Molecular hydrogen line ratios as probes of shocks in dense clouds

Alan Moorhouse

Presented for the degree of Doctor of Philosophy

University of Edinburgh January 1990.

This thesis has been composed by me and
is entirely my own work except where
specifically indicated in the text

Alan Moorhouse

To mum and dad

Abstract

This thesis is concerned with the structure of shocks occurring in dense regions of molecular clouds. These shocks are associated with the outflows from young stars, Herbig-Haro objects, expanding HII regions and the interaction of supernovae remnants with molecular clouds. Momentum, mass and energy are imparted to the cloud. A full understanding of the shock process is thus needed if we are to understand the structure of molecular clouds and the impact on star formation. Emission from the near-infrared transitions of molecular hydrogen is commonly excited in these shocks. A major puzzle is that emission is seen at velocities that would collisionally dissociate molecular hydrogen, and this is a central question that this thesis seeks to answer. This is approached observationally by trying to relate the observed emission to shock models.

Fairly accurate semi-analytic derivations of the emission spectrum expected from hydrodynamic and magnetohydrodynamic molecular shocks are used to fully explore the parameter space of the initial conditions, without resort to expensive numerical calculations. The emission spectrum is then related to that observed.

Most of this work is based on a spectroscopic multi-line study of the near-infrared H_2 emission in two sources, the Orion outflow and the supernova remnant IC443. These observations are then compared with those expected from the models. In both sources it is found that planar hydrodynamic jump-type shocks (J) are consistent with the new observations. Whereas planar magnetically moderated continuous shocks (C), which have been invoked to explain the emission from the shock in Orion, are not. Neither shock types can explain the intensities of CO rotational lines and the H_2 line ratios simultaneously. The high velocities that are observed still present a problem. In IC443 the conclusion is the same but, in addition, the pressure needed to explain the observations is higher than that observed in the supernova remnant. It is suggested that this discrepancy may naturally occur when radiative shocks are driven through a clumpy medium.

This approach of using line ratios as shock discriminators is extended by velocity resolved spectroscopy of three highly excited emission lines from Orion. These observations demonstrate that there are no discernible differences in the line ratios with velocity despite the large change in the energies of the upper energy levels involved. It is discussed how this further constrains the shock type and limits the contribution from non-thermal excitation (such as fluorescence).

The possible physical processes that could lead to high velocity, shocked molecular hydrogen are then discussed. Models proposed in the past are, it is argued, inadequate. It is then shown that the line ratios observed can be closely matched with non-planar continuous type shocks which occur in a bow shock. The densities and pressures needed are still high.

The general conclusions are that previous plane parallel C-shock models invoked to explain the molecular shocks are inconsistent with the observations. The line ratios imply that either J-type shocks, in which the cooling takes a long time compared to the initial heating, or C-type bow shocks which produce a range of temperatures are responsible for the emission. It is finally suggested that C-shocks in gas with a very high magnetic field can produce the high velocity H_2 emission observed without dissociating the molecules.

Contents

List of Figures

List of Tables

Chapter 1

Introduction

Shocks are driven into molecular clouds by a variety of mechanisms, the outflows from young embedded stellar objects; the often associated collimated jets and Herbig-Haro objects; expanding HII regions; supernova blast waves; and cloud-cloud collisions. These shocks can heat the gas, initiating chemical reactions—which can enhance the abundances of certain molecules while destroying others. The shock wave imparts energy and momentum to the molecular cloud, altering its structure. This may induce gravitational collapse or on the other hand support the cloud against collapse (Norman & Silk 1980). The heating of the molecular gas excites the vibrational, rotational and electronic degrees of freedom of atoms and molecules comprising the gas. Emission lines from the radiative decay of these excited states commonly occur over the Infrared to radio wavelengths. Optical emission lines, although visible in a few objects, are generally hard to observe because of the increased attenuation by dust grains at optical wavelengths. Despite much observational and theoretical work over the last decade we will argue in section (1.4) that there are serious problems with the standard interpretation of the conditions in these shocks. Our understanding of the shocks themselves, their role in influencing the above and the physical conditions in these molecular clouds is therefore incomplete.

Molecular hydrogen is readily observable in the near-infrared at gas temperatures close to a few thousand Kelvin, such as those achieved by the passage of a shock wave. It is observations of the emission lines from this molecule that are concentrated on in this

dissertation. The observations are used primarily as a probe of the physical conditions in the molecular cloud and the physics of the shock itself. As will be seen in the discussions on the possible excitation mechanisms multi-line studies, obtaining high signal to noise fluxes and relative strengths, of many transitions are needed to be able to distinguish between the possible exciting mechanisms and the shock types. Such observations form the bulk of this thesis. Why is molecular hydrogen a good diagnostic of the conditions in the shock? Without going into the details we will discuss in the next section, infra-red molecular hydrogen emission lines are good observational probes because

- The lines are quadrupole, so the line emission can be treated as being optically thin. This avoids the problem of modelling the full radiative transfer as well as the shock.
- The levels are a large energy above the ground state. The emission lines are only excited in the hottest parts of the shock, unlike the low rotational transitions of other molecules, such as CO, which are excited by the cold molecular cloud as well.
- The relative intensities of the lines are well known for gas in LTE ($\gtrsim 10^6\,\mathrm{cm}^{-3}$)
- Many shocked clouds are bright sources of H_2 emission lines.

There are many excellent reviews in the literature that are relevant to the work presented in this thesis. Amongst those to highlight on shock waves are: McKee (1986); Shull & Draine (1987) and Lada (1985). Two very good textbooks covering the basics of the dynamics and thermodynamics of fluids and shock waves have been written by Landau & Lifshitz (1987) and Zeldovich & Raizer (1966). On the presence and role of H_2 in the interstellar medium are the reviews of: Shull (1985) and Sternberg (1989). The Orion molecular cloud is unique because of the high apparent luminosity at almost all wavelengths and has had much written concerning the various objects in it. The reader is referred to the numerous papers in the symposium honoring Henry Draper (eds Glassgold, Huggins & Shuckling 1982) and a more up-to-date review by Genzel & Stutzki (1990). A very readable introduction to the physics relevant to the interstellar medium is contained in Dyson & Williams (1980) and in more detail by Spitzer (1978) and Osterbrock (1989). The rest of this chapter is concerned with introducing the reader to the shocks that occur in the interstellar medium (section 1.1). A review of relevant

properties of the hydrogen molecule (section 1.2). The various processes that can induce Infra-red molecular hydrogen emission (section 1.3). The observations of shock excited molecular hydrogen and other molecules (section 1.4) and finally the organisation of the rest of the thesis (section 1.5).

1.1 Shocks in the Interstellar medium

Shocks are amongst the most dynamically active events that occur in the interstellar medium. Stars for instance return matter into the interstellar medium via high-velocity winds when they are born and also throughout their lifetime. Older more massive stars explode as supernovae at their death. The resulting remnant expands at velocities of up to a few thousand $km\,s^{-1}$. They develop when the sound speed of the ambient gas is less than the velocity of the gas that is expanding into it. The ambient gas can only respond to this expansion through a discontinuity, the shock front, which suddenly accelerates, heats and compresses the ambient gas. For this reason shocks are often termed 'surprises', the shock front can only warn of its impending arrival at the sound speed of the gas, which is slower than the speed at which the shock propagates. The structure behind the shock front is determined largely by the shock velocity, density and magnetic field strength. The shock can be divided into four, not necessarily separate, regions (Zeldovich & Raizer 1966)

1. The precursor, where the gas ahead of the shock front is heated and possibly ionised by radiation and/or fast particles produced in the shock.
2. The shock front itself, the gas is accelerated, compressed and heated by collisional or collisionless processes.
3. A relaxation layer, where collisional excitation, dissociation, ionisation, recombination and chemical reactions cause the gas to radiate and change the abundances of atoms and molecules.
4. A thermalization layer; the dense downstream gas absorbs radiation from the shock and re-radiates it as a quasi black body if the column density is high.

The relative sizes of these regions and whether or not they are separate depends crucially on how the dynamical timescale, t_d, compares with the cooling timescale, t_c. A

shock in which $t_c \gg t_d$ is often termed an 'adiabatic' or 'non-radiative' shock because no energy is lost in the shock front itself (hence adiabatic). In this type of shock, typical of young supernova remnants, the eventual cooling of the gas has very little effect on the dynamics of the shock front. The shock front, where all the heating, compression and acceleration occurs is thin compared to the cooling layer. This is equivalent to saying that the shock front is followed by a large column of gas that stays at approximately the same temperature, density and velocity before the gas starts to cool. If the hot gas can cool on a timescale comparable to or shorter than the dynamical timescale ($t_c \lesssim t_d$) then the shock is 'radiative' in the sense that the cooling lowers the temperature and to remain in pressure equilibrium the post-shock gas is compressed almost immediately after passing through the shock front.

In the dense molecular clouds we are concerned with in this thesis the shocks are almost always radiative. The gas jumps from its pre- to post- shock values in a thin shock front and for this reason such shocks are termed J-type (for jump, Draine 1980). An extra important distinction occurs when the gas can be considered as a 'multi-fluid' composed of weakly interacting neutrals, ions and electrons (and sometimes charged dust grains). If there is a significant magnetic field these fluids can achieve different temperatures and flow velocities provided that the fractional ionisation is not too large. Signals in this situation are not solely transmitted by the sound speed(s) of the gas but there are also magnetosonic or Alfvén waves. The Alfvén velocity for the ion-electron plasma (which is only weakly coupled to the neutrals) can be much larger than the sound speed and the shock velocity. Then as far as the charged particles are concerned there is no shock. The charged fluid can propagate signals faster than the shock velocity, and can send signals ahead of the shock front. The pre-shock gas is thus not totally surprised by the shock wave and the ion-electron plasma can respond smoothly to the changes which would otherwise have been discontinuous.

There are several classes of solution that can exist to the multi-fluid MHD shock.

A J-type shock can occur, even though the magnetic field can drive the ions and electrons ahead of the shock front. The charged fluid can heat and accelerate the pre-shock gas in a magnetic precursor through frictional drag. This precursor will only occur when the drag length is longer than the thickness of the shock front. This requires

moderate ionisation fractions and low alfvén velocities (so that the magnetosonic speed is only marginally greater than the shock velocity).

When the Alfvén velocity is increased the ions/electrons are driven further ahead, the neutrals are increasingly accelerated and heated. Eventually no discontinuity occurs in the neutral fluid even though the neutrals can remain supersonic throughout the shock. The neutrals are smoothly accelerated, heated and compressed by collisions with the streaming ions. If the velocity between the ions/electrons and neutrals is too large then the gas becomes too hot, collisional dissociation and ionisation occurs and the shock solution breaks down. However if the gas is able too cool during the drag heating then the temperature is lowered and a C-type shock can still exist. The shock front and the post-shock relaxation layer are co-existent in this type of shock.

There is also another class of C-type shocks in which the neutral gas flows smoothly through a sonic point and becomes subsonic before eventually passing through another sonic point further downstream and becoming supersonic again.

The MHD J-type shock is probably the most difficult to compute since the position at which the jump will occur is not known *a priori*. The position and strength of the jump (from supersonic to subsonic neutral motion) depends on the conditions further downstream in the post-shock gas. This problem of computing self consistently where the jump occurs has been considered by Chernoff (1987) for the simplified cases of adiabatic and isothermal flows and power law cooling functions. Roberge & Draine (1987) discussed how this problem may be treated using realistic cooling functions and chemistry. Despite this work very little has been done on the emission from such shocks, mainly because of the difficulty in obtaining solutions to the flow equations. In the J-type shocks that we discuss in chapter (2) we will ignore this problem and consider the magnetic pre-cursor to be non-existent or insignificant. The emission from a J-type shock is then easily calculated. The C-type shocks are simpler in terms of computing the solutions since no discontinuous jumps occur in the flow. However they are computationally expensive because of all the chemistry and energy and momentum transfer processes that have to be followed (see for example Draine, Roberge & Dalgarno 1983: Flower & Pineau des Forets 1986).

1.2 The Hydrogen molecule

As the emission lines from molecular hydrogen are the primary observational tools that we employ, in this section we will summarize the properties of the hydrogen molecule that are important to a study of shocks and the excitation of line emission.

In the interstellar medium the hydrogen molecule is normally in its ground electronic state, $X^1\Sigma_g^+$. This configuration means the molecule has no component of electronic angular momentum along the inter-nuclear axis (represented by the Σ), the electronic wavefunction is symmetric to reflection in the plane through the axis (+) and the plane through the centre of symmetry which is perpendicular to the axis (g), and the electronic spin is zero (i.e. 2S+1=1). The quantum mechanics of the molecule is described in Herzberg (1950) and the notation used here is summarized by Field, Sommerville & Dressler (1966). The next allowed excited states are the $B^1\Sigma_u^+$ state (11.2 eV above ground $\cong$ 130,000K) and the $C^1\Pi_u$ (12.3 EV above ground $\cong$ 143,000K). Transitions between these two states and the ground state are called the Lyman and Werner bands. The absorption of ultraviolet photons is the most common way in which these electronic states are excited in the ISM, collisions with high energy electrons and cosmic rays are among others. For UV excitation the photon wavelength has to be less than 112 nm and 102 nm for the Lyman and Werner bands respectively. Both these limits are at longer wavelengths than the Lyman limit (atomic hydrogen) at 91.2 nm, non-ionising photons that for example escape HII regions can therefore excite H_2.

The electronic states are split by the vibration and rotation of the nuclei (Fig 1.1). In particular the ground electronic state is split into fifteen vibrational levels, and each vibrational level is further split into a large number of rotational levels. The statistical weight, g_j, of each of these levels is a function of the rotational quantum number, J, and the nuclear spin, I, and is given by $(2J+1)(2I+1)$. The nuclei are identical fermions and the overall wavefunction of the molecule has to be antisymmetric to exchange of nucleons. For even values of J the rotational wavefunction is symmetric, thus the nuclear spin wavefunction has to be antisymmetric, i.e. I=0. The opposite is true for odd J states and I=1. The statistical weights for even J states is $(2J+1)$ and are known as para-hydrogen states whereas odd J are ortho-hydrogen and $g_j = 3(2J+1)$. The vibrational and rotational levels are displayed in the energy level diagram Fig (1.1) and some of the

important transitions are indicated.

Molecular hydrogen is homonuclear and so dipole transitions between the rotational and vibrational levels of the ground electronic state are forbidden. However quadrupole transitions may occur. The selection rules (Field, Sommerville & Dressler 1966) require that the rotational quantum number changes by ΔJ =+2, 0 or -2 (except J=0-0 which is forbidden). The changes in the vibrational quantum number are not restricted. A transition is denoted by the upper and lower vibrational quantum numbers and O(J), Q(J) and S(J), where J is the rotational quantum number of the *lower* level and O, Q and S represent a change, ΔJ, of +2, 0 or -2 respectively. Take the case of the most commonly observed transition, the 1-0 S(1), it is a transition from v=1, J=3 to a lower level v=0, J=1.

Accurate energies for almost all of the ro-vibrational levels in the ground state have been calculated from ultraviolet spectra by Dabrowski (1986). The lowest transition, the 0-0 S(0) line (J=2–0), is at 28 μm and has an upper state energy of 512 Kelvin above the ground (v=0, J=0) state. The energies of the rotational levels ($\approx 85j(j+1)$ K) are widely spaced because of the low moment of inertia compared with other molecules. The highest rotational transitions with $\Delta v = 0$ are visible at 3 μm. The first excited vibrational level is $\approx$ 6000 K above ground. The electronic potential is anharmonic so the separation of higher levels is increasingly reduced. There are fourteen vibrational levels in the ground electronic state, the vibrational continuum (v>14) is at 4.48 eV ($\approx$52000 K), which is the energy needed to dissociate the molecule. In normal molecular cloud conditions it is difficult to detect these emission lines because, although hydrogen is by far the most abundant molecule, collisional excitation is extremely slow at the temperatures (O(50)K) typical of quiescent molecular clouds. Lines will only be emitted after a large amount of energy is input into the molecular gas.

Spontaneous transition probabilities for radiative decay of levels in the electronic ground state have been calculated by Turner, Kirby-Docken & Dalgarno (1977). For most of the $\Delta v = 1$ transitions these rates are a few times $10^{-7}s^{-1}$. The cooling time for hot (a few thousand Kelvin) molecular hydrogen is thus of the order of one year. The H_2 line radiation that is observed is therefore due to a recent event and delineates that event which transferred the energy to the molecule.

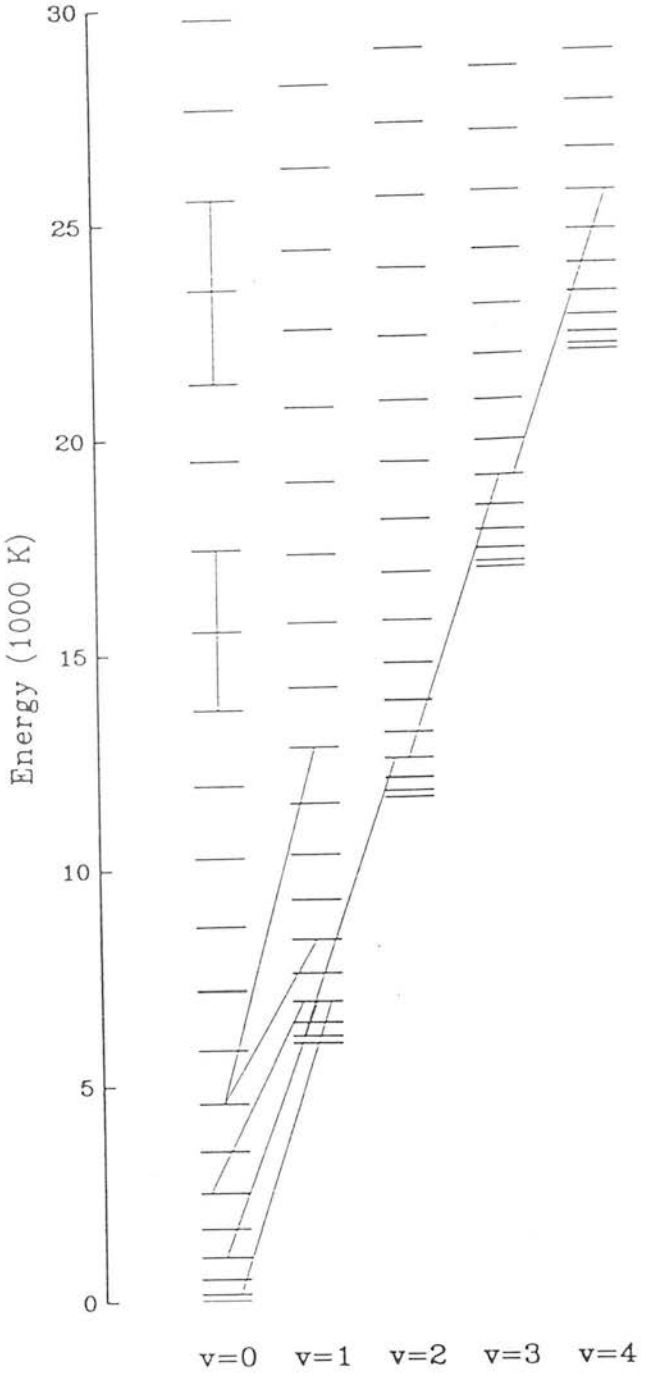

Figure 1.1: Energy level diagram of the ground electronic state of the hydrogen molecule. The vibrational levels increase from the left and each vibrational level is split into rotational levels. Some transitions that have been observed are indicated

The collisional excitation and de-excitation rates (by both H and H_2) between individual levels are not well known, and make calculations of the emission spectrum at low densities (when the molecule is not in local thermodynamic equilibrium LTE) highly uncertain. There are factors of 2–3 in the resulting line intensities depending upon which rates are used (see Burton *et al.* 1989a; Burton 1986). The critical density above which the levels are in LTE is $\approx 10^6\,\mathrm{cm}^{-3}$. Collisional dissociation proceeds through excitation of the v=14 level which is then excited to the vibrational continuum (i.e. Draine & Roberge 1982). The dissociation rate is thus very density sensitive requiring many collisions to excite the v=14 level and because of the uncertainty in the collision rates the dissociation rate is also uncertain at low densities. The total collisional dissociation rates are known to better accuracy at high density. Direct radiative dissociation is unlikely, and radiative dissociation normally goes through the absorption of Lyman or Werner band photons to the excited $B^1\Sigma_u^+$ and $C^1\Pi_u$ states followed by ($\approx$ 10% of the time) a decay to the vibrational continuum of the ground electronic state (see Fig. 1.2). Another important dissociation mechanism is the spin flip caused by the impact of energetic electrons exciting the $b^3\Sigma_u^+$ which is repulsive and immediately dissociates.

Molecular hydrogen is known to form on the surface of dust grains (e.g. Hollenbach & Salpeter 1971; Duley and Williams 1986). The H atoms collide with grains and stick to the surface. These atoms then move around on the surface and tend to combine at preferred sites with ions like OH^- to form H_2. The molecule is subsequently ejected from the grain surface to produce gas phase molecular hydrogen. The exact rate of formation for this process is not well known, but the rate coefficient R_f (in $cm^3 s^{-1}$) is commonly quoted as

$$R_f = 3 \times 10^{-18} y_F \sqrt{T} \tag{1.1}$$

where T is the gas temperature and y_F is the formation efficiency which is close to one for cool grains ($T \lesssim 100$ K). At high temperatures the efficiency is uncertain as it depends upon the ability of an H atom to stick to the surface at high temperatures. For classical graphite and silicate dust grains (e.g. Draine & Lee 1982) y_F drops to near zero at grain temperatures above and below uncertain limits which are probably close to 100 and 20 Kelvins respectively . The lower limit is due to the reduced mobility on the grain surface and the upper limit because the H atom is ejected from the grain before it has had time to find a reaction site. If the grain surface is rough then the H atom may be more tightly bound to the surface and the efficiency is increased at the higher

temperatures (i.e. Neufeld & Dalgarno 1987.). This equation also assumes a typical gas to dust ratio of $\frac{n_H}{n_d} \approx 10^{-12}$ (i.e. Dyson & Williams 1980). Two body reactions in the gas phase are generally too slow to be an important formation mechanism in molecular clouds although reactions of H with H^- can be significant at high gas temperatures (i.e. Hollenbach & McKee 1979) . The reformation timescale is $1/Rn_p$ so behind a fast shock in which the molecular hydrogen is completely dissociated the reformation timescale is (assuming y_F=1) $\approx 10^9/n_p$ years, this is much longer than the cooling timescale behind shock fronts, except for very high gas densities ($n > 10^9\,\mathrm{cm}^{-3}$).

1.3 Excitation of infra-red molecular hydrogen emission

If observations of H_2 lines are to provide information on the physical conditions in clouds and, by implication, information on the details of the excitation process then the differences produced by the many processes which can excite the molecule need to be known to assess their relative contribution in a particular source. The excitation processes can be conveniently divided into two; thermal and non-thermal. When thermally excited collisions populate the low lying levels of the molecule in a bottom-up process, shocks which heat the gas by collisions are a typical thermal process. We will deal with shock excitation in the next subsection. Non-thermal excitation includes such processes as fluorescence, collisions of high energy electrons and formation in excited energy levels. These non-thermal mechanisms tend to populate the higher energy levels first and can be thought of as a top-down mechanism.

1.3.1 Shock excitation

The hot gas behind a shock front can collisionally excite the rotational and vibrational levels of H_2. The temperatures reached behind the shock are a few thousand degrees and the molecules radiate as they cool the gas. There has been much work in the past on the structure of shock waves that can excite H_2 emission and the shocks fall into two broad types. Shocks in which the magnetic field is unimportant to the dynamics of the shock front and the heating occurs at a discontinuity. The opposite case is where the magnetic field has an important effect on the dynamics and smooths out the shock front. The two

cases were termed J-type (for jump) and C-type (for continuous) by Draine (1980) who first realised that strong MHD continuous shocks could exist in molecular material.

In a J-type shock all the heating, acceleration and compression occurs in a thin layer of the order of one mean free path. The pre-shock gas ahead of the front remains undisturbed until the shock itself arrives. This is because the sound speed in the pre-shock gas is less than the velocity of the shock front. The heating in such shocks is thus far quicker than the subsequent cooling. This is the conventional shock which is quite often described in text books (i.e Dyson & Williams 1980; Landau & Lifshitz 1987). In a J-type shock the gas is heated very *quickly* compared to the subsequent cooling. The subsequent emission depends mainly on the form of the cooling function and whether or not the gas is dense enough to be in LTE. When the temperatures behind the shock are greater than about 4000 Kelvin then the collisions become frequent enough to effectively populate the high vibrational levels out of which dissociation can occur. In shocks with temperatures greater than 20000 Kelvin (equivalent to 25 km s^{-1}) the molecules are all dissociated (Kwan 1977).

Conversely in MHD shocks with a moderate ionisation fraction ($< 10^{-5}$) the shock is acting on two fluids, the ions and the neutrals. If the magnetic field is high enough then the ions can be sub-sonic because the ion Alfvén velocity can be greater than the shock velocity. The shock front is still moving supersonically with respect to the neutrals. The ions can thus respond to the passage of the shock wave by sending Alfvénic waves through the gas. However they are prevented from fully dissipating the shock front as a compression wave because the neutrals can only respond to disturbances at the sound speed, which is less than the shock velocity. The ions are driven ahead of the neutrals (in the shock frame they are decelerated faster). The heating is due to the frictional drag between the streaming ions and neutrals. A situation can now develop where the ions and neutrals are accelerated and heated smoothly. A crucial point relevant to the observations is that C-type shocks generally heat the gas on a timescale comparable to the cooling time. C-type shocks like this will therefore produce lower post-shock temperatures than would be be expected for a J-type shock at that velocity. It is the lower temperature behind the shock which suppresses the collisional dissociation of molecules at high shock velocities.

1.3.2 Non-thermal excitation

The non-thermal excitation mechanisms generally produce a different emission spectrum from the thermal shock excitation. Fundamentally this is because all the non-thermal mechanisms excite very high energy levels which are then de-excited either by collisions or by the emission of radiation. On the other hand the thermal mechanisms collisionally excite molecules out of low-lying states to higher ones, only a small change in energy results. The non-thermal mechanisms thus tend to lead to emission from highly excited lines whereas the thermal emission spectrum has a much lower excitation.

The fluorescence process was first proposed as a possible means of producing infra-red emission from H_2 by Gould & Harwit (1963). A molecule in the ground electronic state absorbs a UV-photon and is electronically excited to the Lyman or Werner bands and then rapidly radiatively decays back to a high vibrational level of the ground state (and on average one time in ten to the vibrational continuum, the molecule is photodissociated). Infra-red photons are subsequently emitted in a radiative cascade down the vibrational/rotational ladder, Fig. (1.2) illustrates this mechanism schematically. Detailed models of the emission spectrum from this process have been published by Van Dishoeck & Black (1987) and Sternberg (1988). At low densities ($n < 10^5\,\mathrm{cm}^{-2}$) the intensity of the emission is relatively independent of the density, and is influenced largely by the illuminating ultraviolet intensity and spectrum. The cascade produces very intense emission from the vibrational lines (the [1-0 S(1)/2-1 S(1)] ratio ≈ 2) but the rotational transitions are relatively weak. At high densities ($n \gtrsim 10^5\ \mathrm{cm}^{-3}$) it is now realised that this emission spectrum is altered by both collisional de-excitation interrupting the cascade and by additional thermal heating due to high energy photo-electrons ejected from dust grains (i.e Wagenblast & Hartquist (1986); Burton *et al.* (1989); Hollenbach & McKee 1989; Sternberg 1988).

UV-excited dense gas can look like thermal 'shocked' emission, in particular the above mentioned [1-0 S(1)/2-1 S(1)] ratio increases to a value of about ten in this situation. However, it is still possible to distinguish between thermal (shocked) and UV-excited emission by observing lines from higher vibrational and rotational transitions. For the UV-excited gas transitions from the very high (v> 5) vibrational lines are harder to collisionally de-excite and emission from such lines should be observable, however in

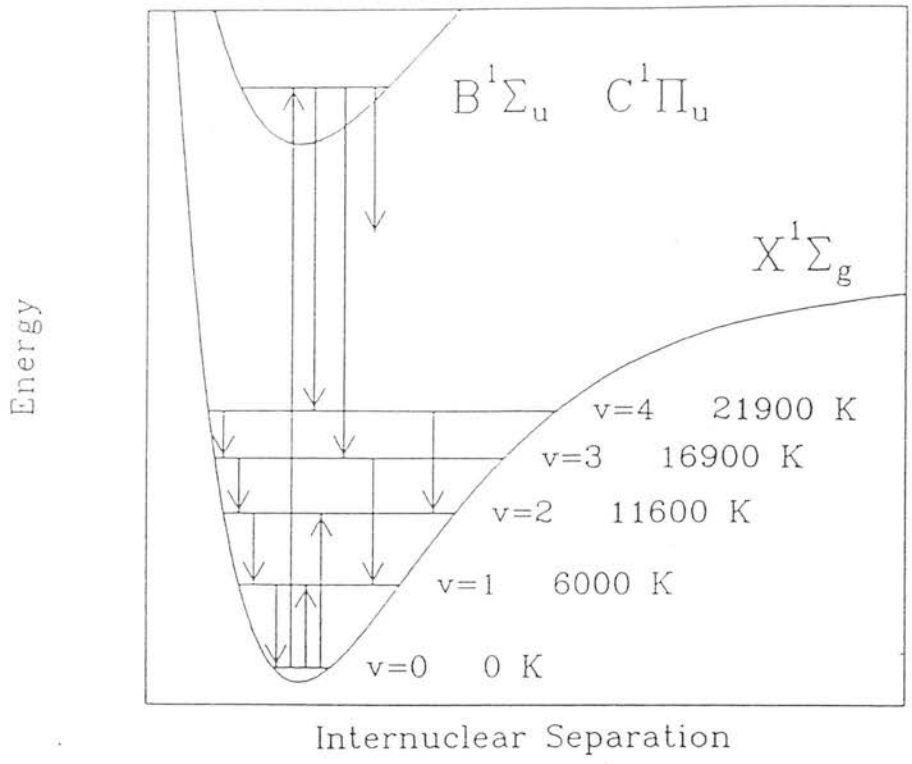

Figure 1.2: Fluorescence and photo-dissociation. Absorption of a UV photon electronically excites the molecule, which then decays either to the continuum or a vibrationally excited level in the ground state. The subsequent radiative cascade and possible thermal excitation are indicated (from Sternberg 1989)

shocked gas these very high vibrational transitions will be weak. The opposite is the case for the high rotational transitions, shocks will collisionally excite these levels (if the gas density is high enough) whereas the fluorescent cascade predominantly excites only the low lying rotational lines (e.g. see Van Dishoeck & Black 1987).

An additional discriminator between shocked and UV-excited emission is the velocity width of the observed lines. Shocks are dynamically active phenomenom which lead to emission from gas accelerated to high velocities, i.e. the emission lines are likely to be broad and shifted with respect to the surrounding material. However, fluorescence is an intrinsically quiescent process imparting no high velocity motions to the gas. UV-excited lines should therefore be narrow (the breadth of the line is only the intrinsic velocity breadth in the cloud, generally the turbulent velocity) whereas shock excited lines are almost always broad. We (Burton, Geballe, Brand & Moorhouse 1990) have tested this hypothesis by observing sources of H_2 emission which are suspected of being UV-excited at very high velocity spectral resolution (≈ 12 km s^{-1} FWHM). In all cases the H_2 emission line was unresolved, as expected for UV-excited gas.

The H_2 lines can also be excited by the impact of high energy electrons or cosmic rays. Such electrons have been hypothesized to arise following the absorption of X-ray photons by heavy elements depleted in dust grains (Lepp & McCray 1983; Voigt & Shull 1989). The spectrum from such an excitation process generally resembles that of UV-excited emission as the large energy of the colliding electron/cosmic ray excites the molecule to a very highly excited vibrational level, which then cascades down the energy levels as in fluorescence. This process tends to convert approximately 10^{-2} of the X-ray luminosity into 1-0 S(1) photons (Lepp & McCray 1983).

When a molecule is formed and ejected from the surface of a dust grain it can leave the grain in an excited state. The distribution of the level populations and the amount of energy injected into these molecules depends on the details of the reformation mechanism and the composition and structure of the grain surface. These are very uncertain properties so at the moment it is impossible to reliably model this excitation process. Early estimates of the reformation state were limited to modelling of atoms on surfaces approximated as rigid lattices (Hunter & Watson 1978) or classical lattices (Leonas & Pjarnpuu 1981). The former authors found that the molecules were highly

rotationally excited ($j > 7$, between 0.5 and 1 eV) and vibrationally excited ($v \leq 8$, 3.5eV). Whereas Leonas & Pjarnpuu calculated that almost all the binding energy is contained in the vibrational modes of the new molecule. Hollenbach & McKee (1979) assumed that 4.2 eV of the binding energy would be deposited in the rotational and vibrational levels in their seminal paper on shocks in molecular gas. Duley and Williams (1986) considered the reformation at OH^- sites (although other ion sites may work as well) and found that the newly reformed molecule should be vibrationally excited ($v < 7$, about 3eV) but rotationally cool ($j \leq 1$) with about 0.2eV of kinetic energy. Thus it is not clear what the product state of H_2 formation will be, however in section (5.4) it is argued that whatever their initial state the re-formed molecules are rapidly de-excited through collisions in gas of densities that we observe. Thus dense atomic gas will produce H_2 which is only moderately excited.

1.4 Observations of shock excited H_2

The first shock models for dense molecular gas followed the discovery by Gautier *et al.* (1976) of the H_2 emission from Orion. It was quickly realised that the luminosities were too great to be explained by UV-excitation from any of the UV sources in the Orion region (Hollenbach & Shull 1977).

The first models were of simple hydrodynamic J-type shocks (Hollenbach & Shull 1977; Kwan 1977; London, McCray & Chu 1977; Shull & Hollenbach 1978). They were able to reproduce the intensities of the few lines that had at that time been observed, in particular reproducing the [1-0 S(1)/2-1 S(1)] ratio of 10 observed in Orion, with shocks of velocities close to $10\,\mathrm{km\ s^{-1}}$ propagating into gas of density $\approx 10^5\,\mathrm{cm^{-3}}$. Kwan (1977) showed that the molecular hydrogen would be completely dissociated in shocks of velocity $> 25\,\mathrm{km\ s^{-1}}$. Problems were created for the J-type shocks when Nadeau & Geballe (1979) observed that the 1-0 S(1) line was broad with radial velocity widths of up to $\pm 100\,\mathrm{km\ s^{-1}}$. CO rotational emission was then observed to be about 2 orders of magnitude stronger than that inferred from the J-type shock models mentioned above (Watson *et al.* 1985).

This prompted the development of C-type shock models. In two concurrent papers

Draine & Roberge (1982) and Chernoff, Hollenbach & McKee (1982) modelled the emission from Orion as C-type shocks. Draine & Roberge attempted to fit the high rotational CO lines and the H_2 emission lines from Peak 1, which at that time included observations of the v=1-0 and 2-1 lines as well as the pure rotational 0-0 S(8) – S(13) lines measured by Knacke & Young (1981). A 38 km s^{-1} shock wave into pre-shock gas of density 7×10^5 cm^{-3} and a transverse magnetic field strength of 1.5 milligauss fitted the intensities of both the H_2 and CO lines. However the relative strengths of both the H_2 and CO lines were not well produced in this model, in particular the very high rotational CO transitions were overestimated by about a factor of 5. Chernoff, Hollenbach & McKee modeled the emission averaged over the entire outflow. They could reproduce the observed intensities as well as the CO rotational lines with a 36 km s^{-1} shock into a gas density of 2×10^5 cm^{-3} and a magnetic field strength of 0.45 milligauss. However only the 1-0 and 2-1 H_2 lines were reproduced in this model, the transitions from more energetic levels were severely underestimated (see McKee, Chernoff & Hollenbach 1984).

The C-shock models are highly dependent on the shock velocity and the initial conditions of the molecular clouds. This is illustrated by noting the differences produced in the two models mentioned in the last paragraph and by examining the more detailed results presented, for example, in Draine, Roberge & Dalgarno (1983). The reason why C-type shocks are sensitive to the shock velocity is easy to explain. The heating rate is determined by frictional heating the amount of which is a function of the velocity difference between the ions and the neutrals (i.e. the drag velocity). The drag velocity in turn increases with the shock velocity. To first order the cooling rate is constant, so that the heating to cooling times are velocity sensitive. Hence the eventual temperature reached in the shock is a function of the shock velocity. The larger the shock velocity the correspondingly larger is the maximum temperature in the C-shock. However most of the observations to date of a number of sources indicate that the temperature behind the shock is about the same, implying for the C-shock models to be correct a constant shock velocity in a large number of sources which presumably have different physical conditions. This is very hard to believe as the shock velocity is determined by, among other things, the velocity of the outflow and the local ambient density. It is almost impossible that these are the same regardless of the local conditions and the type of object which drives the shock.

At this point it should be discussed how from the observations of line ratios excitation temperatures can be determined. An excitation temperature can be defined in the following manner. The specific intensity, I ($W\,m^{-2} per\ steradian$), of an emission line from a source is

$$I = \frac{h\nu}{4\pi} N_j A_{ji} e^{-\tau} \tag{1.2}$$

where ν is the frequency of the line (Hz), h Plancks constant ($J\,s$), N_j (m^{-2}) the column density of molecules in the upper energy level, j, A_{ji} is the spontaneous transition probability (per second) from the upper level j to the lower level i and τ is the optical depth between the observer and the source. The specific intensity is the quantity measured by the telescope+detector. However the entrance aperture is rarely as large as one steradian. To convert the measured intensity per beam diameter b (in arcseconds) to one which is per unit solid angle we multiply the observed intensity by $3.3416 \times 10^{10} b^2$ (this is the number of square arcseconds in one steradian multiplied by the area of the beam). This assumes that the source uniformly fills the beam, if this is true then the column density derived is independent of the distance to the source (because I drops as the distance squared, while the actual surface area from which the detector receives radiation increases as the distance squared).

From the measured intensity the column density in the upper energy level can be found if the frequency, transition probability and the statistical weight are known (these are listed in Table (1.1) for the lines we have observed) and additionally the external extinction can be estimated. If it is assumed that the source is at a single temperature and in Local Thermal Equilibrium (LTE) then the column density of an upper level is given by the Boltzmann formula

$$N_j = g_j \frac{e^{-T_j/T_{exc}}}{Q(T)} \tag{1.3}$$

where g_j is the statistical weight of the upper level (for H_2 see section (1.2)) and Q(T) is the sum over states (see section 2.3), T_j is the energy of the upper level in Kelvins (i.e. $E_j \times k$, Boltzmanns constant), T_{exc} is the excitation temperature of the

Table 1.1: Parameters of lines used in the thesis

Line	Wavelength[1] (μm)	Upper Level[1] Energy (K)	Transition[2] probability 10^{-7} s^{-1}	Statistical[3] weight
1-0 S(11)	1.6504	18979	0.53	81
1-0 S(10)	1.6665	17310	1.05	25
1-0 S(9)	1.6877	15721	1.68	69
1-0 S(8)	1.7147	14220	2.34	21
1-0 S(7)	1.7480	12818	2.98	57
1-0 S(6)	1.7880	11521	3.54	17
1-0 S(1)	2.1218	6956	3.47	21
2-1 S(2)	2.1542	13150	5.60	9
3-2 S(3)	2.2014	19086	5.63	33
1-0 S(0)	2.2235	6471	2.53	5
2-1 S(1)	2.2477	12550	4.98	21
3-2 S(2)	2.2870	18386	5.63	9
4-3 S(3)	2.3445	23955	4.58	33
2-1 S(0)	2.3556	12095	3.68	5
3-2 S(1)	2.3846	17818	5.14	21
1-0 Q(1)	2.4066	6149	4.29	9
1-0 Q(2)	2.4134	6471	3.03	5
1-0 Q(3)	2.4237	6956	2.78	21
1-0 Q(4)	2.4375	7585	2.65	9
1-0 O(4)	3.0039	6471	2.90	5
1-0 O(5)	3.2350	6956	2.09	21
2-1 O(5)	3.4378	12550	3.18	21
0-0 S(17)	3.4857	25541	32.6	117
1-0 O(6)	3.5007	7584	1.50	9
0-0 S(16)	3.5475	23461	28.3	37
0-0 S(15)	3.6261	21413	24.1	105
1-0 O(7)	3.8075	8365	1.06	33
0-0 S(13)	3.8461	17445	16.2	93
0-0 S(12)	3.9960	15542	12.7	29

1 Using energy levels of Dabrowski (1986)

2 Rates from Turner, Kirby-Docken & Dalgarno (1977)

3 Assumes an ortho/para ratio of 3

source. If two lines with different upper level energies are observed then the excitation temperature can be found from the observations by combining equations (1.2) and (1.3)

$$T_{exc} = (T_1 - T_2) ln \left[\frac{I_2 A_1 g_1 \lambda_2}{I_1 A_2 g_2 \lambda_1} \right] (\tau_1 - \tau_2) \tag{1.4}$$

The subscripts 1 and 2 refer to the two different lines that have been observed. Excitation temperatures have been found in this way from observations of a great number of sources. This is not a reliable indicator of the true gas temperature since, in a shock for instance, there are a range of gas temperatures as the gas cools from the high initial temperatures reached in the shock. Nevertheless it is an often quoted estimate of the temperature in the shock. Two particular lines the 1-0 S(1) and the 2-1 S(1) have been observed in many objects because of the relative ease with which they can be observed and the large energy difference of the upper energy levels involved ($\approx 5500K$). The ratio between these two lines has until recently been thought to be a good discriminator between fluoresced and shocked gas because their ratio ([1-0/2-1]) is of order unity for fluoresced gas and ten for shocked gas. However, as discussed in the section on non-thermal excitation mechanisms, at high densities the fluoresced gas is collisionally de-excited and the gas then appears thermalised like a shock. This confusion leads to even more unrealistic excitation temperatures from observations of these lines. With this in mind in Table (1.1) we collate together estimates of the excitation temperature from a number of sources which are quite probably shock-excited. The most striking feature of this table is that all the estimates indicate gas at approximately 2000 Kelvin.

This observation is difficult to explain in C-type shock models because the temperature in the shock is an approximately monotonically increasing function of the shock velocity (see section 2.5). The observation that most shocked sources appear to be close to 2000 Kelvin therefore implies that the shock velocity is required to be constant in a number of different sources which presumably have differing conditions. A constant shock velocity might be thought to be a plausible result if the same process was driving the shock wave in each object, but this is not the case. The objects listed in Table (1.2) range from outflows from young stellar objects, Herbig-Haro objects to supernova blast waves.

Table 1.2: Observed excitation temperatures for shocked sources

Object	Excitation Temperature	Notes	reference
Orion Peak 1	2074± 30	outflow	1
IC443	1900± 100	SNR	2
IC443	1900± 100	SNR	2
Cas A	2400± 300	SNR	3
NGC 2071	1700–2100	Bipolar outflow	4
HH 7	2000± 300	Herbig-Haro	2
DR 21	1950–2250	owtflow	5
CRL 618	2100	proto-planetary	2

[1] This work [2] Burton, Brand, Geballe & Webster (1989a) [3] Doyon & Nadeau (1988) [4] Burton, Geballe & Brand (1989) [5] Garden, Geballe, Gatley & Nadeau (1986)

Fluorescent emission of H_2 has now been positively identified in a number of sources. Hayashi *et al.*(1985) made the first claim based on their observation of the [1-0 S(1)/2-1 S(1)] ratio in Orions bar, subsequently much firmer observations of fluorescence at work has been observed by Gatley *et al.* (1987); Hasegawa *et al.* (1987); Sellgren *et al.* (1988). These observations have been close to, but not perfectly matched by, the models. As was argued earlier the emission spectrum from such sources does indeed show strong emission from highly excited vibrational levels. For instance Gatley *et al.* (1987) identified the v=6-4 Q branch in their spectra of the reflection nebulae NGC 2023. There is as yet no positive identification of the thermalisation that should occur at high densities, although Hasegawa *et al.* claim to observe a mix of thermal and fluorescent gas in some of their sources, but with the increasing sensitivity of infra-red spectrometers this will almost certainly be resolved in the near future. There has been no reported detection of X-ray excited emission.

1.5 Organisation and aims of the thesis

The study presented in this thesis was prompted partly by the observations highlighted in the last section (1.4) that seemed to be in conflict with the accepted C-type shock models. Our understanding of the shock mechanisms acting in molecular clouds (in itself interesting), the physical conditions in the molecular clouds that such shocks are highlighting, the chemistry that is initiated, the total momentum and energy that is transferred and how it is distributed, the possible origin of the molecular outflows and the role in the star formation process are among questions that are therefore incorrectly addressed. We have thus set out to attempt to discriminate between the different classes of shocks. The infra-red emission lines from molecular hydrogen are suited to such a study for the reasons stated earlier. The main result of this thesis is that the plane parallel C-type shocks are inconsistent with the observations. Jump type shocks are shown to be adequately able to explain the emission spectrum, but cannot explain the broad width of the line. If non-planar shocks are employed the C-type shocks can reproduce the observations if the emission is from that of a bow shock.

Before discussing the observations some knowledge is needed of the emission spectrum that molecular shocks will produce. In chapter 2 we therefore discuss in detail how the

H_2 emission from both J-type and C-type shocks can be calculated in the idealized case of plane parallel shocks in which the gas density is high enough for the H_2 energy levels to be in LTE. In particular we present a semi-analytic method by which H_2 line intensities can be calculated from partially dissociative hydrodynamic and MHD (without pre-cursor) Jump-type shocks when the cooling function is assumed to be due to a limited number of coolants and the gas is at constant pressure. It is illustrated how the line ratios from the post-shock region are relatively insensitive to the initial conditions and shock velocity depending more on the dominant coolants of the gas and the shock pressure. We then discuss MHD C-type shocks, reviewing previous work and stressing the sensitivity of the emission spectrum to the initial conditions.

The observations that are used to constrain the shock models are contained in chapters 3, 4 and 5. The observational tool employed has been that of spectroscopy of the emission lines, both unresolved to obtain line intensities and higher resolution observations that can resolve the velocity structure of the emitting gas. Lines from a wide range of upper level energies are sensitive to the temperature and density of the emitting gas and can therefore be used as a probe of shock structure. In chapter 3 are the observations of the shock in Orion. Over 30 emission lines have been measured, including several for the first time. The column densities from these lines are used initially to calculate the extinction to the source, which is found to be lower than previous estimates and places the shock in the photodissociation front. The column densities obtained from the observations are shown to be consistent with J-type shocks of fairly high pressure, which in turn implies high mass loss rates for the source of the outflow which is not at variance with some of the estimates of the mass loss rate.

In Chapter 4 we present similar spectroscopy of two positions in the supernova remnant IC443 which is blasting a shock wave into a nearby molecular cloud. Again the column densities and ratios are shown to be simply explained by J-type shocks and inconsistent with C-type shocks. The pressures needed at the two positions are different from that in Orion and further are higher than the observed pressure of the supernova remnant itself. This discrepancy is discussed at length and a possible mechanism which can solve it is proposed.

Velocity resolved spectroscopy of Orion with a more limited number of lines have been

obtained and are discussed in chapter 5. The line ratios are found to be independent of the velocity of the emitting gas. This rules out contributions to the line emission from fluorescence, reformed molecules and other non-thermal mechanisms. The constraints that this imposes on the process by which the high velocity emission is obtained are further discussed. In particular to an accuracy of 6% the [1-0 S(1)/2-1 S(1)] ratio is identical at all velocities, implying that the excitation temperature is constant to within 50 Kelvin.

This leads on to chapter 6 in which we examine all plausible means by which high-velocity emission can be obtained. These are shown to be inconsistent with the observations. During this discussion shocks that occur around obstacles and are thus bow shaped are investigated. It is shown that C-type shocks occurring in these bow-shaped shocks can produce the correct range of temperatures to reproduce the line ratios in both Orion and IC443, the density is still high and the pressures while still needing to be large are not as high as are needed for the J-type shock to reproduce the observations. It is then proposed that very soft C-type shocks which need magnetic field strengths about a factor of ten larger than are expected in Orion can produce high velocity H_2 emission. This has important ramifications for the origin of the outflow if correct.

Finally we will conclude in Chapter 7 with an overall summary of each chapter and how this fits in with the overall state of the structure of the shocks occurring in molecular clouds. We end with a discussion on the direction that future research should take, both observationally and theoretically.

Chapter 2

Theory of molecular shocks

2.1 Introduction

When H_2 emission lines were first discovered by Gautier *et al.* (1976) it was very quickly recognized that the emission occurred in a layer heated by the passage of a shock wave. Early calculations of hydrodynamic J-type shocks (Kwan 1977, Hollenbach & McKee 1979) concentrated on explaining the few emission lines which at that time had been observed. As has already been discussed in Chapter 1, the discovery that the H_2 emission lines were broad (Nadeau & Geballe 1979) and of pure rotational sub mm lines of CO at an intensity orders of magnitude less than predictions from the J-shock models made such models seem unsatisfactory. Draine (1980) then proposed that MHD C-type shocks could possibly explain the CO emission, and—at the same time—get closer to the observed radial velocities.

The C-shock models which were then developed (Draine & Roberge (1982), Chernoff, Hollenbach & Mckee (1982), Draine, Roberge & Dalgarno 1983) were very successful in accounting for the variety of emission lines from the Orion molecular outflow/BN complex, for example see table 2.1 (taken from Chernoff, Hollenbach & McKee 1982) and the discussion in section (1.4). However the velocities required to fit the emission lines were just less than 40 km s^{-1} which is very close to the limiting velocity above which dissociation/self-ionisation will quickly destroy the molecular hydrogen. The observed radial velocities of up to 100 km s^{-1} still present a problem. Also the high rotational

transitions of CO (Watson, Genzel, Townes & Storey 1985) and the H_2 lines from high energy levels could not be simultaneously fitted by either group (see Mckee, Chernoff & Hollenbach 1984). In section 1.4 it was discussed how the apparent excitation temperatures of shocked gas from different sources appeared close to 2000 K. This is difficult to explain in C-shock models, in which the apparent temperatures are fairly strong functions of many different parameters, such as the shock velocity. Additional problems for the standard C-type shock models has recently come to light by the observation by Geballe & Garden (1987) of vibrationally excited CO (v=1) about 15 times greater than expected from the C-type models.

Here we will examine the emission produced from the various types of molecular shocks, restricting ourselves, for simplicity, to purely planar shock fronts. In the first section we will go through the magnetohydrodynamic flow equations which have to be solved in any shock calculation, these are the equations which simply conserve mass momentum and energy in the gas flow, and will be referred to frequently throughout this thesis. Then we will discuss J-type shocks, initially going through a simple calculation to find the H_2 emission from a shock with power law cooling before talking about partially dissociative shocks and the various cooling processes that may be important. In addition, following this we will review current C-type shock models, which inevitably include much more chemistry and detailed physics than the J-type shocks. This will then finally lead to a section on the various atomic and molecular emission lines which are useful as discriminators between shock types and/or can be used as temperature and density probes.

2.2 Basic flow equations

In any calculation of the structure behind shock fronts it is the basic fluid flow equations that have to be solved. These are the equations that conserve mass, momentum and energy in the flow. In the presence of a magnetic field the ions and neutrals in the gas can act as independent fluids, with some small interaction due to the drag that can occur between the ions and neutrals. The fluid equations are in the frame of the shock front

$$\frac{d}{dt}\rho_n v_n = 0 \tag{2.1}$$

$$\frac{d}{dt}\rho_i v_i = 0 \tag{2.2}$$

$$\frac{d}{dt}(\rho_n v_n^2 + P_n + B^2/2\mu_o) = G_{in} \tag{2.3}$$

$$\frac{d}{dt}(\rho_i v_i^2 + P_i) = -G_{in} \tag{2.4}$$

$$\frac{d}{dt}(\frac{1}{2}\rho_n v_n^3 + U_n\rho_n v + P_n v_n + B^2/\mu_o\rho) = -\Lambda_n + \Gamma_n \tag{2.5}$$

$$\frac{d}{dt}(\frac{1}{2}\rho_i v_i^3 + P_i v_i + U_i\rho_i v + B^2/\mu_o\rho) = -\Lambda_i + \Gamma_i \tag{2.6}$$

Where the subscripts i and n refer to neutrals and ions respectively. The density is given by ρ, v is the velocity and P the pressure. The cooling and heating rates are denoted by Λ and Γ respectively. These rates group together the many different cooling and heating processes, and are functions of both density and temperature. G_{in} represents the rate of momentum exchanged from the ions to the neutrals.

2.3 J-shock models

In a J-shock the heating processes in the shock front occur on a time scale much faster than the subsequent cooling times. The 'shock front' itself is a relatively thin dissipative layer where atoms and molecules are accelerated (heated and compressed) on a length which is of the order of one mean free path. The jump conditions in non magnetized gas are

$$\rho v = \rho_o \mathrm{v}_s \tag{2.7}$$

$$P + \rho v^2 = P_o + \rho_o \mathrm{v}_s^2 \tag{2.8}$$

$$U\,\rho v + P\,v + \frac{1}{2}\rho v^3 = U_o \rho_o \mathrm{v}_s + P_o \mathrm{v}_s + \frac{1}{2}\rho_o \mathrm{v}_s{}^3 \tag{2.9}$$

These are the well known Rankine-Hugoniot jump conditions. The temperatures, density and velocity just behind the shock front are simply given by the solution of these equations. For a strong shock (i.e. Mach no. $\gg 1$) $P \gg P_o$ and $U \gg U_o$. The P_o and U_o terms are thus dropped. Now dividing by ρv and noting that the enthalpy is given by the following equation

$$U + P/\rho = \frac{\gamma}{\gamma - 1}\frac{n}{\rho} kT \tag{2.10}$$

After some trivial algebra we obtain the following results

$$\frac{\rho}{\rho_o} = \frac{\gamma + 1}{\gamma - 1} \tag{2.11}$$

$$\frac{v}{\mathrm{v}_s} = \frac{\gamma - 1}{\gamma + 1} \tag{2.12}$$

and finally for the temperature immediately behind the shock front

$$T_{max} = \frac{2(\gamma - 1)}{(\gamma + 1)^2}\frac{\mu m_h \mathrm{v}_s^2}{k} \tag{2.13}$$

the molecular gas reaches this temperature and then subsequently cools, through both dissociational and radiative processes. To calculate the emission resulting from such a shock we could impose the last three conditions on the fluid flow and integrate the flow equations until some point at which the temperature is low. There is a simple

analytic approximation to the total emission from J-type shocks that can be obtained using a formulation similar to that of London, McCray & Chu (1977). Firstly, the column of molecules in a particular energy level integrated through this cooling layer is

$$N_j = \int_0^\infty n_j \, dx = \int_0^\infty n_j v \, dt \tag{2.14}$$

And as the mass flux (equation 2.7), nv = constant = $n_o v_s$,

$$N_j = n_o v_s \int_0^\infty \frac{n_j}{n} \, dt \tag{2.15}$$

Where n_o is the preshock density and v_s is the shock velocity. If the molecules are thermalized (n_j/n) is given by the Boltzmann formula. Conservation of energy in the flow, neglecting bulk energy (the ρv^2 term in equation 2.9), implies

$$\frac{dT}{dt} = -\frac{(\gamma - 1)}{\gamma} \Lambda(n, T) \tag{2.16}$$

where $\Lambda(n, T)$ is the total cooling rate per molecule. Thus

$$N_j = n_o v_s \int_0^{T_{max}} \frac{e^{-T_j/T}}{Q(T)\Lambda(n, T)} \, dT \tag{2.17}$$

where Q(T) is the partition function, which for H_2 is given approximately by

$$Q(T) = 2\frac{T}{T_{rot}} \frac{1}{1 - e^{-T_v/T}} \tag{2.18}$$

where $T_v = 4700$ K is the vibrational partition energy (note that this is smaller than the energy seperation of the v= 1 & 0 levels because of the contribution from higher v levels which are increasingly closer together in energy), and $T_{rot} \approx 83$K. Equation 2.17 can be solved when the cooling processes are known. For purely radiative H_2 cooling at thermalized densities the cooling rate is $\Lambda(n, T) \propto T^s$, s=4.6, for temperatures < 2000 K (see section 2.3.1). The solution for thermalized H_2 lines of equation 2.17 for power law cooling is then simply given by the solution of the incomplete gamma function

$$\frac{N_j}{g_j} \propto (T_j + T_v)^{-s} - T_j^{-s} \tag{2.19}$$

This simple calculation implies that the relative column densities of different energy levels will be the same in every source, regardless of shock velocity and density, providing that the maximum temperature is greater than that in the region where most of the emission is produced and the density is high enough to thermalize H_2. For the 2-1 S(1) and 1-0 S(1) lines (upper level energies of 12550 and 6956 Kelvins respectively) this implies an excitation temperature of 1900 K. This provides the basis of a plausible explanation as to why the excitation temperatures of shocks derived from the 2-1/1-0 ratio are always close to 2000 K. The temperatures obtained using equation 2.19 are not strictly correct. More realistically the cooling function is not a power law for all temperatures and is further altered by other processes that can cool the gas (such as H_2 dissociation, CO radiative cooling, H_2O radiative cooling, among others). The importance of H_2 dissociational cooling at high temperatures means that the fractional abundances in the gas change throughout the shock, the pressure then has two terms for atomic and molecular hydrogen. Instead of conserving the total volume density the number density of protons should be conserved and the equation for the rate of H_2 dissociation, mainly by collisions with other H_2 and atomic H, has to be followed.

In the next section we will discuss the important cooling mechanisms for molecular gas at the temperatures we are considering (500—20000 K), and following that we will derive the method by which line emission from these more complex shocks can be calculated.

2.3.1 Major coolants

If we know the cooling processes involved we are then able to calculate the emission from any molecule providing that at the same time the relative level populations can also be ascertained. We have considered situations where the major coolants are as follows: H_2 radiative (Infrared), and dissociative cooling, as well as CO and H_2O radiative cooling. We have ignored cooling from species such as OH,O^o,O^+ and C^o as these are only important at low temperatures (< 500 K) where the H_2 energy levels are not

significantly populated.

The total H_2 radiative cooling is simple to calculate when the lower lying levels are in LTE. The total cooling rate is then given by the sum over all allowed transitions of

$$\frac{\Lambda_r}{n} = \sum_{ij} E_{ij} A_{ij} N_i / N = \sum_{ij} E_{ij} A_{ij} \frac{g_i e^{-T_i/T}}{Q(T)} \tag{2.20}$$

Where N_i/N is the relative number of molecules in upper level i, given by the Boltzmann formula. A_{ij} is the spontaneous radiative transition probability from level i to j (calculated by Turner, Kirby-Docken & Dalgarno 1979) and E_{ij} is the energy of the transition (calculated using the energy levels of Dabrowski (1983)). This sum is easy to perform and the total radiative cooling rate per molecule against temperature is shown in Fig. 2.1. The dotted curve in Fig 2.1 is the following expression which provides a good approximation to the results of the sum (equation 2.20).

$$\frac{\Lambda_r}{n} = \begin{cases} 3.0 \times 10^{-32} T^{4.62} & T < 2000 \text{ K} \\ 1.7 \times 10^{-25} e^{-7210/T} & T > 2000 \text{ K} \end{cases} \text{ W molecule}^{-1} \tag{2.21}$$

This cooling rate is only true for high densities when all the energy levels are in LTE. Each level becomes sub-thermally populated below some critical density, this critical density is determined by the collision rates appropriate to the level and these are not well known (e.g. Burton *et al.* 1989) but are typically close to $10^6\,\mathrm{cm}^{-3}$. The critical density below which the cooling rate per molecule becomes density dependent is $\approx 3 \times 10^6\,\mathrm{cm}^{-3}$ (Hollenbach & Mckee 1979).

For the partition function of H_2 we have used two methods of calculation, one is to output the sum over states ($\sum_{ij} g_i e^{-T_i/T}$) while performing the radiative cooling calculation in equation 2.20 and this is the solid curve plotted in Fig. (2.2). Also plotted in Fig. (2.2) is the analytic approximation obtained by assuming that the rotation and vibration terms are separable (equation 2.18).

To investigate any errors that may be introduced by assuming LTE we have calculated the cooling rate and partition function for a variety of cases where the population is assumed to be zero above a critical upper level energy to simulate non LTE. The dashed

curves in Figs. 2.1 and 2.2 show the results of this for two cutoff energies appropriate to no molecules in the 3^{rd} vibrational state (17000 K) and the 2^{nd} vibrational state (12000 K). It can be seen that the cooling rate and partition function are dominated by the lower lying energy levels. As is expected because of the exponential energy term in the Boltzmann distribution and the fact that the low v transitions are the brightest observed. We can be confident then that when the density is above the critical value that the cooling rate and partition function are correct, although the highest lying energy levels (especially those which require many collisions to become excited) may still be populated below their LTE values.

At high temperatures and densities collisional dissociation of H_2 proceeds mainly through the v=14 level being collisionally excited to the vibrational continuum (Roberge & Dalgarno 1982 and references therein). This is the important pathway of collision induced dissociation at the temperatures of the shocked sources we are considering (i.e. about 2000K). As such the total dissociation rate is extremely temperature and density dependent, the collisions from v=14 to the continuum are competing against both the relatively fast de-excitation through collisions and spontaneous radiative transitions (i.e. the v=14 is sub-thermally populated). Dissociation rates have been calculated for collisions by many authors. We adopt the following rates (in cm ^{3} s^{-1}) given by Lepp & Shull (1987) for collisions with H_2 and H

$$k_d^{\mathrm{H_2}} = 5.48 \times 10^{-9} exp^{-53000/T} \tag{2.22}$$

$$k_d^{H} = 3.59 \times 10^{-9} exp^{-46000/T} \tag{2.23}$$

These rates are severely depressed at low densities ($< 10^4\,\mathrm{cm}^{-3}$, Dove & Mandy (1986)) and the exact functional form of the dissociation rates are unknown at such low densities. The binding energy of H_2, E_{bind} = 4.5eV and so, combining equations 2.22 and 2.23, the total H_2 dissociational cooling rate is

$$\Lambda_d = E_{bind} n_{H_2} [n_H k_d^H + n_{H_2} k_d^{\mathrm{H_2}}] \tag{2.24}$$

The CO radiative cooling rate is harder to calculate than the H_2 radiative rate, although at the high densities we are considering the dominant levels are in approximate LTE. The cooling rate has been calculated by McKee *et al.* (1982) using a master equation technique to find the level distribution at specific density and temperature, they give

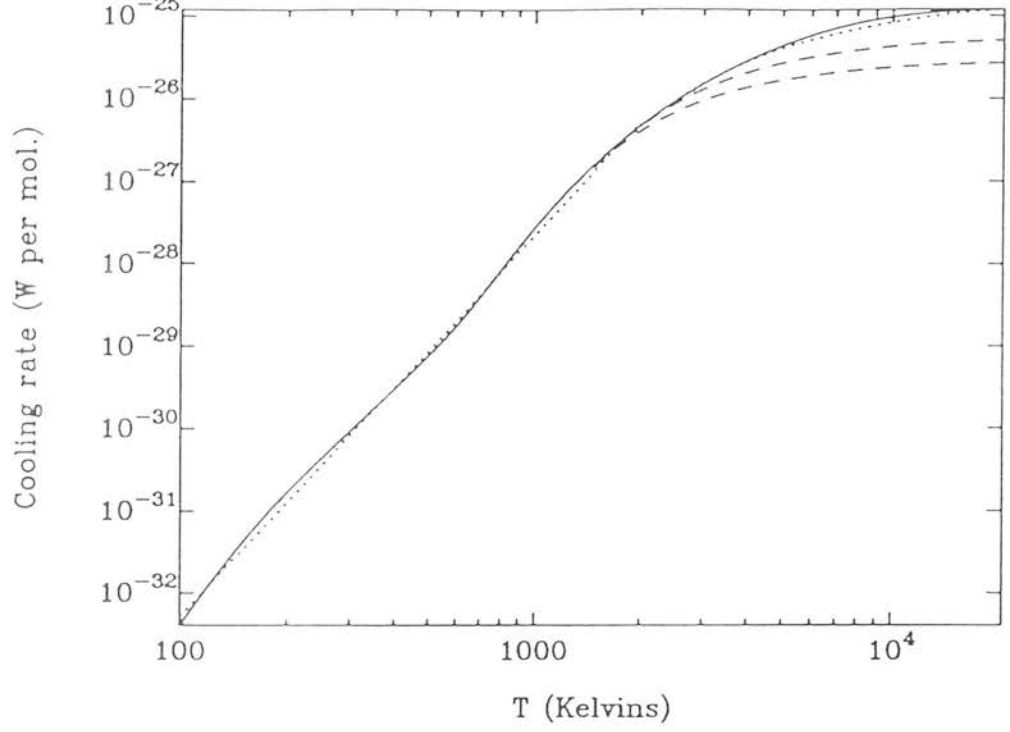

Figure 2.1: Radiative cooling rate of H_2 in LTE, due to spontaneous transitions in the ground electronic state. The dashed curves below the LTE curve are those for a zero population in the energy levels above 17000 and 12000 Kelvin.

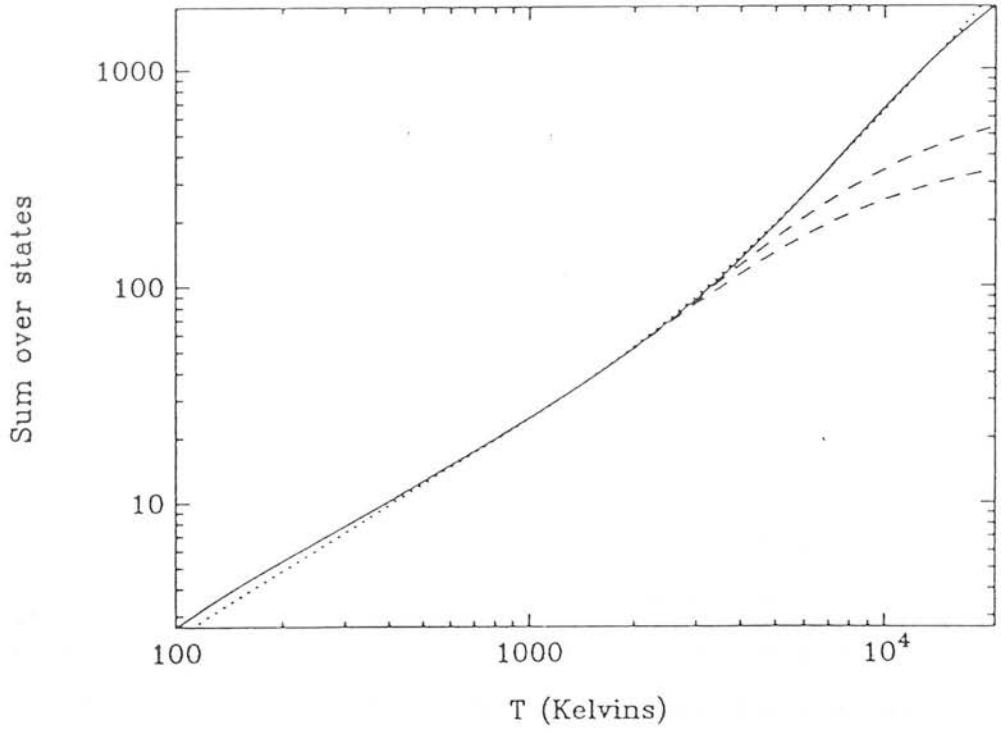

Figure 2.2: The partition function of ground state molecular hydrogen against temperature, the solid curve is the result of the sum over states assuming a full LTE distribution. The dotted curve is the theoretical approximation and the dashed curves represent an LTE distribution cut off as in Fig. 2.1

two approximations to their results for high density ($n > n_{crit}$)

$$\frac{\Lambda_{CO}}{n} = 2.24 \times 10^{-30} T^2 X(CO) \tag{2.25}$$

and low density ($n < n_{crit}$)

$$\frac{\Lambda_{CO}}{n} = 1.2 \times 10^{-34} T^{1.25} n X(CO) \tag{2.26}$$

Where n_{crit} is a function of temperature given by the equation

$$n_{crit} = 1.86 \times 10^4 T^{3/4} \text{ cm}^{-3} \tag{2.27}$$

H_2O radiative cooling may also be an important coolant, as any atomic oxygen that is produced in the post-shock gas is quickly converted to water (Hollenbach & Mckee 1977), first by producing OH which then reacts with H_2.

$$O + H_2 \rightarrow OH \tag{2.28}$$

followed by

$$OH + H_2 \rightarrow H_2O \tag{2.29}$$

OH also reacts with O and C in the following reactions

$$OH + O \rightarrow O_2 \tag{2.30}$$

$$OH + C \rightarrow CO \tag{2.31}$$

$$OH + C^+ \rightarrow CO \tag{2.32}$$

All these resultant molecules can react with atomic H to produce OH. If H_2O is produced in warm (i.e. post-shock) gas as is suggested by the reaction scheme above then it can be an important coolant at modest (a few 1000K) temperatures. We use the results presented by Hollenbach (1988) which are calculated using the universal cooling function of Hollenbach & Mckee (1979). Note that there is a discrepancy of about a factor of three between the results of Hollenbach & Mckee (1979) and a more accurate calculation by Neufeld & Melnick (1987). The cooling function of Hollenbach (1988) was calculated using the total de-excitation rate of Neufeld & Melnick (1987) and is thus in agreement with their results. The expression we use for H_2O cooling is

$$\frac{\Lambda_{H_2O}}{n} = 3.3 \times 10^{-35} n_p T^{1.5} X_{H_2O} \text{ W } cm^3 \tag{2.33}$$

Both CO and H_2O can suffer from severe line optical depth effects. The line optical depth effects depend on the details of the radiative transport. An estimate as to when the

cooling lines become optically thick can be obtained by using the results of Hollenbach & Mckee (1979). For the column density of each molecule required to produce an average optical depth of one in the lines responsible for the radiative cooling, N_{t1}, is $\approx 10^{26} - 10^{27}\,\mathrm{m}^{-2}$ at 1000 K. The cooling length, l_c, of a typical molecular shock (see chapter 1) is of the order the cooling time ($\approx 10^7$ s for H_2 radiative cooling) multiplied by the shock velocity, i.e $l_c \approx 10^{12}$-10^{13}m. The abundances of CO & $H_2O$are $< 10^{-4}$. The density needed to produce an optical depth of one is $N_{t1}/(l_c 10^{-4}) \approx 10^{18}\ \mathrm{m}^{-3}$. These densities are almost always larger than the regions that we are concerned with. So the radiation from these molecules is assumed to be optically thin and able to escape the cooling layer without being absorbed.

2.4 Partially dissociating J-shocks

The structure of a partially dissociating shock can be summarized as follows;

(i) The shock front, where dissipative processes heat and compress the gas.
(ii) A further layer where the kinetic energy relaxes into internal energy of the molecules.
(iii) A cooling region, in which first dissociation and then radiation act to cool the gas.
(iv) A final region in which the magnetic pressure supports the gas and prevents further compression.

At the high temperatures, immediately behind the shock front, cooling by dissociation can be important. The change in the fractional abundances of atomic and molecular hydrogen then have to be followed in the flow equations. The largest change is made to the pressure terms in the energy equation. The aim of this section is to rewrite the energy equation. So that as in the derivation of the power law cooling (equations 2.19) the time integral can be changed to one of temperature . There are now terms in the energy equation due to both atomic and molecular hydrogen

$$\frac{d}{dt}((U_h + P_h/\rho) + (U_{\mathrm{H}_2} + P_{\mathrm{H}_2}/\rho) + \frac{1}{2}v^2) = -\Lambda/\rho_o \mathrm{v}_s \qquad (2.34)$$

The sum of the internal energy and pressure is related to the temperature for an

ideal gas through the enthalpy equation

$$U + P/\rho = \frac{\gamma}{\gamma - 1}\frac{n}{\rho}kT \tag{2.35}$$

Where n is the number density of the particular atomic or molecular species. For atomic gas the ratio of specific heats (γ) is equal to 5/3 and for fully populated molecular gas 9/7. The hydrogen molecules may not, however, be populated (in the internal modes) according to equipartition. The $\frac{\gamma}{\gamma-1}$ term can be approximated by $\frac{7}{2} + \xi$ where ξ represents the amount of energy distributed in the vibrational states

$$\xi = \frac{T_v/T}{e^{T_v/T} - 1} \tag{2.36}$$

This tends towards 1 when the temperature $T \gg T_v$, the vibrational levels are then fully populated and $\gamma = \frac{9}{7}$. This approximation also assumes that the rotational levels are effectively fully populated, not too unreasonable as the temperature at which this occurs is only a few hundred Kelvin for densities above $10^6\,\mathrm{cm}^{-3}$.

If we now define the atomic hydrogen fraction as $f = n_H/n_p$, the H_2 number density is $\frac{1-f}{2}n_p$. The energy equation is then

$$\frac{d}{dt}([\frac{5}{2}f + (\frac{7}{2} + \xi)\frac{1-f}{2}]kT + \frac{1}{2}v^2) = -\frac{\Lambda}{n_p} \tag{2.37}$$

The bulk velocity term is insignificant, behind a strong molecular shock $\rho = 6\rho_o$ and $v = v_s/6$. Therefore

$$\rho v^2 = \frac{1}{6}\rho_o v_s^2 \tag{2.38}$$

which implies through the momentum equation that

$$P = \frac{5}{6}\rho_o v_s^2 \tag{2.39}$$

using the last four equations to express the bulk velocity and energy terms in units of v_s^2.

$$\frac{7}{2}\frac{P}{\rho} = \frac{35}{72}v_s^2 \qquad \text{and} \qquad \frac{1}{2}v^2 = \frac{1}{72}v_s^2 \tag{2.40}$$

Hence dropping this term introduces an error of at most 3 percent. This rapidly gets smaller as the velocity drops. The energy equation is now

$$\frac{d}{dt}([\frac{5}{2}f + (\frac{7}{2}+\xi)\frac{1-f}{2}]kT) = -\frac{\Lambda}{n_p} \tag{2.41}$$

or alternatively allowing for He at 10% of n_p gives an extra $\frac{1}{4}kT$

$$\frac{d}{dt}([2 + \frac{\xi}{2} + (\frac{3}{4} - \frac{\xi}{2})f]kT) = -\frac{\Lambda}{n_p} \tag{2.42}$$

In the derivation that follows we will ignore region (i) and assume that the density and temperature are simply given by the strong shock solutions, in which a complete redistribution of the available energy occurs throughout the available degrees of freedom.

The rate of change of atomic hydrogen fraction is

$$\frac{df}{dt} = \frac{2R}{n_p} \tag{2.43}$$

The energy equation is now

$$\frac{d}{dt}([4 + \xi + (\frac{3}{2} - \xi)f]T) = -T_{diss}\frac{df}{dt} \tag{2.44}$$

T_{diss} is the dissociation energy in temperature units ($\approx 52000K$). Behind the shock front T = T_{max} and the gas is still fully molecular so f = 0 and $\xi = 1$. Which imply that

$$f = \frac{5T_{max} - (4+\xi)T}{(T_{diss} + (\frac{3}{2} - \xi)T)} \tag{2.45}$$

Now by noting that from the definition of ξ (equation (2.36))

$$\frac{d(\xi T)}{dt} = \xi^2 e^{T_v/T} \frac{dT}{dt} \tag{2.46}$$

Then the energy equation is again rewritten in the form

$$\frac{dT}{dt}(2 + \frac{1}{2}\xi^2 e^{T_v/T} + \frac{3}{4}f - \frac{1}{2}\xi^2 e^{T_v/T} f) = -\frac{\Lambda}{k n_p} - \frac{TR}{n_p}(\frac{3}{2} - \xi) \tag{2.47}$$

This finally gives us an explicit expression for $\frac{dT}{dt}$ in terms of known variables. We can then use this expression to convert the time integral of equation (2.14) into a Temperature one.

2.4.1 H_2 emission

To calculate the line emission from such a shock we follow the procedure taken in section (2.3) and write the column density of a particular level as

$$\frac{N_j}{g_j} = \int_t^0 n_{H_2} v \frac{e^{-T_j/T}}{Q(T)} dt \tag{2.48}$$

and substituting in 2.48 to change the time integral into a temperature one, we get

$$\frac{N_j}{g_j} = k n_{po} \mathrm{v}_s \int_0^{T_{max}} \frac{1-f}{2} \frac{e^{-T_j/T}}{Q(T)} \frac{2 + \frac{3}{4}f + \frac{1}{2}\xi^2 e^{T_v/T}(1-f)}{[\Lambda - kTR(\frac{3}{2} - \xi)]/n_p} dT \tag{2.49}$$

From the preceeding discussion it can be seen that f and ξ are purely functions of temperature, however the cooling function terms in the denominator are also density dependant. By assuming that the pressure is constant (i.e nT is constant) then this density dependance is written as a function of temperature by replacing the density, n, with $r_c n_o \frac{T_{max}}{T}$ (where r_c is the initial post-shock compression ratio given by equation 2.11 which equals 6 for a $\gamma = 7/5$).

It is then a simple matter to integrate 2.49 numerically, and obtain the column densities of H_2through the shock. The cooling function (a combination of the functions presented in section 2.31) and the pressure are pre-specified. The Integration also needs to start at the maximum post-shock temperature, which is obtained from the shock velocity through equation 2.13. For a given set of abundances the column densities are just a function of the two input parameters, pressure (NT) and velocity (v_s).

At high temperatures the dissociative cooling is so much faster than the radiative cooling that there is insignificant emission from the H_2 until radiative cooling begins to dominate. In Fig. (2.3) we show the the structure behind a typical partially dissociative shock, illustrating this point. The dissociative and radiative cooling are delineated by *dotted* and *dashed* lines respectively, also plotted is the Column of molecules at each temperature ($\frac{dN}{dT}\delta T$) for the energy levels appropriate to the 1-0 S(1) and 2-1 S(1). It can be seen that there are few molecules in each level for temperatures where dissociation dominates and also that the dissociative cooling reduces the column density of the higher line disproportionately compared with the lower energy level. This will alter the excitation temperatures, and in fact the [1-0 S(1)/2-1 S(1)] temperature is pressure dependant. The differences are small but not insignificant. In Fig. (2.4a) we plot the [1-0 S(1)/2-1 S(1)] temperature against pressure, also in Fig. (2.4b) we plot the dependance on shock velocity. It is thus clear that partially dissociative J-shocks produce line emission which is very close to 2000K over a wide parameter range.

2.4.2 CO emission

Rotational CO line emission can be calculated in much the same way as H_2. We will assume that the CO abundance remains constant throughout the flow. This is reasonable because although CO can be collisionally and photo-dissociated it is rapidly re-formed through the chemical reaction network outlined in equations 2.28- 2.32 In particular equation 2.49 has to be multiplied by the CO fraction and the H_2 partition function replaced with that of CO. The CO partition function can be written down as

$$Q_{CO} = (T/2.77)Q_{CO}^{vib} \tag{2.50}$$

Where Q_{CO}^{vib} is the vibrational part of the partition function (it has been assumed that rotation and vibration are separable). The radiative transitions of CO, unlike H_2,

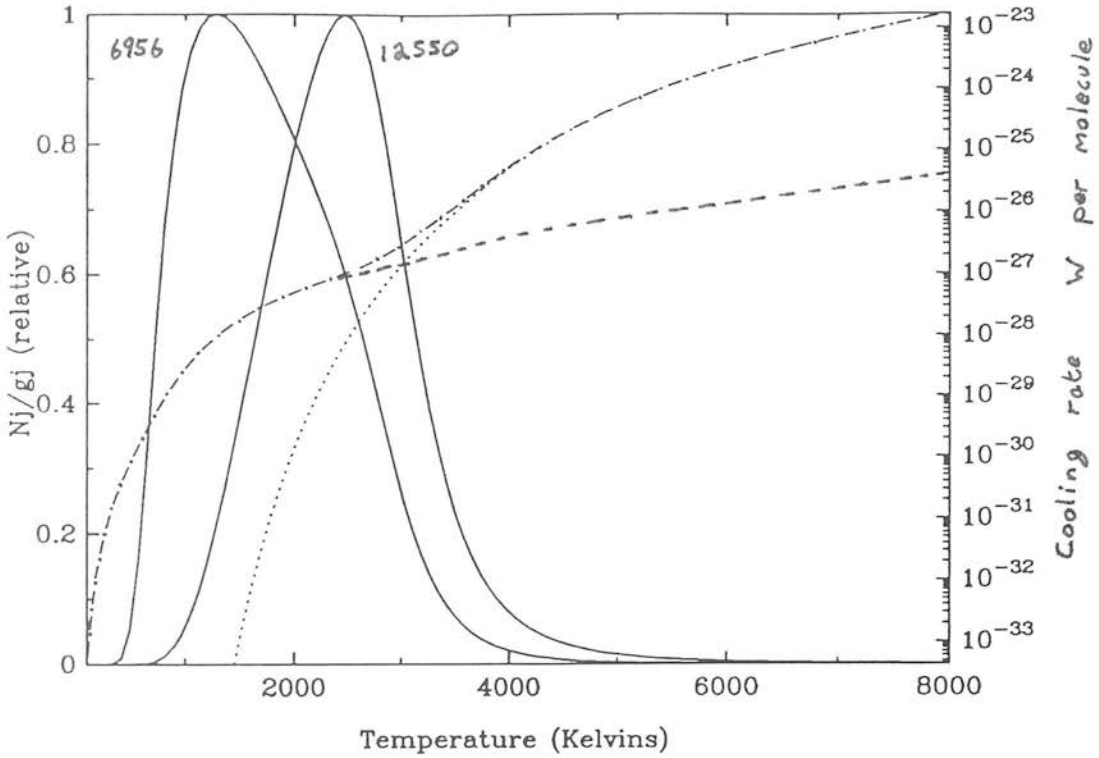

Figure 2.3: The structure behind a 15 km s^{-1} shock with a pressure of $10^{11} K\ cm^{-3}$. The dissociative cooling and radiative cooling are shown as dotted and dashed lines. The column from two energy levels at 12550 K and 6956 K are shown. The contribution to the 12550 K line peaks at temperatures higher than the 6956K line.

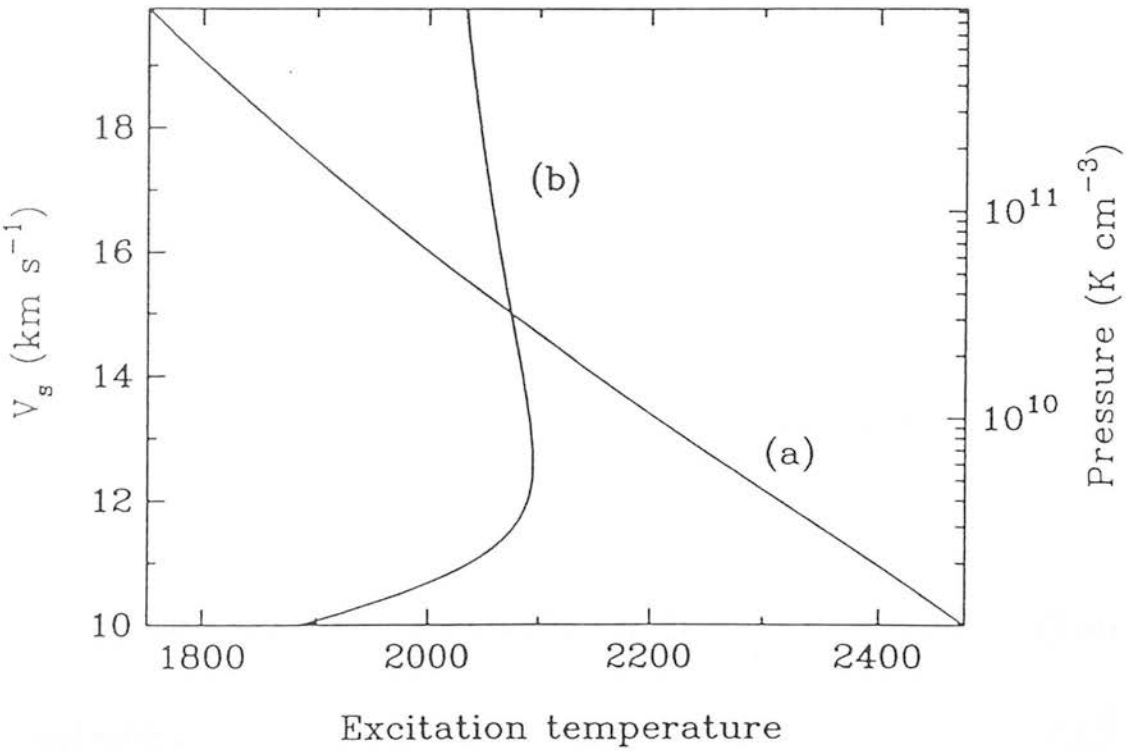

Figure 2.4: The dependance of the [1-0 S(1)/2-1 S(1)] excitation temperature on (a) Pressure, and (b) shock velocity.

are dipolar. As such the spontaneous transition probabilities are much higher than H_2(typically of the order of one second). The critical densities of vibrationally excited CO are thus very high, and for most of the situations we will consider vibrational CO will be significantly under populated. Then the vibrational term $Q_{CO}^{vib} \approx 1$. Substituting in equation 2.49 we get for rotational CO

$$\frac{N_j}{g_j} = 2.77 k n_{po} X_{CO} \int_{\emptyset}^{T_{max}} \frac{e^{-T_j/T}}{T} \frac{2 + \frac{3}{4}f + \frac{1}{2}\xi^2 e^{T_v/T}(1-f)}{[\Lambda - kTR(\frac{3}{2} - \xi)]/n_p} dT \tag{2.51}$$

Again this is easy to integrate numerically, providing that the pressure (and by implication the density) is specified. To relate the absolute emission from CO to the H_2 introduces an extra free parameter, the CO abundance.

2.4.3 Pressure in the flow

The cooling layer is very nearly isobaric. Through the shock front the pressure rises dramatically to reach its initial post-shock value ($\approx 2\,\rho_o\,\mathrm{v}_s^2/(\gamma+1)$ for a strong shock), this pressure then gradually rises as the gas cools to reach the pressure appropriate to an isothermal shock ($\rho_o\,\mathrm{v}_s^2$). Here we will demonstrate that the assumption of constant pressure introduces only a small error.

The pressure in an ideal gas is ρc^2, so the momentum equation is

$$\rho c^2 + \rho v^2 = \rho_o v_s^2 \tag{2.52}$$

now conservation of the mass flux implies $v^2 = \frac{\rho_o^2\,\mathrm{v}_s^2}{\rho^2}$, substituting this in and multiplying by ρ gives a quadratic equation in ρ

$$\rho^2 c^2 + \rho_o{}^2\,\mathrm{v}_s^2 = \rho_o\,\mathrm{v}_s^2 \rho \tag{2.53}$$

and solving

$$\frac{\rho}{\rho_o} = \frac{1 + \sqrt{1 - 4c^2/\,\mathrm{v}_s^2}}{2c^2/\,\mathrm{v}_s^2} \tag{2.54}$$

multiplying both sides by c^2/v_s^2this becomes

$$\frac{P}{\rho_o v_s^2} = \frac{1}{2}(1 + \sqrt{1 - 4c^2/v_s^2}) \tag{2.55}$$

Now for pure a molecular hydrogen gas $c^2 \approx 16$ (T/4000) in units of (km $s^{-1})^2$ and for a strong shock the maximum temperature is given by equation 2.13

$$\frac{P}{\rho_o v_s^2} = \frac{1}{2}(1 + \sqrt{1 - 0.54T/T_{max}}) \tag{2.56}$$

So initially behind the shock front the constant pressure approximation results in an error of 16 percent, which subsequently decreases. So throughout the cooling layer we will assume that the pressure is constant (i.e. nT $\simeq$ constant), this approximation is equivalent to the temperature being overestimated by 16 percent.

2.4.4 Magnetohydrodynamic J shock

The flow equations written down in section 2.2 include magnetic terms. In the above calculations of the line emission the dynamical effects of the magnetic field were ignored, and these terms were dropped. In this section we will examine the effects that the magnetic field can have on the shock structure, still considering the case when the ionisation fraction is small, or zero. Qualitatively the effects the magnetic field will have on the post shock gas are as follows. Initially the magnetic field will lower the maximum post shock temperature. This is because a portion of the shock energy is used in compressing the magnetic field along with the gas, which also results in a lower initial compression ratio. Subsequently as the gas cools the thermal pressure remains constant (see section 2.4.3) but the density is increasing, it follows that the magnetic pressure will increase (assuming the magnetic flux is 'frozen') because the magnetic field strength will increase along with the density. A point will thus occur in the flow at which the magnetic pressure will exceed the thermal pressure and it is at this point that any further compression will be halted.

To calculate the jump conditions and the resulting effect on the molecular emission

we shall define

$$A = \frac{B_o^2/\mu_o}{\rho_o v_s^2} \tag{2.57}$$

which represents the ratio of the pre shock magnetic pressure to the total ram pressure of the shock. If the magnetic field is 'frozen', then $B = B_o\rho/\rho_o$ and by noting that the thermal pressure $P = \rho c_{th}^2$. We can find the post shock temperature, velocity and density simply by conserving momentum and energy across the shock front. These equations divided by $\rho\, v_s^2$ across the shock are, for momentum

$$(\frac{c}{v_s})^2 + u^2 + \frac{A}{2u} = u(1 + A/2) \tag{2.58}$$

and correspondingly for energy

$$\frac{\gamma}{\gamma - 1}(\frac{c}{v_s})^2 + \frac{u}{2} + \frac{A}{u} = \frac{1}{2} + A \tag{2.59}$$

Where u is the ratio of the velocity of the gas (in the shock frame) to the shock velocity. These simultaneous equations are simple to solve for c and u although the resulting expressions are complex. A reasonably approximate solution for $\gamma = \frac{7}{5}$ is

$$u = \frac{1}{6} + \frac{5}{6}A^{0.6} \tag{2.60}$$

and

$$(\frac{c_{th}}{v_s})^2 = \frac{5}{36}e^{-10A(1-1.2A)}\,(A < 0.3) \tag{2.61}$$

So this gives for the maximum temperature

$$T_{\max} \simeq 33\, v_s^2 e^{-(V_{A0}/v_s)^2/0.15} \tag{2.62}$$

where V_{A0} is the Alfven velocity ($\sqrt{B_o^2/\mu_o\,\rho_o}$).

The final limiting compression ratio will depend only on the initial magnetic field strength and the shock velocity. However the region where the post shock gas is magnetically supported may occur far downstream where the gas is cool, having no effect on the 'hot' lines that we are interested in. The magnetic pressure equals the thermal pressure when

$$\frac{\rho c_{th}^2}{\frac{1}{2}B^2/\mu_o} = \frac{2u}{A}(\frac{c_{th}}{v_s})^2 \approx \frac{5}{18}\frac{(\frac{1}{6}+\frac{5}{6}A^{0.6})}{A}e^{-A/0.15} = 1 \tag{2.63}$$

Note that if A is small (< 0.05) then this is greater than 1, and thermal pressure dominates initially. But if this is the case, magnetic pressure will eventually dominate further upstream in the cooler gas when

$$uc_{th}^2 = \frac{v_s^2 A}{2} \tag{2.64}$$

Which is, assuming that thermal pressure is constant (see section 2.4.3)

$$T \leq 157\, v_s^2 \sqrt{A} \tag{2.65}$$

For a shock of 15 km s^{-1} and an A of 0.01 this is a temperature of 3500 K. This is in the region where dissociational and radiative cooling become equal.

What effect does this have on the line emission? The density in the flow is now constant implying that the velocity v is fixed. The emission from the shocked region in which H_2 radiative cooling is dominant is not affected by this change. It is the length of time a parcel of gas is in a particular temperature range that determines the amount of emission. The crucial parameter is thus the cooling rate per molecule for calculating this time. This change will effect the density dependant cooling terms, such as H_2 dissociation, CO and H_2O radiative cooling which are all proportional to n^2. The thermal pressure (nT) will now fall as the temperature decreases. This has the effect of making these coolants less effective at lower temperatures (previously the gas density would have increased as the temperature dropped) relative to H_2 radiative cooling. This directly translates into an extra factor of T^{-1} in the cooling rates for the H_2O, CO and

H_2 dissociation. This leads to more emission from lower temperature gas, i.e. the excitation temperatures will be reduced.

2.5 Magnetohydrodynamic C shocks

The physical processes which occur in C-type shocks have been reviewed in chapter 1, however for completeness we will review them here in more detail than in the cursory introduction in chapter 1.

A magnetic field in a partially ionised gas exerts a force on the charged particles, which causes the ions to move with a different velocity than the neutrals. This velocity difference can be large and it is this process, ambipolar diffusion, which governs the whole structure of C-type shocks. Frictional drag between the ions and neutrals can then be an important source of heat input in the flow. The drag length scale for the ambipolar diffusion is found by equating the magnetic force on the ions with the collisional drag on them due to the neutrals (Spitzer, 1978)

$$\frac{B^2}{8\pi l_a} = n_i \rho (v_n - v_i) < \sigma v > \tag{2.66}$$

where v_n and v_i are respectively the neutral and ion velocities. The gradient in the magnetic field strength (increasing downstream from the shock front as the gas cools and compresses) forces the ionic particles in the upstream direction. That is, the ions are decelerated (in the shock frame) much faster than the neutrals. This tells us that the drag on the ions due to the neutrals $(v_n - v_i)$ is in the downstream direction (the neutrals are moving faster than the ions) Hence the ions and magnetic field are compressed before the neutrals. In other words the compressed field behind the shock front propagates upstream (towards the shock front itself) as a hydromagnetic wave (which is attenuated by the increasing velocity of the ions). It is useful to rewrite equation 2.66 in terms of the Alfven Mach number of the ions (M_{Ai}) (Mckee, Chernoff & Hollenbach 1984)

$$M_{Ai}^2 = (\frac{v_s}{v_{Ai}})^2 = 4\pi \rho_{io} \frac{v_s^2}{B_o^2} = M_A^2 x_{io} \tag{2.67}$$

Where M_A is the Alfven mach number of all the gas, x_{io} is the initial fractional ionisation and as usual the Alfven velocity of the ions, v_{Ai}, is

$$v_{Ai} = \frac{B_o}{\sqrt{4\pi\rho_{io}}} \tag{2.68}$$

The magnetic field is tied to the ions at this point so B_i/n_i is a constant. Rewriting equation 2.66 for the collisional drag length in terms of the ion neutral mean free path, $\lambda_{in} = 1/n_o\sigma_{in}$

$$l_a = \lambda_{in}\frac{B/B_o}{M_A^2 x_{io}} \tag{2.69}$$

Where $< \sigma v > v \approx \sigma_{in}\, \mathrm{v}_s^2/2$ (assuming that the ions are very quickly decelerated so that $v_n - v_i \approx \mathrm{v}_s$ is true)

There are several classes of solutions that can occur, depending on the ion and neutral Mach no. and the cooling length w.r.t. the drag length. The simplest of these is just the case we have considered in the last section, where the Mach nos $M_{Ai}, M_A > 1$. Now equation 2.69 tells us that the drag length will be small, possibly smaller than the ion-neutral mean free path. Both the ions and neutrals are accelerated and compressed in a shock front which is shorter than the drag length scale. The shock is purely J type and the standard Rankine-Hugoniot conditions can be applied to find the conditions behind the shock.

C-type shocks will occur when the ion-Alfven Mach no. $M_{Ai} < 1$ and $M_A > 1$. The ions remaining subsonic while the neutrals are supersonic. Equation 2.69 now tells us that the drag length l_a is longer than the ion-neutral mean free path, i.e. heating occurs over length scales much longer than the collision scales. The first condition that the neutrals are moving supersonically is possible because the ions are subsonic and it is the Alfven velocity at which signals are transmitted. Another requirement generally needed for the shock to be of pure C-type is that the cooling length is comparable to the drag length. If this is not true then two situations develop. If the cooling length is longer than the drag length then the gas is heated at a faster rate than it cools, the gas may become so hot that full dissociation and ionisation takes place. This may lead to the ions

becoming supersonic and a J-type shock may develop. Conversely if the cooling length is shorter than the drag length the gas is cooling very quickly, and the shock appears as a J-type one where the gas is quickly heated and then subsequently cools.

C-type shocks can only develop for a small range of magnetic field strengths and ionisation fractions. The fact that there are upper and lower bounds beyond which the shock is no longer C-type is simple to see. If the ionisation fraction is too small (or even zero), then there is no frictional drag between the ions and neutrals, the shock is then of the simple Jump type discussed above and the magnetic field only has the effects described in section 2.4.4. If the ionisation fraction is large then the frictional ion-neutral drag length is small, smaller in fact than the cooling length. The heating then occurs in a region much smaller than the cooling and the shock behaves as a magnetized J-type shock. Similar arguments apply to the strength of the magnetic field.

One of the difficulties in calculating the emission from C-type shocks, is the many heating and cooling processes which are followed in the flow at the same time solving (simultaneously) the full flow equations. This is very expensive computationally and there are many free parameters which can be changed, which can and do, produce a different result. Thus making physical insights as to the important processes underlying the emission/acceleration mechanisms difficult. Nevertheless several authors have modelled C-type shocks over the past decade. In this section we will review their work and the central results to have arisen from them.

Draine (1980) was the first person to consider the possibility of strong Continuous type shocks. Previously Mullan (1971) studied C-type shocks in atomic gas where radiative losses are not important to the dynamics. This restricted him to finding only weak C-type shocks. Draine found strong C-shocks because in the molecular gas he was considering radiative losses were important. The approach that he took was to solve the fluid dynamics in detail, while calculating at several points in the flow the cooling rates, chemistry, heating rates. This then allows the computation to be treated as an initial value problem. Specifying the initial conditions allow a calculation of the shock structure and the emission from it. He presented numerical solutions for $10\,\mathrm{km\ s^{-1}}$ shocks propagating into diffuse ($n < 20\,\mathrm{cm^{-3}}$) gas, demonstrating that the ion-neutral drag was important in moderating the shock structure.

A few years later Draine, Roberge and Dalgarno (1983) then extended the study of C-shocks to denser molecular material they considered densities up to $10^6\,\mathrm{cm}^{-3}$. They were able to show that for the magnetic fields and fractional ionisation thought to be present in molecular clouds that C-type shocks would be the norm. Importantly they were able to calculate the line intensities from vibrational-rotational H_2 and of the fine structure lines of OI and CI. They found that C-shocks were able to accelerate and heat the H_2 up to speeds of $45\,\mathrm{km\ s}^{-1}$ before the molecules are fully dissociated, this appeared to be the basis at which the problem of fast H_2 could be solved. In Fig 2.5 we present figure 9 of Draine, Roberge & Dalgarno (1983) which shows the Temperature with shock velocity for molecular gas of density $10^6\,\mathrm{cm}^{-3}$, $x_e = 10^{-8}$ for two values of the magnetic field. Of interest in relating the observations to these models is the excitation temperature that would be derived from ratios of certain H_2 lines. There are two illuminating features that are apparent from these results. Firstly, the excitation temperatures are quite strong functions of the shock velocity, in contrast with the J-type shocks which have excitation temperatures almost independent of shock velocity. Also note that the maximum temperature achieved before dissociation cuts in is 4000 K, and the second point is that the excitation temperatures from the different lines remain very close together. This is a common feature of emission from planar C-type shocks, *the excitation temperature of H_2 lines is constant for a large range of upper level energies.*

The H_2 emission from behind a C-type shock thus appears as a constant temperature slab. The physical reason for this is that C-type shocks exist because over a large distance the heating due to ion-neutral drag is approximately balanced by the cooling. This is not necessarily true, but if a C-shock is to maintain the central feature of slowly accelerating molecules, and if the shock velocity is chosen to be very close to the dissociation limit (as per Orion), then it is a good approximation.

The principal coolants in C-shocks are OI, H_2, CO, OH & H_2O (see for example Fig. 4 of Draine, Roberge & Dalgarno 1983). Strong emission lines of these species are thus produced in C-type shocks. Strong OH and H_2O cooling occur because partial dissociation of H_2 produces a large atomic H fraction then any free O reacts with H (reactions 2.28–2.32) to produce OH and H_2O. Table (2.1) is the result of the C-shock fit to the emission from the Orion molecular outflow of Chernoff, Hollenbach & Mckee (1982). In the introduction to this chapter we discussed the difficulty that Draine &

Roberge (1982) had in modelling the high-J CO lines, while at the same time attempting to fit the high-J H_2 lines. Chernoff, Hollenbach & Mckee were able to reproduce the CO line intensities by using a lower density *and ignoring the high-J H_2 lines.* In the next chapter we will encounter evidence that the outflow is emitting these high-J H_2 lines everywhere, so the CO emission still presents a problem for shock modellers.

Chernoff (1987) produced an important piece of work on the detailed mathematics and physics of C-shocks. He was able to produce analytic solutions to the energy conserving flows and present the theory for the momentum conserving case, and thereby examine the effects of cooling and ionisation changes in the flow on the shock structure. For general cooling this was achieved by numerical analysis. His major result was that depending upon the ionisation fraction (and by how much it changes) shocks in astrophysical gas were either C or J-type with very few intermediate cases.

Recently Smith & Brand (1990a) have pointed out that it is possible to solve, analytically, the flow equations for 'cool' C-shocks under certain approximations to the equations for the momentum and energy transfer between the ions and neutrals and the cooling function. The essential requirement here is that the Mach no. is high and cooling is strong (not unreasonable), then the temperature is low (w.r.t. the equivalent J-type shock) and the thermal pressure is divorced from the dynamics. This is an extension of the analytic results of Chernoff (1987) for 'cold' energy conserving flows. This has made it possible to explore a much larger range of parameter space than was previously possible with numerical calculations. Several important results have emerged out of this work. The first is a general method for solving the C-shock flow equations (under the given approximations). This makes it possible to use these analytic results to calculate the structure and emission from more realistic situations than the plane parallel case. Secondly they were also able to calculate when the shock would no longer be C-type. Figs 2.6 and 2.7 are their figures 5 and 6, they show the parameter space under which C-shocks would occur for H_2 and H_2O cooling dominant. These are plots of the quantity $\chi(n/10^6)^{0.5}/(B/1000)$ versus shock velocity. Where χ is the ionisation fraction in the gas and n is the density (cm^{-3}), B the magnetic field strength (Gauss). In both these plots can be seen some of the limits we qualitatively mentioned earlier, for relatively low magnetic field strengths/ high ionisation fractions the shock becomes J-type. At higher velocities either dissociation or self ionisation cuts in.

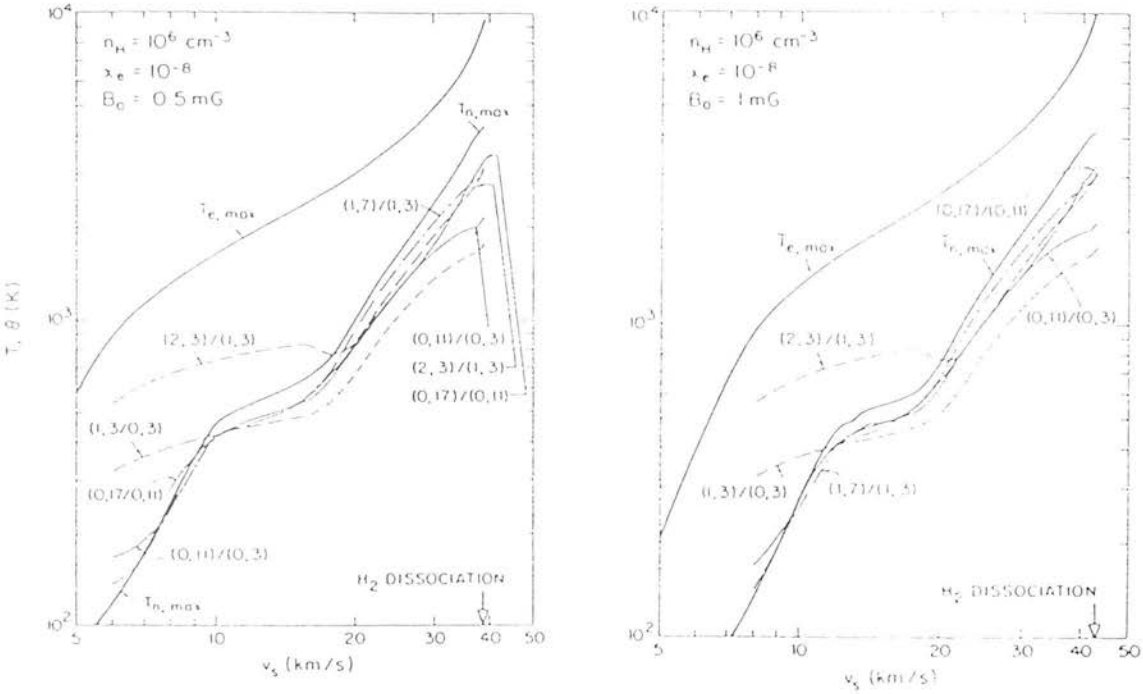

Figure 2.5: Plot of Temperature versus shock velocity from a C-shock (Draine, Roberge & Dalgarno 1983), for two magnetic field strengths

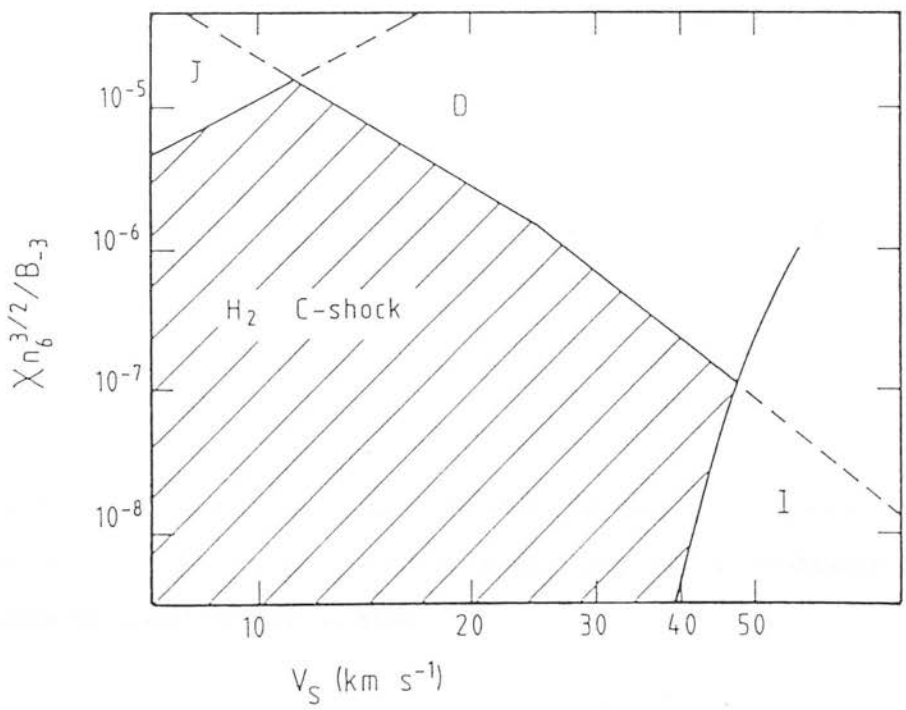

Figure 2.6: Parameter space in which C-type shocks occur (Smith & Brand, 1989).

Line (1)	Intensity[a] or Line Ratio: Predicted[b] (2)	Observed[c] (3)	References (4)
H_2 1–0 $S(1)$	1.0×10^{-4}	1.0×10^{-4}	1
0–0 $S(2)$	6.4×10^{-5}	5.0×10^{-5}	2
2–1 $S(1)$/1–0 $S(1)$	1/12	1/12	3
3–2 $S(3)$/1–0 $S(1)$	1/200	...	
CO 6–5	1.0×10^{-3}	1.0×10^{-3}	4
21–20	9.0×10^{-3}	1.0×10^{-2}	5
27–26	4.0×10^{-3}	6.5×10^{-3}	5
30–29	2.3×10^{-3}	2.4×10^{-3}	5
34–33	9.8×10^{-4}	6.0×10^{-4}	6
OH $^2\pi_{3/2}(5/2–3/2)$	3.7×10^{-3}	4.8×10^{-3}	7
$^2\pi_{1/2}(7/2–5/2)$	2.2×10^{-3}	...	
H_2O $9_{55}–9_{36}$	$\sim 10^{-3}$	...	
$10_{56}–10_{47}$	$\sim 10^{-3}$	...	
$11_{57}–11_{48}$	$\sim 10^{-3}$	...	
O I (63 μm)	1×10^{-4}[d]	...	
H I (21 cm)	4×10^{20}[e]	...	

[a] In ergs cm^{-2} s^{-1} sr^{-1}.

[b] Fit to the observed average surface brightness and line ratios of OMC-1 with ambient density of 2×10^5 cm^{-3}, shock velocity of 36 km s^{-1}, magnetic field of 0.45 milligauss, and $f_A = 3.7$.

[c] Surface brightness averaged over a 1′ beam, corrected for 2 μm and 12 μm extinction of 2.5 and 0.94 mag, respectively. The 1–0 and 2–1 $S(1)$ intensities have been adjusted upward by an additional factor of 2 to allow for the more heavily attenuated blue component.

[d] Oxygen intensity depends sensitively on preshock O abundance, assumed to be 2.4×10^{-4}.

[e] Atomic hydrogen column density through OMC-1, with 75 km s^{-1} width.

References.—(1) Beckwith *et al.* 1978; (2) Beck, Lacy, and Geballe 1979; (3) Scoville *et al.* 1981; (4) Goldsmith *et al.* 1981; (5) Storey *et al.* 1981; (6) Watson 1982; (7) Storey, Watson, and Townes 1981.

Table 2.1: C-shock model of Chernoff, Hollenbach & Mckee (1982) fitted to the Orion outflow. The high J-CO lines were fitted because they used a low density which could not match the highly excited H_2 lines

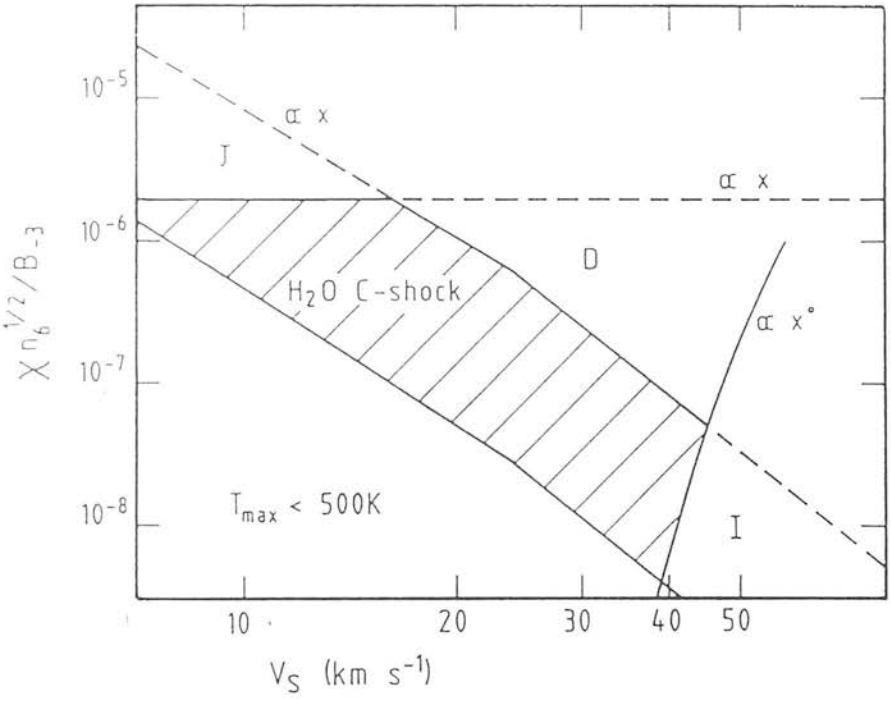

Figure 2.7: As Fig. 2.6 but for H_2O cooling dominant (Smith & Brand, 1989).

When the cooling can be approximated as a power law ($\Lambda \propto T^{\alpha}$) they were able to show that, as indicated in Fig. 2.5, the maximum temperature in the shock is close to a monotonically increasing function of shock velocity and is given by (for strong H_2 cooling $\alpha \approx 3.3$ for 1000 $T <$ 5000 Kelvin)

$$T_{max} = 1.27[(1 - 6.5/M_A)n^{1.5}\chi/B]^{0.3}\, v_s{}^{1.2} \tag{2.70}$$

Where n is in units of cm^{-3}, B in Gauss and v_s in km s^{-1}. In the second of the series (Smith & Brand 1990b, Paper2) they applied their results to calculate the emission and line profiles from planar shocks of H_2. In addition they were also able to calculate an approximate function for the column density of a particular H_2 level of energy T_j

$$\frac{N_j}{g_j} = 4.4 \times 10^{16} \frac{1}{\chi M_A} \left(\frac{1}{T_j} + \frac{0.1}{T_{max}} \right) e^{-T_j/T_{max}} \text{ cm}^2 \tag{2.71}$$

This is not quite a constant temperature but as we will see in later chapters the curvature when $T_j > T_{max}$ is relatively small.

2.6 Summary

In summary we have gone through the flow equations needed to calculate the emission from behind a hydrodynamic Jump-type shock. The emission from such shocks is shown to be relatively insensitive to the initial conditions, producing excitation temperatures close to those which are nearly always observed (2000 K for H_2 gas) over a wide range of pressures and over all velocities which can excite significant amounts of H_2 emission. It has been argued that the presence of a magnetic field will make little difference to the observed emission, only reducing the initial post-shock temperature and supporting the gas from compression at some point downstream in the flow. The shock is radically changed when there is a small ionisation fraction. Then as pointed out by Draine (1980) the ions are decelerated faster than the neutrals, heating due to ion-neutral drag takes place at the same time as cooling and the shock becomes continuous. A review of the current C-shock models suggests that the temperatures from these shocks are velocity dependant, at contrast with the observations. Further it is argued that such shocks appear as a constant temperature slab, wheres the J-type shocks have a smooth increase in excitation temperature with the energy of the line being observed. It is this last point

that provides an observable difference between the two types of shocks, and in the next two chapters we will examine this difference through observations of H_2 emission lines.

Chapter 3

The Orion Molecular outflow

3.1 Introduction

In the last two chapters we have illustrated that the discovery of line emission from molecular hydrogen in the Orion molecular cloud, OMC-1 (Gautier *et al.* 1976) stimulated a series of theoretical studies (Kwan 1977, London, McCray and Shu 1977, Hollenbach and Shull 1977) of the structure of molecular shocks. Observations of an extremely supersonic range of velocities in the H_2 1-0 S(1) line profile (Nadeau and Geballe 1979) prompted several workers (Draine 1980, Chernoff, Hollenbach and McKee 1982, Draine, Roberge and Dalgarno 1983) to develop magnetically moderated C-shock models. These could achieve velocities of over 40 km s^{-1} before shock heating dissociated the hydrogen molecules, and might therefore form the basis of an explanation for the observed velocity range of 150 km s^{-1}. Furthermore, these shock models seemed better able to explain the observed far-infrared CO intensities (Storey *et al.* 1981) than the earlier J-shock hydrodynamic shock models, in which hydrogen molecules are dissociated behind shocks of speeds of more than 25 km s^{-1} (Kwan 1977). Recent observations, however, by Geballe and Garden (1987) find that the mid-infrared vibrational CO line emission is more than an order of magnitude stronger than the C-shock model predictions. It is these problems that prompted us to undertake a program to study in detail the line emission from the shocked gas in Orion.

In this chapter we present observations of the H_2 emission from the Orion molecular

outflow, which we use as discriminators between shock models and temperature and density probes of the hot shocked gas. Before discussing our new observations we will first discuss the many observations that have been made in the past. This will begin with a description of the morphology of the Orion outflow region, in both H_2 and other atomic and molecular emission. We will then discuss more detailed observational work performed on the shock excited emitting gas, basically this is confined to observations of H_2 and CO line ratios. This will be followed by a presentation of our spectroscopy of H_2 lines, after a brief description of the observing techniques involved. The extinction to the shocked gas is shown to be lower than most of the early estimates. Finally, the implications for the type of shock involved, the state of the pre-shock gas and the origin of the outflow will then be explored.

3.1.1 An overview of the Orion molecular outflow

The Orion molecular cloud is an extremely active region of star formation. The great nebula in Orion, Messier 42, is the brightest HII region in the sky and is thought to be a champagne type HII region at the front surface of a molecular cloud. Behind this HII region is one of the brightest embedded infrared sources, the Becklin-Neugabauer object and the Kleinmann-Low nebula. At high spatial resolution the BN/KL object is seen to be comprised of several sources. The most luminous object in this region is IRC 2 (Wynn-Williams *et al.* (1984)), and is thought to be the source of the momentum driving the molecular outflow. This molecular outflow, the brightest in the sky, is the object that we are concerned with in this chapter. An excellent review on star formation and the Orion molecular cloud has been written by Genzel & Stutzki (1990). There appear to be several dynamically distinct outflows around IRC 2 and the relationship between them all is not clear (except that they probably have a common origin). A low velocity flow is concentrated within 20″ of IRC 2 with a full velocity extent of about 35 km s^{-1} and is traced by OH and H_2O masers and mm/submm lines of heavy molecules. A higher velocity outflow is seen in CO and many other molecular transitions at velocities up to 150 km s^{-1}. Shocks are associated with this outflow, and it is these shocks in which molecular hydrogen, as well as CO and OH emission is excited. On much larger scales are many HH objects and there are faint streamers (Hasegawa 1987; White 1988) which appear to be connected with the outflow and HH objects.

It is unfortunate that the molecular outflow, located about one arc minute to the North of the trapezium stars which power the ionisation, lies directly behind the HII region. This line of sight makes it almost impossible to observe the outflow in the light of ionised species. Although Hasegawa & Akabane (1985) have detected broad lines in radio recombination lines spatially coexistent with the outflow and with a similar velocity width to the shocked molecular emission. At optical wavelengths there is no sign of the outflow. It is only when observations are carried out at longer wavelengths, where the extinction is less, that the outflow appears. This suggests that the outflow, and other Infrared sources, are embedded deep in the molecular cloud. The exact depth into the cloud is poorly known, mainly due to the uncertain extinction to these sources.

Fig. (3.1) is a low spatial resolution ($\approx 5''$) contour map of the H_2 1-0 S(1) emission (from Scoville *et al.* 1982). The continuum sources are marked as solid circles. The brightest H_2 emitting position in a $5''$ beam was named Peak 1 by Beckwith *et al.* (1978), the fainter positions are numbered increasingly in order. Upon inspection of Fig. (3.1) it is apparent that the H_2 emission arises from a loosely bipolar structure, but from IRC 2 the emission is not symmetric and appears as a dog leg. A similar morphology is seen in the emission from high velocity CO (e.g. Erickson 1982).

As we have already seen the observed high velocities ($>100\,\mathrm{km\ s^{-1}}$) present difficulties for theoretical models. Global models of the emitting region are made even more difficult by the observation that over the whole source the lines are broad, display slightly extended blue wings, and show only a very small shift in the peak velocities (e.g. Nadeau, Geballe & Neugebauer 1982; Geballe *et al.* 1986). This leads to the inescapable conclusion that the outflow is almost in the plane of the sky. The true velocities are thus likely to be much larger than the observed radial velocities and the additional problem arises of how to transfer momentum travelling in the plane of sky (the outflow) into the observed velocities perpendicular to this plane. The shock excited rotational CO and $63\,\mu$m OI emission are as broad as the H_2 lines (Crawford *et al.* 1986).

Emission from highly rotationally excited CO has been measured by Watson *et al.* (1985) using the Kuipier Airborne observatory. These lines have been measured with large beams 30–40$''$ centered on the BN object. Watson *et al.* demonstrated that the high J lines are sub LTE. Draine & Roberge attempted to model this CO emission

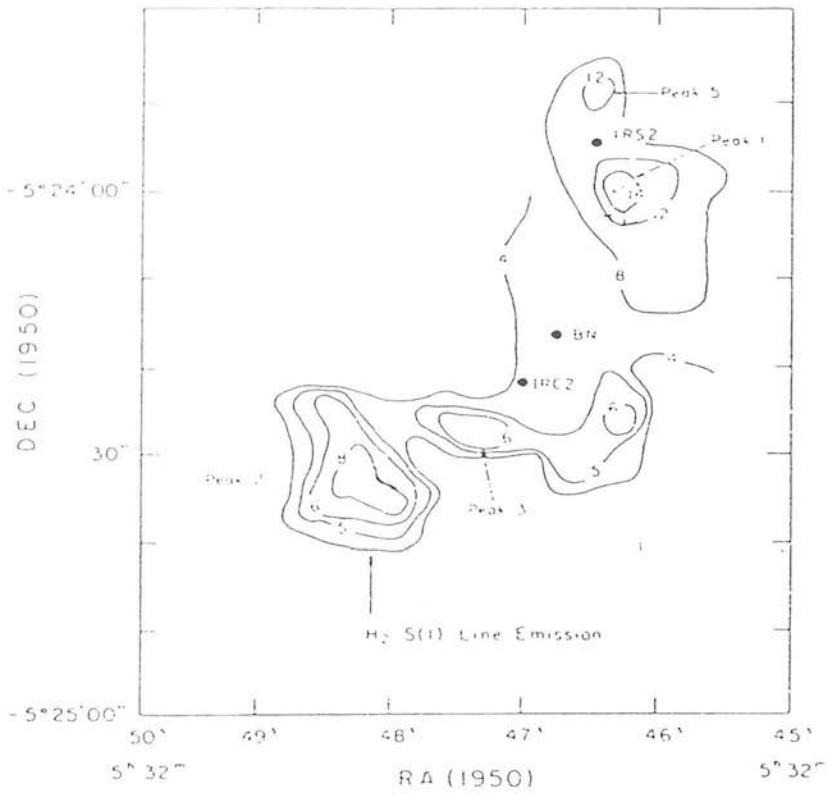

Figure 3.1: Morphology of the outflow region. The contours are H_2 1-0 S(1) emission. Continuum sources are also marked.

from their C-shock. However their model over-predicted the high J Intensities (see Fig. (3.2)). In order to fit these lines they introduced a suppression factor to reduce the populations of these high J levels, this factor was about 6 for the highest level. Viscuso & Chernoff (1988) have recalculated the the cooling rates using the revised cross sections of Schinke *et al.* (1985) and find no evidence for such a suppression factor. Further difficulties for the C-type shock models have arisen because of the new observation by Geballe & Garden (1987) of vibrationally excited CO emission at more than an order of magnitude stronger than the predictions from C-shock models. Chernoff, Hollenbach & Mckee (1982) applied a C-shock to the averaged emission from the outflow, ignoring the emission from the highly excited H_2 lines. By doing this they could fit the CO emission quite well. But they under predict the strength of the higher H_2 lines by a factor of 4. Mapping of the H_2 1-0 O(7) and 0-0 S(13) lines by Brand *et al.* (1989b) has presented constraints for any shock models. These lines are close enough together to be measured simultaneously and it was found that the ratio of these two lines is a constant everywhere from the outflow. This is surprising since these two lines arise from energy levels of 8365 and 17445 Kelvins respectively. As such they are sensitive indicators of temperature and density. The shock in Orion must be of a type that is insensitive to the local conditions (such as velocity and density).

3.2 Infrared Spectroscopy

Observing in the infrared is made difficult for many reasons. Thermal emission from the sky background, the telescope and instruments are all strong in the infrared. In fact a blackbody at a temperature of 300 Kelvin peaks at 10 μm. Any source is generally far fainter than this background emission. To overcome this Infrared astronomers use a technique called chopping. A vibrating secondary mirror is used to point, usually at a few Hertz, the detector on and slightly off the source. As long as there are no sources in the off beam position then subtracting the two signals should leave only emission from the infrared source. This is a standard technique but is not perfect since the vibrating mirror does not necessarily return to the same position and so errors are introduced due to variable pointing. The sky emission can, and does, vary on very short timescales introducing further errors. Secondly the sky is not perfectly transparent in

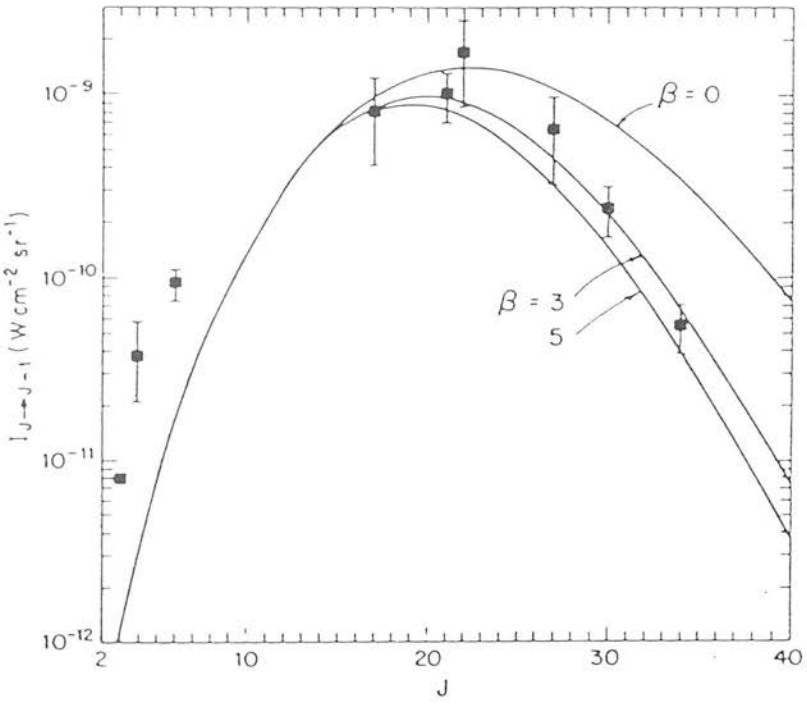

Figure 3.2: Intensities of CO (J→J-1) versus the rotational quantum number J (from Draine & Roberge 1982). The solid curves are C-shock model predictions. β is a parameter used to reduce the collision rates of the high J values. Revised rates using better cross sections suggest that this is zero (Viscuso & Chernoff 1988).

the infrared. In fact there are only a few spectral regions, called windows, where ground based observations can be carried out. Outside of these windows the blending together of many water and OH absorption lines reduces the transmission to zero. This attenuation is compounded because the strength depends on the amount of water vapour in the air above the telescope which can change in a matter of minutes, even on a good site. If spectroscopy is being conducted then a smooth spectral source (a ratioing star) is observed and used to correct for the atmospheric transmission by dividing the source spectrum with this reference spectrum. To obtain flux calibration a flux standard (a star whose infrared magnitudes are known) should be observed as well. These stars (which are often the same) should be as close to the air mass of the object as possible to avoid the uncertainties involved in performing air mass corrections.

It is thus essential that if reliable observations are to be made then a telescope at a high site, or from an aeroplane in the case of the KAO, is used. There the amount of water will be less and calibration correspondingly more accurate. The 3.8m United Kingdom Infrared Telescope (UKIRT) on Mauna Kea Hawaii at an altitude of 13800 feet is therefore an ideally suited to a study of this type. This is the telescope that we have used for all the new observations presented in this and the following chapters.

Most of the observations utilised the Cooled Grating Spectrometer CGS2 (Wade 1983). We will briefly describe this instrument here. CGS 2 is a seven channel grating spectrometer that operates efficiently at wavelengths between 1–5 μm. Two gratings are mounted back to back which give resolving powers of approximately 300 and 600. Several broad blocking filters are available, some of which allow observations across different windows. There is a maximum available beam diameter of $\approx 5''$ and beyond 3 μm only the lower resolution grating can be used. The detector itself is a seven element one dimensional InSb array. The pixels are separated by a very small distance and in use each channel is effectively separated by the resolution of the instrument. The detector and grating are cooled to a temperature of 66 Kelvins by a combination of both solid and liquid Nitrogen, hence the name cooled grating spectrometer.

The intensities of lines measured by the cooled grating spectrometer were determined by least-squares fitting Gaussian profiles to the observed lines, together with polynomials to the continua (which is normally flat). The gaussian profile is a very reasonable

approximation to the transmission of the instrument to a delta function. The procedure adopted was to fit a gaussian to the very bright lines, leaving as extra free parameters the wavelength of the line centre and the FWHM of the line. This enabled a determination of the resolution of the instrument and the wavelength calibration on the actual source rather than using a lamp line. This FWHM was then used in fitting gaussians to the fainter lines. The resolution of CGS 2 is not a constant with wavelength (although it does not vary a great deal) so isolated lines away from a bright reference line were fitted using an extrapolated/interpolated FWHM using the theoretical expression for the wavelength dependence of the resolution of the instrument.

As in the infrared the signal is determined by the co-addition of the on-off beam signal over many chopping cycles the error bar on each data point is a realistic indicator of the uncertainty. There are many contributions to this error but most of it is simply the change in the sky/instrument emission and the accuracy with which the chopping secondary returns to the observed position. So, each error bar is representative and it is possible to formally calculate the error on the fitted line intensity, simply from the covariance matrix of the fit (see Press, Flannery, Teukolsky & Vetterling 1986). In most cases this provides a reasonable estimate of the internal error. However this does not take into account the observational errors, such as pointing in a slightly different position, the beam size changing and more importantly the sky transmission changing. For all lines other than the reference 1-0 S(1) the errors on the line intensities are calculated from the statistics of all the observations of that particular line. An estimate the true line intensity is obtained from a weighted mean (using the formal error as a weight), and the error is then given by the following equation

$$\sigma_{Im} = \sum \left(\frac{I(\sigma I)^{-2} - \frac{\sum (I(\sigma I)^{-2})}{\sum (\sigma I)^{-2}}}{\sum (\sigma I)^{-2}} \right) \tag{3.1}$$

This is particularly useful where the lines are partly blended, because although the fitting routine copes with this fairly well, the extra free parameters allow a much greater leeway in the intensity estimates. Also although most of the lines that are used in the subsequent analysis are free from telluric absorption, some of those used are partly attenuated by the atmospheric transmission. In this case a good estimate of the line intensity can only be obtained with many observations.

3.3 Observations

Most of the observations utilized the facility cooled grating spectrometer CGS2 described in the last section. The beam diameter of this instrument was set to 5″; and the resolving power was typically 500. Standard chopping and nodding (60″ EW) practices were employed. The stars BS 1552 (K=4.14) and BS 1713 (L=0.11) were used for ratioing and flux calibration.

All of the three micron lines were measured in 1985 November; most of the two micron lines were observed in January and February of 1987. In addition, during the latter period a number of the strong lines in the two and three micron bands were measured in a single scan so that their relative intensities could be determined, this observation was repeated in February of 1989. Also during January of 1988 measurements of several fainter lines were taken using the combination of the single channel bolometer UKT9 and a Fabry-Perot interferometer. In Table (3.1) are the details of the observations of Peak 1. The reduction procedure used was that outlined in the last section.

The reduced 2 μm spectrum from the January 1987 observations is shown in Fig. (3.3). This spectrum is a coadd of all the observations taken on these two nights. As such the observations around 2.2 and 2.35 μm are of much higher signal to noise than other parts of the spectrum because more observations were taken there. This is apparent by examining the error bars on the continuum in different parts of the spectrum. Note also the apparent absorption feature at 2.166 μm, the wavelength of the atomic hydrogen Brackett γ line. This is really an emission line, the chopper throw was large enough to be off of the outflow but was still within the extent of the ionised HII region. There is simply more Brγ emission from the H^+ region in the off-source chop position (60″ W) than towards Peak 1. Fig. (3.4) is a plot of the spectrum of the faint 3-2 S(3) line and the gaussian fit through it as a solid line.

The 3 μm spectrum has been published elsewhere (Geballe 1986) and is shown in Fig (3.5). This is a very long spectrum covering the whole of the L, L′ and M windows and parts of the spectrum are very noisy due to poor (near zero!) atmospheric transmission. This is especially apparent beyond 4.07 μm in Fig (3.5b). There are two other interesting points to note about this spectrum (other than the many H_2 lines visible). Firstly, the

continuum is depressed at around 3.1 μm, this is the the well known ice-absorption feature. Secondly, the 3.3 μm emission feature can be seen, this is presumably emission associated with the PDR in front of the outflow (e.g. Sellgren 1981). It is potentially useful as an extra estimate as to the likely strength of UV-excited H_2 emission from the PDR. Again note the negative intensity of the hydrogen recombination Brα line due to brighter recombination emission in the off beam position.

Several two micron H_2 lines, including the 4-3 S(3) and 3-2 S(2) (which had not previously been observed), were measured at Peak 1 January of 1988. These data were obtained using the facility UKT9 bolometer/spectrometer in series with an ambient temperature Fabry-Perot interferometer and a circular variable filter (CVF) as order isolator. The beam diameter was 12″, and the velocity resolution ~120 km s^{-1}, so that the H_2 lines are only marginally resolved. This instrument set up was used rather than the cooled grating spectrometer because the increased beam size allows 4 times more flux to enter the detector. Chopping and nodding practices were as above. The 1-0 S(1) and 2-1 S(0) lines were measured with this instrument, so that the former two line intensities could be scaled to previously measured H_2 lines and thus be included in the analysis. These spectra are displayed in Fig. (3.6). The feature on the blue side of the 4-3 line is a higher FP order of the 1-0 Q(1) line transmitted partially by the CVF.

3.3.1 Column densities and extinction estimates

Because of pointing and beam size differences between the different observations sets, the spectra were scaled to one another using the previously described spectrum that contained lines common to the various two and three micron spectra. The resulting line intensities found using the method outlined in section (3.2) are presented in Table (3.2). This is the largest collection of H_2 emission lines for any one object. While the absolute fluxes may be in error for the reasons discussed in section 3.2 the relative fluxes of these lines are accurate to the quoted errors as care was taken to make sure that every observation could be included as a ratio by always observing one, or more, of the bright v=1-0 lines (usually including the 1-0 S(1)) as well as the fainter line of interest. We note that the relative intensities of the two micron lines measured by us are consistent with those observed by Oliva and Moorwood (1988). The errors quoted in Table (3.2)

Table 3.1: Journal of Orion Peak 1 observations

Wavelength range or lines observed	Date	Integration time (minutes)	Standard
3–4 μm	01-86	100	BS1713
1.7–2.4 μm[1]	06-01-87	50	BS1552
2 μm	06-01-87	140	BS1552
2 μm	07-01-87	104	BS1552
2 μm	22-02-87	80	BS1552
FP; 1-0,2-1 S(1) 3-2 S(2), 4-3 S(3)	15-01-88	60	BS1552
1-0 S(1),S(7)	16-01-88	10	BS1552
2–3 μm	20-02-89	65	BS1552

1. Concentrating on the bright lines.

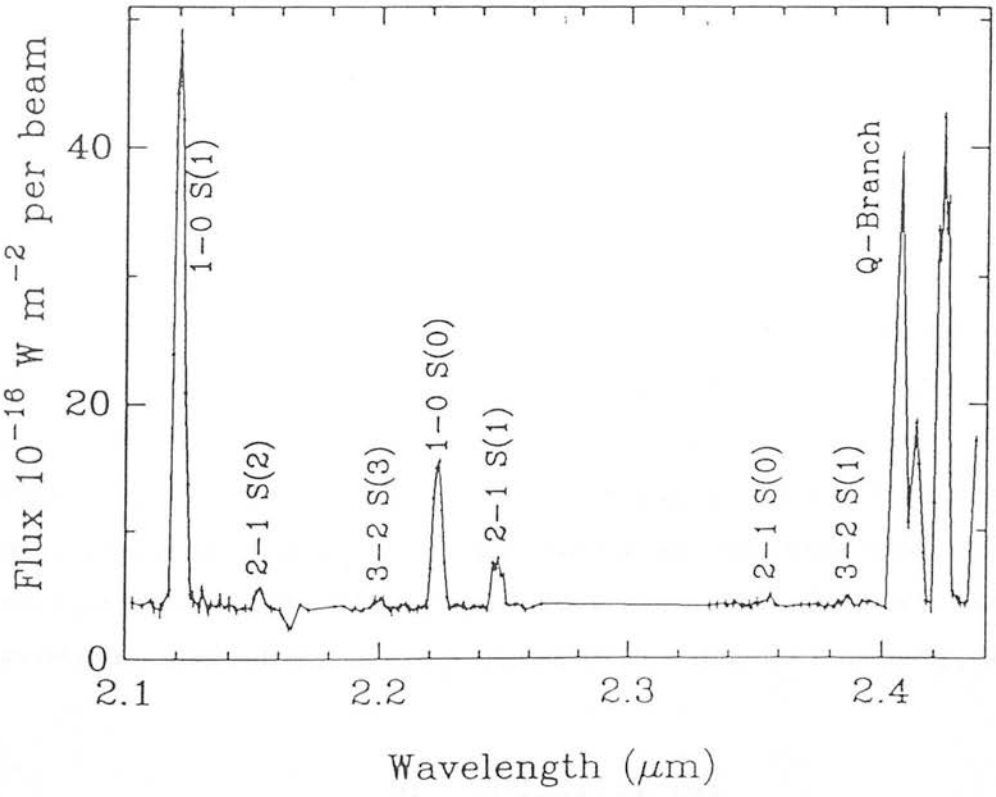

Figure 3.3: Raw 2 μm spectrum from 1987 January, obtained at a resolution of 0.004 μm. Lines used in the analysis are labelled. The feature at 2.166 μm is due to Br γ in the offset beam.

are either the formal errors of the Gaussian fit to the spectral line, or— for all but the brightest lines— the statistical error from the many observations. Both give reasonable results, but the latter method is preferred because the many observations (over more than one night) reduce errors due to atmospheric transmission/emission and detector variations.

Of the approximately 30 H_2 lines detected, only those 19 lines whose intensities were believed to be free from significant uncertainties (e.g., due to attenuation by telluric absorption lines) were considered for further analysis. Observed column densities, N_0 (assuming no extinction), were determined from the observed intensities using transition probabilities from Turner, Kirby-Docken, and Dalgarno (1979) and the formula for optically thin transitions stated in chapter 1 (equation 1.2). The relative accuracy of these column densities is limited only by the accuracy of the observations. However, there are sources of systematic errors. The largest systematic error is due to the partially unknown beam size and the absolute calibration.

The intrinsic intensity and hence the column density is extinguished by dust grains. There can be attenuation both from foreground dust outside the emitting region (external extinction) and inside (internal extinction). In what follows we will assume that there is negligible internal extinction although there is some evidence, which we will discuss in chapter (5), that there is some internal extinguishing material. This assumption if wrong will result in an overestimate of the average extinction to the emitting gas.

Gautier *et al.* (1976) in their paper announcing the discovery of H_2 emission from outside the solar system pointed out that it would be possible to measure the extinction using the ratios of lines from common energy levels. In the present data set there are several sets of lines all of which come from the same level, but which branch to different lower energy levels and so appear at different wavelengths. Knowing the branching ratio enables one to work out the foreground extinction assuming some extinction law. Any deviations from the branching ratio are due to differential extinction at the different wavelengths involved. The intensity ratio of two lines from the same energy level is

$$\frac{I_1}{I_2} = \frac{A_1\lambda_2}{A_2\lambda_1} 10^{(A_{\lambda_2} - A_{\lambda_1})/2.5} \tag{3.2}$$

Table 3.2: Parameters and Intensities of Observed H_2 Lines

Line	Wavelength[a] (μm)	Upper Level[a] Energy (K)	Flux Density[b] (10^{-16} W m^{-2})	Dereddened Column[c] Density / g_j (10^{18} m^{-2})
1-0 S(7)†	1.7480	12818	4.2 ± 0.4	...
1-0 S(1)	2.1218	6956	50.1 ± 0.5	326.3 ± 2.9
2-1 S(2)	2.1542	13150	1.6 ± 0.1	14.8 ± 1.2
3-2 S(3)	2.2014	19086	0.8 ± 0.1	1.9 ± 0.2
1-0 S(0)	2.2235	6471	12.2 ± 0.2	467.5 ± 11.1
2-1 S(1)	2.2477	12550	4.3 ± 0.1	18.8 ± 0.8
3-2 S(2)	2.2870	18386	0.8 ± 0.2	2.5 ± 0.6
4-3 S(3)	2.3445	23955	0.5 ± 0.1	0.6 ± 0.1
2-1 S(0)	2.3556	12095	0.9 ± 0.1	22.5 ± 4.5
3-2 S(1)	2.3846	17818	0.8 ± 0.1	3.1 ± 0.8
1-0 Q(1)†	2.4066	6149	40.0 ± 5.0	...
1-0 Q(2)†	2.4134	6471	16.5 ± 2.0	...
1-0 Q(3)	2.4237	6956	45.1 ± 5.0	367. ± 41.
1-0 Q(4)†	2.4375	7585	16.0 ± 2.0	...
1-0 O(4)†	3.0039	6471	13.4 ± 2.0	...
1-0 O(5)	3.2350	6956	25.7 ± 2.1	299. ± 25.
2-1 O(5)‡	3.4378	12550	2.1 ± 0.3	16.9 ± 2.4
0-0 S(17)	3.4857	25541	1.5 ± 0.5	0.21 ± 0.07
1-0 O(6)	3.5007	7584	4.3 ± 0.6	167. ± 22.
0-0 S(16)	3.5475	23461	0.8 ± 0.4	0.38 ± 0.18
0-0 S(15)	3.6261	21413	3.5 ± 0.6	0.74 ± 0.13
2-1 O(6)†	3.7236	13150	}	...
0-0 S(14)†	3.7244	19405	} 2.2 ± 0.3	...
1-0 O(7)	3.8075	8365	9.2 ± 0.8	145. ± 12.
0-0 S(13)	3.8461	17445	8.4 ± 0.9	3.11 ± 0.03
0-0 S(12)	3.9960	15542	3.8 ± 0.4	5.8 ± 0.6
2-1 O(7)†	4.0540	13891	1.4 ± 0.4	...

a Obtained from Dabrowkski (1984).

b In a 5″ aperture at Peak 1, except for the 3-2 S(2) and 4-3 S(3) lines, which were in a 12″ aperture. These latter two fluxes need to be divided by 2.9 to scale with those in a 5″ aperture (based on a measurement of the 1-0 S(1) line through the 12″ aperture). The 2μm line fluxes combine two sets of measurements. The 3μm line fluxes have been multiplied by a factor of 1.07 from the observed values based on a composite 2 and 3μm spectrum.

c Assumes $A_\lambda \propto \lambda^{-1.5}$ with $A_K = 0.8$. All values apply to a 5″ aperture.

† Line detected, but either contaminated by telluric absorption lines, blended with other lines, or observed with incomplete spectral coverage. Intensities not reliable enough to be included in the analysis.

‡ Blended with 0-0 S(18), but we estimate the contamination is < 5%.

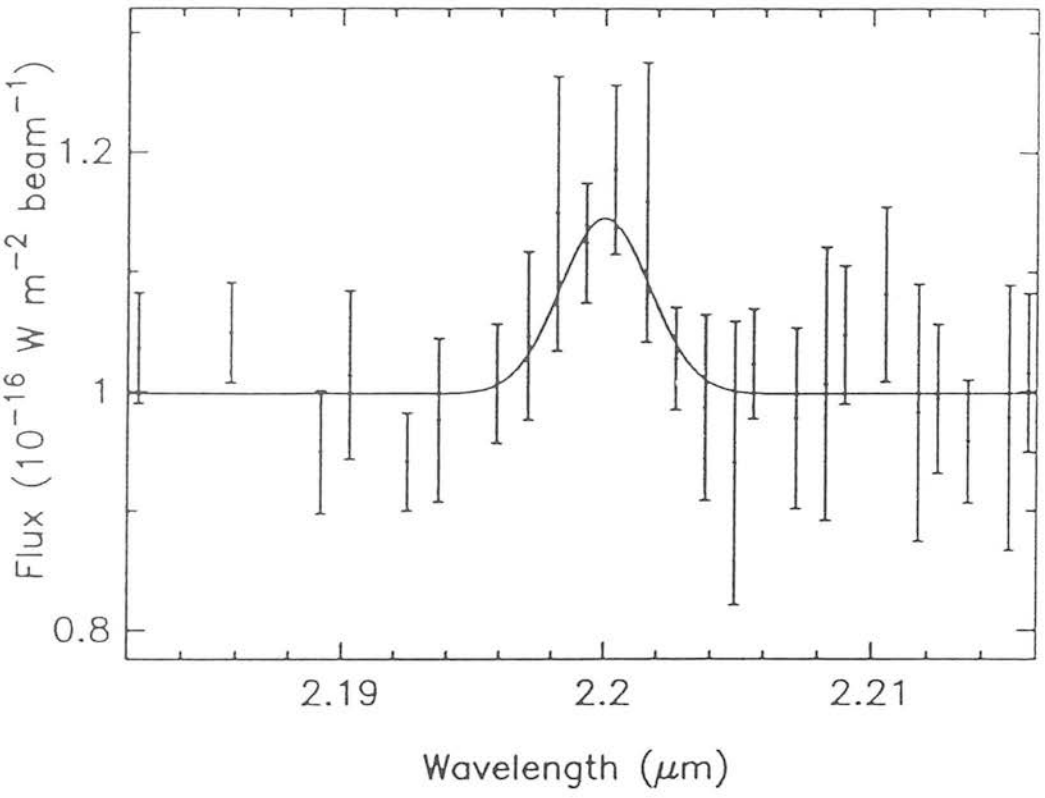

Figure 3.4: Gaussian fit to the faint 3-2 S(3) line.

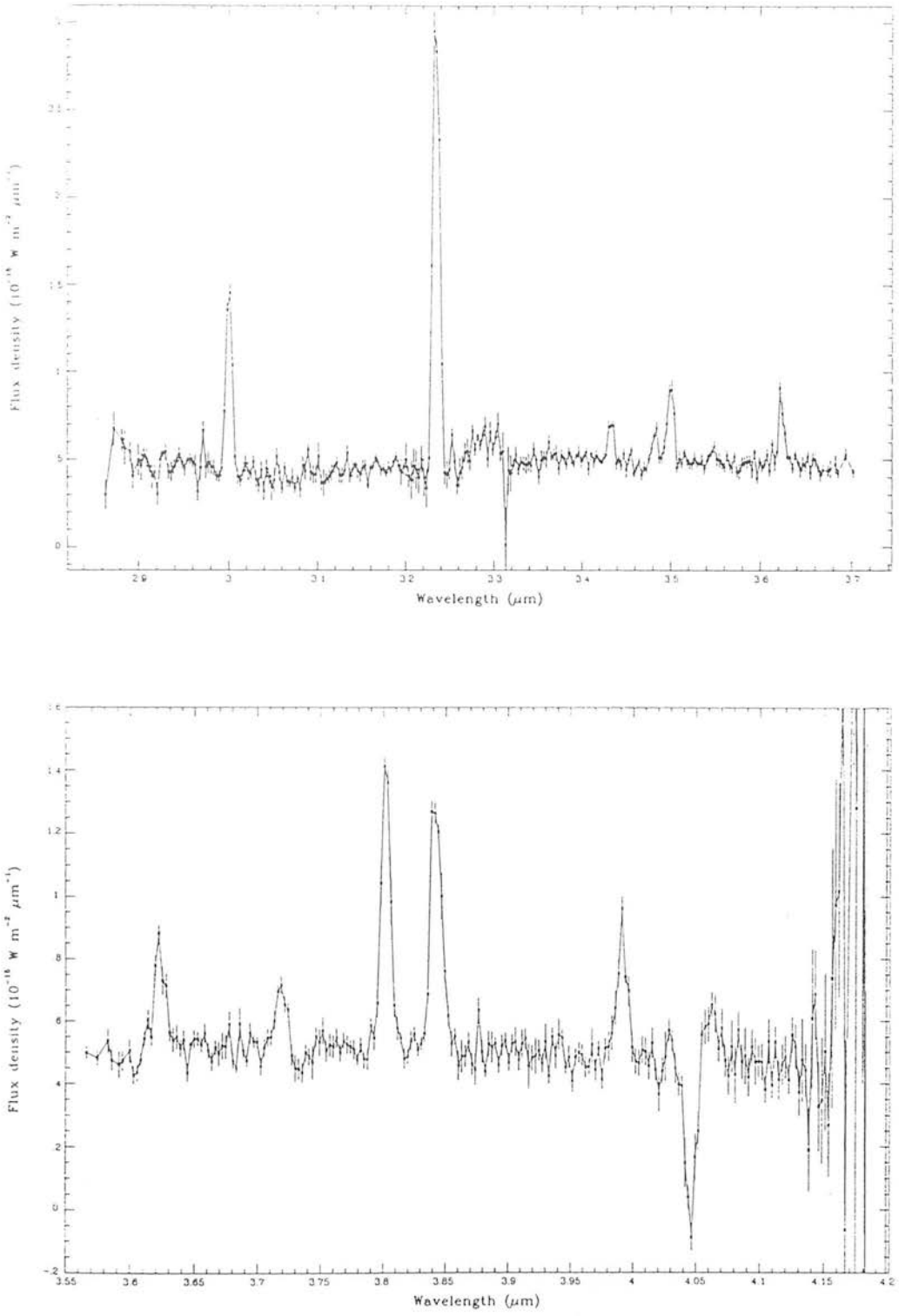

Figure 3.5: 3 μm spectrum of peak 1

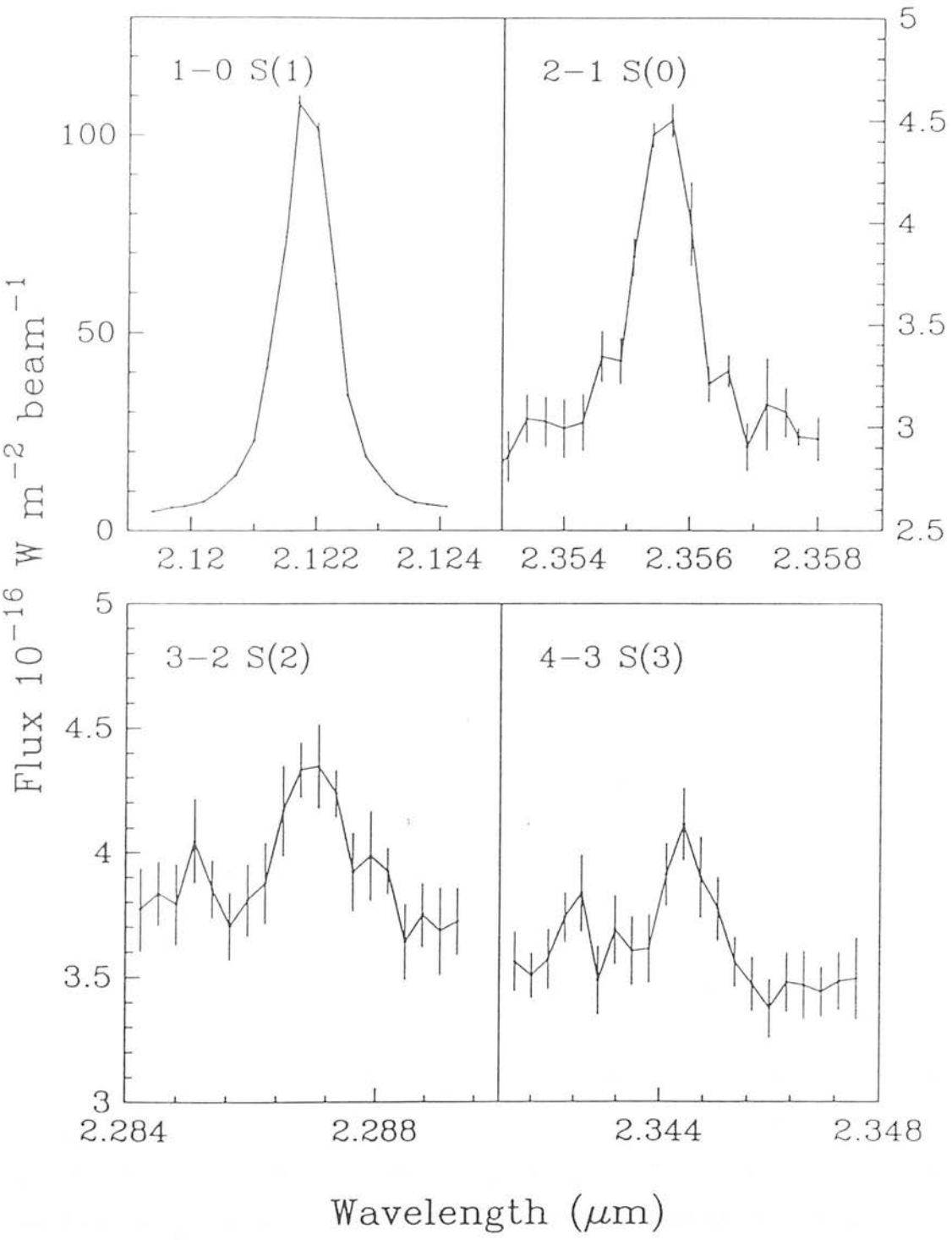

Figure 3.6: Orion Peak 1 spectra obtained using the UKT9+FP system

The differential extinction ($(A_{\lambda_2} - A_{\lambda_1})$) between the two wavelengths can be used to infer the total extinction to the source by comparison with a particular extinction law. This is difficult because of the unknown form of the curve in the infra-red (e.g. see Beckwith *et al.* 1983). If we assume that the extinction law is a power law, $A_K \propto \lambda^{\propto}$, then the extinction at a particular wavelength (we choose the K band because that is where most of our observations are) is

$$A_K = 2.5 \frac{(\lambda_1/\lambda_K)^{\alpha}}{(1-(\lambda_1/\lambda_2)^{\alpha})} log \frac{I_1 A_2 \lambda_1}{I_2 A_1 \lambda_2} \tag{3.3}$$

and the associated error is

$$(\delta A_K) = 2.5 \frac{(\lambda_1/\lambda_K)^{\alpha}}{(1-(\lambda_1/\lambda_2)^{\alpha})} [(\delta I_1/I_1)^2 + (\delta I_2/I_2)^2]^{0.5} \tag{3.4}$$

Table (3.3) lists the extinction estimates derived from lines with common energy levels and assuming power laws of α = -1.0, -1.5 and -2.0 for the wavelength dependance of the extinction. We also quote estimates from bright, widely separated lines of similar upper level energies, however for reasons we discuss below we are cautious of relying on such estimates alone.

It is seen by examining the results in Table (3.3) and equations 3.4 that the error in the extinction estimates is very large because of the restricted wavelength coverage and the sensitivity to the line intensities. More extinction estimates can be found by using other lines which come from different upper energy levels. But, this involves estimating the population of each energy level. This can introduce inaccuracies since the population of two different levels depend on the physical state of the emitting gas. The temperature distribution is not known, so only lines with similar upper energies can be trusted. The last two chapters have highlighted that the population distribution is density dependant, high densities are needed to bring a particular level to its LTE value. Further, it is not necessarily the case that the ortho/para ratio has the statistical equilibrium value of 3:1. For these reasons we do not generally include extinction estimates using lines from different upper levels. However several lines with long baselines (wavelength separation) and with a similar energy (so that the temperature dependance is not severe) of the upper level are useful indicators of the extinction. We point out that the extinction

derived from these lines should not be trusted especially if they are only measured in isolation. We quote them here as checks against systematics in the measurements of the line intensities.

For an extinction law $A_\lambda \propto \lambda^{-1.5}$, appropriate for the Mathis Rumpl & Nordsick (1977) grain distribution, the best estimate of the extinction is $A_K = 0.8 \pm 0.3$. The dereddened column densities in the last column of Table 1 assume this form of the extinction law. If it is assumed that $A_\lambda \propto \lambda^{-1.0}$, the derived extinction is $A_K = 1.0 \pm 0.3$. However, the derived ratios of dereddened column densities are only marginally different from those in Table 1, as the total extinction is small in either case. This is a small value for the extinction to Peak 1 compared to previous estimates. However we tend to believe our results because the data is largely a homogeneous set, carried out by the same observers with mostly the same instrument and beam size, and more importantly care was taken to ensure that the relative intensities of *all* the lines are correct (i.e. by taking spectra of the bright lines over all bands, to be used as reference lines). In the next paragraph we will examine why most of the previous estimates overestimated the extinction.

In Table (3.4) are all the published extinction estimates over the last decade using this technique. There are clearly large discrepancies in the various results. Part of this, we assert, is due to the difficulties in estimating the extinction from H_2 line ratios mentioned above.

Beckwith, Persson & Neugebauer were the first to publish an estimate using the H_2 lines. Their value of $A_K = 4$ is inaccurate because they used old values of the transition probabilities which suggested that the intrinsic ratio of the [1-0 Q(3)/1-0 S(1)] lines equals 0.55 rather than the more accurate value of 0.70 (using Turner, Kirby-Docken & Dalgarno 1977). Also Geballe, Russell & Nadeau (1982) have shown that there is considerable difficulty in calibrating spectra near the wavelength of the Q-branch lines, and throw doubt on the accuracy of their observations.

Note that Simon *et al.* (1979) observed Peak 2 and found $A_K = 4 \pm 0.6$ for a van de Hulst #15 law using measurements of the 1-0 S, Q and O lines and the better transition rates.

Beck & Beckwith applied a correction factor of 1.5 at Peak 1 to the 2 μm lines. This was based on the assumption that the 5 μm (0-0 S(8)) line they observed was intrinsically symmetric, and that the asymmetries in the 2 μm lines are due to internal extinction. Observations since then suggest that at least some of the asymmetry in the H_2 lines is real (Geballe *et al.* 1986). We will defer a discussion on the extent of any internal extinction until Chapter (5), but point out that this correction factor decreases the external extinction estimate.

Knacke & Young derived their value of the extinction by comparing their measurements of the 0-0 S(8) and the S(12)—S(15) over a 7″ beam with the 1-0 S(1) flux of Beckwith *et al.* (1978) measured through a 10″ beam. This resulted in the intensities of their 3 μm lines being overestimated by 57% relative to the 1-0 S(1) line, due to the different beam filling factors involved.

Twelve lines were combined in the analysis of Beckwith *et al.* (1983). However, their results are severly compromised by combining measurements from 3 different telescopes with correspondingly different beam sizes.

The only remaining measurement differing from our estimate is that of Davis, Larson & Smith (1982). At first sight there are no obvious flaws in their analysis. But they mention the lack of the 1-0 Q(6) line in their spectrum and speculate that this could be due to some non-LTE process, this line was subsequently observed at an intensity similar to the other Q branch lines (Geballe *et al.* 1982) . This throws into doubt the accuracy of their data.

For these reasons we believe the extinction to Peak 1 is close to 1 magnitude at K (for a $\lambda^{-1.5}$ law), in section 3.4 the question of the value of the extinction will be examined further using all the lines measurements presented in Table (3.2). It is interesting to note that the estimates of the extinction towards Orion have been steadily declining with advancing publication date.

3.4 Shock models

Figure 3.7 is a plot of the dereddened column density in each level divided by that predicted for a slab of gas at 2000 K. The data are presented in this way in order to show the deviation from such a constant temperature environment, which has often been considered to be characteristic of the H_2 line-emitting region (see references in Chapter 1). A Boltzmann distribution at any other temperature is a straight line in this diagram. Lower temperatures have progressively smaller gradients while higher temperatures have steeper gradients. The best-fit single excitation temperature for the data is about ~2200K, which is consistent with most previous observations of H_2 lines in OMC-1 (e.g. Knacke and Young 1981). However, it is clear that no straight line will be a satisfactory fit to all of the data points. The weak, high-excitation lines are considerably more intense than would be expected from a straight line fit based on the strong high S/N, low-excitation lines. Since weak and strong lines come from both the two and the three micron spectra and correspond to both ortho and para H_2, neither errors in scaling, errors in dereddening, nor any particular ortho-para ratio can be the cause of the curvature in the locus of data points in Fig. 3.7.

A significant contribution to the faint ($1/50^{th}$ of the 1-0 S(1)) high-v lines from fluorescence is highly unlikely at Peak 1. Firstly, the 1-0 S(1) line intensity from the PDR is about $1/500^{th}$ (Burton & Puxley 1989) that at Peak 1. In fact our observation of the 3.3 μm feature allows us to improve this estimate for peak 1. Sellgren (1981) mapped at low resolution the nebula in the 3.3 μm feature, their results suggests that the ratio of the 1-0 S(1) to 3.3 μm flux is $\approx$ 30. This implys that the 1-0 S(1) flux from the PDR is $\approx 1/300^{th}$ of that from the shock. We have measured the intensity of the 3-2 S(2) line decreasing with that of the 1-0 S(1) line just off-source, but within the ionized nebula. Thus suggesting that the [3-2 S(2)/1-0 S(1)] ratio is not greatly enhanced at the PDR and the contribution is at most only at the 10% level. It is clear on theoretical grounds that intensities of the weak, high-J pure rotational lines at Peak 1 cannot be significantly enhanced by fluorescent emission. This is due to the fluorescent cascade which tends to populate high-v but only the low lying rotational levels (see for example van Dishoeck & Black 1988). In chapter (5) we will present further evidence that the fluorescent contribution to the H_2 emission at Peak 1 is insignificant.

Table 3.3: Extinction estimates using the data presented here

Line pair	wavelengths microns	extinction at K α =1.0	α =1.5	α =2.0
Lines with a common upper energy level				
1-0 S(1)/ 1-0 Q(3)	2.1218/ 2.4237	2.2±1.1	1.5 ± 0.7	0.8±0.4
1-0 S(1)/ 1-0 O(5)	2.1218/ 3.2350	0.8±0.3	0.6 ± 0.2	0.5±0.2
1-0 S(0)/ 1-0 Q(2)	2.2235/ 2.4134	3.5±0.8	2.3 ± 0.5	1.9±0.4
2-1 S(1)/ 2-1 O(5)	2.2477/ 3.4378	0.7±0.7	0.5 ± 0.5	0.4±0.4
Lines with similar upper level energy				
1-0 S(1)/ 1-0 O(7)	2.1218/ 3.8075	0.9±0.3	0.7 ± 0.2	0.6±0.2
1-0 S(1)/ 1-0 O(6)	2.1218/ 3.5007	0.8±0.8	0.6 ± 0.6	0.5±0.5
1-0 S(7)/ 2-1 O(5)	1.7480/ 3.4378	1.1±0.5	0.8 ± 0.4	0.7±0.3

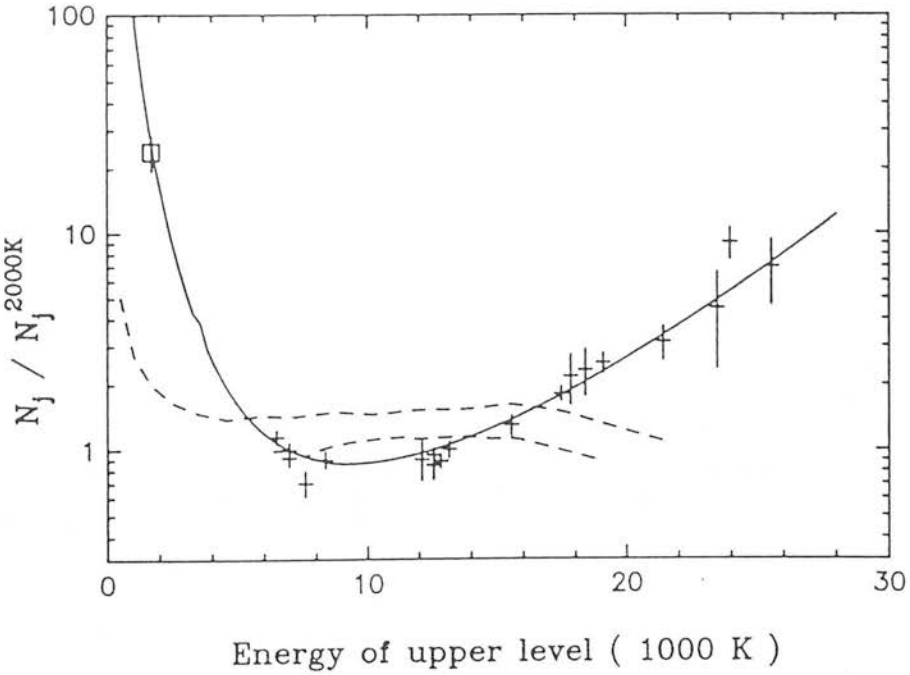

Figure 3.7: Plot of the ratios of observed, dereddened H_2 column densities to those from a Boltzmann distribution at 2000K (normalised so that the 1-0 S(1) ratio is unity) versus upper energy level. Error bars are $\pm 1\sigma$. The continuous line is from the cooling flow model described in the text, drawn through the 1-0 S(1) point. The dashed lines are the predictions of the C-shock models for OMC-1 by Draine and Roberge (1982) and by Chernoff, Hollenbach and McKee (1982). The upper line is for pure rotational lines.The box represents the value of the 0-0 S(2) line observed by Beck *et al*, (1979).

Table 3.4: Previous estimates of the extinction towards Peak 1 in Orion.

Date of observation	Quoted extinction	lines used	Assumed law	A_K $\lambda^{-1.5}$	ref
1978	4 ± 1^a	S(1)/Q(3) S(2)/Q(4)	Vdh #15	4.9	1
1980	3.8 ±0.5	0-0 S(8) + S(9) /1-0 S(1)	Vdh # 15	4.2	3
≈1980	2.1±0.3	Q(3)/S(1) Q(2)/S(0)	Vdh#15	2.6	6
1980	1.2 ± 0.1^d	Q(3)/S(1)	Vdh#15	1.5	7
1980	$1.7–2.5^c$	many lines	λ^{-1}– $\lambda^{-2.5}$	2	4
1981/82	1.4 ± 0.3^b	0-0 S(8)/ 1-0 S(1) Q(3)/S(1)	Vdh # 15	1.2	2
1981	$\approx 1^d$	S(1)/O(7)	$\lambda^{-1.7}$	1	5

[1] Beckwith, Persson & Neugebauer (1979) [2] Beck & Beckwith (1983) [3] Knacke & Young (1981) [4] Beckwith, Evans, Gatley, Gull & Russell (1983) [5] Geballe, Persson, Simon, Lonsdale & Macgregor (1986) [6] Davis, Larson & Smith (1982) [7] Scoville, Hall, Kleinmann, & Ridgway (1982)
a Observational errors, see text
b Correction factor of 1.5 applied to the 0-0 S(8) flux to account for differential internal extinction
c Used many lines observed with different telescopes and beam sizes.
d High resolution profiles at ≈ 20 km s^{-1}

The solid curve in Fig. 3.7 is the result of a simple partially-dissociative J-shock fitted to the data, using the equations developed in section (2.3). The cooling mechanisms included in this model were dissociation and radiation of H_2 and radiation from CO. The H_2O cooling was artificially suppressed by putting the water abundance to zero. For the curve plotted in Fig. 3.7 a CO abundance of one hundredth times solar was chosen (fractional abundance = 3.7×10^{-6}). Only if the CO abundance is greater than solar does CO cooling begin add to the H_2 radiative cooling and significantly affecting the line-ratios curve shape. However, even with such high abundances the extra cooling at low temperatures can be offset by increasing the pressure (which reduces the emission from the high temperatures). The absolute column density of this model was forced to pass through the 1-0 S(1) line. The model results were thus multiplied by a factor of ~ 0.3 , this is related to the beam filling factor, line of sight through the shock and other such effects. The high-excitation lines in the figure are then fitted by varying the *only other free parameter, the shock pressure.* The pressure thus derived is $8 \times 10^{10} K\ \mathrm{cm}^{-3}$.

As we have argued in chapter (2) in a C-shock, the temperature increases to a flat maximum, as heating by friction matches cooling, and then drops. Thus a slab of gas, approximately at a constant temperature, emits most of the energy. The temperature of this slab depends on the velocity of the shock. This seems to be at variance with the data presented here and in Brand *et al.* (1989b) (who show that the ratio of the 0-0 S(13) and 1-0 O(7) lines does not vary within OMC-1). Discrepancies are particularly evident for lines from the v=3 and 4 levels and for high-J rotational lines, whose strengths are hard to explain in the C-shock models. The dashed lines in Fig. 3.7 show predictions of H_2 line intensities made from the C-shock model of Chernoff, Hollenbach & Mckee (1982), normalized to the 1-0 S(1) line and superposed on our model fit. This particular model is clearly not in agreement with the data. In Fig 3.8 we plot our data points with the prediction from the plane parallel cool C-shock approximation described in chapter (2). The best fit maximum temperature for this data set is 2500 K. It is clear that this provides a poor fit to the data and so it thus appears that the current C-shocks fitted to the Orion shock (Draine & Roberge (1982); Chernoff, Hollenbach & Mckee (1982)) are poor models for the H_2 exciting shocks and further that all plane parallel C-shock models are ruled out as viable models for the Orion shock. This does not rule out the possibility that a series of C-shocks of different velocities, and hence temperatures, could combine to reproduce the temperature distribution we observe here.

The shock pressures needed for the J-type shock to reproduce the column density ratio's are rather high but are needed in any shock model that seeks to explain these observations. The fact that we see emission from highly excited molecules implies large pressures. Bearing in mind that we are discussing collisionally excited gas, the highly rotationally excited molecules imply gas that is in, or very close to, LTE. This is because collisions can only increase, or decrease, the rotational quantum number by 2. So many collisions are needed to populate the high J levels. The temperatures and densities needed to excite the highly rotationally excited lines in LTE are not very well known, but Burton *et al.* (1989a) calculated the critical density for the 0-0 S(13) line using three published values for the collisional excitation rates. They found that densities of between 10^6 and 10^7 cm^{-3} were needed to obtain LTE populations. As this gas is at temperatures of at least 3000 Kelvin, there is a lower limit to the pressure of $\approx 3 \times 10^9$ K cm^{-3}.

The suppression of H_2O cooling is important. Water is a very efficient coolant and has a weak temperature dependence. So the effect on the line emission if water dominates the cooling is to cool the lower temperature gas more efficiently. The shock will therefore produce far too much hot gas. The pressure does not have a large effect in this case as the H_2O cooling goes as the density squared, the same as H_2 dissociation. Fig. 3.9 shows the column density ratios produced from behind a J-type shock with a water abundance assuming that half of the Oxygen is in H_2O. It is apparent that this is a poor fit to the data as expected from the discussion above. There is no theoretical basis for suppressing the water cooling as the Oxygen chemistry is thought to be well understood (e.g. Neufeld & Melnick 1987).

Our lower estimate of the extinction to the outflow does place it within the photodissociation region (which extends out to an $A_v \approx 10$, see for example Tielens & Hollenbach 1985 and Genzel, Harris & Stutzki 1990) and the strong UV flux here may be photodissociating H_2O. Van Dishoeck (1987) point out that H_2O has several resonances near the Lyman and Werner bands, and so its photodissociation rate is higher than other molecules. Recently Melnick *et al.* searched for water emission from the Orion shock. They did not detect any emission at an upper limit $\approx$100 times fainter than the predictions of Neufeld & Melnick (1987) from a C-type shock. For these reasons we believe that H_2O is an unimportant coolant for the shock in Orion.

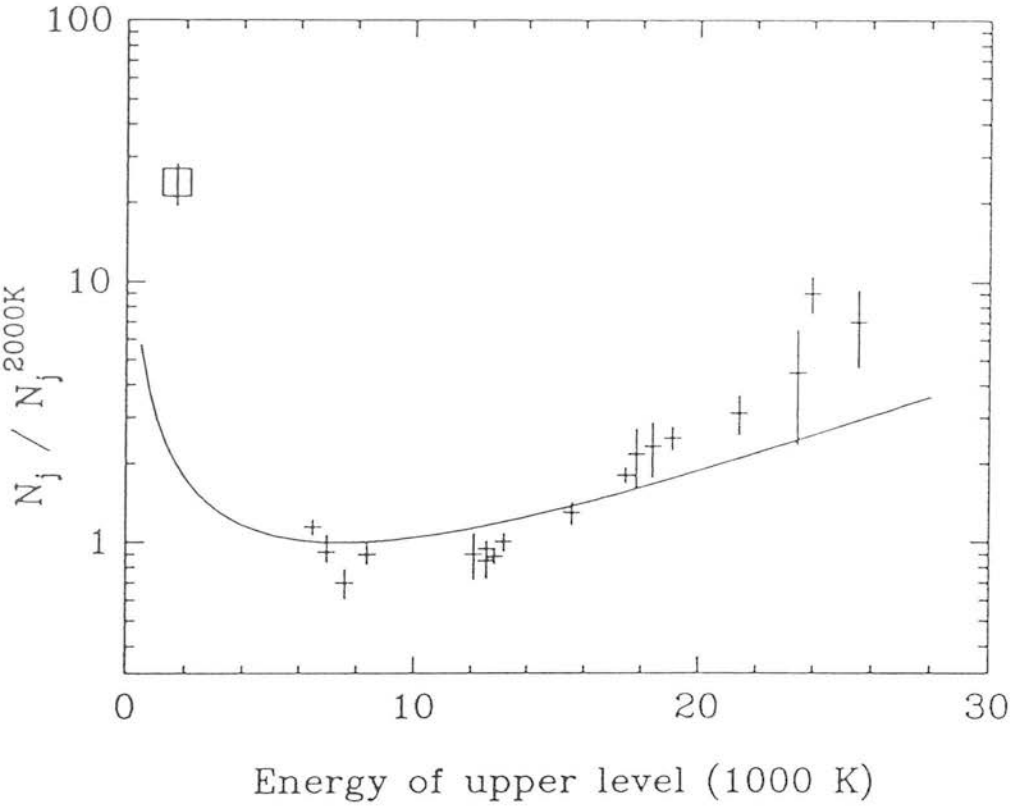

Figure 3.8: A planar C-shock with a maximum temperature = 2500 K using the approximation in section (2.5), assuming H_2 cooling dominates.

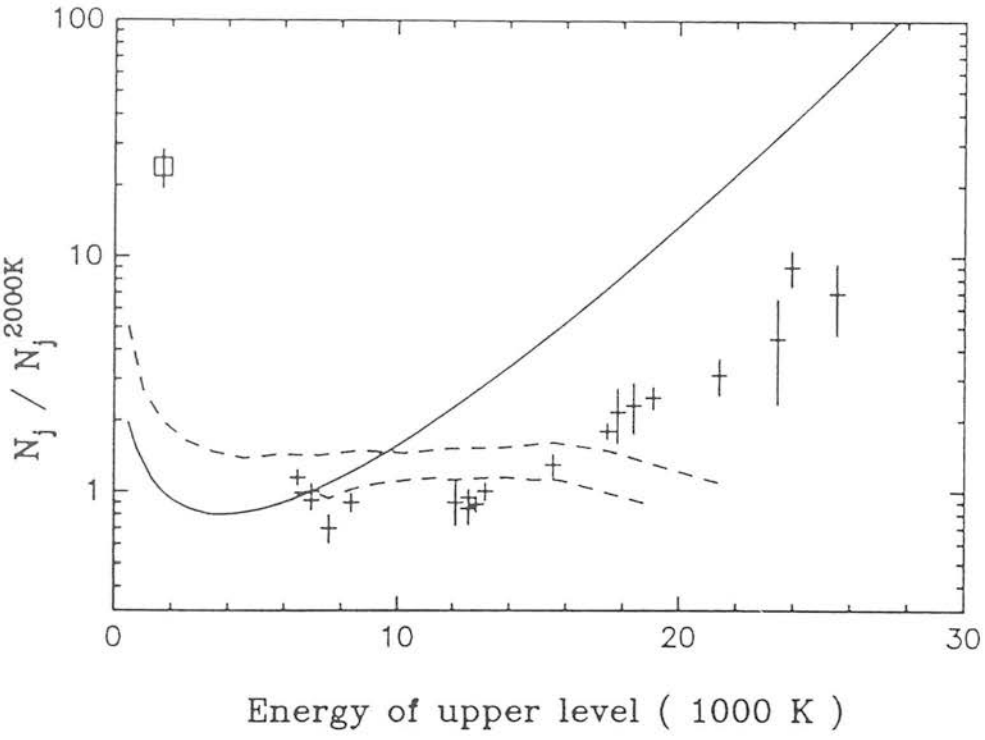

Figure 3.9: Line ratios compared with a J-type shock including significant water cooling. The H_2O cooling dominates so the shape of the curve does not depend on shock pressure

3.4.1 CO emission

In section 2.4.2 we derived the equations necessary to obtain the strengths of CO emission lines from the J-type shock model. First a word about the absolute intensities of these lines. We are attempting to model the shocked gas to be consistent with the observed H_2 intensities. So the pressure used to fit the H_2 line ratios is the one that should be used to infer CO line strengths. However, the total H_2 emission in partially dissociative shocks is velocity dependent. Higher shock velocities lead to more dissociation and subsequently less H_2 emission (although the ratios remain the same, if the *shock pressure* is constant). The CO emission is not as sensitive to the shock velocity, as CO rapidly reforms after dissociation. The model column density of the 1-0 S(1) line was normalized to the observed column density for the purpose of fitting to the column density ratios. This correction factor represents physical details of the shocked gas, such as the beam filling factor or the line of sight to the shock plane, and for the reasons stated above depends upon the velocity. This (unknown) factor is reflected as an uncertainty in predicting absolute CO column densities from the models fitted to the H_2 emission.

Combined with the above is the unknown abundance of the CO, which has two effects. One is to alter the absolute intensities. The second is more important because changing the abundance changes the relative amount of CO to H_2 cooling. As the functional forms of these two coolants is different (see section (2.3.1)) this changes the cooling function and hence the line ratios. The changed cooling curve has only a marginal effect on the resultant ratios because the shock is still forced to fit through the H_2 lines (by changing the pressure slightly). If the transition between CO/ H_2 cooling occurs at temperatures less than the H_2 emitting gas, yet still within the CO emitting gas, differences may appear between lines which arise from the CO and H_2 cooling regions.

In Fig. 3.10 we plot the observed intensities of the rotational CO lines against the rotational J-number as in Fig. 3.2. The crosses are the predicted line strengths from shocks forced to fit through the H_2 lines. The parameters found for peak 1 are then applied to the area over which the CO measurements were made (with a multiplicative factor to take into account the H_2 emission through the different beams). The model intensities were multiplied by a somewhat arbitrary number, forcing the curve to pass

through the J=21-20 transition. This factor is typically 10^{-2}. It can be seen that the model provides a poor fit to the high rotational transitions, overestimating their strength by about an order of magnitude.

Including the effect of the magnetic field (see section 2.4.4) results in the gas compression being halted when the magnetic pressure dominates over the thermal pressure. To simulate this rather than solve the full MHD equations we have used equation 2.49 for the emission from behind a Hydrodynamic J-shock and at an arbitrary temperature (related to the magnetic field strength) fixed the density to be a constant. This has a slight effect on the shape of the predicted CO curve, but does not suppress the high J transitions. This can be seen physically as follows. CO and H_2O cooling depend only on a single power of the density (as the densities are high enough for CO to be in LTE). Halting the compression will have the effect of making the lower temperature cooling slightly less efficient, but only by a factor of T_b/T (T_b is the temperature at which the magnetic pressure first dominates). As the CO energy levels are between 1000 and 3000 Kelvin ($20 < J < 34$) the line emission is produced in gas with only a small temperature difference, so only a small suppression of the high J transitions can occur.

So the problem of the strength of the CO lines remains a difficulty for theorists. Neither C-type shocks nor the J-type shocks appear able to explain the relative strengths of the CO and H_2 lines simultaneously. The discrepancy is not due to errors in the excitation rates as suggested by Draine & Roberge (1982). Recent calculations by Viscuso & Chernoff (1988) using improved calculations of the collision cross sections found, despite the changes in the particular rates, that the cooling rates and the emissivities of the lines are the same as the original calculations of Mckee *et al.* (1982). The suppression factor proposed by Draine & Roberge is not supported by these new rates.

It is possible that the CO line ratios could be due to an observational confusion. The CO line intensity observations have up until recently been exclusively centered on the BN object using large beams (30-40″) which just include Peak 1. It is quite possible that the BN/KL object is producing a strong flux of CO emission at rather low temperatures. This would produce excess emission from the mid-range ($J \ll 20$) transitions, giving the appearance that the shocked emission has weaker high J lines. The CO J=17-16 line is indeed stronger from the BN object than Peak 1 when measured with a 43″ beam

(Borieko, Betz & Zmuidzinas 1989). As the H_2 intensity is much smaller from BN than Peak 1 this difference is exaggerated in terms of the [CO 17-16/ H_2 1-0 S(1)] ratio which is approximately 0.4 at Peak 1 and 1.6 at BN, although this difference could simply be due to higher on average shock velocities around the BN region.

Of more importance are the ratios of the CO lines from these two positions. Spectra taken with smaller beams (33″) and centered on IRC2 (which is approximately 7″ south east of BN) and Peak 1 of the J=22-21 transition have been obtained by Boreiko & Betz (1989). Bearing in mind the slightly different areas of the shock emission sampled their results do suggest that the J=22-21 line is relatively stronger than the J=17-16 at peak 1 than BN. The emission spectrum from Peak 1 is possibly flatter than at the BN object, which would bring the theory into agreement with the observations. This problem will not be solved until CO line ratios centered on Peak 1 are obtained, to see if the shock models really are incorrect. Further to this higher spatial resolution observations tracing the differences that clearly exist between the morphologies of the CO and H_2 emission are needed. This is because even these moderately high-J CO lines are contaminated from ambient molecular cloud emission (the PDR) and it is not clear whether this emission arises in the shocks we have described in some detail, the so called "hot-core" or following reformation from faster dissociative shocks (i.e. Hollenbach & Mckee 1989; Neufeld & Dalgarno 1989).

3.4.2 More on the extinction

A further handle on the amount of external extinction can be derived in the following manner. If we assert that the column densities in the ratio diagram of Fig. 3.7 intrinsically follow a smooth function of the upper level energy, then the scatter in the points about a smooth function represents within the observational errors the amount that the intensities are reddened. To calculate the extinction using this method we first de-redden the data by some amount of extinction and then plot the data on the shock curve. This is illustrated in Fig. 3.11 which is the best fit J-shock, a pressure equal to 8×10^{10}K cm^{-3}, in order from (a) to (d) the extinction is increased from 0.5 to 1.1 in steps of 0.2. It can be seen that there is large scatter in the data points for extinctions at either side of this range. The value of the extinction which closely matches a smooth curve is

for a $\lambda^{-1.5}$ law an $A_K = 0.8 \pm 0.1$. This does rely on knowledge of the underlying level distribution, but, providing the gas is *collisionally excited and in LTE* the ortho/para ratio should be 3:1 and the run of N_j/g_j with T_j is a smooth function. It is comforting that the extinction derived using this technique is the same as that from the more direct method in section 3.3.1. There we used the bright lines close in energy and not the fainter ones that display the scatter most clearly in Fig. 3.11 because of their larger wavelength separation.

This new value of the extinction actually places the outflow well within the photodissociation front (i.e. Hollenbach & Mckee 1988). An extinction of 0.8 magnitudes at K corresponds to approximately 8 magnitudes visual. While this is large enough to wipe out most of the non-ionising UV photons that are responsible for heating and dissociation the conditions in Orion are extreme . This small extinction places the outflow in the photo-excited OI/CI region.

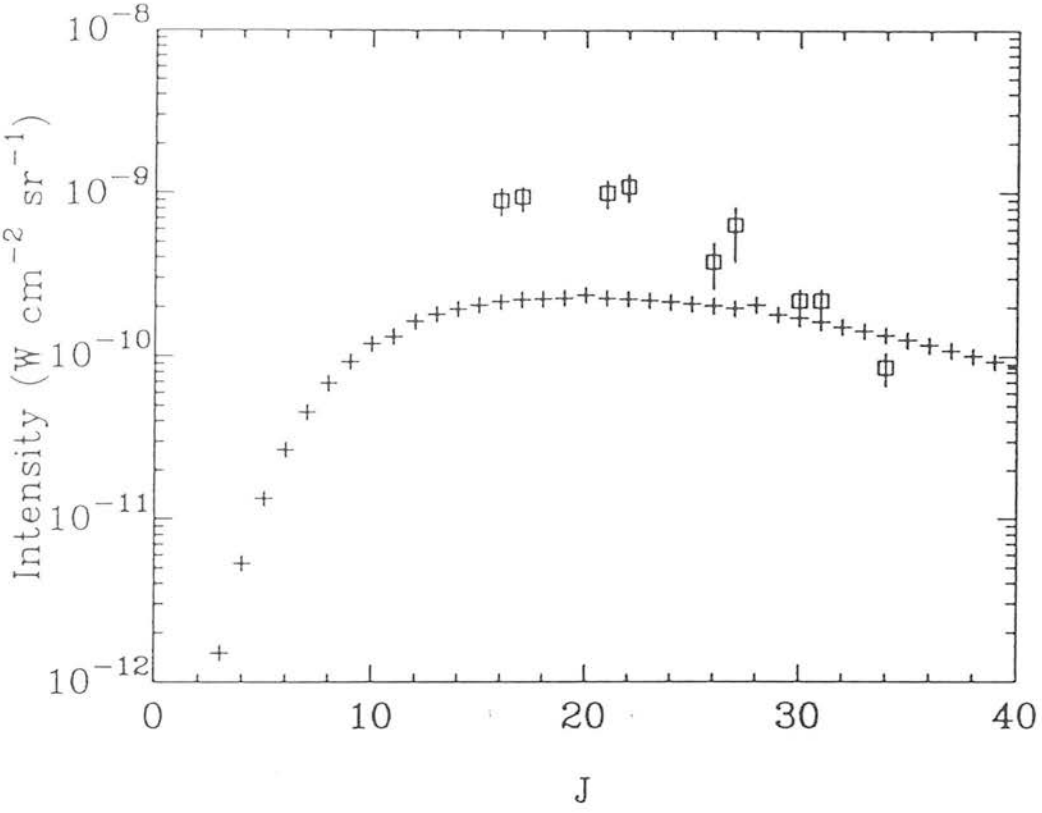

Figure 3.10: CO intensities predicted from the J-shock applied to Peak 1. Squares are all the observed points (of BN, Watson *et al.* 1983), crosses are the predictions

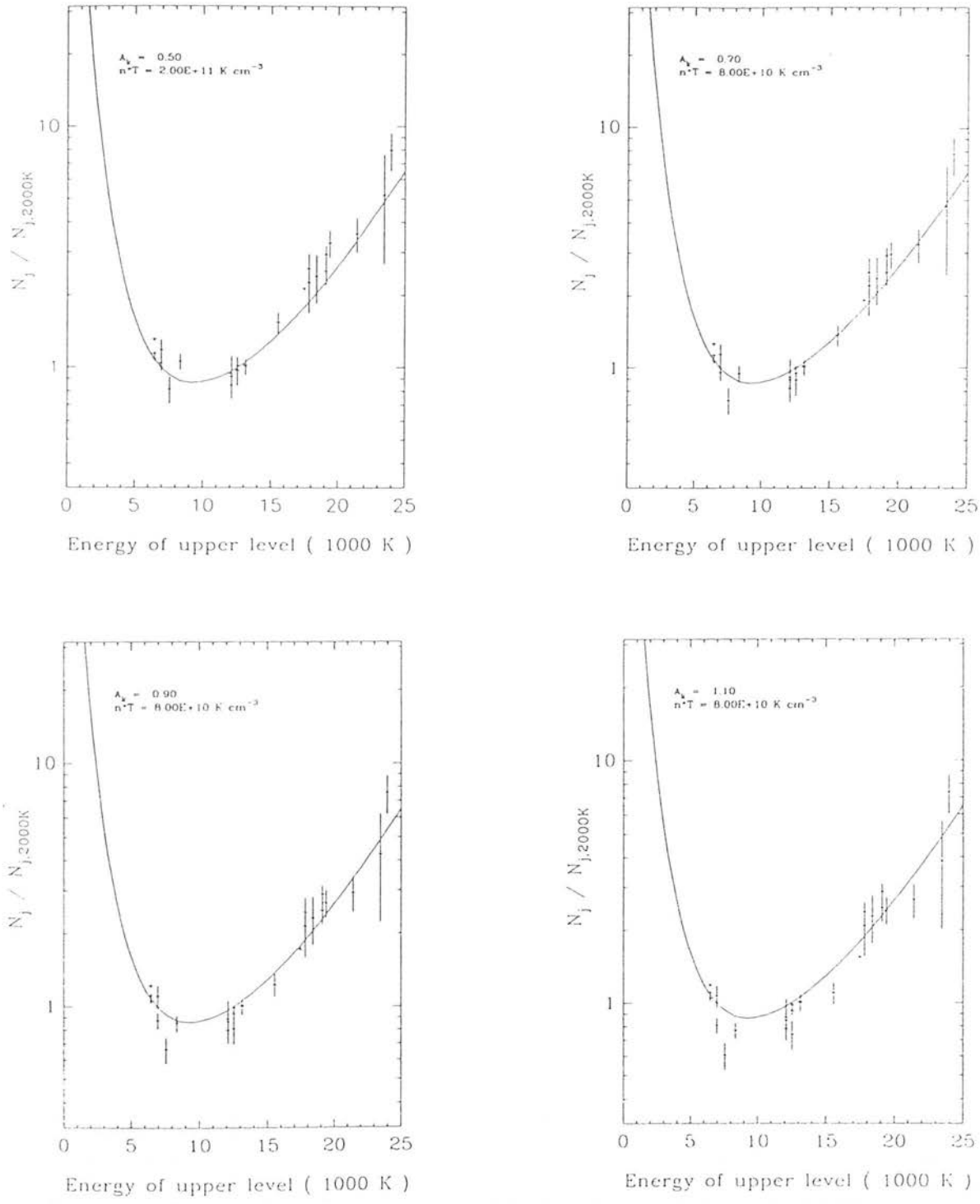

Figure 3.11: Scatter in the data introduced by varying the extinction

3.5 The state of the outflow

How does this all fit in with the global picture of the molecular cloud and the state of and origin of the outflow?

If the J-type model is correct then the high pressures that we derive at peak 1 must be the same everywhere to account for the constant [0-0 S(13)/1-0 O(7)] line ratio. The shock pressure all over the outflow is therefore equal to 8×10^{10}K cm^{-3}. Ignoring the problem of the high velocity emission and the CO rotational lines we can ask the question what can produce constant shock pressures? Probably the simplest way is if the shocks are pressure driven by a high pressure bubble which is expanding out into the surrounding cloud. If this is the case then the pressure in this bubble is approximately the same as the shock pressure. The total mass loss rate of the outflow source can now be estimated, although it should be noted that such an estimate is highly uncertain. The outflow in Orion has a radius of about 2×10^{15} m (assuming a distance of 500pc and apparent angular radius of 30″). If we further assume that the expansion velocity is of the order of the maximum velocity we see, i.e. 100 km s^{-1}. Then the mass loss rate, $\dot{M}$, is simply given by

$$\dot{M} = 4\pi R^2 P/3v \approx 2 \times 10^{20} kgs^{-1} \approx 2 \times 10^{-3}\,\mathrm{M}_{\odot} yr^{-1} \tag{3.5}$$

This is a large mass loss rate for a bipolar outflow, which typically have $\dot{M} \approx 10^{-5}\,\mathrm{M}_{\odot} yr^{-1}$ (i.e see review by Lada 1985), but is comparable with previous estimates which place the mass loss rate of IRC2 as high as $10^{-3}\,\mathrm{M}_{\odot} yr^{-1}$ (Elitzur 1982; Genzel & Downes 1982). So although the pressures needed for a J-type shock to be consistent with the line ratios are high (or equivalently high density) this is not inconsistent with the global properties of the flow estimated by other means.

The extinction is lower than previous estimates. So the luminosity of the shocked gas, and hence the total mass, is correspondingly lower. Integrating over the H_2 1-0 S(1) maps the luminosity of the shocked component in this line is $\approx 2.5\,\mathrm{L}_{\odot}$ (i.e. Garden *et al.* 1986). Assuming the total hot H_2 is given by that appropriate to J-type shocks (for which the 1-0 S(1) line contributes about $\frac{1}{15}^{th}$ of the total emission) then the luminosity

of the outflow in H_2 line emission, correcting for 0.8 magnitudes of extinction, is 80 $L_\odot$. This corresponds to a mass of the hot H_2 of about 10^{-2} $M_\odot$.

If planar J-type shocks are responsible for the emission then the heating has to be quicker than the subsequent cooling for the shock to appear J-type. This requires either very small magnetic fields, low ionisation fractions ($< 10^{-8}$) or very high ionisation fractions ($> 10^{-5}$) (see section 2.5 and Smith & Brand 1989). Inspection of Fig (2.6) reveals that $n^{1.5}/B \gtrsim 10^4$ (where is the ionisation fraction, n the H_2 number density in cm^{-3} and B the magnetic field strength in milligauss) for a J-type solution to occur. For a density of 10^6 cm^{-3} this requires $/B > 10^{-5}$. In dense molecular clouds, with high extinction, there is a lower limit to due to cosmic ray ionisation of about 10^{-7}. If was this low then the magnetic field would have to be less than 10μgauss. The strength of magnetic fields in molecular clouds is highly uncertain, but observational studies of low density clouds (i.e. Troland & Heiles 1986) and the theoretical investigation of self gravitating clouds by Mouschovias (1976) suggests that $B \approx n^{0.5}/1000$ milligauss. This gives a value of the field strength of about 1 milligauss. If this is correct the shock should be C-type.

Alternatively the magnetic field strength could be 'normal' yet the ionisation fraction may be high ($> 10^{-5}$) giving a J-type shock. The estimated extinction of 0.8 magnitudes at K (equivalent to 8 magnitudes visual) places the outflow inside the photodissociation region produced at the HII/molecular cloud edge by the trapezium stars. The ionisation fraction is thus enhanced by the photo-ionisation of atoms and molecules by photons of wavelengths longer than the Lyman limit. A detailed model of PDR's has been constructed by Tielens & Hollenbach (1985a), they found a good fit to the observations of the Orion region (Tielens & Hollenbach 1985b) for parameters close to the standard model of the first paper. For an $A_v = 8 - 10$ their results suggest that the ionisation fraction is a few times 10^{-6}, at lower extinctions this can rise to $10-5$ at $A_v < 6$ by sulfur ionisation and to a few times 10^{-4} at $A_v < 4$ due to the ionisation of atomic Carbon. The ionisation fraction thus produced in such PDR's may possibly be large enough to turn the shock J-type, although this number is highly uncertain. Interestingly these models also show that the water molecules are destroyed for $A_v < 10$. This would fit in with the J-type shock model fits which suggest that the water cooling is suppressed.

3.6 Conclusions

The H_2 line emission from Peak 1 in the Orion molecular outflow has been studied in detail spectroscopically. The spectra that we have obtained have concentrated on obtaining accurately the relative strengths of many lines spread over a large range in the energy of the upper level. This enables the temperature distribution of the gas to be studied. In summary the evidence that we have presented in this chapter suggests that the shocked H_2 line ratios at Peak 1 in Orion are consistent with those expected from the simple hydrodynamic model outlined in chapter (2), with cooling by water molecules suppressed. The shock pressures needed are large, $8{\times}10^{10}$K cm^{-3}. It is shown that planar MHD C-type shocks are inconsistent with the data. The previous published shock models that have been applied to the Orion emission (Draine & Roberge 1982; Chernoff, Hollenbach & Mckee 1982) cannot explain the large intensities of the fainter lines which come from high energy levels. The analytic approximation of Smith & Brand (1990) can produce higher temperatures, but the shape of the curve is flatter (it is close to a constant temperature) than is observed.

Collaborators involved in this work were Peter Brand, Tom Geballe, Mike Burton, Richard Wade and Mark Bird. A letter based on a large number of the observations presented here has been published in the Astrophysical Journal Letters (Brand, Moorhouse, Burton, Geballe, Bird, & Wade, 1988.).

Chapter 4

The Supernova remnant IC443

4.1 Introduction

There are many other sources of shocked molecular hydrogen emission other than the Orion molecular outflow. Unfortunately most of them are more than an order of magnitude fainter than Orion. This meant that until recent increases in detector sensitivity it was impossible to probe spectroscopically the H_2 emission from the very faint lines which are crucial to understanding the shock structure. Here we will present new observations, of the supernova remnant (SNR) IC443. The H_2 emission here is most certainly excited by shocks, an issue that is not so clear in other slightly brighter sources. IC443 then, provides another opportunity to study the shock structure in detail and in, as we shall see, a situation that has the added constraint that the driving pressure is known. Furthermore, IC443 has been observed many times in the past—being one of the few known examples of a Supernova remnant interacting with a molecular cloud. This places IC443 in the almost unique position of being an object in which the very end process of high mass star formation (a supernova) is influencing the environment that forms stars (the molecular cloud).

The previous observations have indicated that the shock here may be different from the one in Orion. Initially we will describe the present state of knowledge on the SNR/molecular cloud shock. We have decided, as for Orion, to tackle the question of the shock structure spectroscopically, concentrating on the H_2 emission lines emit-

ted by the shock. Following the presentation of the new observations the implications for the shock structure will be discussed. Lastly these new results will be discussed in terms of the global picture and energetics of IC443.

4.2 Morphology

IC443 is visible on sky survey plates as a bubble almost a degree across and contains tenuous X-ray emitting gas at a temperature of $\approx 2\times10^7$ K (Petre *et al.* 1983; Watson *et al.* 1983; Petre *et al.* 1988). A molecular cloud appears to bisect this bubble along an axis NW-SE (Cornett, Chin & Knapp 1977). The optical/X-ray emission is concentrated in two lobes either side of the molecular cloud. Cornett, Chin & Knapp (1977) argued that the molecular cloud ran in front of the face of the supernova remnant, thus obscuring the Southern part of the supernova remnant. This view was supported when it was discovered from observations of high velocity neutral atomic hydrogen (DeNoyer 1978) that the remnant is interacting with the molecular cloud. Shock excited line emission from OH and CO (DeNoyer 1979a,b) and molecular hydrogen (Treffers 1979) were subsequently discovered near to the remnant/cloud interface.

An almost complete ring of 'shocked' H_2 emission has been mapped by Burton *et al.* (1988). They suggest that this provides strong evidence that the supernova explosion occurred very close to, or possibly inside, the molecular cloud. The expansion of the remnant into the cloud has then punched a hole through the cloud, and shocks on the inside edge of this hole are propagating into the cloud, visible as the ring of H_2 emission. The Shock accelerated CO, OH, HCN, HCO^+ (White *et al.* 1987; De Noyer 1979a,b) and high velocity atomic hydrogen emission (21cm, Braun & Strom (1986)) are morphologically similar to the H_2 ring, on the rather large scales of the available resolution ($\approx 20''$), at the distance of 1500pc to IC443 (e.g. Fesen 1984) this is $\equiv$0.1pc. Figure (4.1) is a low spatial resolution ($20''$) contour map of the shocked H_2 emission (Burton *et al.* 1988). The incomplete 'ring' is clearly evident. Also note the irregular structure, suggesting an inhomogeneous source. In fact on arcsecond scales available with Infrared arrays the H_2 emission is seen to be very spotty. The H_2 emission lines are broad (up to 100 km s^{-1}) and there are large changes in the peak velocity from different positions, with no obvious systematic trend in these changes. Overall the impression is

gained of large density variations, with fast —possibly dissociative—shocks producing the atomic emission and combined with the slower shocks into the denser material the molecular emission.

Shock excitation of the H_2 in IC443 is further supported by K band spectra observed by Burton *et al.* (1989) at several of the brighter points in their H_2 map, the v=1-0 & 2-1 transitions have intensity ratios similar to those of other shocked sources (e.g. Garden *et al.* (1986), Lane & Bally (1986), Burton, Geballe & Brand (1989), Burton *et al.* (1989), Doyon & Nadeau (1988), and see Chapters (1) and (3)). Interestingly the [0-0 S(13)] to [1-0 O(7)] ratio has been found to differ in IC443 and other shocked sources (Burton *et al.* 1989), in the four sources where they looked this ratio ranged from 0.8 to 2.3. Brand *et al.* (1988) have shown that the ratio of these two lines is 1.0 all over the Orion molecular outflow (see Chapter (3)). This suggests that the shocks are of different types or have different pressures from those in Orion. In section (4.3) we will present new spectroscopy of H_2 lines from IC443, which when combined with previous observations will be used to gain some constraints on the physical state of the gas.

Far infrared observations of OI (63 μm) and CO (J=22-21, 119 μm) have recently been obtained at the (20″W,20″S) position (Burton *et al.* 1990). The CO line was not detected, but the OI emission was coarsely mapped and is consistent with the distribution of the H_2 emission. In fact the OI/ H_2 ratio does not appear to vary across the source. Burton *et al.* combined these new observations with previous measurements of H_2 and atomic hydrogen recombination lines (note that at this position only upper limits exist), and attempted to fit the emission to a variety of shock models, with the constraint of forcing the driving pressure to be equal to that in the supernova remnant.

Over 50 different model calculations were made, covering situations ranging from soft C-shocks to partially dissociative J-shocks. Tables (4.1) and (4.2) summarises the seven classes of models they ran and the best fits that they found. As can be seen from examining Table (4.2) no single model could simultaneously explain the H_2, CO and OI lines. However they found that a J-shock similar to the calculation we have presented here, with cooling from water molecules suppressed was very close to the observations. However, on theoretical grounds they argue that such a shock is not to be expected. The shock for the given parameters (of density, magnetic field strength and shock velocity)

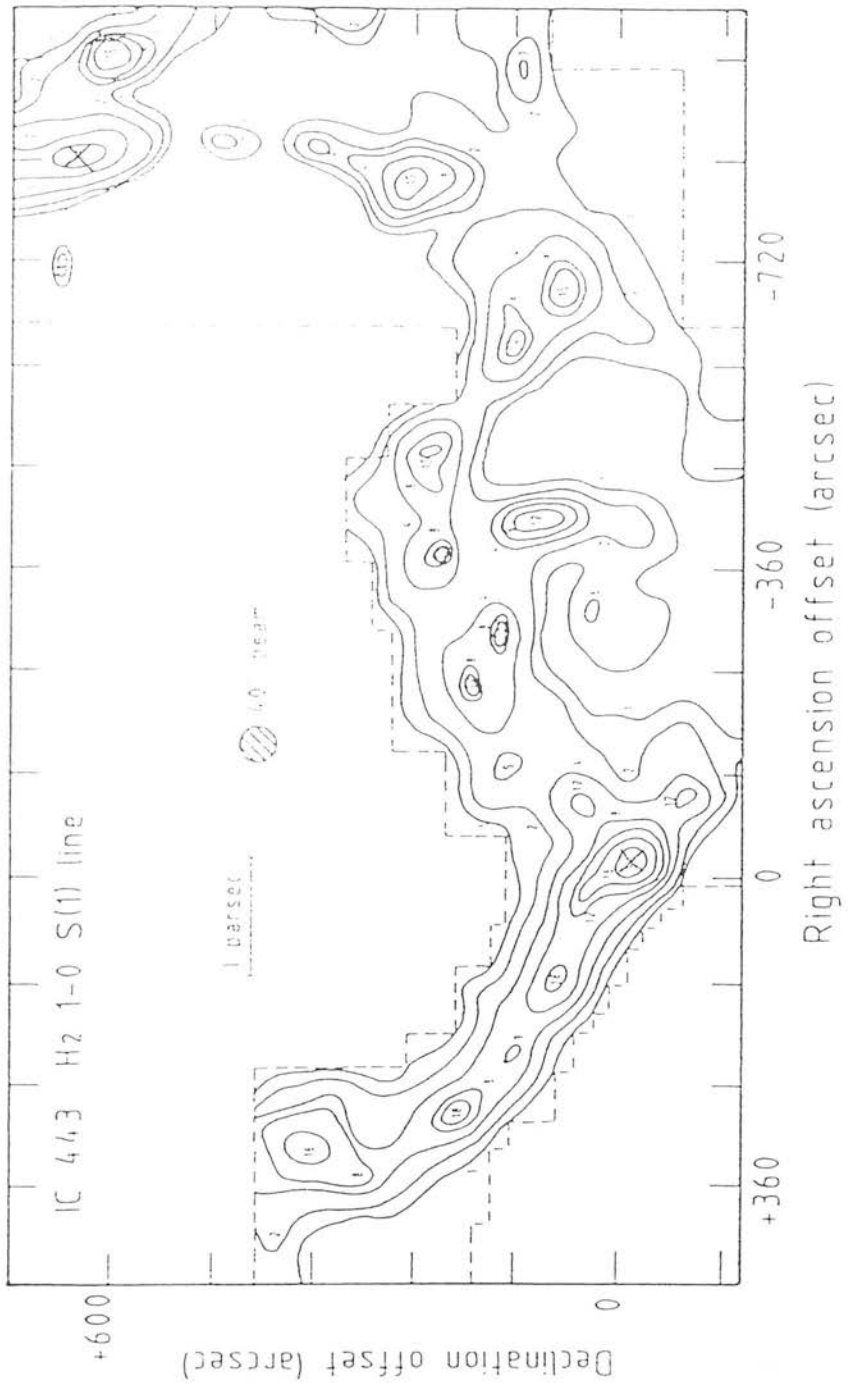

Figure 4.1: Map of H_2 v= 1-0 S(1) emission from IC443 from Burton *et al.* 1988.

should be C-type and secondly, the oxygen chemistry was artificially suppressed so as to reduce cooling from H_2O. There is no theoretical basis for either of these conditions. It was found that a superposition of many, constant pressure, C shocks with different velocities could reproduce the data, the OI being produced in slow shocks and the faster shocks providing the H_2 emission. This seems, however to be at variance with a constant OI/ H_2 ratio. The same number of low and high velocity shocks would be needed at every point in the shock.

4.3 Observations

The observations presented here were all made at the (UKIRT). Several observations over a period of time were made at the two brightest positions in the molecular ring and these are indicated by crosses in fig (4.1) . The coordinates quoted in table (4.3) are offsets from an arbitrary zero position with R.A. = 6^h 14^m 43.0^s, Dec. = 22^o $23'$ $0.0''$ (1950).

On the nights of the 20^{th} and 21^{st} February 1989 spectra were obtained using the cooled grating spectrometer CGS2 at a resolving power of $\approx$ 600 and an aperture size of $5''$, chopping $90''$ E-W (Figs.4.1–4.4). Flux calibration was achieved using the standard stars BS3314 (K=3.94) and BS1552 (K=4.07). Each spectrum was over-sampled by a factor of three or four. Tables 4.4 and 4.5 provides the line intensities. Additional data for both positions are include in tables 4.4 and 4.5 which simultaneously measured some of the bright 2 and 3 μm lines. Part of this data (the 3 μm lines) has already been published elsewhere (Burton *et al.* 1989), and was obtained on the nights of the 6^{th} and 7^{th} january 1987, again using CGS2 but with a lower spectral resolution of $\approx$ 300, the beam size was again $5''$. This data is displayed in Figs. 4.5 and 4.8.

Much lower resolution spectra obtained using a circular variable filter (resolution $\approx$ 0.018 μm) in conjunction with the InSb photometer UKT9 were obtained between the 6^{th} and 9^{th} of January 1986. The beam size for these observations was $19''$. Two spectra, one covering the K window and a second running from H to K were taken. The K window spectrum has been published by Burton *et al.* (1989) and that covering H and K by Burton (1987). These spectra are shown in Figs. 4.6, 4.7 and 4.9. Several of the line

Table 4.1: Physical parameters of the classes of shock models fitted to the IC443 emission by Burton *et al.* (1990).

Shock Parameters	Model A[a]	Model B[b]	Model C[b]	Model D[c]	Model E[c]	Model F[c]	Model G[d]
Type	'Fast' J	'Slow' J	'Slow' J	'Slow' C	'Fast' C	'Fast' C	'Fast' C
Speed (km/s)	100	10	10	10	40	40	25
Pre-shock Density (cm^{-3})	10^3	10^5	10^5	10^5	10^4	10^4	10^6
Pressure (cm^{-3} $(km/s)^2$)	10^7	10^7	10^7	10^7	1.3×10^7	1.6×10^7	6.3×10^8
$B_{0.1}$[e] (μG)	10	100	100	316	100	100	1000
Ionization[f] Fraction	-	-	-	$\leq 10^{-6.5}$	$\leq 10^{-6.5}$	$\leq 10^{-6.5}$	$\leq 10^{-6.5}$
Area Filling Factor	2	4	4	2	4	4	1
∂(C)	0.62	0.62	0.62	0.25	0.25	0.25	0.20
∂(O)	0.80	0.80	0.80	0.50	0.50	0.50	0.56
∂(Si)	0.10	0.10	0.10	0.03	0.03	0.03	-
∂(Fe)	0.04	0.04	0.04	0.03	0.03	0.03	-
Other			O Chemistry suppressed			O Chemistry suppressed	

Table 4.2: Results of the shock models in Table (3.1), from Burton *et al.* (1990).

Line	Observed	A 'Fast J'	B 'Slow J'	C 'Slow J'	D 'Slow C'	E 'Fast C'	F 'Fast C'	G 'Fast C'
H_2 1-0 S(1)	3.5(-4)	3.6(-5)	5.3(-4)	6.9(-4)	<1(-10)	3.6(-3)	3.6(-3)	3(-3)
	2.2(-3)[a]							
H_2 2-1 S(1)	2.6(-5)	1.7(-5)	4.3(-5)	4.1(-5)	<1(-10)	3.2(-4)	3.2(-4)	1(-4)
	1.6(-4)[a]							
H_2 0-0 S(2)		1.0(-6)	4.5(-5)	1.1(-4)	4.2(-5)	3.8(-3)	3.8(-3)	2(-3)
H_2 0-0 S(13)	2.7(-5)	3.8(-6)	1.7(-5)	1.9(-5)	<1(-10)	not available		1(-5)
	7.0(-5)[a]							
H_2 Total		2.6(-4)	1.0(-2)	1.4(-2)	6.4(-4)	1.4(-1)	1.4(-1)	1.4(-1)
CO J=22-21	<2.5(-4)	2.4(-8)	1.6(-4)	3.4(-4)	1.7(-8)	3.8(-5)	3.8(-5)	2(-3)
CO Total		2.2(-5)	3.2(-3)	6.5(-3)	1.2(-3)	2.5(-3)	2.5(-3)	1.4(-2)
H_2O Total		6.0(-7)	1.0(-2)	5.3(-7)	7.2(-4)	2.3(-2)	<1(-6)	1.3(0)
OH Total		1.7(-6)	1.2(-5)	3.2(-9)	2.6(-6)	5.2(-4)	<1(-6)	4.3(-3)
Br γ	<2.8(-5)	4.0(-5)	<1(-10)	1.2(-14)	<1(-10)	<1(-10)	<1(-10)	<1(-10)
H51 α	<7.5(-10)	3.4(-11)	<1(-14)	<1(-14)	<1(-14)	<1(-14)	<1(-14)	<1(-14)
[OI] 63μm	2.9(-3)	3.0(-3)	2.1(-7)	2.9(-3)	2.2(-3)	8.2(-5)	~2(-3)	3(-3)
[OI] 145μm		9.0(-5)	6.8(-9)	7.2(-5)	6.8(-4)	4.8(-6)	~1(-4)	1(-4)
[CI] 370μm		4.2(-5)	1.4(-12)	3.1(-10)	1.4(-4)	5.2(-6)	5.2(-6)	3(-4)
[CI] 609μm		7.4(-6)	2.0(-13)	5.2(-11)	1.4(-5)	6.4(-7)	6.4(-7)	1(-5)
[CII] 158μm		3.2(-4)	<1(-10)	2.9(-10)	<1(-10)	<1(-10)	<1(-10)	<1(-10)
[NeII] 12.8μm		6.6(-4)	<1(-10)	<1(-10)	<1(-10)	<1(-10)	<1(-10)	<1(-10)
[SiII] 35μm	<1.9(-4)	2.0(-4)	<1(-6)	<1(-6)	<1(-6)	<1(-6)	<1(-6)	<1(-6)
[FeII] 26μm		1.8(-4)	<1(-6)	<1(-6)	<1(-6)	<1(-6)	<1(-6)	<1(-6)
Grain 60μm		1.2(-1)[e]	4(-4)[f]	4(-4)[f]	-	-	-	-
Grain 100μm		6(-2)[e]	2(-4)[f]	2(-4)[f]	-	-	-	-
IRAS 60μm[b]	~8(-3)[d]	1.2(-1)	4(-3)	4(-3)	3(-3)	9(-3)	≤2(-3)	5(-1)
IRAS 100μm[c]	~4(-3)[d]	6(-2)	3(-3)	2(-3)	2(-4)	4(-3)	8(-4)	2(-1)

intensities obtained are inaccurate due both to the difficulty of calibrating emission lines close to telluric absorption features and also blends, due to the relatively low spectral resolution. Any lines which are close to such features have subsequently been excluded from the analysis. Integration times and further details are given in table (4.3).

4.4 Results

The spectra at the two locations in IC443 are shown in Figs. (4.1)— (4.8). The spectra at (844″W,635″N) obtained on the 21 February 1989 (Fig (4.3)) were degraded badly by cirrus and should be regarded with some caution. The ten individual spectra at this position were scaled to the maximum observed intensity of the 1-0 S(0) line before co-addition. This increased the signal to noise on the lines when compared with the straight coadd, but the line intensities obtained should be regarded as preliminary until further observations can be obtained. Weather conditions were good when the (20W,20S) spectra were measured.

The H_2 line intensities and derived column densities are given in tables (4.1) and (4.2). The line intensities were estimated by least square fitting of Gaussian profiles to the data as explained in section 3.2. The solid lines in figs. (4.2) and (4.3) are the gaussian fits to the emission lines. Uncertainties are dominated by the accuracy of the observations. There is also a systematic percentage error of about 10 percent in the absolute column densities because of the uncertainty in the beam size.

It is apparent from Figs (4.2) and (4.3) and from Tables (4.1) and (4.2) that the intensities of the high excitation 3-2 lines relative to those of the stronger 2-1 and 1-0 lines are considerably different at the two locations in IC443. The ratio [3-2 S(3)]/[1-0 S(0)] is 0.13 $\pm$ 0.02 at (20W,20S), but 0.05 $\pm$ 0.02 at (844W,635N). Burton *et al.* (1989a) found that the intensity ratio [1-0 O(7)]/[0-0 S(13)] was considerably different at these two positions; their measurements and derived column densities are also included in Tables (4.2) and (4.3).

Burton *et al.* (1988) argued that the extinction to IC443 was similar to that towards Peak 1 of the Orion molecular outflow. This was based on their observation that the

Table 4.3: Journal of observations

Date observed	Wavelength range μm	Integration time (s)[1]	Calibrating star	Resolution microns	Aperture arcseconds
20″W 20″S					
20 Feb 89	1.7–2.5	3000	BS3314	0.0033	5
21 Feb 89	2.2–2.25	3600	BS1552	0.0033	5
6 Jan 87	2.1–3.8	10000	BS2821	0.0098–0.0069	5
6-8 Jan 86	K band	1800	BS3188	0.018	19.6
6-8 Jan 86	H–K bands	2800	BS3188	0.018	19.6
844″W 635″N					
21 Feb 89	2.2–2.25	4800	BS3314	0.0033	5
7 Jan 87	2.1–3.8	5000	BS2821	0.0098–0.0069	5
7 Jan 86	K band	2300	BS3188	0.018	19.6

Note: 1. Total integration, includes time spent on/off source.

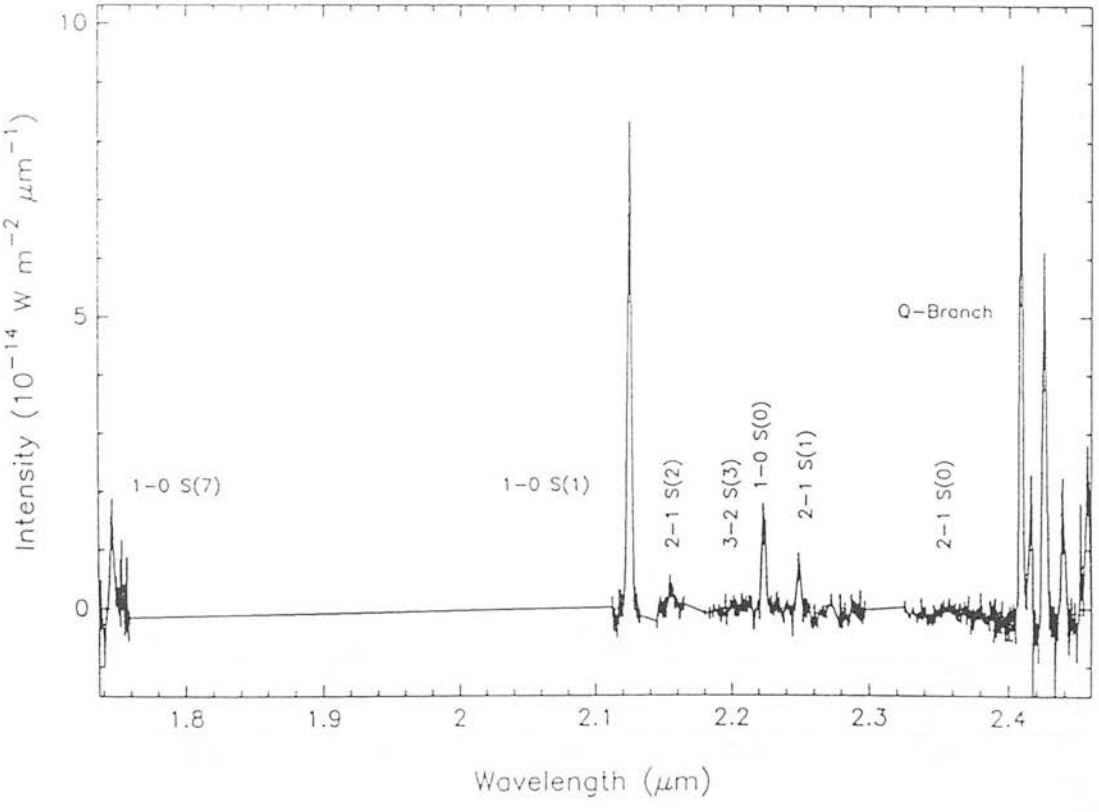

Figure 4.2: Spectra of the H_2 emission lines at the (20″W,20″S) position. Labels indicate the lines visible in the spectra, error bars are 1 sigma.

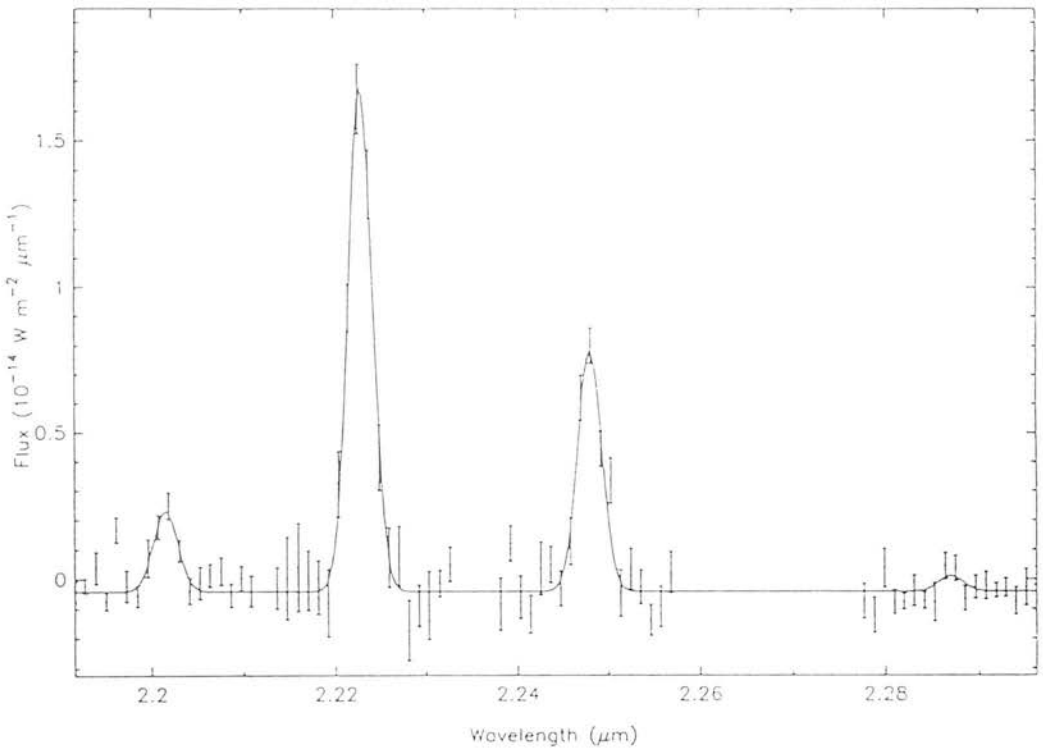

Figure 4.3: A deeper Spectrum than fig. (3.1), detecting the 3-2 S(3), 1-0 S(0), 2-1 S(1) and 3-2 S(2) lines (in wavelength order. The solid line is the gaussian fits to the data points. Flux density is that in the 5″ beam.

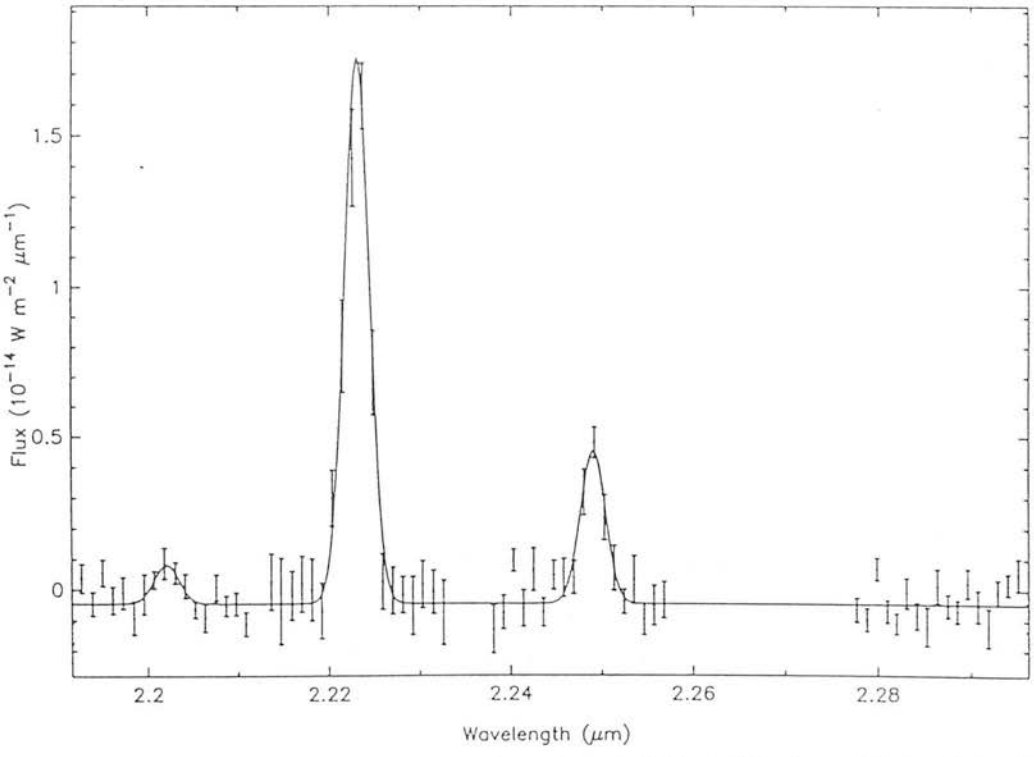

Figure 4.4: Same as in fig. (3.2) except for the 844″W 635″N data. Note that the 3-2 S(2) line is not detected.

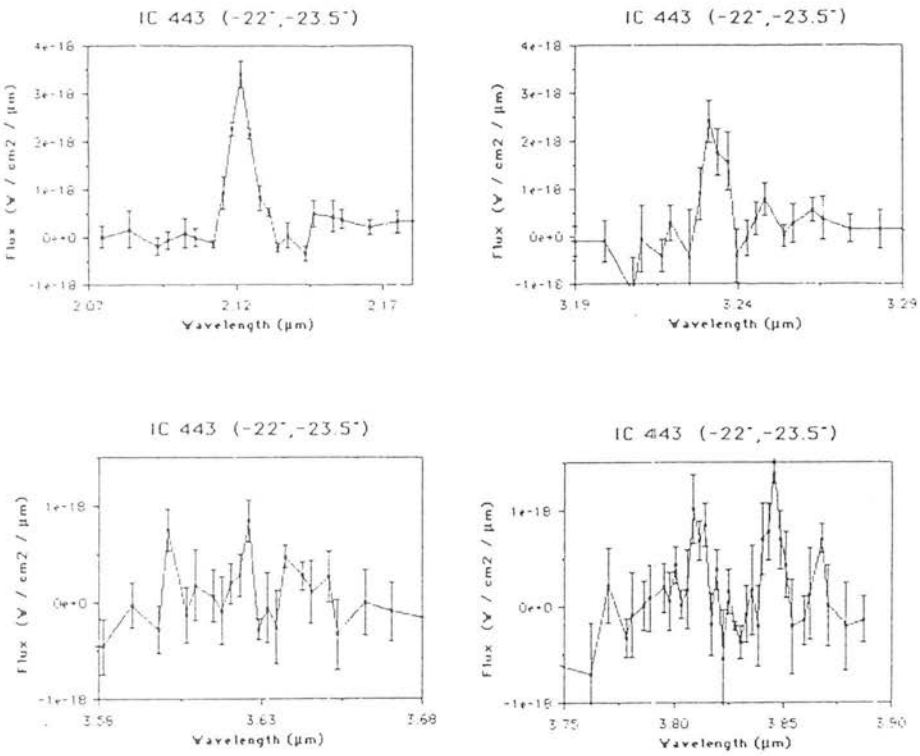

Figure 4.5: CGS2 spectra obtained during January 1987, at (22″W, 23″S). (a) 1-0 S(1), (b) 1-0 O(5), (c) 1-0 O(7) & 0-0 S(13) and (d) 0-0 S(15). The O(7)+S(13) spectrum (c) has been published by Burton *et al.* (1988)

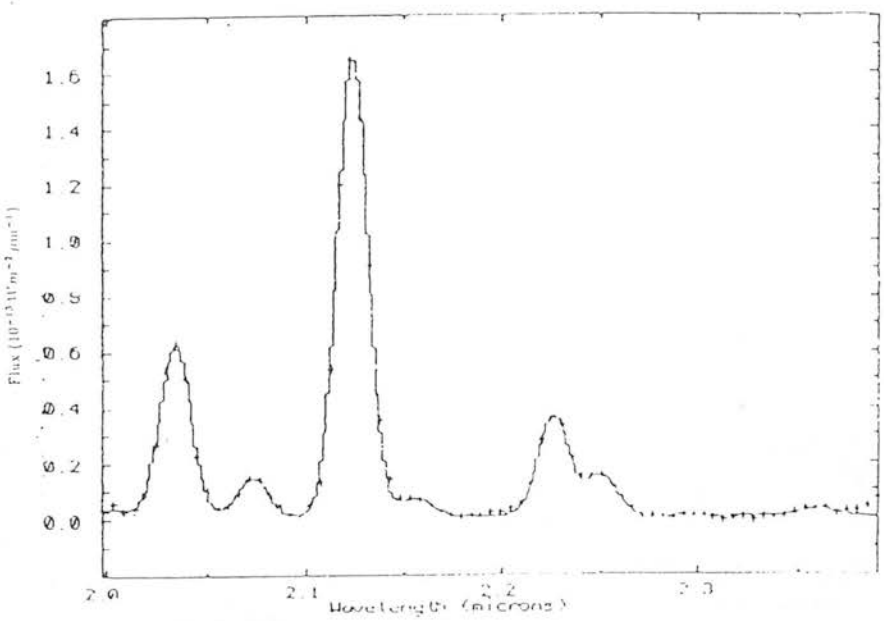

Figure 4.6: CVF spectra at (25″W, 22″S) obtained in January 1986 with a 19.6″ beam

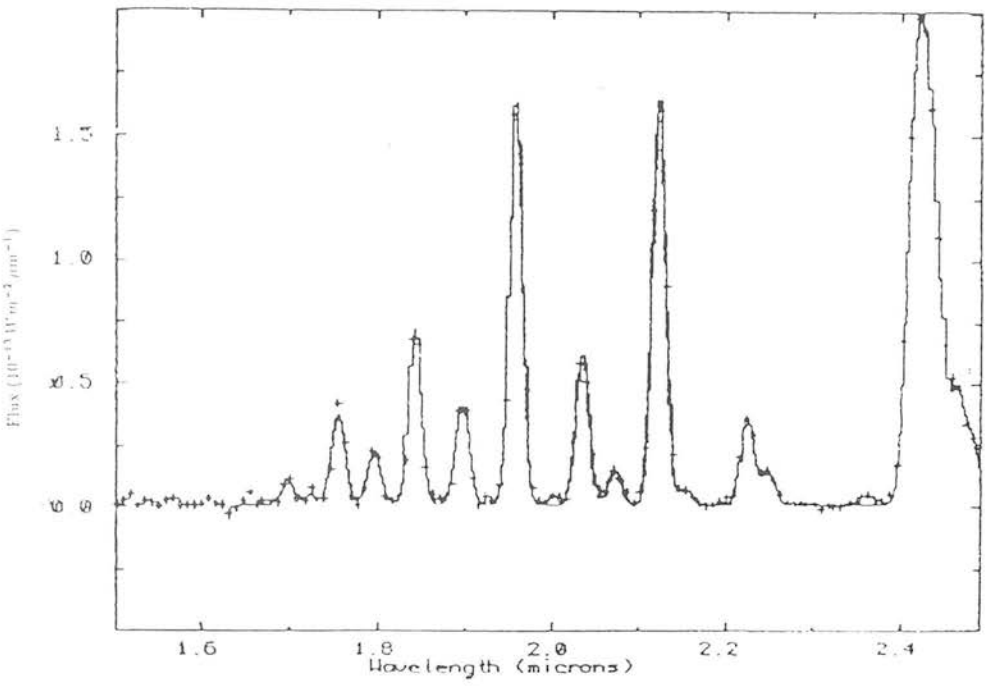

Figure 4.7: Similar to Fig. (3.5) but covering both H and K bands

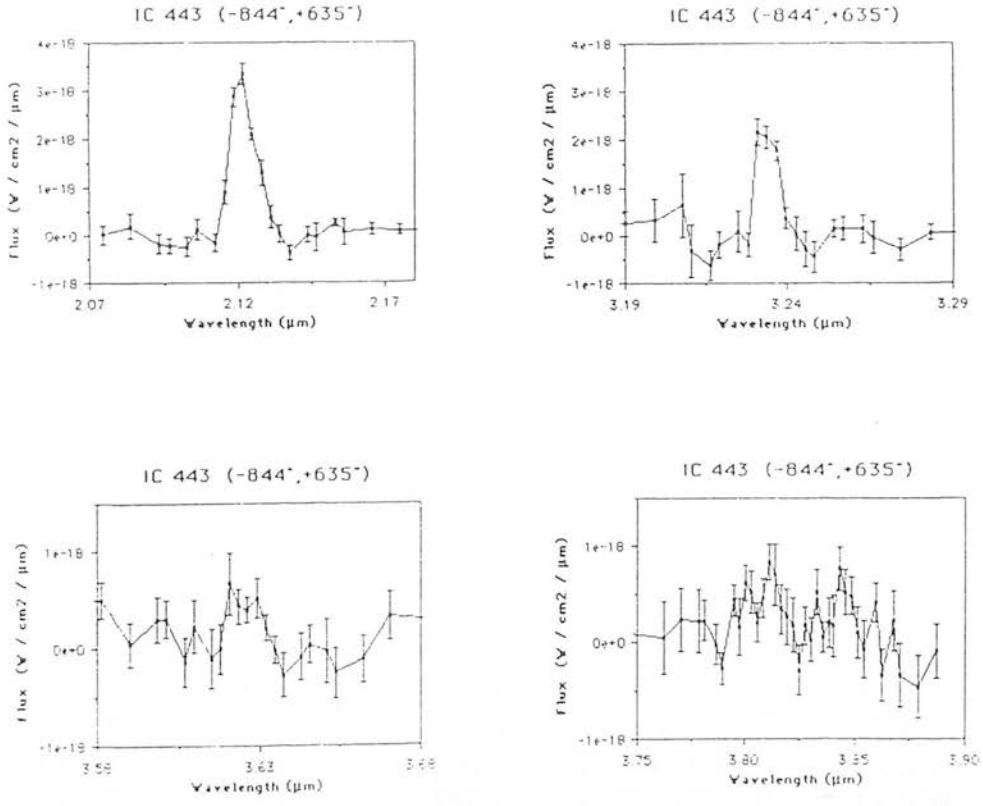

Figure 4.8: CGS2 spectra obtained during January 1987, at (844″W, 635″S). (a) 1-0 S(1), (b) 1-0 O(5), (c) 1-0 O(7) & 0-0 S(13) and (d) 0-0 S(15). The O(7)+S(13) spectrum (c) has been published by Burton *et al.* (1988)

Table 4.4: **Intensities and column densities for the (20″W 20″S) position**

Line	Wavelength[1] (microns)	Energy[1] of upper level (K)	Intensity[2]	Column density N_j/g_j $10^{18}m^{-2}$
Febuary 1989 (5″ beam)				
1-0 S(7)	1.7474	12817	5.8 ±0.4	0.82 ± 0.06
1-0 S(1)	2.1218	6951	28.0 ±0.8	11.18 ± 0.32
2-1 S(2)	2.1535	13150	1.03 ±0.09	0.60 ± 0.05
3-2 S(3)	2.2014	19084	0.81 ±0.12	0.13 ± 0.02
1-0 S(0)	2.2235	6471	6.05 ±0.42	14.6 ± 1.0
2-1 S(1)	2.2474	12550	2.73 ±0.18	0.80 ± 0.05
3-2 S(2)	2.2872	18386	0.16 ±0.08	0.10 ± 0.04
1-0 Q(1)	2.4060	6149	23.5 ±2.0	20.4 ± 1.7
1-0 Q(2)	2.4135	6471	7.2 ±0.4	15.7 ± 1.5
1-0 Q(3)	2.4235	6951	20.3 ±0.8	11.6 ± 0.5
1-0 Q(4)	2.4375	7584	5.6 ±0.3	7.8 ± 0.4
January 1987 (5″ beam)				
1-0 S(1)	2.1218	6951	31.66 ±1.28	12.6 ±0.5
1-0 O(5)	3.2350	6951	18.19 ±2.40	18.4 ±2.4
1-0 O(7)	3.8077	8365	5.38 ±0.76	8.0 ±1.1
0-0 S(13)	3.8464	17444	9.80 ±0.76	0.34 ±0.03
0-0 S(15)	3.736	21294	3.77 ±1.54	0.08 ±0.03
January 1986 (K band) (19″ beam)				
1-0 S(1)	2.1218	6951	322.9 ±3.15	8.39± 0.08
1-0 S(0)	2.2235	6471	70.06 ±3.15	10.99± 0.49
2-1 S(0)	2.3556	12094	5.16 ±3.15	0.59± 0.36
2-1 S(1)	2.2474	12550	27.70 ±3.15	0.53± 0.06
2-1 S(2)	2.1535	13150	12.58 ±3.15	0.48± 0.12
January 1986 (H & K bands) (19″ beam)				
1-0 S(1)	2.1218	6951	321.0 ±2.5	8.34± 0.07
1-0 S(0)	2.2235	6471	71.5 ±2.5	11.21± 0.39
1-0 S(6)	1.7880	11521	41.7 ±5.5	1.11± 0.15
1-0 S(7)	1.7474	12817	72.2 ±5.5	0.66± 0.05
1-0 S(8)	1.7147	14220	8.3 ±5.5	0.26± 0.17
1-0 S(9)	1.6877	15721	18.6 ±5.5	0.24± 0.07
1-0 S(10)	1.6665	17310	<5.5[3]	<0.3[3]
1-0 S(11)	1.6504	18979	<5.5[3]	<0.2[3]
2-1 S(0)	2.3556	12095	9.3 ±2.5	1.06± 0.28
2-1 S(1)	2.2477	12550	26.7 ±2.5	0.51± 0.05
2-1 S(2)	2.1535	13150	12.7 ±2.5	0.48± 0.10

1. Calculated from energy levels of Dabrowski (1984).
2. Units of 10^{-17} W m^{-2} $beam^{-1}$.
3. 3 sigma upper limits

relative strength of the total 1-0 Q-branch emission (observed at low spectral resolution) was similar in both sources. The extinction to the Orion molecular outflow is not well known, but the observations of chapter (3) indicate a value of 0.8 magnitudes at K.

Following the method outlined in section 3.3.1 the extinction can be estimated from ratios of lines which are transitions from a common upper energy level or bright lines very close in energy with a large wavelength base. There are several such line pairs that we have observed. At both positions the combinations of 1-0 S(1), 1-0 O(5) and 1-0 O(7) can be used, and at (20W,20S) the S(1)/Q(3) and S(0)/Q(2). We assume an extinction law of $A \propto \lambda^{-1.5}$, and the extinction estimates at K thus derived are shown in table (4.6). There is some scatter in the results, but the averages are for the (20″W,20″S) $A_K = 0.7 \pm 0.3$ and at (844″W,635″N) $A_k = 0.4 \pm 0.4$. These are very similar values, and we will assume an average extinction to IC443 of 0.6 magnitudes. This is similar to the Orion extinction and so is not inconsistent with Burton *et al.* (1988). This lower extinction will reduce the total luminosity from the shocked H_2 gas.

Table 4.5: **Intensities and column densities for (844″W 635″N) position**

Line	Wavelength[1] (microns)	Energy[1] of upper level (K)	Intensity[2]	Column density N_j/g_j $10^{18}m^{-2}$
Febuary 1989 (5″ beam)				
3-2 S(3)	2.2014	19084	0.30± 0.08	0.049± 0.013
1-0 S(0)	2.2235	6471	5.78± 0.30	13.93 ± 0.72
2-1 S(1)	2.2474	12550	1.58± 0.14	0.47 ± 0.04
3-2 S(2)	2.2872	18000	< 0.1[3]	< 0.06[3]
January 1987 (5″ beam)				
1-0 S(1)	2.1218	6951	34.98 ±1.19	13.96± 0.5
1-0 O(5)	3.2350	6951	17.81 ±1.66	18.0 ± 1.7
1-0 O(7)	3.8075	8365	5.98 ±1.26	8.9 ± 1.9
0-0 S(13)	3.8464	17443	4.81 ±1.26	0.17± 0.04
0-0 S(15)	3.736	21294	4.11 ±1.26	0.08± 0.03
January 1986 (19″ beam)				
1-0 S(1)	2.1218	6951	227.7 ±2.3	5.92± 0.06
1-0 S(0)	2.2235	6471	51.4 ±2.3	8.07± 0.37
2-1 S(0)	2.3556	12094	3.0 ±2.3	0.34± 0.27
2-1 S(1)	2.2474	12550	18.5 ±2.3	0.35± 0.05
2-1 S(2)	2.1535	13150	7.0 ±2.3	0.27± 0.09

1. Calculated from energy levels of Dabrowski (1984).
2. Units of 10^{-17} W m^{-2} $beam^{-1}$.
3. 3 sigma upper limits

Table 4.6: **Extinction estimates**

position	Line pair	A_K (magnitudes)[1]
20″W 20″S	1-0 O(5) / 1-0 S(1)	0.9 ±0.3
	1-0 Q(3) / 1-0 S(1)	0.2 ±0.3
	1-0 Q(2) / 1-0 S(0)	0.8 ±1.1
	1-0 S(1)/ 1-0 O(7)	0.9 ±0.3[2]
844″W 635″N	1-0 O(5) / 1-0 S(1)	0.6 ±0.3
	1-0 S(1)/ 1-0 O(7)	0.4 ±0.4[2]

1. Assuming A$\propto \lambda^{-1.5}$
2. For an excitation temperature = 2000K

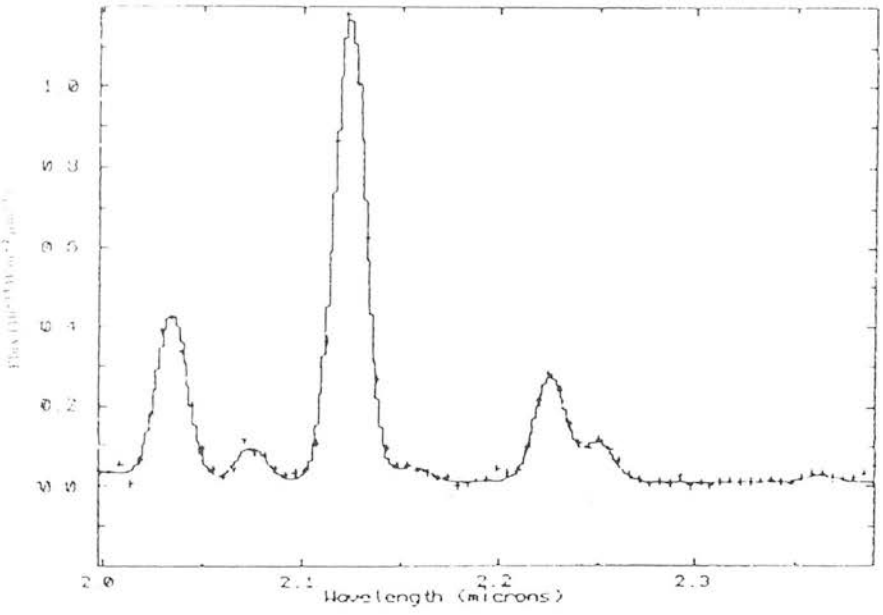

Figure 4.9: K-band CVF spectra at (846″W, 637″S) obtained during January 1986 with a 19.6″ beam

4.5 Model fits

Interestingly the S(13) to O(7) ratio has been found to differ in other shocked sources (Burton *et al.* 1989). In the four sources where they looked it ranged from 0.8 to 2.3. This variation initially seemed to pose a difficulty for the J-type shocks, and it was postulated that different velocity C-type shocks leading to different temperatures may be the cause of the variation. However, as we have already seen in Chapter (2) J-type shocks in molecular gas are actually dependant on the pressure of the gas which regulates the relative amounts of dissociational and radiative cooling. The data we have presented in the last section are of the two brightest positions, and are the two locations where the S(13)/O(7) ratio was measured to be 0.84 and 1.9 by Burton *et al.* (1989). We next apply the J-type shock model to this column density data and it is shown to provide a very good fit simultaneously to both the 2 μm and the 3.8 μm data.

The dereddened column density ratios are plotted in Figs. 4.10 and 4.11, ratioed again with a 2000K boltzmann slab, to highlight the temperature changes. It is apparent that a single temperature is a bad representation of the data, and as in Orion there is a smooth increase in excitation temperature with upper energy level. Note also that the temperatures of the highly excited lines are different from those in Orion, being relatively stronger at the (20″W,20″S) and weaker at the (844″W,635″N) positions.

The solid curves in Figs. 4.10 and 4.11 are the result of the J-shock model fits. Again there are only two free parameters, the absolute intensity of the shocked lines (dependent on the angle of sight through the post shock layer and beam filling factor) and the pressure. The first of these is fixed by forcing the absolute intensity to fit the bright 1-0 S(1) or S(0) line, the pressure is then varied to fit the relative intensities of the other lines to the 1-0 S(1). The simple J-shock is consistent with both the new 2 μm data and the 3 μm data of Burton *et al.* (1989) at both positions, thus offering an explanation for the 'odd' S(13) to O(7) ratios, with driving pressures of 2×10^{10} K cm^{-3} and 6×10^{11} K cm^{-3} at (20″W,20″S) and (844″W,635″N) respectively. The model predictions for the absolute intensities were multiplied by about 10^{-2} at both (20″W,20″S) and (844″W,635″N) to fit the model curve through the 1-0 S(1) line. J-type shocks can thus successfully account for both the line ratios and the absolute intensities (assuming the beam is not filled).

The dashed curves in Figs 4.10 and 4.11 are the results of the C-shock approximation explained and employed in Chapters (2) and (3). As expected the planar C-type shocks are very poor fits to the data points.

The hot gas in the SNR has been presumed to be driving the shock wave into the molecular cloud. From X-ray and optical observations the pressure of the SNR is in the range 10^7—10^9 K cm^{-3} (Burton *et al.* 1988, and references therein) and is more likely to be in the middle of this range (Petre *et al.* 1988). The thermal pressure in the post shock gas should be very close to this driving pressure. However, the pressures derived for the shocked H_2 gas are larger, for the (20″W 20″S) position the pressure needed is 2×10^{10} K cm^{-3} and at the (844″W,635″S) position the pressure is even greater at 6.0×10^{11} K cm^{-3} . In section (4.5.1) we will examine possible mechanisms that could produce an apparent pressure enhancement. Again for the reasons stated in chapter (3) it is worth noting that even if a collection of many C-type shocks could be made to fit the data the pressure needed to explain the observed highly excited lines would still be high, because of the large critical density (10^6 cm^{-3}) and temperatures needed to populate the highly excited energy levels.

Rotational CO line emission can be calculated using the equations developed in Chapter (2). We have already discussed in Chapter (3) the uncertainties in predicting CO line intensities by extrapolating from the parameters used in fitting to the H_2 lines. The total H_2 emission in partially dissociative shocks is velocity dependant, higher shock velocities lead to more dissociation and subsequently less H_2 emission (although the ratios remain the same, for constant pressure). The model column density of the 1-0 S(1) line was normalized to the observed column density for the purpose of fitting to the column density ratios. This correction factor represents physical details of the shocked gas, such as the beam filling factor or the line of sight to the shock plane, and for the reasons stated above depends upon the velocity. This (unknown) factor is reflected as an uncertainty in predicting absolute CO column densities.

The CO (J=22-21) upper limit (Burton *et al.* 1990) of 2.5×10^{-7} W m^{-2} sr^{-1} at the (20″W,20″S) position was obtained with a beam size of 45″. In order to extrapolate CO predictions from the H_2 shock we need to correct for the different filling factors of the 45″ and 20″ beams (the aperture for the 1986 measurements). Averaging over the contours

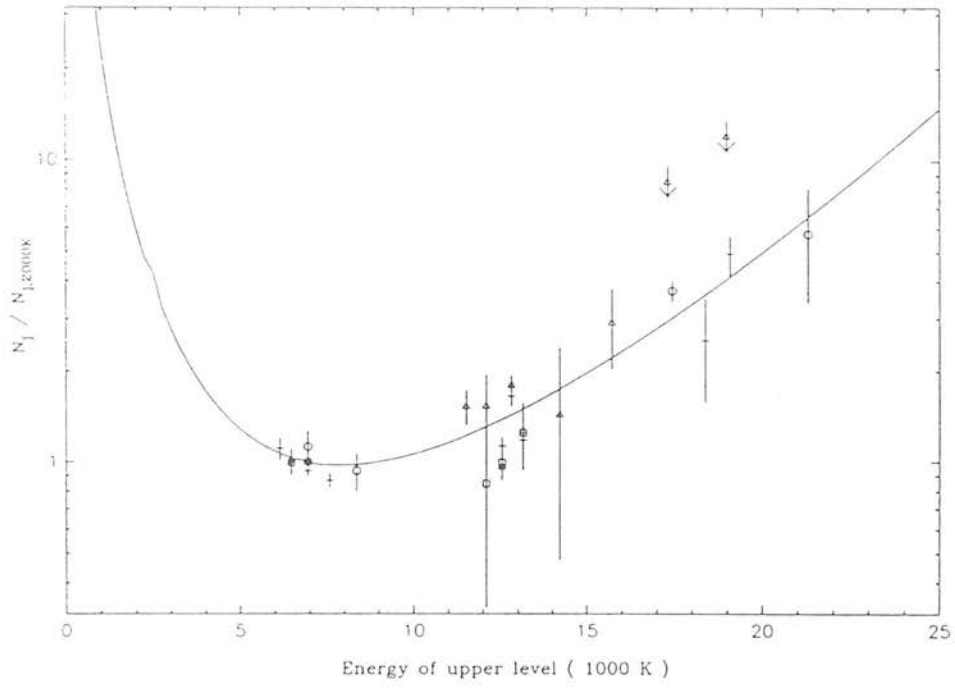

Figure 4.10: Result of the J-shock fit to the column densities of the 20″W 20″S position. The solid curve is the model fit for a pressure of 2×10^{10} K cm^{-3}. Crosses are the CGS2 data from Feb 1989; open circles, Feb 1987; squares the K-data of jan 1986 and the triangles the H—K data of jan 1986. Arrows through data points are 3 sigma upper limits.

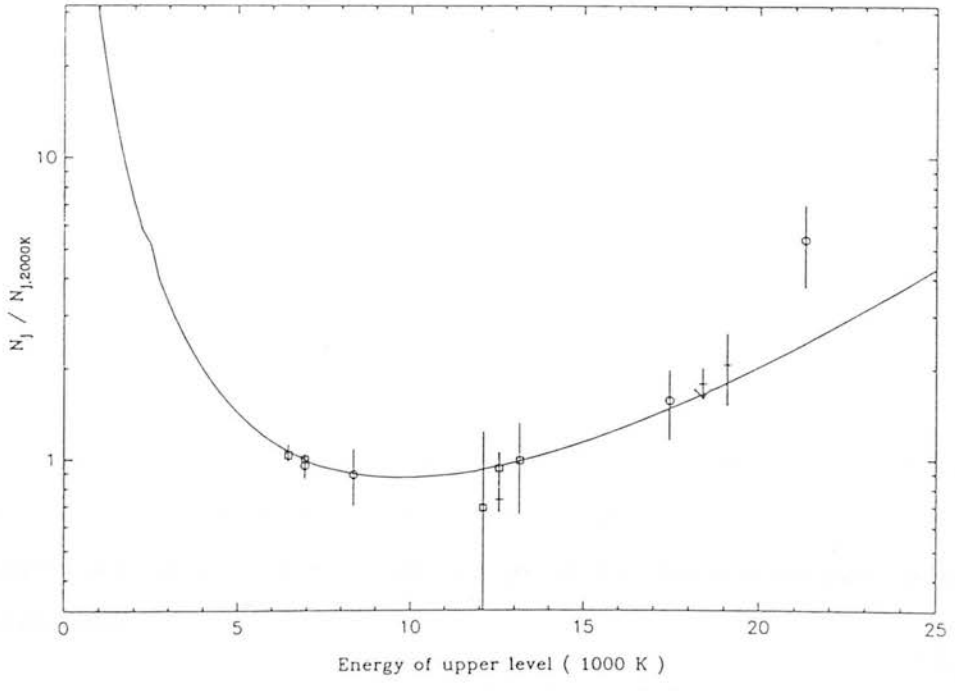

Figure 4.11: As fig. (4.10), except for the (844″W,635″N) position and a pressure of 6×10^{11} K cm^{-3}.

in Fig. (4.1) there is about 3 times more 1-0 S(1) flux in a 45″ than a 20″ beam So that the specific intensity of the H_2 lines is reduced by about 2. For a shock appropriate to the (20″W 20″S) position (i.e. n×T = 2×10^{10} K cm^{-3}) and a shock velocity in the range 13-20 km s^{-1} the CO J=22-21 line intensity is $\leq 6 \times 10^{-8}$ W m^{-2} sr^{-1}, for a CO abundance of $< 3 \times 10^{-4}$. This is consistent with the observed upper limit on the line strength. If the abundance is higher then the CO line intensity is increased. But, because of the interplay between the CO/ H_2 cooling the shock pressure needs to be increased to match the H_2 line ratios this partly offsets the increases in CO intensity. Alternatively if the shock velocity is higher there is a large amount of dissociation (effectively increasing the CO/ H_2 abundance) and the extrapolated CO intensity would be increased. Despite the last two difficulties over a wide range of parameters the Rotational CO emission is not in conflict with the observations.

4.5.1 Overpressured shocks

As was pointed out in the last section, the pressures implied by the apparent observed J-shocks in IC443 are greater than that in the supernova remnant which is the principle driving force of the molecular cloud shock. In this section we describe a situation that could explain this apparent paradox.

The pressure in the post-shock gas is approximately equal to the pressure in the supernova remnant. Conservation of momentum across the shock front gives

$$P \simeq \frac{2}{\gamma+1}\frac{\mu m_H}{k} n_o v_s^2 \tag{4.1}$$

The gas behind this shock cools and condenses. It's final density (probably limited by magnetic field) may be several hundred times the pre-shock density. This cool high density layer has a ram pressure (ρv^2) which is greater than the thermal pressure by the compression ratio.

If this compressed layer overruns a dense clump in the pre-shock medium, then a shock is reflected back into the layer, and a shock propagates into the clump. On scales large enough that the cooling zone behind the shock can be treated together with the

shock as a single discontinuity, the resultant interaction is shown in Fig. 4.12. A high pressure section now develops, bounded on one side by the shock propagating into the clump and on the other by a corresponding shock into the cooled layer. The pressure in this region will be constant, even though there may be a contact discontinuity at the clump/dense layer boundary. This pressure can be found by conserving mass and momentum across the two shocks, assuming that the shocks are isothermal

$$\frac{P_{final}}{P_{SNR}} = \frac{\rho_{clump}}{\rho_{amb}} \frac{1}{[1 + M_o^{-1}(\rho_{clump}/\rho_{amb})^{0.5}]^2} \tag{4.2}$$

Where P_{final} is the final pressure, P_{SNR} is the pressure in the supernova remnant, ρ_{clump} and ρ_{amb} are the densities of the clump and ambient material, and M_o is the initial Mach number in the ambient material. The shock into the clump has a velocity of

$$V = \frac{\mathrm{v}_s}{[1 + M_o^{-1}(\rho_{clump}/\rho_{amb})^{0.5}]} \tag{4.3}$$

And the corresponding velocity of the reflected shock is

$$V = \mathrm{v}_s - \frac{\mathrm{v}_s}{[1 + M_o^{-1}(\rho_{clump}/\rho_{amb})^{0.5}]} \tag{4.4}$$

For an example, consider the case of an ambient density of $3{\times}10^3$ cm^{-3} and a clump of $3{\times}10^5$ cm^{-3}, and assume the final compression ratio to be one hundred so that the shocked ambient gas eventually reaches the density of the clump. Using equation 4.1, and a pressure of 10^9 K cm^{-3}, the initial shock velocity into the ambient material will be 41 km s^{-1}, fully dissociating the H_2. The initial shock into the dense material, driven by the pressure of the SNR, is only 3 km s^{-1}, far too small to excite H_2 emission. Thus the cooled and compressed layer, following the shock in the dilute gas, (which because it has been compressed is moving at very close to the shock velocity) is travelling at around 38 km s^{-1} towards the dense material. At this point the densities of the clump and layer are nearly equal, it thus follows that two shocks form with the same velocity, one at 19 km s^{-1} into the clump and another slowing down the compressed layer to the same

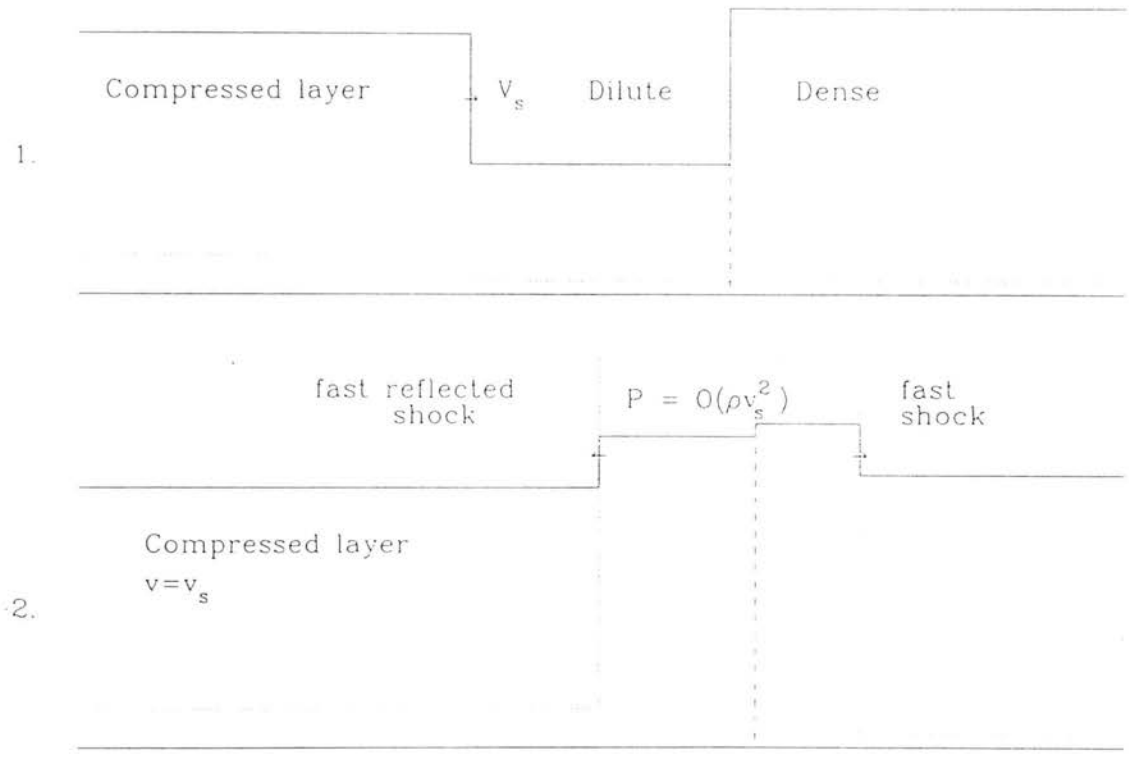

Figure 4.12: Schematic showing the situation that develops when two clouds collide

velocity. What is the pressure of this shocked gas? To answer this we use equation 4.1 again, the density is higher than the ambient density by one hundred times, however the shock velocity is down by a factor of $\approx$ two, so that the overall pressure increase is twenty five times the pressure driving the blast wave.

The densities do not have to be equal for this process to work. Note that faster shocks will be driven into the lighter gas, but the pressure will still be high. Further, it is not necessarily the dense clump shock that is producing the H_2 emission we see. It is perfectly feasible, given enough time, that H_2 has reformed following the initial dissociative shock in the dilute gas (e.g. Duley & Williams 1986; see section 1.2). Then the reflected shock into this reformed material could be the one that produces the visible emission.

The shocks that emit H_2 are therefore, in this scenario, the clumps that are in the right density range such that shocks of between 10 and 24 km s^{-1} are driven through them (if the shocks are actually C-type these limits could be changed). For the pressures we observe these limits imply densities of between 2–8$\times 10^5$ cm^{-3} dominate the emission at (20″W,20″S) whereas at the other position shocks into clumps of intial densities 5–20$\times 10^6$ cm^{-3} are emitting there. The fast SNR driven shock in the low density ambient medium is fully dissociative and presumably is the origin of the high velocity atomic H. The velocity of this shock cannot be too high because then ionisation of the post-shock gas would lead to H recombination emission which is not detected.

This is a transient phenomenom. The high pressure shocks will last only for a length of a time which is comparable to the crossing time of the shock through the clump, or if the reflected shock is producing the emission the crossing time through the cooled layer. What would be the crossing time across such a clump? Obviously this depends on the radius of the clump, this is likely to be less than the beam size i.e. 2×10^{16} cm. For a shock velocity of 100 km s^{-1} this gives an upper limit to the crossing time of $\approx$ 100 yr. This is not inconsistent with the observations taken over the last three years which show no evidence of variability in the H_2 emission line intensities and ratios. The size distribution of clumps in molecular clouds is not well defined although it appears that the velocity dispersion has a simple power law dependance (velocity dispersion, $\sigma \propto R^p$ where the best estimates for p are 0.5) on the radius over a large range of

masses and radii (i.e. Larson 1981; Myers 1983; Perault, Falgarone & Puget 1985; Dame *et al.* 1986; Scoville *et al.* 1987; Solomon *et al.* 1987). If the clump is governed by this size-line width relations then the column density is a constant $\approx 10^{22}\,\mathrm{cm}^{-2}$ (see McKee 1989 and references therin). Using the above upper limit on the radius implys a density $> 5 \times 10^5\,\mathrm{cm}^{-3}$. These numbers although uncertain are not inconsistent with the observations presented here.

This mechanism may be occurring in the Orion molecular outflow, it would explain the high pressures needed to explain the observations there and also the high densities that are implied by the H_2 line ratios. In fact, as on every scale shocks, and clouds, are observed they become increasingly clumped then it is likely that the faster shocks going through the diffuse medium will shock the denser clumps in the way described here.

Mckee *et al.* (1987) have considered a similar situation in which a high density clump is overrun by a supernova blast wave with application to the grain destruction by such shocks. However they considered the energy conserving case (for the SN blast wave) and a blast wave that was only weakly time dependent (so that the changes in the shock driving pressure are slow compared to the sound travel time in the shocked gas). The pressure in the remnant has thus dropped because of the increased volume that the remnant occupies and the pressure in the shocked clump thus appears to be larger than that in the supernova remnant. As the SNR expands the driving pressure drops and the momentum of the shocked clump plus the local ram pressure of the remnant material is what drives the shock into the high density clump. Can this explain the high pressures observed in IC443? In order to gain an apparent increase of one hundred in the shock pressure the SNR will have had to increase in volume by the same amount. This corresponds to an increase in radius of 4-5 assuming spherical symmetry. However from the appearance of the H_2 and the optical remnant the extent of the blast wave is to first order the same. We therefore conclude that there has been insufficient expansion of the blast wave to produce the apparent high pressure.

4.6 Conclusions

In this chapter we have presented spectroscopy of the Supernova remnant molecular cloud shock IC443. The observations are of two bright points in the shock where previous spectra (of the [0-0 S(13)/1-0 O(7)] ratio) indicated different conditions in the shocked gas. The column densities were found to lie on a smoothly increasing curve of excitation temperatures, as in Orion. At both positions the observations are well matched by the J-type shock model in which H_2 is the dominant coolant and that from water is suppressed but the shock pressures are different from that in the Orion molecular cloud. The observations are not well matched by planar C-type shock models. The pressures needed to explain the observations are higher than the observed pressure in the remnant itself. We hypothesize that this is due to the interaction of a post-shock cooled layer with higher density clumps. As the shocks are Isobaric the density, and thus the ram pressure, of this layer are considerably increased. The shock in the clump/compressed layer is thus of a higher pressure than the SNR driving the shock. Further we argue that this is a process which may be occurring in many H_2 exciting shocks.

A paper based on this chapter has been submitted to Monthly notices of the Royal Astronomical society. This work was performed in collaboration with Peter Brand, Tom Geballe and Michael Burton.

Chapter 5

H_2 Velocity profiles

5.1 Introduction

Observations in Orion of the v=1-0 S(1) molecular hydrogen line (e.g. Nadeau & Geballe, 1979) demonstrated that some of the shocked gas is undergoing motions in excess of 100 km s^{-1} relative to the quiescent molecular cloud. Similar highly supersonic motions of shocked H_2 have been observed in many other star forming regions (*e.g.* Doyon & Nadeau 1988; Garden *et al.* 1986), and are presumed to be associated with the interaction of a high velocity wind from a young stellar object and a molecular cloud being impacted by the wind. However the line emission at these high velocities defies easy explanation (*e.g.* Brand *et al.* 1989a).

The atomic and molecular line emission in Orion has been modelled by several authors as arising in a magnetically moderated C-type shock (Draine & Roberge 1982; Chernoff, Hollenbach & McKee 1982). However as we have seen in chapter (3), the intensities of weak, high excitation, molecular hydrogen lines are considerably stronger than the predictions from the C-shock models, and appear consistent with a hydrodynamic or J-type shock (Brand *et al.* 1988). This conclusion presupposes that there is insignificant emission in these weak high excitation lines from fluorescence, which would be observed as a narrow unresolved component to the line core. Conversely in C-shocks the excitation temperature increases as the shock velocity increases (Draine, Roberge & Dalgarno 1983).

Comparison of the 1-0 S(1) line with lines of similar excitation energy, but from longer wavelengths (Geballe *et al.* 1986; Scoville *et al.* 1982), show that this line displays slightly stronger high velocity wings. This was interpreted by the above authors as an effect of extinction through the outflow and different locations of the high and low velocity gas. That is the molecular emission arises from spatially separate regions, which suffer from different levels of total extinction. Differences in the line profiles of the long and short wavelength lines are then simply due to the effects of reddening. Geballe *et al.* (1986) found that at long wavelengths the high velocity wings were relatively more intense, suggesting, if this model is correct, that the highest velocity emission arises from the most heavily obscured regions.

However, it is not clear if these observed differences are due, in part, to real variations in the velocity distributions of the energy levels involved or the effects mentioned in the last paragraph. It is possible that changes in the velocity profile could arise if the shocks exciting the emission lead to a different temperature distributions with velocity. As is the case with C-type shocks, where the excitation temperature is an approximately monotonically increasing function of the shock velocity. It would be very difficult to produce the observed changes by invoking variable pressure J-shocks as outlined in Chapter's 2, 3 & 4. The pressure change that would be needed to produce ten percent more flux in the 1-0 O(7) line (8365 K) than the 1-0 S(1) (6956) is greater than 10^3 K cm^{-3}, the higher excitation lines would be orders of magnitude stronger from such a shock. Such a large change would result in very 'odd' line ratios that would be nothing like those observed towards Orion (see Chapter 2). If there is a fluorescent (from the PDR) component to the observed emission this would be expected to lead to different line shapes. We will postpone a full discussion of this for a later section. Briefly this is because fluorescence is a quiescent process, and should thus produce narrow lines and the relative strengths of lines is totally different from the shocked spectrum (except when the density is high, see chapter 1).

In this chapter we will present high spectral resolution observations of Peak 1 of lines which are from widely spaced upper energy levels, but are very close in wavelength. The effects of reddening are thus minimal, and any intrinsic variations in the velocity distributions can be ascertained. The motivation for carrying out these observations was to determine if there are any changes in the profile shape with the energy of the

upper level, this may provide clues as to the acceleration mechanism responsible. Before presenting the results we will briefly describe the observing techniques required to obtain high resolution observations using Fabry-Perots.

5.2 High resolution spectroscopy with FP's

The use of Fabry Perot etalon's as tunable filters has already been briefly discussed in chapter 3. However, in that case the FP used was of low resolution, the aim being to increase the contrast between a faint line and the continuum. In that mode of course the optimum resolution to use is one that barely resolves the line. For the observations presented in this chapter the intention is to resolve the line and obtain accurate velocity information. It is vital when making observations like this that the FP is monitored both for drift of the plate separation (due to temperature variations), and alignment.

Absolute velocity calibration of the H_2 lines is achieved by comparing their wavelengths calculated from the energy levels of Dabrowski (1984) with nearby lines from an argon lamp. In order to convert the FP step number to a velocity the following procedure is followed:

1. Using the known wavelengths of the astronomical and lamp line the number of orders separating the two lines is calculated.
2. This order correction (if any) is applied to the lamp line, to give an apparent wavelength of the lamp line appropriate to the order in which the astronomical line is observed.
3. The observed velocity of the astronomical line is now the difference between FP velocity and the velocity of the wavelength shift.
4. This is the velocity of the emission relative to the Earths velocity at that time. This is corrected for by calculating the velocity (magnitude and direction) of the Earth to the local standard of rest (LSR) in the direction of Orion.

The LSR is defined as the reference frame in which nearby stars are at rest. The motion of the earth in the LSR is thus a combination of the Earths motion around the sun plus the solar motion toward the solar apex. At the time of the observations we

calculate that the Earth was receding from the Local Standard of Rest (LSR) in the direction of Orion at a velocity of 34 km s^{-1}.

These observations were all carried out at UKIRT. The indium antimonide photometer/low resolution spectrometer (UKT9) was used in conjunction with an ambient temperature FP, whose passband has a full width at half maximum of 25 km s^{-1} in parallel light. The circular variable filter (CVF) in UKT9 acted as an order isolator, although within it's resolution it transmits several orders adjacent to the one of interest. The FP was stepped at intervals of 10 km s^{-1}, providing a fully sampled spectrum. The aperture size was 12 arcsec, which leads to a slightly divergent beam, thus degrading the resolution of the FP to 32 km s^{-1}. This is the observed FWHM of an Argon lamp line used in the alignment procedure. Standard nodding and chopping (60 arcsec E-W) were performed. All observations were of Peak 1 (R.A. = $5^h\ 32^m\ 46.2^s$, Dec = $-5^o\ 24'\ 02''$; Beckwith *et al.* 1978). The Molecular hydrogen 1-0 S(1), 2-1 S(1) and 3-2 S(3) lines were observed. The blue wing of the 3-2 S(3) line is blended with the 4-3 S(5) line, which is observed for the first time. Further observational details are given in Table (5.1).

In practice it is desirable to measure lamp lines as close in frequency to the line of interest. This is to avoid any errors that can be introduced by making the order corrections (although the order separation is reasonably well known and does not vary a great deal). For this reason before the start of the observations we measured the following Argon lines; 2.0992 (monitoring), 2.134, 2.208 (actually a triplet, the strongest line was measured) and 2.314 μm.

The FP was then regularly monitored for velocity drift, by observing the 2.0992 μm argon line before and after each observation set. The uncertainty in the velocity calibration is ± 5 km s^{-1} , the main sources of error being drift of the FP during the observations (which thus very slightly degrades the instrumental profile for the long integrations) and the limited resolution ($\approx$ 30 km s^{-1}). In figure (5.1) we plot the velocity drift against time, the open circles are the observations of the 2.0992 μm Argon line. The solid curve is an exponential function fitted to these points, this is as expected a reasonable approximation to the contraction of the FP plates following the temperature drop at the start of the night. Also indicated are the time periods over which each observation was made. It can be seen that there are significant variations of the velocity over the timescale of

these observations. In particular the measured velocity of the lines is shifted by about 20 km s^{-1} over the whole period when the observations were obtained. A correction has been applied to the lines when calculating the LSR velocity to allow for this velocity drift. We have made no attempt to correct for the velocity shifts between individual scans in an observation (≈ -1 km s^{-1} for the 2-1 and 3-2 observations) and coadded the spectra as though there were no velocity shifts.

The measured peak velocity for each of the profiles is quoted in Table (5.2) as well as the relative intensities and upper energy levels of the lines. The peak of the 1-0 S(1) profile is at +4 km s^{-1} close to the velocity of the ambient molecular cloud (+9 km s^{-1}; Goldsmith, Plambeck & Chiao 1975). The velocity of the peaks of the other profiles are, within the measurement errors, identical to that of the 1-0 S(1). The absolute flux scale was not determined because of uncertainties in the numbers and relative strengths of other orders transmitted by the CVF. Making it impossible to calibrate to a continuum source. It is interesting to note that Geballe *et al.* (1986) also found that the 1-0 S(1) line from Peak 1 was at +4 km s^{-1}.

5.3 The similarity of line profiles

The spectrum of the 1-0 S(1) line is shown in Fig. (5.2 a). The error bars are plus/minus one standard deviation. The signal to noise in this spectrum is very high, so for clarity a bar ten times the length of the average error bar (± 1 sigma) is plotted in the top right of this figure. The solid curve is a cubic spline that is fitted through the data points. The dashed line is the measured lamp profile which, since the lamp line is unresolved, may be taken to be the instrumental profile. The spline fit will be used to compare other lines to the 1-0 S(1) line. It is clear from Fig. (5.2 a) that the errors in the 1-0 S(1) data are very small (Signal to noise ratio at the peak is *180*). Errors in comparing the profiles of fainter lines with the spline fit will thus be due largely to the measurement errors in these lines. The line is obviously broad, and resolved, there is emission out to ± 150 km s^{-1}. Which, crudely deconvolving, is about an intrinsic velocity extent of ± 100 km s^{-1}, consistent with all other previous measurements (i.e. Nadeau, Geballe & Neugabauer 1986; Scoville *et al.* 1982; Brand *et al.* 1989).

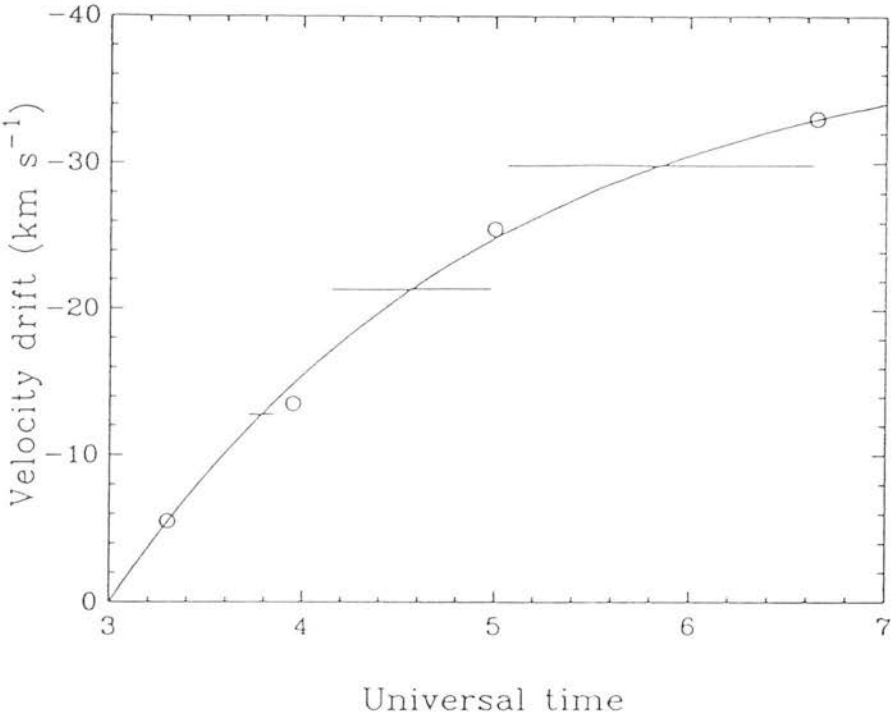

Figure 5.1: The observed drift of the FP with time. Open circles are the observed velocity change of the Argon line. The solid curve is an exponential through these points and the solid horizontal lines show the time periods over which, with increasing time, the 1-0 S(1), 2-1 S(1) and 3-2 S(3) observations were made.

Table 5.1: Observing Log

Line	Wavelength[1] (microns)	U.T. start of integration	Integration time[2] per point (sec)	Number of points	Number of scans
Argon	2.0992	$3^h\ 18^m$			
1-0 S(1)	2.1218	$3^h\ 43^m$	8	43	3
Argon	2.0992	$3^h\ 57^m$			
2-1 S(1)	2.2477	$4^h\ 9^m$	48	42	6
Argon	2.0992	$5^h\ 0^m$			
3-2 S(3)	2.2014	$5^h\ 4^m$	96	39	12
4-3 S(5)	2.2009				
Argon	2.0992	$6^h\ 39^m$			

1. Calculated from energy levels of Dabrowski (1984).
2. Total integration time includes time spent on and off source.

Table 5.2: Velocity peaks

Line	Energy Level[1] (Kelvins)	relative intensity	Velocity of peak[2] intensity (km s^{-1})
1-0 S(1)	6956	100	4
2-1 S(1)	12550	9	0
3-2 S(3)	19086	2	3
4-3 S(5)	25623	0.2	6[3]

1. Calculated from energy levels of Dabrowski (1984).
2. With respect to local standard of rest.
3. Not well constrained by data, error is 10 km s^{-1}.

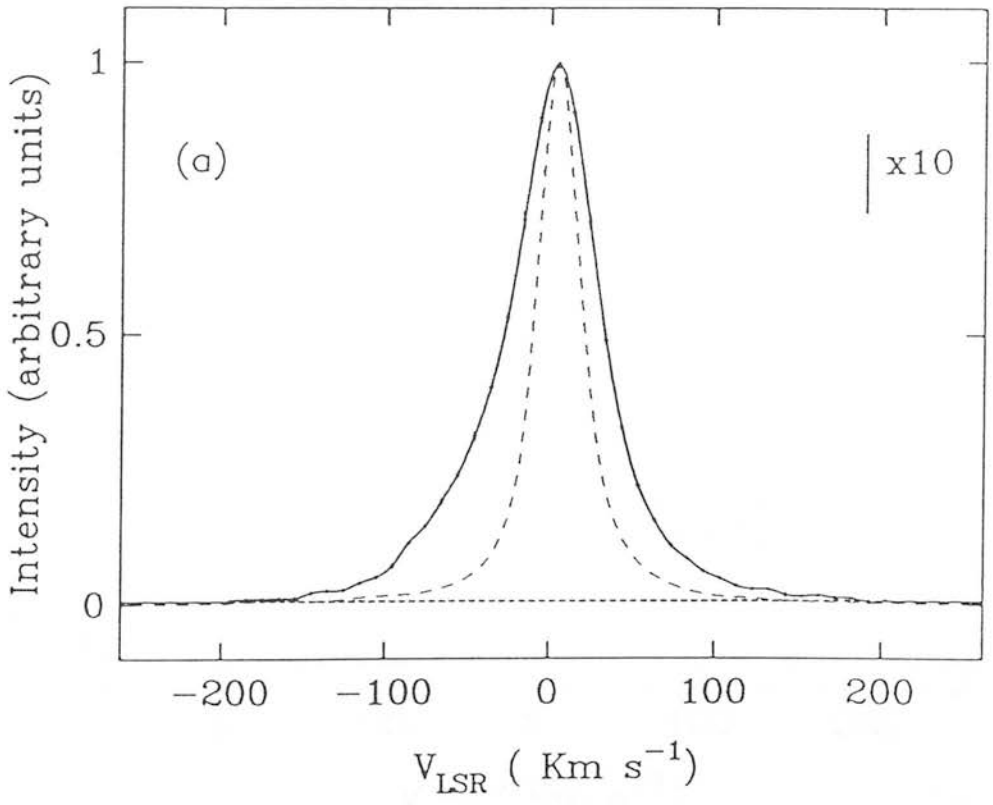

Figure 5.2: Profiles of molecular hydrogen lines at Peak 1 in OMC—1; (a) The 1-0 S(1) line (dots, with error bars); a cubic spline (solid curve) fitted through the data points and an Argon lamp line (dashed curve) profile.

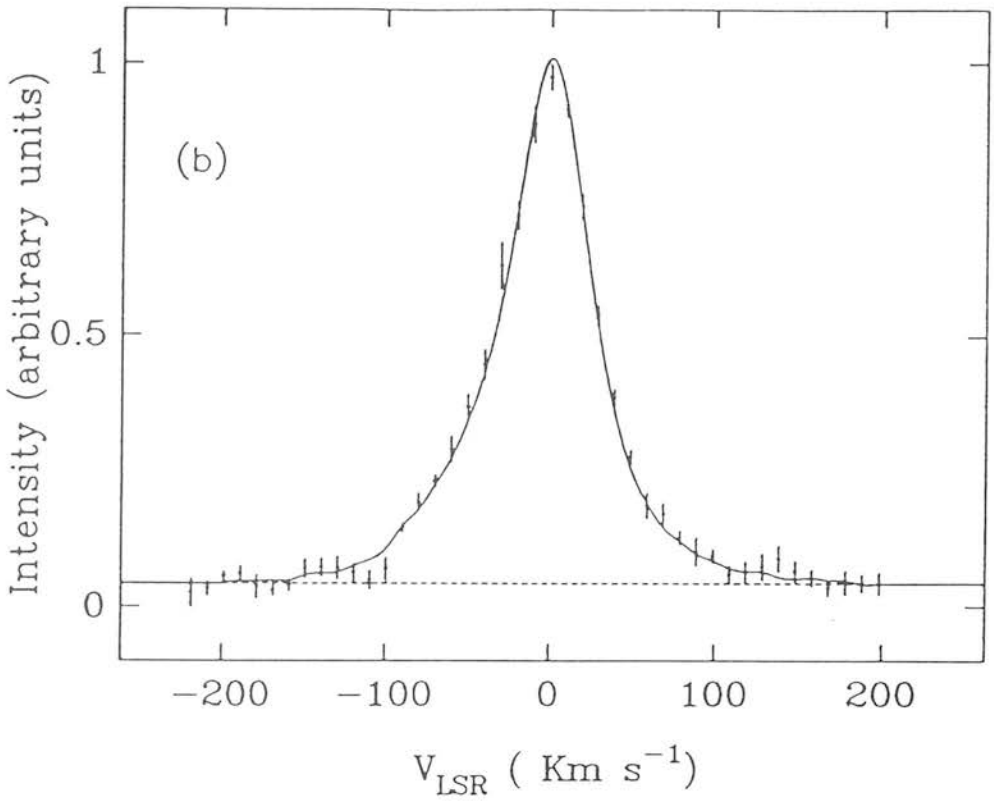

Figure 5.2(b): The 2-1 S(1) line where the spline shown in (a) is fitted to the data (solid curve)

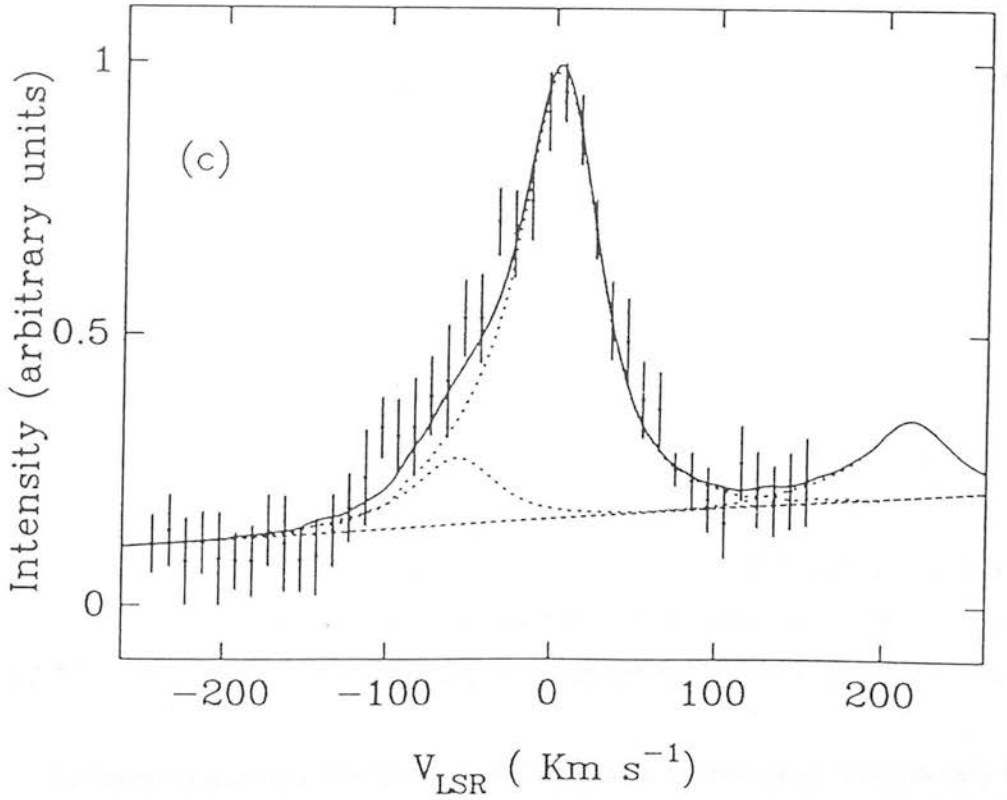

Figure 5.2(c): The 3-2 S(3) line, fitted by a spline model with components due to (dotted curves) the 3-2 S(3) (v=0 km s^{-1}), 4-3 S(5) (v= -61 km s^{-1}), and the 1-0 S(0) (v=215 km s^{-1}) lines. In all of the above diagrams the dotted line represents the underlying continuum.

The 2-1 S(1) line profile is presented in Fig. (5.2 b). The solid line is the least squares fit to these data using the cubic spline from the 1-0 S(1) line plus a flat continuum. In this fit $\chi^2 = 39$ with 42 data points. There were three free parameters in this fit, the height of the baseline, the amplitude and velocity offset of the spline. It is thus apparent that there are no measurable differences between the observed 1-0 S(1) and 2-1 S(1) profiles.

The 3-2 S(3) line profile is displayed in Fig. (5.2 c). It is blended with the 4-3 S(5) line (2.009 μm) at -61 km s^{-1} relative to the 3-2 S(3) line. The rise in intensity beyond $+100$ km s^{-1} is the blue wing of the 1-0 S(0) line, approximately two FP orders away from the 3-2 S(3) line and partially transmitted by the CVF. On the LSR velocity scale in the diagram it would peak at 215 km s^{-1}. The solid line is again a least squares fit to the data, except that in this case a flat continuum plus three cubic splines with the correct velocity offsets were fitted to the data. The amplitude of the 4-3 S(5) line was set to 0.10 times the 3-2 S(3) line. This is the ratio calculated from the J shock model fitted to the molecular hydrogen lines in the 2-3 μm region (Chapter 3 and Brand *et al.* 1988). The value of χ^2 is 22. There are 39 data points, and three free parameters. The dashed lines show the individual contributions from the lines. Again it is evident that there are no differences between the 3-2 S(3) profile and the 1-0 S(1) profile. If the ratio of blended lines is left as a free parameter, the best fit value is 0.3, with a χ^2 of 20. It is noted that the values of χ^2 for this data is smaller than would be expected, this is likely due to the high continuum to line ratio (about 10), so the formal errors of the data points are dominated by continuum variations.

The 4-3 S(5) line is the highest excitation line yet detected in shocked gas, it's upper energy level is at 26500 Kelvin above ground. It is weak, and so it is not obvious that the data constrain its profile. This question was partly examined by fitting an instrumental profile instead of the 1-0 S(1) spline to this line. The result is shown in Fig. (5.3). It is clear that this a worse fit, and in this case the χ^2 increases to 26. So we infer that the 4-3 S(5) line possesses a broad profile, which is not inconsistent with the 1-0 S(1) profile.

In order to quantify the fraction of flux that a narrow (*e.g.* fluorescent) line could contribute to the broad lines, a combination of the instrumental profile and the 1-0 S(1) spline was fitted to the data , the relative amplitudes being left as free parameters. This

will effectively measure any extra narrow component to the faint lines relative to the 1-0 S(1) (as would be expected if there is a combination of shocked/fluoresced emission, see next section). The 3-sigma upper limit to the fraction of each observed profile which could be produced by a narrow line was : for the 2-1 S(1) line 0.03, for the 3-2 S(3) line 0.20, and for the 4-3 S(5) line 0.6. This made no significant improvement to the fits. For the 2-1 S(1) case it was found that the addition of a small (3%) negative component slightly improved the fit (χ^2 = 37 *c.f.* 39). A negative component implies that the template (the 1-0 S(1) spline) overestimates the level of a narrow component to the 2-1 S(1) line and this would require an excitation mechanism that produces a [2-1 S(1)/1-0 S(1)] ratio less than the thermalized value. Gas heated by the absorption of X-rays can produce low ratios (Lepp & McCray 1983), but is not favourable energetically. The luminosity of the 1-0 S(1) line is about 10^{29} Watts (assuming a distance of 500 pc) based on the flux from a 5″ beam (chapter (3)). So a narrow 1-0 S(1) luminosity of 10^{26} Watts would overestimate the 2-1 S(1) flux by 3% (assuming no 2-1 S(1) flux is produced). A 1-0 S(1) luminosity of this value would be produced by an X-ray source of 10^{29} Watts (Lepp & McCray). There are no known sources with this high an X-ray luminosity in Orion.

It is useful to quantify how strong the limit is that the 1-0 S(1) and 2-1 S(1) line ratios are the same. A meaningful way to do this is to calculate the excitation temperature at each data point. The absolute fluxes are not known from these profiles, because of the order sorting of continuum sources. We reference any deviations from the spline fit as differences from an excitation temperature of 2074 (±18) Kelvin. This is the excitation temperature from the dereddened [2-1 S(1)/1-0 S(1)] ratio of these lines using the observations of Orion presented in Table (3.3). In Fig. 5.4 we plot the excitation temperature against velocity for all points that are more than 5 sigma above the continuum signal, this allows only velocities less than 100 km s^{-1} to be used. The dotted line in Fig. 5.4 is the excitation temperature of 2074 K and corresponds to a data point which passes through the spline fit. The temperatures are scattered within 30 Kelvins of the assumed temperature. Apparent in Figs. (5.4) and (5.2b), and the reason that a negative component to the line core improved the fit, is tentative evidence that the higher velocity material (v> 30 km s^{-1}) is at a slightly higher temperature than the low velocity gas. This temperature difference of ≈ 40 Kelvin corresponds to an increase of six percent in the [2-1 S(1)/1-0 S(1)] ratio for the high velocity wings. The line ratio is thus tightly

constrained, even though there is slight evidence for a change with velocity. It would be very useful to test this result by obtaining at higher resolution the 2-1 S(1) profile. Over the wavelength separation of these two lines an extra magnitude of extinction (at K) would enhance the 2-1 line by 6% , this is consistent with the observations of Geballe *et al.* (1986) and Scoville *et al.*(1982). In the following section we will discuss how this restriction constrains the state of the emitting gas.

5.4 Limits on fluorescence and reformation

The Orion molecular outflow lies behind the optical HII region M42. The interface layer between the two gives rise to fluorescent H_2 emission (Hayashi *et al.* 1985). Such fluorescent emission is a likely contaminant of the line emission observed toward the molecular outflow region. However, the fluorescent emission for theoretical reasons is expected to be narrow (see discussion in chapter (3)).

UV-excitation is a quiescent process, imparting no acceleration to the gas. The line widths from UV-excited gas will thus just reflect the velocities present in the excited gas (likely to be turbulent, but much smaller than the velocities observed here). Because molecular clouds typically display velocities of only a few km s^{-1} the width of the UV-excited gas is expected to be considerably narrower than the present resolution. Burton *et al.* (1989b) have indeed observed that the 1-0 S(1) line, from sources believed to be fluoresced, is unresolved at the highest resolution available of 12 km s^{-1}. It thus follows that the line emission at moderate and high velocities must originate in shock accelerated gas. The 60 arcsec chop, was chosen in order to sample line emission away from the outflow, but still within the HII region, largely subtracting any foreground fluorescence. The upper limits to narrow features in the profiles represent limits to fluorescent contamination of the line emission seen toward the outflow region. From the similarity of all the lines we conclude that any fluorescent contribution from the photodissociation region is insignificant.

Theoretically the fluorescent contribution to the v = 3 and 4 lines is expected to be much less than the above limits. The average intensity of the 1-0 S(1) line emission observed from the photodissociation region is approximately 500 times smaller than that

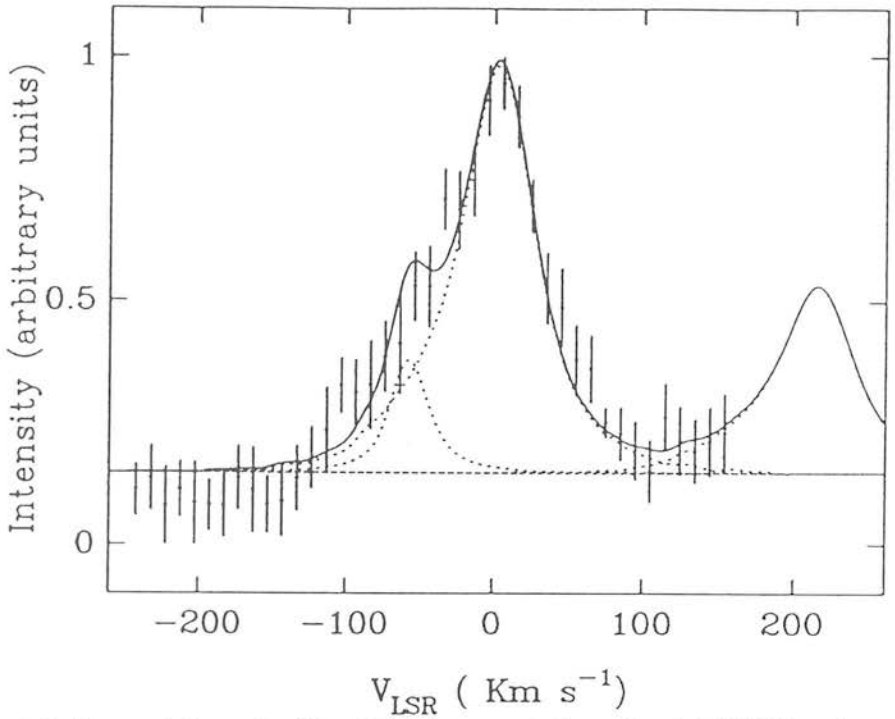

Figure 5.3: Same data as in Fig. (5.2 c), except that the 4-3 S(5) has been fitted with the instrumental profile.

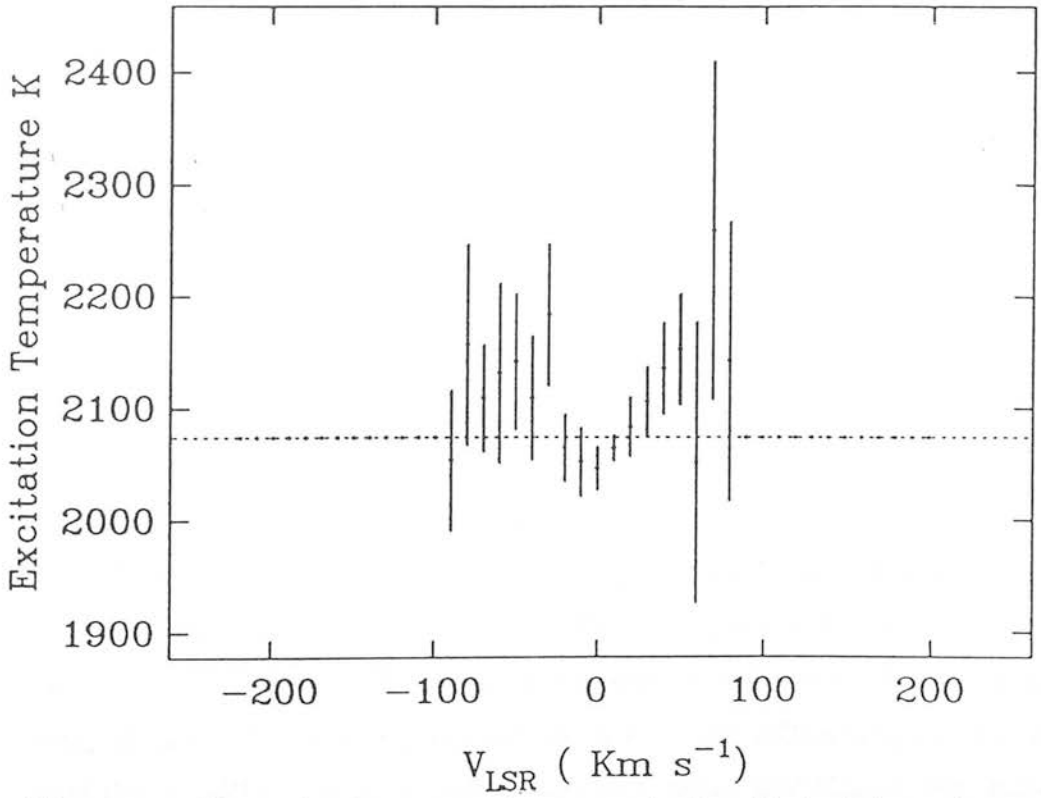

Figure 5.4: The excitation temperature v. velocity. Derived from the ratio of the 2-1 S(1) and 1-0 S(1) lines. The dotted line is a temperature of 2074 Kelvin, appropriate to the Peak 1 data of chapter (3). This dotted line is equivalent to the best fit curve of Fig. (5.2b).

from Peak 1 (Tielens & Hollenbach 1985). At Peak 1 the 3-2 S(3) line is one fiftieth of the 1-0 S(1) (see Chapter (3)). Even if fluorescence were able to produce as much flux in the 3-2 S(3) line as the 1-0 S(1), the contribution from the photodissociation region to the shocked 3-2 S(3) line flux would be only ten percent of that from the shocked outflow. The fluorescent component is likely to be much less, since the fluorescent models of Black & van Dishoeck (1987) predict that at most the 3-2 S(3) is twenty percent of the 1-0 S(1). A similar argument holds for the 4-3 S(5) line.

The above discussion refers only to the foreground fluorescence from the photodissociation region. Fluorescence occurring in pre-accelerated gas can be ruled out by the observed line ratios (see Chapter 3), which are unlike any of the pure fluorescent models (i.e. Van Dishoeck & Black 1988; discussion in Chapter 1). Recently it has been pointed out that in regions of high density, collisions will thermalize the lower vibrational levels of UV-excited molecules (i.e. see review by Sternberg 1989, and references therein; and chapter 1), however this cannot produce the range of excitation temperatures observed. The maximum temperatures that such regions can reach is of the order of 1000 K, much less than the excitation temperatures of 4000 K appropriate to the highly excited lines (see Chapter 3). More importantly, there would still be strong emission from high vibrational levels in the cascade, but which require very large ($\gg 10^6$ cm^{-3}) densities to become collisionally quenched.

5.4.1 Reformation limits

An important puzzle that we have mentioned several times in preceeding chapters is the origin of the high velocity emission. One possible solution of this problem concerns H_2 reforming in an excited state. Molecular hydrogen is known to reform on the surfaces of cool dust grains (Hollenbach & Salpeter 1971; Duley & Williams 1984), at gas temperatures so low that H_2 line emission is no longer collisionally excited. It is likely that the H_2 will reform in an excited state (*e.g.* Duley & Williams 1986, Hollenbach & McKee 1989), although the distribution of levels excited in this way is unknown. Duley & Williams (1986) suggested that the origin of the high velocity H_2 emission might be due to the emission from such reformed molecules downstream of a fast fully dissociating shock. The reformation time, although long, is short enough that the distance from the

shock front to the downstream reformation layer is too small to be resolved with present techniques. The appearance is given of molecules surviving a fast shock. In this picture then the fast ($> 22/40$ km s^{-1}) line emission is all from these reformed molecules. The spectrum resulting from such a process is not known, but at low densities it may look like pure fluorescence (i.e. Hollenbach & Mckee 1989). At high densities, such as are expected in the cooled post shocked gas, the molecules will become thermalized, as is the case in dense photo-dissociation regions's (see Chapter 1, and discussion in last section). Indeed such excited molecules will be collisionally de-excited in the dense ($\geq 10^{13}$ m^{-3}) gas behind the shock front. The ratio of the formation rate to the collision rate is

$$\frac{R_f n}{n\sigma v} = \frac{3 \times 10^{-24}\sqrt{T}n_H}{n_H 10^{-19}\sqrt{5kT/3\mu m_H}} = 3 \times 10^{-3}\sqrt{\frac{3\mu m_H}{5k}} = 3 \times 10^{-5} \ll 1 \qquad (5.1)$$

Where σ is the H_2 collision cross section ($O(10^{-19}m^2)$) and R_f is the rate coefficient for H_2 formation on dust grains (Hollenbach & Salpeter 1971). So collisions are more frequent than the rate of formation (largely due to the fact that there are more atoms and molecules to collide with than there are dust grains to form on). The collisional de-excitation timescale (about $1/n\sigma v \approx 10^{17}/n\sqrt{T}$ s) now has to be compared with the radiative de-excitation time (approximately 107s). For collisions to de-excite the molecules therefore requires the density $n > 10^{10}/\sqrt{T}$ m^{-3}.

This formation energy will provide an extra heating source to the gas, in much the same way as occurs in dense PDR's. It is interesting to calculate what temperatures could be obtained by this process. Assuming steady state this temperature can be found by equating the heating with the cooling rate. The heating rate due to H_2 formation is simply the formation rate (given above, and in chapter 1) multiplied by the energy (both internal and kinetic) given to the new molecule. The binding energy which is released when a molecule forms is 4.5eV. However, not all this energy is available to the molecule. Some is used in breaking the bonds which were binding the atoms/molecule to the grain surface. This is an unknown factor, although C-H bonds are typically about 1eV. Cooling can be provided from several sources; H_2, CO, H_2O and OI radiative cooling are likely contributors as well as thermal radiation from dust grains. The H_2 radiative cooling is a strong function of temperature (see Chapter 2) because of the wide spacing of the energy levels, and all the Oxygen is probably locked up in CO and

H_2O because of reactions (2.27-2.32). An upper limit to the temperature can be found by assuming the most inefficient coolant is responsible, at low temperatures ($\ll$ 1000 K) this is likely to be H_2 radiative cooling. So assuming full LTE H_2 cooling the balance of heat input via formation against the cooling due to H_2 is

$$3 \times 10^{-18}\sqrt{T}(1 - f/2)^2 {n_p}^2 \, 4.5 \, 1.6 \times 10^{-19} = f n_p \, 3 \times 10^{-23} T^{4.6} \qquad (5.2)$$

Where f is the fraction of molecular hydrogen to n_p the proton n umber density and T the temperature. Which gives temperatures of O(100 K) for $f > 10^{-4}$ and density of $n_p \geq 10^7$. This is insufficient to excite the high vibrational lines of H_2. The emission, and subsequent reformation, from fast interstellar shocks has been considered in detail by Hollenbach & Mckee (1989). They found that the temperatures reached in the formation layer are between 100–500K, the specific intensity of H_2 1-0 S(1) emission produced is less than 1% of the observed value in Orion. Neufeld & Melnick (1989) have also calculated the emission from fast molecular shocks, they argued that the efficiency of reformation on hot ($> 50K$) dust grains may be large if the surface of the grain is rough, allowing hydrogen atoms to remain attached. Nevertheless the reformation timescale is still longer than the cooling time and efficient reformation like this cannot lead to hot shocked H_2 emission.

As molecule reformation can not account for the observed line ratios the bulk of the emission must be produced by some other process than reformation (i.e. shocks). The line wings could still be produced by reformation, but the line ratios would be different and the profiles of the lines would be expected to appear dissimilar. For example consider the situation discussed above, the reformation following a fast shock leads to thermalized gas at 500 K. This excitation temperature is far too small to explain the constant [2-1 S(1)/1-0 S(1)] excitation temperature of 2074 $\pm$ 30 Kelvin. In terms of the observed intensity ratios of these two lines 500 Kelvin gas is only 2% of that produced in gas at 2074 Kelvin. Therefore we do not believe that molecule reformation can account for the high velocity, high excitation line emission.

5.5 Implications for Shock models

It is clear from the discussions in previous chapters that an individual simple shock wave (either J- or C-type) cannot lead to the large range of emission velocities observed in excited H_2 lines. A high velocity bow shock, either from a wind passing a high density clump or a bullet propagating into a lower density medium, suffers from similar problems, and cannot in itself lead to broad profiles (Brand *et al.* 1989a). An oblique C-type shock can broaden the profile beyond what would be produced by a J-type shock, but the range is still too small to account for the observations.

The possibility that the high velocity line emission is due to scattering off fast moving grains has been ruled out by measurements of profiles of the 1-0 O(7) line at 3.8 μm (Geballe *et al.* 1986). The 1-0 O(7) line is broad, but at such long wavelengths the scattering efficiency is severely depressed, scattering of dust grains would therefore produce narrow lines at long wavelengths. Spectropolarimetry of the 1-0 S(1) line (Burton *et al.* 1988) has indicated that there is no change in the polarisation with velocity of the emission, which would be expected if the wings are scattered.

We will examine in the next chapter possible means by which the high velocity emission may be obtained. Here we will discuss the extra requirements that any model which seeks to answer this problem has to meet. Namely the Line profiles imply that the line ratios are constant with velocity. This suggests, especially when noting that although there are variations in the line ratios from source to source these are not huge, that the particular shock excitation mechanism is a *very weak function of the shock velocity.*

It therefore seems plausible that the observed H_2 line profile along a given line of sight is produced by an ensemble of low velocity shocks, some of which are occurring in molecular gas that is co-moving with the molecular outflow, as suggested by Chevalier (1980) and by Nadeau, Geballe & Neugebauer (1982). Observational evidence for this interpretation has been found by Scoville *et al.* (1982), Geballe *et al.* (1986) and, perhaps most strongly, by Geballe & Garden (1989), although geometric models of the emission region are not obvious (*e.g.* Brand *et al.* 1989a).

If indeed the line emission is due to a superposition of shocks, the similarity of the profiles of lines with widely differing upper energy levels constrains the shock type. This is because in a J-shock, the line emitting H_2 has already been accelerated and is cooling rapidly, so the temperature distribution is independent of the shock velocity. In a C-shock, much of the line emitting gas is in LTE. at a temperature which is a strong (monotonically increasing) function of the shock speed. For example, J-shocks give significant emission only for shock velocities between 10 km s^{-1} (below this the temperature behind the shock front is not high enough to excite much H_2 before the gas cools) and 25 km s^{-1} (the dissociation limit). For shock velocities between these limits the excitation temperature of any particular line pairs is constant. The emission from J-shocks is more dependent on the pressure (through the amounts of dissociational to radiative cooling($\propto n^2$ and n respectively)), even over two orders of magnitude the excitation temperature derived from the 2-1 S(1)/1-0 S(1) ratio varies only from 1800 to 2200 K. The restriction of the excitation temperatures seen in Fig. (5.4) implies that the pressure is constant to within an order of magnitude. The appearance of C-shocks is dependent on many parameters (i.e shock velocity, magnetic field strength, ionisation fraction and density) in a 36 km s^{-1} shock (applied to Orion by Draine, Roberge & Dalgarno 1983) the excitation temperature of the 2-1/1-0 lines is 2700 K and drops to 800 K for 20 km s^{-1} . The line profiles of a superposition of J-shocks will be similar for all upper state energies, unless there are large variations in the shock pressure . However, for a superposition of C-shocks, higher excitation lines are very sensitive to the parameters of the shock. The present results then, when interpreted in terms of multiple shock events along the line of sight, clearly favour J-type over C-type shocks. Several recent and independent observational tests (Brand *et al.* 1988, 1989b; Burton *et al.* 1989a), in Orion and elsewhere, also favour J-shocks.

5.6 Extinction in the high velocity gas?

We have already seen that the high velocity wings of the 2-1 S(1) line are slightly enhanced. This could be produced if this higher velocity material is suffering more extinction than the low velocity core. The 2-1 S(1) line which is at a slightly longer wavelength than the 1-0 S(1) would therefore be less attenuated at long wavelengths and

the 2-1 S(1) line wings would be stronger than the 1-0 S(1) wings. If these measurements are to be believed about one magnitude of extra extinction would be needed towards the high velocity gas. The results of Scoville *et al.* (1982) also suggest that there is one magnitude of extra extinction to the high velocity gas. They obtained profiles of the low rotational (J<4) 1-0 S and Q transitions, although their signal to noise was lower than the results presented here. Later Geballe *et al.* (1986) measured the profile of a line at 3.8 μm line, comparing this with 1-0 S(1) line they came to the same conclusion that there is an extra magnitude of extinction in the high velocity wings. It is at this point that a word of caution should be introduced. In Chapter (3) we discussed the difficulties of deriving the extinction using the ratios of H_2 emission lines, all the problems mentioned then apply now. In particular all of the differences in the line profiles are slight and are only just detected at each point. The resulting error in the extinction estimate is thus large (Geballe *et al.* quote $A_K = 0.6 \pm 0.3$ extra extinction in the wings) and it is not clear whether there is an extra component to the extinction or not.

The question of the amount of internal extinction in the high velocity wings has been heightened by the recent measurement of a pure rotational line at 4 μm (the 0-0 S(9), Geballe & Garden 1990). In Fig. 5.5 we reproduce their measured peak 1 profile. The most striking feature of the Peak 1 spectrum is that it is flat topped. Comparison with the 1-0 S(1) line at similar resolution (20 km s^{-1}) reveals that this is an extra component to the blue wing of this line. Note that a profile of the same line, measured just after the peak 1 observation, but from Peak 2 does not show this component and is consistent with other profiles measured here and the intensity maximum is at a velocity close to 0 km s^{-1}. This seems to be very difficult to be explained in terms of extinction alone, for reasons we outline below. But it also seems impossible to be an excitation effect as this line has an upper energy level of 9000 Kelvin. It is thus at the very nadir of the locus of points in the line ratios v upper energy level diagram. It is very hard, especially as all previous evidence suggests the gas is in LTE, to avoid producing copious amounts of emission in the other 1-0 and 2-1 lines. The 0-0 S(9) line can be plotted on the column density ratio plot of Fig. 3.7 and is a factor of two higher than the shock curve (although there are the usual uncertainties in the absolute calibration).

This extra component (v_{lsr} =−30 km s^{-1}) is as strong, and as broad, as the peak (zero velocity) flux. This line is at 4 μm where the extinction is very much reduced

compared to that at 2 μmbut is very similar to that at 3.8 μm. Yet there is no evidence for such a strong component to the 1-0 O(7) line at 3.8 μm. The flux at -30 km s^{-1} in the 3.8 μm line is one half that of the peak (zero velocity). This corresponds to a very large differential extinction between these two wavelengths, comparatively free from extinction. The implied total extinction is huge, between 3 and 10 magnitudes at K depending on the extinction law chosen. These values seem hard to reconcile with the observed [2-1 S(1)/1-0 S(1)] ratio which would increase by more than 20% for so large an extinction. The observed flux in the 0-0 S(9) when plotted on the column density diagram of Fig. 3.7 does indeed fall a factor two greater than would be expected, consistent with two components to this line of equal strength.

Taken together all this does suggest that there is an extra component to the line emitting gas which suffers from extra extinction. Although the exact amounts of extinction and the locations of the emitting gas relative to each other are questions that will require more careful observations before they can be answered. What effect does this have on the observed line ratios? To address this question we have attempted some crude modelling by assuming that there are two components to the line emitting gas, of equal intensity and one of which suffers more extinction than the other. Initially we take a value of one magnitude for the extra extinction. Then dereddening both components of the line has little effect on the line ratios for values of $A_K < 0.5, 1.5$, where the two limits are those for the low and high extinctions respectively. If the upper limit for the highly extinguished gas is breached the 3 μm lines are severely depressed away from the 'shock' curve. Nevertheless we can argue that the dereddened column densities of the lines we have observed (1.7–3.9 μm) will not be seriously changed by this new observation because the profile of the 1-0 O(7) 3.8 μm line is not incredibly different from the 2 μm line profiles. Extra data on the extinction to the different velocities are clearly needed to resolve the importance of this observation.

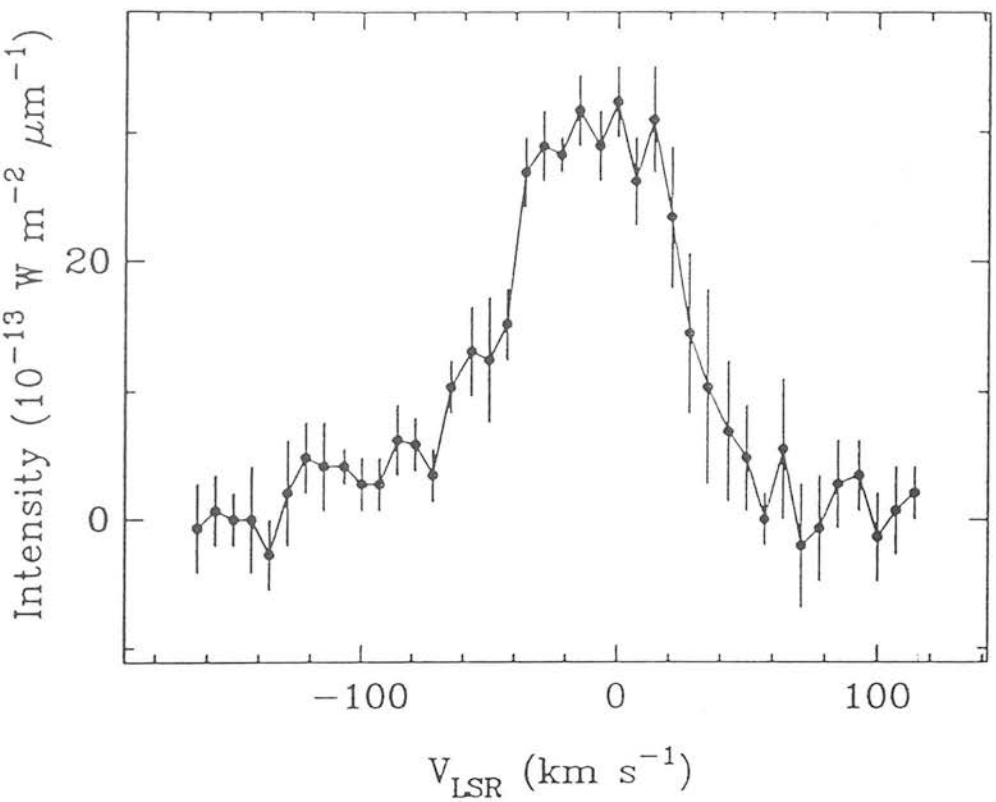

Figure 5.5: Velocity profile of the 0-0 S(9) line at 4 μm from Geballe & Garden (1990). Measured from Peak 1 in a 5″ beam.

5.7 Summary

In conclusion, we have obtained medium resolution velocity profiles of the Orion shock at Peak 1. The lines observed span a large range in upper energy level and are thus very sensitive to the type of shock. The wavelengths of these lines are very close, so the effects of differential extinction although noticeable are minimised. The central result of this chapter is that these lines are identical in shape, even though they cover an energy range of 7000– 20000K in their upper energies. This provides stronger constraints on the detailed shock mechanism exciting the emission, which has to excite the gas to the same temperatures regardless of the shock velocity. This is true for the J-type shocks described in chapter (2), providing that the *shock pressure is constant.* The emission from behind planar C-type shocks is velocity dependent and so an unchanging distribution of shock velocities would be required to account for the constancy in the line ratios with velocity of the gas. Further, combined with the observation of Burton *et al.* (1989) that the ratio of two temperature dependent lines is constant over the orion outflow and the fact that the excitation temperatures observed in shocked gas are always close to 2000K, this result implies that the shock excited emission everywhere is restricted to producing a narrow distribution of allowable temperatures. It is argued on the basis of the similarity of these profiles that UV-excitation is an unimportant contributor to the line flux at Peak1, and cannot be an important excitation process in the high velocity line wings. It is also argued that 'hot' reformation of molecules behind a fast dissociative shock cannot account for the line emission observed.

There is some evidence of slightly enhanced emission in the wings of the lines at longer wavelengths than the 1-0 S(1). However it is impossible to tell with this data alone whether this is an effect of increased extinction to the high velocity gas or a real increase in the excitation temperatures at the higher velocities. However, previous work suggests that the former is the case and about 1 magnitude, at K, of extinction to the high velocity gas compared to that of low velocity is needed to explain the observed differences. This question has become an important one to address further since the discovery of a strong blueshifted component to a line at 4 μm (Geballe & Garden 1990) , where dust extinction is negligible. This results in this profile appearing flat topped. This line has a similar upper energy level to those of the first vibrational level, and it is difficult to see how this line could be excited in isolation. However this is not seen at

shorter wavelengths (although the profiles of lines at 2.1, 2.4 and 3.8 μm suggest some extinction variable with velocity) and the extinction implied is very large, between 30 and 100 visual magnitudes. It becomes imperative then for a higher S/N study of how the line ratios vary with velocity, with new improvements in spectrometer sensitivity and especially the imminent arrival of sensitive infra-red grating array spectrometers (i.e. CGS4) this will be possible for a larger number of lines than was possible in this study.

This work was carried out in collaboration with Peter Brand, Tom Geballe and Michael Burton. A paper based on the work described here has been accepted for publication in Monthly Notices of the Royal Astronomical Society.

Chapter 6

More complex shock models and the high velocity emission

6.1 Introduction

We have already encountered in previous chapters the perplexing problem of how to both accelerate and excite H_2 emission to velocities of over 50 km s^{-1}, without dissociating the molecules. In this chapter we will examine most possible scenarios by which high velocity H_2 emission could be obtained. This extends the discussion on planar shocks in chapter (2) to non-planar and oblique cases, where the bulk velocity may be high but the shock velocity can remain small. This leads on to a discussion on the emission from bow-type shocks. In fact neither J- nor C-type bow shocks can lead to a sufficient extension of the velocity widths of the lines. At this point it is discussed how column density ratios similar to those seen in Orion and IC443 can be reproduced by high density C-type bow shocks. The central feature of the high shock pressure remains the same, and because of the geometry the emission is not highly dependent on the velocity. Finally we will conclude by a discussion on some very recent work performed in collaboration with Michael Smith and Peter Brand, which can solve the acceleration problem by invoking a very high magnetic field in Orion.

Apart from explaining the observed high velocity emission any model that hopes to realistically explain the shock excited emission from Orion has to be able to explain the

following observations;

1. The observed H_2 line ratios and intensities (chapter (3)).
2. The constancy of these line ratios over the entire outflow (the [0-0 S(13)/1-0 O(7)] ratio is 1.0 everywhere (Brand *et al.* 1989b)).
3. The observed velocity width and, preferably, the observed shape as well.
4. The profile appearing identical for all the $2\,\mu$m lines, regardless of the upper energy level (chapter 5).
5. The velocity profile appearing smooth and peaking very close to $0\,\mathrm{km\ s^{-1}}$ Brand *et al.* (1989a).
6. The outflow is centre-filled. i.e. maps of the emission do not show any limb enhancement.
7. The observations from other shocked species (such as the CO).

The last two points are slightly weaker than the rest. Point 6 on the outflow being centre filled is important, but requires construction of three dimensional models before this can be tackled quantitatively. The last point can constrain the shock models but care has to be taken since one is often comparing observations using different beam sizes which are sometimes pointing to different parts of the outflow. The J-type shock model can account for the first of these and, if the shocks are of constant pressure, points 2 and 4 as well. However as the shock velocity is limited to below $25\,\mathrm{km\ s^{-1}}$ the other points remain inexplicable. Planar C-type shocks cannot explain the line ratios or the observed velocities but may be able to reproduce the CO observations (as in the models of Chernoff, Hollenbach & McKee). Planar shock properties are also more sensitive to the shock velocity, making it difficult to envisage a series of multiple shocks accounting for the similar profiles with upper level energy.

The arguments as to why reformed molecules are not an important contributor to the high velocity highly excited emission we see from shocked sources were presented in the last chapter. The important point is that the reformation timescale (on dust grains) is a lot longer than the cooling timescale, so that the gas has cooled before significant reformation has taken place. To be able to see H_2 emission after such a reformation period would then require some extra heating mechanism which, because

of the data presented in the last chapter, would have to exactly mimic the excitation conditions at the lower velocities and look like a J-shock. Some authors have argued that the high velocity emission is occurring from slow shocks in fast moving material (Chevalier 1980). This is unsatisfactory for several reasons but may nevertheless form the basis of an explanation. Firstly the gas has to be accelerated to very fast velocities and then shocked at velocities which are too low to lead to full dissociation. Secondly the densities implied by our observations are very high and it is difficult to see how gas of this density could be moving at high velocities without having been shocked at a high velocity in the first place. However it may be possible to avoid these difficulties if clumps can be accelerated to high velocities without disruption. Two possible ways this may be achieved are (i) a smooth acceleration from a massive disc or (ii) by entraining a clump in a jet and then slowly accelerating the clump by the ram-pressure of the jet.

6.2 Clumps, Instabilities and oblique shocks

In this section we will discuss a variety of possible physical mechanisms which might be thought able to produce the fast emission we see. This section is confined to simple geometries, in the next section (6.3) we will examine the non planar case of emission from behind bow shocks. Discussing each process in turn

6.2.1 Co-moving clumps

It has been suggested by Chevalier (1980) and by Nadeau, Geballe & Neugebauer (1982) that low velocity shocks occurring in the fast moving outflow could lead to the high velocity H_2 emission. The low velocity emission is, in this picture, from lower velocity shocks at the boundary of an expanding shell. The fast moving wind, including the co-moving clumps, is internal to and drives the expansion of this shell into the ambient cloud (see Fig. 3. of Geballe *et al.* 1986).

These shocks are thus required to be non-dissociative into dense gas which is moving at speeds of over 100 km s^{-1} within the molecular outflow. Each individual shock will be very narrow in this picture. In order to explain the smoothness of the emission profile

many clumps would be required to be moving at distributed velocities throughout the beam. Brand *et al.* (1990) calculate that at least 30 such sources would be needed if the shocks are J-type (and therefore narrower than the highest resolution available ($\approx$ 12 km s^{-1})) and the profile is to appear smooth. This number would be smaller if the shocks are C-type, but even then the velocity width of a fast C-shock is only 20 km s^{-1} (most of the emission is located near the peak temperature, i.e. Smith & Brand 1990). Such a large number of evenly distributed clumps along the line of sight is very ad hoc. This is made even more difficult with the new observation that the lines remain broad on scales as small as one arcsecond (Burton *et al.*1989), many clumps moving at radial velocities between $\pm$100 km s^{-1} would therefore need to be included in a beam size approximately equivalent to 10^{14} m (at a distance to Orion of 500pc). The lines are also broad all over the outflow (e.g. Nadeau, Geballe & Neugabauer (1982); Burton *et al.* 1989)). The number of co-moving clumps would therefore need to be high at all places in the outflow and also evenly distributed to avoid producing large changes in the profiles shapes and peaks. Shocks that would develop in such clumps would have variable velocities and pressures- a very restricted range of density would be required to retain the constant excitation temperature that is observed (i.e. see chapter 3). Further it is a matter of debate as to whether dense clumps can be accelerated to such high velocities without being destroyed (i.e. McKee 1988). Although none of the above rules out the possibility that the high velocity emission is produced by shocks in material which is moving with the outflow, it requires much more work before it can be considered to form the basis of an explanation.

6.2.2 Density gradients

The protoplanetary nebula CRL 618 displays even higher velocity H_2 emission than in Orion (emission is seen out to $\pm$200 km s^{-1} ,Burton & Geballe 1986). Hartquist & Dyson (1987) have argued that the high velocity material in this source is an expanding shell which has swept up ambient molecular material, in an earlier slower phase, and is moving down a steep density gradient. The density gradient allows the shell to accelerate. This accelerating shell is subject to the Rayleigh-Taylor instability and this shell fragments due to thermal instabilities at speeds close to 100–130 km s^{-1}. This fast moving molecular gas now has to excite H_2 emission. Hartquist & Dyson showed that

mixing of the hot shocked stellar wind with this dense gas is insufficient to heat the gas to more than 600 Kelvin. They suggested that the H_2 emission could be due to UV-excitation of these high density fragments.

This may well apply to CRL 618 (although the high [0-0 S(13)/1-0 O(7)] ratio observed in this source makes UV-excitation appear unlikely), but in Orion the line ratios (chapter 3) and the fact that the profiles are the same regardless of the energy of the upper level (chapter 5) rules out UV-excitation of the high velocity gas in Orion. Hence an extra means of driving slow, non-dissociative, shocks through the accelerated shell has to be found for this mechanism to work. The same problem as with reformation. Further, it is not obvious that such a well directed acceleration mechanism could lead to the wide profiles seen all over the Orion shock. For these reasons we do not believe that this mechanism can account for the observed high velocity emission.

6.2.3 Oblique shocks

Oblique shocks, those where the flow direction is inclined at a large angle to the shock plane, can allow very fast moving gas to be shocked at only a small velocity. The velocity component parallel to the shock front is constant. While the perpendicular component determines the shock velocity.

However this only acts to shift the peak of the emission. The velocity width of the line is still as narrow as in the plane parallel case. A combination of discrete oblique shock components with a range of angles to the line of sight could combine to produce a broad smooth profile, but similar arguments to those in the last two subsections make this seem unsatisfacory. C-type bow shocks will be slightly broader than J-type but again the same objections apply.

6.2.4 Instabilities

Scoville *et al.* (1982) suggested that some form of instability in the shocked material may broaden the profiles. The onset of instability generally requires the cooling post shock gas to be a shallow function of temperature. This is so that the cooling leads

to temperature changes on a faster timescale than the sound crossing time, pressure gradients then develop which can lead to catastrophic cooling or secondary shocks being formed. The onset of a thermal-type instability by radiative cooling was first investigated by Falle (1975,1981). He found that multiple shocks will form in supernova remnants if the cooling function index $\alpha < 1.5$ (i.e for a power lower cooling function $\Gamma \propto T^{\alpha}$) Since then more studies (i.e. Chevalier & Imamura 1982; Innes, Giddings & Falle 1987; Smith 1989) have confirmed that such instabilities will develop but the exact value of α is uncertain (ranging from 1.5–0.0). Could such instabilities develop in the dense molecular gas we are observing?

In a strong molecular J-type shock of velocity 100 km s^{-1} the temperature just behind the shock front is over 300,000 Kelvin. At such high temperatures the molecules are quickly dissociated and ionized. The situation is now like the radiatively cooling supernova remnant shocks considered by Innes, Giddings & Falle (1987) except the density is much higher. They found that shocks speeds greater than 150 km s^{-1} for the shocks to become unsteady. The secondary shocks that form would need to propagate far downstream into the reformed molecular material. In other words this provides an acceleration mechanism but not a shock-heating mechanism. A fully ionising shock like this would produce intense recombination radiation, that is not observed (either in Orion or IC443).

How much recombination radiation arises from these fast ionising shocks? For a hydrodynamic shock the temperature behind the shock front is given by equation (2.13). For molecular gas ($\gamma = 7/5$ appropriate for full excitation of the rotational modes only) the temperature is

$$T = 31.8 \left[\frac{\mathrm{v}_s}{\mathrm{km\ s^{-1}}} \right]^2 \tag{6.1}$$

$\mathrm{v}_s$is the shock speed. Assuming that the gas is in steady state the collisional ionization is balanced by the radiative recombinations', the fraction of H that is ionised, χ, is given as in Spitzer 1978 by

$$\chi \approx \frac{1}{1 + \alpha/\Gamma} \tag{6.2}$$

Γ and α are the rate coefficients for ionization and recombination to the ground

state. Assuming collisional ionization by $H + H \rightarrow e^- + H$ (rate coefficient from Draine, Roberge & Dalgarno 1983) and the recombination coefficients of Spitzer (1978) then 50% ionisation occurs at a temperature of approximately 10^5 K. Which is the temperature achieved in a 60 km s^{-1} shock. If there is a magnetic field then this shock velocity is increased (see section 2.4.4).

So in fast shocks the gas becomes ionized, recombination occurs further downstream. We can estimate the strength of the recombination radiation by assuming the ionised gas is like an optically thin HII region. From Osterbrock (1974) and Giles (1977) the Brγ line flux is for case B emissivities

$$F_{Br\gamma} \approx 1.57 \times 10^{-11} \frac{n_e M(HII)}{d^2} \text{ W cm}^{-2} \tag{6.3}$$

Where n_e is the electron number density (in cm^{-3}), M(HII) is the mass of the HII region (in g) and d is the distance (cm) The mass of the HII region is estimated as

$$M(HII) \approx t_{rec} \frac{5}{6} v_s n_o m_{H_2} d^2 \Delta\Omega \tag{6.4}$$

where t_{rec} is the recombination time of the ionised gas ($\approx 3 \times 10^{12}/n_e$ s, Osterbrock 1974), $\frac{5}{6} v_s$ is the velocity of the post-shock gas, n_o is the pre-shock number density, m_{H_2} is the mass of molecular hydrogen and $\Delta\Omega$ is the beam size. The Brγ flux through a beam size of 5″ is

$$F_{Br\gamma} \approx 10^{-26} n_o v_s \tag{6.5}$$

The $Br\alpha$ flux is approximately three times this value (Giles 1977). Which for a 100 km s^{-1} shock into gas of density $10^5\,cm^{-3}$ is a flux of $\approx 3 \times 10^{-19} W\,cm^{-2}$ for the $Br\alpha$ line. This is greater than the upper limits on the fast Brα, for Orion there is an upper limit of 6×10^{-21} W cm^{-2} (in a 5″ beam Geballe & Garden 1987). Note that this approximate calculation is in close agreement with more realistic shock models: Hollenbach & Mckee (1989) calculate a $Br\alpha$ flux of 2.5×10^{-21} W cm^{-2}.

Slower shocks, that do not produce as much ionising radiation, may be unstable. But then secondary shocks need to form which can accelerate the molecular gas to the higher velocities.

6.2.5 Working surfaces of jets

When a collimated wind (a jet) strikes the surface of a cloud a bow shock forms around the shock. The bow shock cannot produce the broad line emission for reasons we describe below. The situation behind the bow shock has been considered by Dyson (1987) as a possibility for explaining Herbig-Haro objects. The hot shocked gas at the front surface of the jet is at a higher pressure than the gas to the side which has been shocked at the bow. Consequently this high pressure forces the hot gas back through the nozzle that is formed between the edge of the jet and the wall of the bow shock. The gas velocity at this point is equal to the sound speed ($\approx v_s/4$) and could interact with the cooled bow shock material further downstream. Brand *et al.* (1989a) have argued that the possibility of producing the high velocity molecular emission from this region would require shock velocities of over 300 km s^{-1}. Again this mechanism would also produce intense recombination radiation (as in Herbig-Haro objects) at the front of the jet. Furthermore if such a structure is to explain the widespread high velocity emission then a large number of jets, moving in different directions, are required to be emanating from IRC2.

6.3 Emission from bow shocks

Bow shocks are an ensemble of the oblique shocks mentioned above added together in a definite way (unless the cooling time exceeds the flow fly-by timescale). These will occur when a fast moving fluid encounters an obstacle (such as a clump). The shape of the bow shock is determined by balancing local pressure. This results in a shape which should be very close to being parabolic, and only deviates from a parabola when the emissivity from the shock is low or if the obstacle is not spherical. In that case the bow shock approaches the shape of a Mach cone (Raga 1985)-far downstream. Brand *et al.* (1989a) have considered this problem. They assumed that the bow shock was parabolic and that the shock was J-type. Not unexpectedly they found that the line widths from such shocks were still too narrow to explain the observed profiles. They derived a simple expression as to the maximum width of an emission line behind bow type shocks which illustrated that a single bow shock could not produce profiles broader than twice the

breakdown velocity (i.e. the dissociation limit; 25 or 40 km s^{-1}).

A similar problem, but this time when the exciting shocks are C-type has been tackled by Smith & Brand (1990c). They considered three shapes for the bow shock: a parabola, hemispherical cap and a cone. The velocity widths of the lines produced is never greater than ≈ 40 km s^{-1} for parabolic and hemispherical caps. The observed velocity can be doubled if the bow shock is conical in shape, but the velocity width is still too small and very particular conditions are needed to produce such a width.

6.3.1 Line ratios from Bow shocks

At this point we digress a while, to discuss whether the line emission from behind bow type shocks are consistent with the observations. The discussion on the J-type bow shocks is limited and it is argued that an insignificant change in the line ratios will result because of the limited velocity range involved. The discussion on the emission from C-type bow shocks uses many of the results from Smith & Brand (1990a, b & c) which solve analytically the MHD flow equations for C-type shocks under reasonable approximations for the equations of ion-neutral drag and the cooling function.

The Line ratios expected from behind a bow shock are calculable, since the problem is well defined. Here we will only consider the case where the bow is parabolic in shape. The emission from parabolic J-type shocks is very easy to calculate. In fact the line ratios will not vary a great deal from the plane parallel case. This is because for any wind that is driving the shock emission comes from the section of the bow shock where the velocity is between 10 and 25 km s^{-1}. The pressure (for a constant density) thus only varies by a factor of 7 from the front to the back of the shock. This has only a small effect on the line ratios (see section 2.4.3) and the emission from behind the J-type bow shock will look largely the same as before.

The situation is very different for C-type shocks, because of the increased sensitivity of the emission to the shock velocity. The fast shocks at the nose of the bow produces hot gas, and as the Mach angle decreases downstream of the clump the shock velocity falls producing a lower excitation component to the emission. This has the effect of rapidly decreasing the excitation temperature at low energy levels-the curvature of the

column density ratios is decreased (i.e. see Fig. 2.4). We can calculate the emission from behind a C-type bow shock by combining equations 2.70 and 2.71 for the column densities and maximum temperature behind a planar C-type shock, and then integrating this over the parabolic shock surface, allowing for the change in the shock velocity as we move downstream and the change in the transverse component of the magnetic field as we move around the bow. The relevant angles are shown in Fig. 6.1, here we will only consider flows in which the magnetic field is perpendicular to the flow velocity and which is also perpendicular to the line of sight (ψ and $\theta = 0$). Setting the line of sight angle to zero will have no effect on the line ratios in the optically thin case, which is appropriate for emission from H_2.

If the velocity is greater than the critical velocity (for dissociation or ionisation) then the H_2 line emission does not arise from the whole bow shock, but rather is excited further downstream—in the tail of the bow—where the shock velocity is smaller than the critical velocity. Consequently the critical velocity has to be known for each point on the surface. This is not simply the 40 km s^{-1} limit commonly quoted, but is in fact dependent on the ionisation fraction, transverse magnetic field strength and the density (see Fig. 2.6). For accurate modelling this limiting velocity should be calculated accurately for a plane parallel shock. However, inaccuracies in the breakdown limit chosen only lead to small differences in the predicted steepness of the high excitation column Densities.

It is assumed that the emission stops at velocities above the critical velocity (because the gas is fully dissociated or ionised). While this is not strictly the case, the exponential dependence of the dissociation rate (see chapter (2)) leads to a very small range of velocities about the critical velocity where the dissociated fraction increases from zero to unity. To calculate the breakdown velocity for different values of the transverse magnetic field we use the approximation that $v_b \propto B^{1/4}$ (Smith & Brand 1990a). We can now express the column density in a particular level by integrating over the surface and allowing for the change in the transverse components of v and B (transverse v and B $\propto sin\alpha$).

$$\frac{N_j}{g_j} = 7 \times 10^{22} \int \frac{B_{-3}}{\chi_{o-7}\sqrt{n_6}v_{10}}\left(\frac{1}{T_{max}} + \frac{1}{T_j}\right)e^{-T_j/T_{max}}dA \qquad (6.6)$$

The area dA is found (as in Smith & Brand 1990c) by noting that an element $d\alpha d\phi$

has an area (R $d\phi$)(dz/cosα), where R is the radius at distance z from the front of the parabola. The equation for a parabola is z = $R^2/(2L)$ and $dR/dz = tan\alpha$. So the area is

$$dA = L^2 \frac{cos\alpha}{(sin\alpha)^4} d\alpha d\phi \tag{6.7}$$

where L is the of the parabola. We can approximate $T_{max} \approx T_b(\frac{sin\alpha}{sin\alpha_b})^{4/p}$ with p being the power law cooling index (1.5 for H_2O, 4.7 for H_2). T_b and α_b are the temperatures and shock angle at which dissociation occurs ($sin\alpha_b = v_b/v$). After some algebra the integral (6.1) can now be expressed as

$$\frac{N_j}{g_j} = 4.3 \times 10^{21} L^2 [\frac{B}{n\chi T_j}] \frac{1}{v} [\frac{v}{v_b}]^4 \int_0^1 \frac{0.1 + y}{x^4 y e^{1/y}} dx \tag{6.8}$$

Where v is in km s^{-1} and $y = \frac{T_b}{T_j} x^{(4/p)}$. The limiting temperature T_b is for dissociation between 3700–4000K. So the line ratios from this bow shock are determined only by the cooling function. Take the following initial conditions. A density of 3×10^6 cm^{-3} is chosen so that the H_2 is in LTE, a magnetic field $B_o = 10^{-3}\sqrt{n_o}$ mG (where n_o is in cm^{-3}) perpendicular to the direction of the flow, and ionisation fraction of $\chi_o = 10^{-7}$ and an variable H_2O abundance of $\epsilon = f\epsilon_o$ ($\epsilon_o = 4.25 \times 10^{-4}$, so that for f=1 H_2O cooling dominates over H_2). The results of such calculations are shown in Figs. (6.2) and (6.3) for the line ratios observed in Orion and IC443 using the values of indicated ϵ. These are reasonably close to the observed column density ratios considering the assumptions in the calculation. The line ratios from such a bow shock are altered by changing either the shape of the bow (i.e. notice the change from the planar to the parabolic case) or the form of the cooling function. The cooling function is dependent on the relative abundances of the coolants that are important to the 'hot' molecular gas (see section (2.3.1)).

For large or small H_2O abundances either H_2 or H_2O dominate the cooling and the function is independent of density at intermediate abundances the cooling is a function of density. Large differences will be apparent if the velocity falls below the breakdown velocity, as then the maximum temperature is never reached, the high excitation energy lines will thus fall in intensity. However, the actual line ratios from such a shock structure is independent of the velocity once this is over the breakdown velocity. The breakdown

velocity is generally between 40 and 50 km s^{-1} depending upon whether the breakdown is due to dissociation or ionisation. The relative weakness of the line ratios on the actual shock velocity is a result of increasing the wind velocity only pushes the line emitting region further down the bow, and essentially the same range of temperatures is produced.

These C-type bow shocks can thus explain many of the observed features that are also consistent with the J-shock model. In particular the line ratios are fairly insensitive to the initial conditions. Thus the observation of excitation temperatures $\approx$ 2000K in most sources is naturally explained. In the J-shock model this observation was explained most naturally by the similar shape of the cooling function, variations occurred with different shock pressures due to the different amounts of dissociational and radiative cooling but are small for large changes in the shock pressure (see chapter (4)). The emission is insensitive to the shock velocity as changes only lead to more or less dissociative cooling. The dissociational cooling is an exponential function of temperature and effectively stops any emission from temperatures at which it dominates. In constant pressure shocks the temperature at which dissociation dominates is constant, so regardless of shock velocity the gas cools from a temperature which is the same in all sources. In the C-type bow shock model a large velocity (> 50 km s^{-1}) and a reasonably constant shape of the bow is required.

For Orion this implies that there are either many bullets shocking the dense molecular cloud, which has a fairly low H_2O abundance, or an outflowing massive wind is being impeded by many dense clumps. Whichever scenario is finally chosen the pressures needed are still high (because of the density and temperature arguments developed in sections 3.4 and 4.5).

For IC443 the situation is more constrained, it is unlikely that the shocks are produced by many fast moving clumps striking the molecular cloud in an even fashion. However, high density bow type shocks may develop in the situation envisaged at the end of chapter (4), where the emission is produced by the interaction of the cooled and compressed layer following behind a fast shock with a high density clump. The shock that is formed in this layer when it meets a high density clump will be bow type in shape.

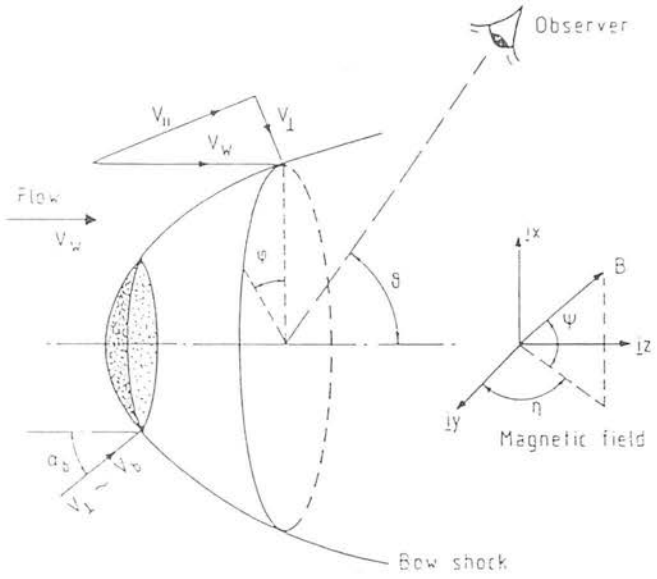

Figure 6.1: Schematic of the geometry of the bow shock, showing the relevant angles referred to in the text. The stippled area at the front of the bow represents the area over which molecular hydrogen is dissociated (from Smith & Brand 1990c).

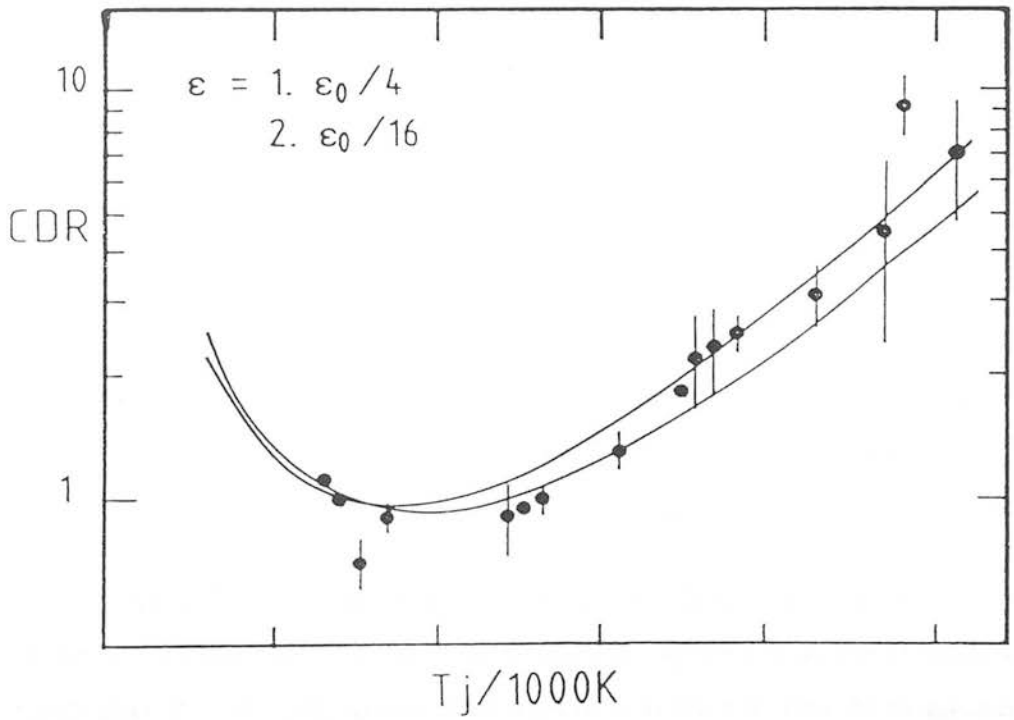

Figure 6.2: Orion data of Fig. (3.7) compared to the C-type bow shock with the parameters described in the text and two differing abundances of water.

6.4 Very fast C-type shocks

It will have been noticed in the last section that the maximum velocity before full dissociation or ionisation occurs is $\propto B^{1/4}$. This provides a clue as to how C-type shocks can possibly accelerate H_2 to velocities much faster than 40 km s^{-1} without destroying the molecules. Simply all that is needed is a high magnetic field to increase the limiting velocity. The Alfven velocity is larger, the ions can dissipate the waves produced by ion-neutral collisions at a faster rate, the neutrals and the ions are increasingly tied together. The drag velocity $(v_n - v_i)$ is thus reduced. The shock is 'softer' and reaches a lower temperature. So a high velocity shock, which previously would have dissociated or ionised all the molecules, is kept at a lower temperature which does not destroy the molecules.

The structure in a shock front through such a medium is compared in Fig. 6.5 with that when the magnetic field is 'normal', the structure is calculated using the C-shock approximations outlined in section (2.5). The neutral and ion velocities are given by $r\,\mathrm{v}_s$ and $q\,\mathrm{v}_s$ respectively. The temperature, t_m, is ratioed to the maximum temperature reached in the shock.

This is equivalent to saying that the Alfven velocity is larger than expected in quiescent clouds and hence the Alfven Mach number $((\mathrm{v}_s/v_A)^2 = 4\pi\rho(\mathrm{v}_s/B)^2)$ is reduced. The drag length (equation 2.69) is thus longer. Increasing the drag length allows much more cooling to take place (relative to ion-neutral frictional heating) and so the temperature reached in the shock is lower. It follows that the shock velocity can be increased until the critical point is again reached where the drag length is reduced (while, to first order, the cooling length remains the same) and the gas reaches the temperature at which dissociation and/or ionisation destroys the molecules.

The magnetic field strength required to increase the breakdown velocity from around 50 km s^{-1} to 150 km s^{-1} is about 30 times that expected from the Mouschovias (1976) result that $B \propto n^{1/2}$, the actual value implied is at least 30 mG. Most measurements of the field strength in and around Orion have found values of the magnetic field between 50-120μG (Troland, Crutcher & Kazes 1986 and references therin). These measurements are relevant to the parts of the cloud that are at a much lower density than the densities

implied by our results. At the higher densities ($\approx 10^{10}\,\mathrm{cm}^{-3}$) of the OH and H_2Omaser sources in BN/KL the magnetic fields are a few to tens of milligauss (Norris 1984; Fiebig & Gusten 1989). These field strengths are consistent with the Mouschovias result. High magnetic fields have been suggested by Pudritz & Norman (1986) in their outflow model. Also compressive shocks could increase the magnetic field strength above the $\sqrt{n}$ value (assuming that the magnetic field is frozen to the neutrals, $B \propto n$).

If a bow shock calculation is now performed (as in the last section) for a high magnetic field strength then the line ratios and the breadth of the line should be achievable (Smith, Brand & Moorhouse 1990b).

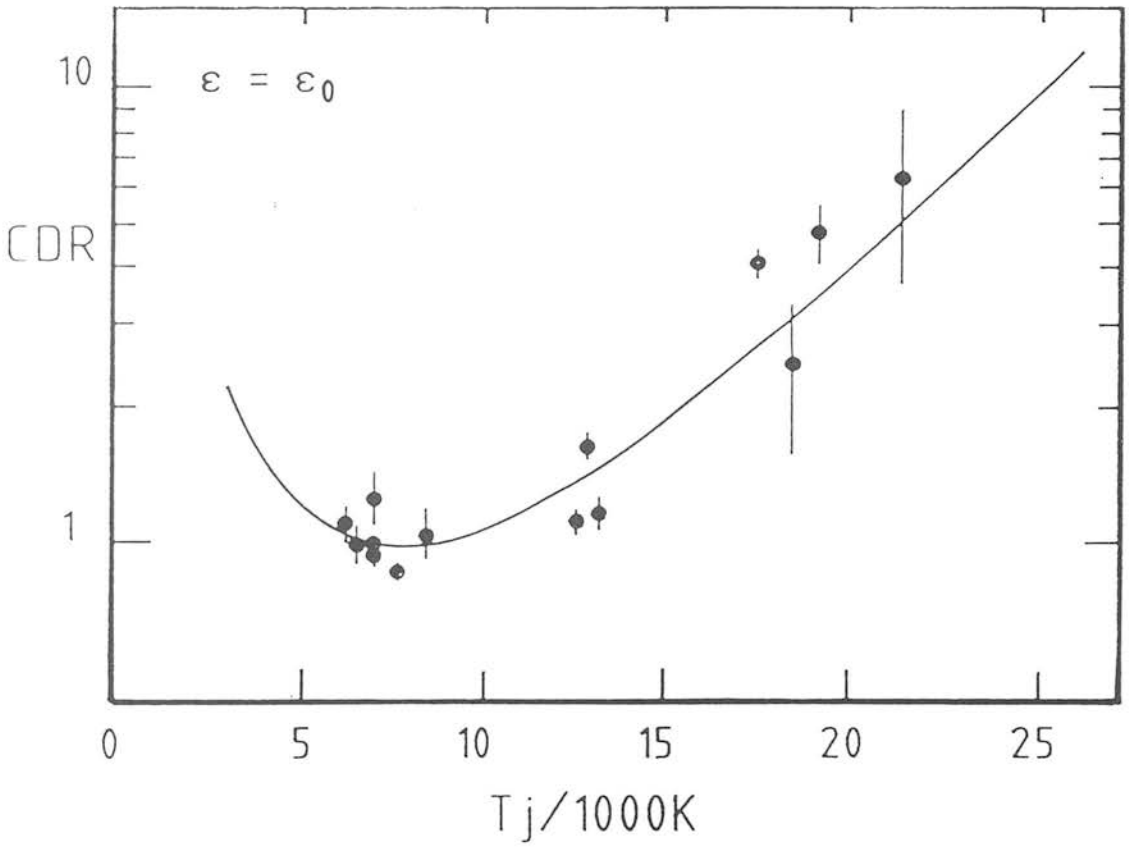

Figure 6.3: The IC443 data of Fig. (4.?) and the predictions from a C-type bow shock of abundance $\epsilon_o (= 4.25 \times 10^{-4})$.

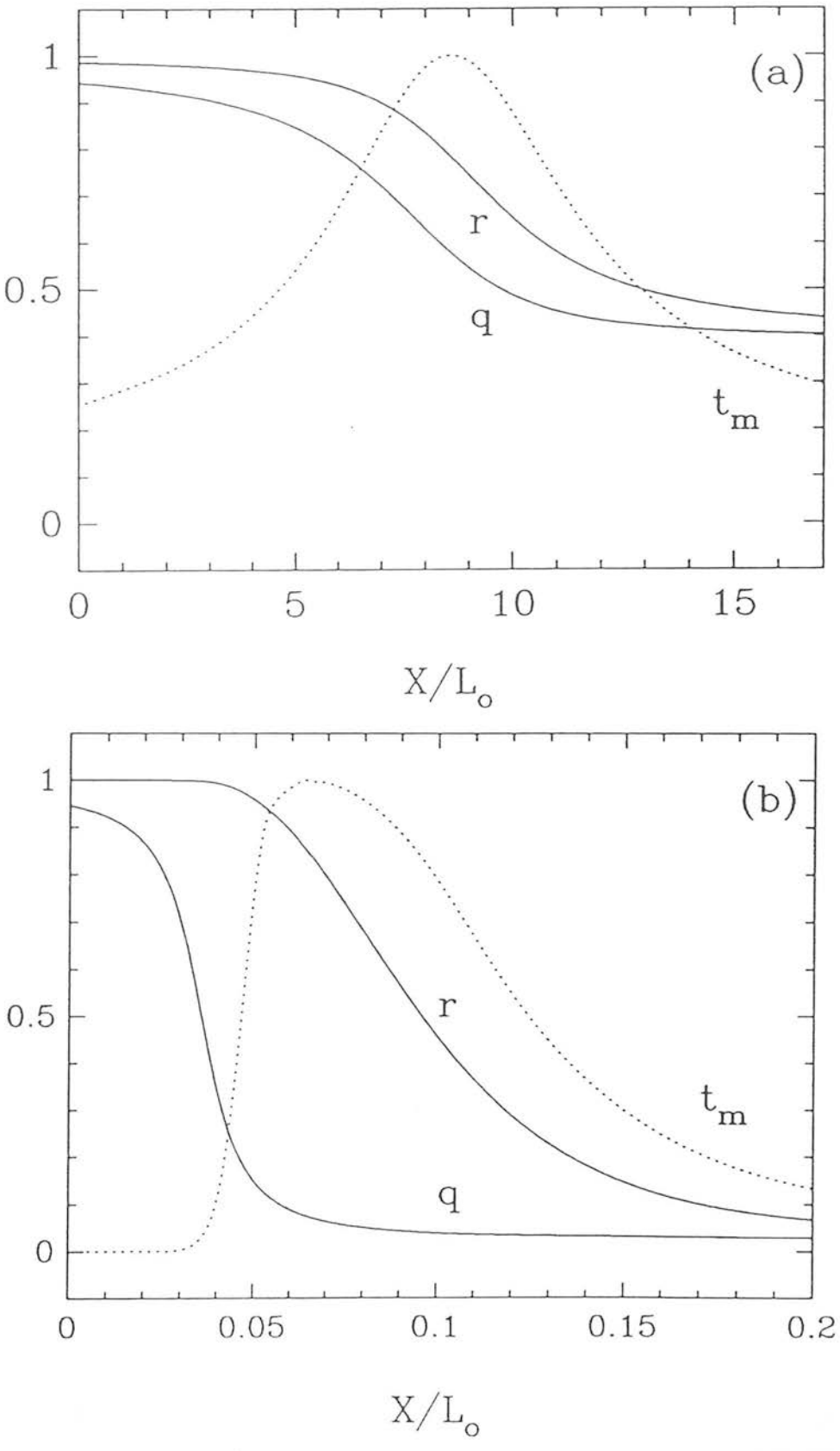

Figure 6.4: The velocity and temperature structure in C-shocks (a) A normal shock with a magnetic field strength of 1.7 milligauss, density $3 \times 10^6\,\mathrm{cm}^{-3}$ and velocity $40\,\mathrm{km\ s}^{-1}$ (b) A high magnetic field of 100 milligauss, and velocity of $200\,\mathrm{km\ s}^{-1}$. The drag velocity is never more than $40\,\mathrm{km\ s}^{-1}$, so the temperaure remains low.

6.5 Summary

Various possibilities have been discussed as mechanisms by which high velocity H_2 could be obtained. For most of these it is argued that there are serious flaws if they are to form the basis of an explanation. MHD C-type shocks occurring in bow shocks are shown to be able to reproduce the line ratios observed in Orion and IC443. The pressures needed remain high and the suppression of H_2O cooling is relaxed. Finally we suggest that if the magnetic field is very high then the ion-neutral drag length is increased allowing the breakdown velocity for C-type shocks to increase, possibly solving the problem of the high velocity H_2 emission that is observed.

Michael Smith is the inspiration behind the C-type bow shock models. Two papers have been submitted to Monthly notices of the Royal astronomical society based on the last two sections of this chapter.

Chapter 7

Conclusions and prospects for future research

7.1 Introduction

This thesis has presented a detailed study of the shock-excitation of molecular hydrogen in dense molecular clouds. The aim of observing this excited molecule is to understand the shock physics that is exciting the emission. This was partially prompted by the observation that most of the shock excited sources suggested that the temperature in the post-shock gas is $\approx$ 2000K. A remarkable observation in view of the different conditions that must be present in the large number and variety of sources that have been observed.

The bulk of this thesis has concentrated on a multi-line spectroscopic study. In Orion over 30 different H_2 emission lines have been observed. These lines cover a wide range of upper level energies (6000–26000 Kelvins) and are thus ideal as probes of the temperature structure in the post-shock gas. The column density ratios that can be derived from these observations have been modelled using approximate, but fairly accurate, semi-analytic solutions for the emission spectrum expected from both hydrodynamic Jump-type shocks and Magnetohydrodynamic Continuous-type shocks. One of the major results implied by this data is that the plane parallel C-type shocks previously thought able to explain the emission are in fact unable to do so. Simple J-type shocks in which H_2 is the dominant coolant are, however, consistent with the H_2 line ratios. Later on it is shown

that high density bow shocks, such as those that are formed when a high velocity, high density wind encounters an obstacle, which are C-type can reproduce the right range of temperatures and provide a reasonable match to the line ratios. The density and temperature distribution produced by such C-type bows are significantly different from the plane-parallel C-shocks.

The extinction derived to the orion outflow is found to be much lower than previous estimates. In fact it is now so low that the outflow itself is within the confines of the photodissociation front at the molecular cloud/HII region interface produced by the trapezium stars. This radically changes the ionisation state of the molecular outflow material. The pressures needed to explain the observed emission lines are high for both the J-type and C-type bow shock models. These observations combined with the apparent constancy of the line ratios over the face of the shock throw open the question as to whether the outflow is pressure or momentum driven. The implied mass loss rates for the driving source are large.

Observations of the supernova remnant/molecular cloud shock IC443 suggests the same result. The slight differences in the line ratios here and in Orion are it is argued due to different shock pressures if the shock is J-type. The pressures needed are higher than the pressure observed in the supernova remnant. It is suggested that this discrepancy is due to the high ram pressure which results when a high density clump interacts with the cooled and compressed layer following behind the radiative shock in the lower density ambient medium. The line ratios here can also be matched with a C-type bow shock. The pressures needed are still large due to the high densities and wind velocities required. The differences could be due to either a different cooling function in the two places, which can occur if the water abundance is changed, or by changing the shape of the bow. The large ram pressure shocks offer one way of escaping the large mass loss rates implied by the orion observations.

Much higher resolution spectroscopy has been employed to investigate the dependance on velocity of the line ratios. It was found that within the observational errors the line ratios were identical even at the very high velocities at which molecular hydrogen would be destroyed in normal shocks. This imposes tight restrictions on any models invoked to explain the high velocity emission. It is further argued on the basis of this

and other data that the effects of fluorescence are insignificant compared to the shock excited emission.

Finally it is proposed that the high velocity H_2 emission that is observed is due to C-type shocks in gas with a very high magnetic field strength. The alfven velocity is thus much larger than normal allowing larger shock velocities to be reached without dissociating H_2. Such high magnetic fields have been invoked in some models of the origin of the bipolar outflows and if this is correct would lend support to those models. If the field is high in a bow shock then the line ratios can be simultaneously explained as well as the breadth of the lines. The C-type bow shocks also have another neat feature. The emission is naturally a weak function of the shock velocity. Higher shock velocities only push the emission region farther to the back of the bow surface the same spread of temperatures are achieved and the emission line ratios appear the same.

7.2 Prospects for future research

The near future appears promising for studies into the shock condition. Observationally the advent of sensitive 2D array spectrometers (such as CGS4) in the infrared will allow line intensities and ratios to be determined in many more sources that were previously too faint to study. Further such spectrometers will be able to measure many lines simultaneously, overcoming one of the major difficulties of obtaining accurate line ratios. Observations of this type will help to determine if planar shocks exist anywhere or whether the molecular clouds are intrinsically so clumpy as to make planar models unrealistic. Combining this with more line profile data will help to check the universality of the shock models.

Already underway, for Orion, are high spatial ($1''$) and spectral ($12\,\mathrm{km\ s^{-1}}$) resolution observations of the shocked regions, this is allowing a detailed study of the velocity field to take place. Real three dimensional modelling of the shock is now needed. The fact that there is now a reasonable means of exciting the high velocity H_2 emission makes this potentially much more exciting. Problems still exist with regards to understanding the Orion outflow. Probably the largest of these is the heavily extinguished blue wing, this is hard to construct in any single structure which produces the velocity profile of

the line. It is difficult to escape the conclusion that there is a spatially separate *blue shifted* H_2 emitting region at Peak 1 which is extinguished by about an extra magnitude at K. This is something that again CGS4 is ideally suited to, obtaining accurate high resolution profiles of lots of lines to determine the velocity dependance of the extinction.

Other points only briefly mentioned in the text are the breadth of the lines even at the smallest scales observable ($\approx 1''$) which corresponds to 10^{14} m. The broad lines have to be producible on scales this small. If the high B bow type shocks are responsible then it has to be checked if the scale lengths can be this small and further realistic models that would produce a widely distributed set of such bow shocks need to be invoked. Such work should relate directly to the origin of the outflow. As the magnetic fields needed are so high the impact on the state of the clouds and the origins of the outflows are many. For instance is the high magnetic field present in the ambient cloud and it is the shocks into this cloud we see or is the high magnetic field associated locally with the outflowing gas which is then shocked? It is important to further test such shocks by comparison with observations, one possibility is to refine the shock models to include other atomic and molecular species. This is then linked to the IC443 observations in which the H_2, atomic H, CO and OI emission appear inconsistent with any single shock model.

This leads on to such satellite observatories as ISO and SIRTF which will enable observations in between the windows and at long wavelengths free from atmospheric effects, increasing the accuracy of the line ratios obtainable by a large factor. Of potentially more importance, for the CO problem at least, is NASA's planned replacement of the Kuiper Airborne observatory a Boeing 747 with a 3m IR telescope, SOFIA. This will give sensitivity and resolution comparable to that presently obtainable in the near-IR. Related to this, but for longer wavelengths are the mm and sub mm interferometers that are now coming on line and being planned which will again allow high spatial resolution observations of molecules excited in much cooler parts of the outflow.

The future thus appears bright with both advances in theoretical and observational powers just round the corner. Undoubtedly these advances, as they always tend to, will produce many more problems than the few that have been addressed here. As this occurs our understanding advances one level deeper promising that we may eventually

get to a root understanding of the physical processes in molecular clouds and how they effect the star formation that occurs in them This thesis has considered only one very small part of this, but as the different parts of the painting are coming into view an exciting time is promised for all who work in this field.

References

Beck, S.C., & Beckwith, S., 1983. *Astrophys. J.*, **271**, 175.

Beck, S.C., Bloemhof, E.E., Serabyn, E., Townes, C.H., Tokunaga, A.T, Lacy, J.H. & Smith H.A., 1982. *Astrophys. J.*, **253**, L83.

Beckwith, S., Persson, S.E., Neugebauer, G. & Becklin, E.E., 1978. *Astrophys. J.*, **223**, 464.

Beckwith, S., Persson, S.E. & Neugebauer, G., 1979. *Astrophys. J.*, **227**, 436.

Beckwith, S., Evans II, N.J., Gatley, I, Gull, G. & Russell, R.W., 1983. *Astrophys. J.*, **264**, 152.

Black, J.H. & van Dishoeck, E.F., 1987. *Astrophys. J.*, **332**, 412.

Borieko, R.T., Betz, A.L., 1989. *Astrophys. J. (letters)*, **346**, L97.

Borieko, R.T., Betz, A.L. & Zmuidzinas, J., 1989. *Astrophys. J.*, **337**, 332.

Brand, P.W.J.L., Moorhouse, A., Burton M.G., Geballe, T.R., Bird, M., Wade, R., 1988. *Astrophys. J.*, **334**, L103.

Brand, P.W.J.L., Toner, M.P., Geballe, T.R. & Webster, A.S., 1989a. *Mon. Not. R. astr. Soc.*, **237**, 1009.

Brand, P.W.J.L., Toner, M.P., Geballe, T.R., Webster, A.S., Williams, P.M., & Burton, M.G., 1989b. *Mon. Not. R. astr. Soc.*, **236**, 929.

Braun, R., & Strom, R.G., 1986. *Astron. Astrophys. Suppl.*, **63**, 345.

Burton, M.G., & Geballe, T.R., 1986. *Mon. Not. R. astr. Soc.*, **223**, 13P

Burton, M.G., 1986. PhD thesis, University of Edinburgh.

Burton, M.G., 1987. *Q. Jl. R. astr. Soc.*, **28**, 269.

Burton, M.G., Brand, P.W.J.L., Geballe, T.R. & Webster, A.S., 1989a. *Mon. Not. R. astr. Soc.*, **236**, 409.

Burton, M.G., Geballe, T.R., Brand, P.W.J.L., & Moorhouse, A., 1990a. *Astrophys. J.*, January 1990.

Burton, M.G., Hough, J.H., Axon, D.J., Hasegawa, T., Tamura, M., McCaughrean, M.J. & McLean, I.S., 1988. *Mon. Not. R. astr. Soc.*, **235**, 161.

Burton, M.G., Geballe, T.R., Brand, P.W.J.L., & Webster, A.S., 1988. *Mon. Not. R. astr. Soc.*, **231**, 617.

Burton, M.G., Geballe, T.R., Brand, P.W.J.L., 1989b. *Mon. Not. R. astr. Soc.*, **238**, 1513.

Burton, M.G., Bland, J., Axon, D., Brand, P., Garden, R., Geballe, T., Hollenbach, D., Hough, J., McLean, I., Moorhouse, A., 1989c. to appear in: *Evolution of the interstellar medium*, proccedings of the ASP centennial meeting, Berkley, California, June 21-23, 1989. ed. L. Blitz, publisher Astronomical Society of the Pacific.

Burton, M.G., & Puxley, P.J., 1989. to appear in: *Second Wyoming conference on the Interstellar Medium in external galaxies*, Grand Tetons National Park, July 3-7, 1989.

Burton, M.G., Hollenbach, D.J., Haas, M.R., & Erickson E.F., 1990b, submitted to *Astrophys. J.*,}

Chernoff, D.F., 1987. *Astrophys. J.*, **312**, 143.

Chernoff D.F., Hollenbach, D.J. & McKee C.F., 1982. *Astrophys. J. (letters)*, **259**, L97.

Chevalier, R.A., 1980 *Astrophys. lett.* **21**, L.57

Chevalier, R.A., & Imamura, J.N., 1982. *Astrophys. J.*, **261**, 543.

Cornett, R.R., Chin, G., & Knapp, G.R., 1977. *Astron. Astrophys.*, **54**, 889.

Crawford, M.K., Lugten, J.B., Fitelson, W., Genzel, R. & Melnick, G., 1986. *Astrophys. J. (letters),* **303,** L57.

Dabrowski, I., 1984. *Canadian J. Phys.,* **62,** 1639.

Dame, T.M., Elmegreen, B.G., Cohen, R.S., & Thaddeus, P., 1986. *Astrophys. J.,* **305,** 892.

Davis, D.S., Larson, H.P., & Smith, H.A., 1982. *Astrophys. J.,* **259,** 166.

DeNoyer, L.K., 1978. *Mon. Not. R. astr. Soc.,* **183,** 187.

DeNoyer, L.K., 1979a. *Astrophys. J.,* **228,** L41.

DeNoyer, L.K., 1979b. *Astrophys. J.,* **232,** L165.

Dove, J. & Mandy, M., 1987. *Astrophys. J. (letters),* **311.** L93.

Doyon, R. & Nadeau, D., 1988. *Astrophys. J.,* **334,** 883.

Draine, B.T., 1980. *Astrophys. J.,* **241,** 1021.

Draine, B.T. & Roberge W.G., 1982. *Astrophys. J. (letters),* **259,** L91.

Draine, B.T. & Roberge W.G. & Dalgarno A., 1983. *Astrophys. J.,* **264,** 485.

Duley W.W. & Williams, D.A., 1984. *Interstellar Chemistry,* Academic press, London.

Duley W.W. & Williams, D.A., 1986. *Mon. Not. R. astr. Soc.,* **223,** 177.

Dyson, J., & Williams, D.A., 1980. *The physics of the interstellar medium,* Manchester University press.

Dyson, J. 1987. In: *IAU Symposium 122 Circumstellar Matter,* ed. Appenzeller, I., & Jordan, C., Reidel, Dordrecht.

Erickson, N.R., Goldsmith, P.F., Snel, R.L., Berson, R.L., Huguenin, G.R., Ulich, B.L., & Lada, C.J., 1982. *Astrophys. J. (letters),* **261,** L103.

Elitzur, M., 1982. *Astrophys. J.,* **262,** 189.

Fesen, R.A., 1984. *Astrophys. J.,* **281,** 658.

Fiebig, D., & Gusten, R., 1989. *Astron. Astrophys.,* **214,** 333.

Field, G.B., Sommerville, W.B. & Dressler, K., 1966. *Ann. Rev. Astron. & Astrophys.,* **4,** 207.

Flower, D. & Pineau des Forets, G., 1986. *Mon. Not. R. astr. Soc.,* **220,** 149.

Garden, R., Geballe, T.R., Gatley, I., & Nadeau, D., 1986. *Mon. Not. R. astr. Soc.,* **220,** 203.

Gatley, I., Garden, R., Brand, P.W.J.L., Lightfoot, J., Glencross, W., Okuda, H. & Nagata, T. 1987. *Astrophys. J. (letters),* **318,** L73.

Gautier III, T.N., Fink, U., Treffers, R.R. & Larson, H.P., 1976. *Astrophys. J. (letters),* **207,** L129.

Geballe, T.R., 1986. In: *Summer school on Interstellar processes,* eds Hollenbach, D.J. & Thronson, H.A. (NASA TM 88342), p. 129.

Geballe, T.R., & Garden, R.P., 1987. *Astrophys. J. (letters),* **317,** L107.

Geballe, T.R., & Garden, R.P., 1989, in preparation.

Geballe, T.R., Persson, S.E., Simon, T., Lonsdale, C.J., & McGregor, P.J., 1986. *Astrophys. J.,* **302,** 693.

Geballe, T.R., Russell, R.W. & Nadeau, D., 1982. *Astrophys. J. (letters),* **259,** L47.

Genzel, R., & Downes, D., 1982. In: *Regions of recent star formation,* p. 251, eds. Roger, R.S. & Dewney, P.E., Dordrecht, Reidel, Holland

Genzel, R., Harris, A.I., & Stutzki, J., 1990. In: *the proceedings of 22nd Eslab symposium on infrared spectroscopy in astronomy,* Salamanca, 7-9th December 1988 (ESA SP series)

Genzel, R., & Stutzki, J., 1989. *Ann. Rev. Astron. & Astrophys.,* **27,** 41.

Giles, K., 1977. *Mon. Not. R. astr. Soc.,* **180,** p57.

Goldsmith, P.F., Plambeck, R.L. & Chiao, R.Y., 1975. *Astrophys. J.,* **196** L39.

Gould, R.J., & Harwit, M., 1963. *Astrophys. J.,* **137,** 694.

Hartquist, T.W., Dyson., J.E., Pettini, M., & Smith, L.M., 1986. *Mon. Not. R. astr. Soc.,* **221,** 715.

Hartquist, T.W., & Dyson., J.E., 1987. *Mon. Not. R. astr. Soc.,* **228,** 957.

Hasegawa, T. & Akabane, K., 1984. *Astrophys. J. (letters),* **287,** L91.

Hasegawa, T., 1987. In: *Star forming regions,* p. 123, eds Piembert, M. & Jugaku, J., Dordrecht, Reidel, Holland.

Hasegawa, T., Gatley, I., Garden., R.P., Brand, P.W.J.L., Ohishi., M., Lightfoot, J.F., Hayashi, M. & Kaifu, N., 1987. *Astrophys. J. (letters),* **318,** L77

Hayashi, M., Hasegawa, T., Gatley, I., Garden, R.P. & Kaifu, N., 1985. *Mon. Not. R. astr. Soc.,* **215,** 31p.

Herzberg, G., 1950. *Spectra of Diatomic molecules.* New York van Nostrand Reinhold.

Hollenbach, D.J., 1988. *Astro. Lett. and communicatios,* **26,** 191.

Hollenbach, D.J. & McKee, C.F., 1979. *Astrophys. J. Suppl.,* **41,** 55.

Hollenbach, D.J. & McKee, C.F., 1980. *Astrophys. J. (letters),* **241,** L47.

Hollenbach, D.J. & McKee, C.F., 1989. *Astrophys. J.,* in press.

Hollenbach, D.J. & Salpeter, E.E., 1971. *Astrophys. J.,* **163,** 155.

Hollenbach, D.J. & Shull, J.M., 1977. *Astrophys. J.,* **216,** 419.

Hunter, D.A. & Watson, W.D., 1978. *Astrophys. J.,* **226,** 477.

Imamura, J.N., & Chevalier, R.A., 1982. *Bull. Am. Astr. Soc.,* **13,** 791.

Innes, D.E., Giddings, J.R., & Falle, S.A.E.G., 1987. **226,** 67.

Knacke, R.F. & Young, E.T. 1981. *Astrophys. J. (letters),* **249,** L65.

Kwan, J., 1977. *Astrophys. J.,* **216,** 713.

Lada, C.J., 1986. *Ann. Rev. Astron. & Astrophys.,* **23,** 267.

Lane, A.P., & Bally, J., 1986. *Astrophys. J.,* **310,** 820.

Landau, L.D., & Lifshitz, E.M., 1987. *Fluid Mechanics second edition: Course of theoretical physics vol. 6,* Pergamon press.

Leonas, V.B., & Pjarnpuu, A.A., 1981. *Sov. Astr. Lett.* **7(1),** *19.*

Lepp, S., & McCray, R., 1983. *Astrophys. J.,* **269,** 560.

Lepp, S. & Shull, J.M., 1987. *Astrophys. J.,* **270,** 578.

London, R., McCray, R. & Chu, S-I., 1977. **217,** 442.

Mathis, J.S., Rumpl, W. & Nordsieck, K.H., 1977. *Astrophys. J.,* **217,** 425.

McKee, C.F., 1986 In: *Spectroscopy of Astrophysical plasmas* eds. Dalgarno & Layzer, p. 226.

McKee, C.F., 1988. *Supernovae remnants and the interstellar medium,* IAU Colloquium 101, p.205. eds. Roger, R.S., & Landecker, T.L. Cambridge University press.

McKee, C.F., 1989. *Astrophys. J.,* **345,** 782.

Mckee, C.F., Chernoff, D.F. & Hollenbach, D.J., 1984. In: *Galactic and extragalactic infrared spectroscopy,* p. 103, eds. Kessler, M.F. & Phillips, J.P., Dordecht, Reidel, Holland.

Mckee, C.F., Storey, J.W.V., Watson, D.M. & Green, S., 1982. *Astrophys. J.,* **259,** 647.

McKee, C.F., Hollenbach, D.J., Seab, C.G., & Tielens, A.G.G.M. 1987. *Astrophys. J.,* **318,** 674.

Mouschovias, T.C., 1976. *Astrophys. J.,* **207,** 141.

Myers, P.C., 1983. *Astrophys. J.,* **270,** 105.

Mullan, D.J., 1971. *Mon. Not. R. astr. Soc.,* **153,** 145.

Nadeau, D., Geballe, T.R., 1979. *Astrophys. J.,* **230,** 1169.

Nadeau, D., Geballe, T.R. & Neugebauer, 1982. *Astrophys. J.*, **253**, 154.

Neufeld, D.A. & Dalgarno, A., 1989. *Astrophys. J.*, **340**, 869.

Neufeld, D.A. & Melnick, G., 1987. *Astrophys. J.*, **322**, 266.

Norman, C., & Silk, J., 1980. *Astrophys. J.*, **238**, 158.

Norris, R.P., 1984. *Mon. Not. R. astr. Soc.*, **207**,

Olivia, E., & Moorwood, A.F.M., 1988. *Astron. Astrophys.*, **197**, 261.

Osterbrock, D.E., 1974. *Astrophysics of gaseous nebulae,* W.H. Freeman-San Francisco.

Perault, M., Falgarone, E., & Puget, J., 1985. *Astron. Astrophys.*, **152**, 371.

Petre, R., Canizares, C.R., Winkler, P.F., Seward, F.D., Willingale, R., Rolf, D., & Woods, N., 1983. In: *Supernova Remnants and their X-ray Emission,* p. 289, eds Danziger, J. & Gorenstein, P., Reidel, Dordrecht, Holland.

Petre, R., Szymkowiak, A.E., Seward, F.D., & Willingale, 1988., *Astrophys. J.*, **335**, 215.

Press, W.H., Flannery, B.P., Teukolsky, S.A., & Vetterling, W.T. 1986. *Numerical Recipes,* Cambridge University press.

Pudritz, R.E., & Norman, C.A., 1983. *Astrophys. J.*, **274**, 677.

Roberge, W.G., & Dalgarno, A., 1982. *Astrophys. J.*, **255**, 176.

Roberge W.G., & Draine, B.T. 1987. *News Lett. Astr. Soc. N.Y.*, **3**, 8.

Schinke, R., Engel., V., Buck, U., Meyer, H. & Diercksen, G.H.F., 1985. *Astrophys. J.*, **299**, 939.

Scoville, N.Z., Hall, D.N.B., Kleinmann, S.G. & Ridgway, S.T., 1982. *Astrophys. J.*, **253**, 136.

Scoville, N.Z., Min, S.Y., Clemens, D.P., Sanders, D.B., & Waller, W.H., 1987. *Astrophys. J. Suppl.*, **63**, 821.

Sellgren, K., 1981. *Astrophys. J.*, **245**, 138.

Sellgren, K., 1986. *Astrophys. J.*, **305**, 399.

Shull, J.M. & Beckwith, S., 1982. *Ann. Rev. Astron. & Astrophys.*, **20**, 163.

Shull, J.M. & Draine, B.T., 1987. In: *Interstellar Processes,* p.283, eds. Hollenbach, D.J. & Thronson, H.A., Reidel, Dordrecht, Holland.

Shull, J.M. & Hollenbach, D.J., 1978. *Astrophys. J.*, **220**, 525.

Simon, M., Righini-Cohen, G., Joyce, R.R., & Simon, T., 1979. *Astrophys. J. (letters),* **230**, L175.

Smith, M.D. 1989. *Mon. Not. R. astr. Soc.*, **238**, 235.

Smith, M.D., & Brand, P.W.J.L., 1990a. *Mon. Not. R. astr. Soc.,* in press.

Smith, M.D., & Brand, P.W.J.L., 1990b. *Mon. Not. R. astr. Soc.,* in press.

Smith, M.D., & Brand, P.W.J.L., 1990c. *Mon. Not. R. astr. Soc.,* submitted.

Smith, M.D., Brand, P.W.J.L. & Moorhouse, A., 1990a. *Mon. Not. R. astr. Soc.,* submitted.

Smith, M.D., Brand, P.W.J.L. & Moorhouse, A., 1990b. *Mon. Not. R. astr. Soc.,* submitted.

Solomon, p.m., Rivolvo, A.R., Barrett, J.W., & Yahil, A., 1987. *Astrophys. J.*, **319**, 730.

Spitzer, L. Jr., 1978. *Physical processes in the interstellar medium,* Wiley Interscience-London.

Sternberg, A., 1989. in the proceedings of 22^{nd} Eslab symposium on infrared spectroscopy in astronomy, Salamanca, 7-9^{th} December 1988.

Storey, J.W.V., Watson, D.M., & Townes, C.H., 1981. *Astrophys. J. (letters),* **244**, L27.

Tielens A.G.G.M. & Hollenbach D., 1985a. *Astrophys. J.*, **291**, 722.

Tielens A.G.G.M. & Hollenbach D., 1985b. *Astrophys. J.*, **291**, 747.

Troland, T.H., Crutcher, R.M., & Kazes, I., 1986. *Astrophys. J. (letters)*, **304**, L57.

Treffers, R.R., 1979. *Astrophys. J.*, **233**, L17.

Turner, J., Kirby-Docken, K., & Dalgarno, A., 1977. *Astrophys. J. Suppl.*, **35**, 281.

Viscusso, P.J. & Chernoff, D.F., 1988. *Astrophys. J.*, **327**, 364.

Wade, R., 1983. In: *Instrumentation in Astronomy* V eds. Boksenburg, A. & Crawford, D.L., Proc. SPIE, **445**, 47.

Watson, D.M., Genzel, R., Townes, C.H. & Storey, J.W.V., 1985. *Astrophys. J.*, **298**, 316.

Watson, M.G., Willingale, R., Pye, J.P., Rolf, D.P., Wood, N., Thomas, N., & Seward, F.D., 1983. In: *Supernova Remnants and their X-ray Emission*, p. 289, eds Danziger, J. & Gorenstein, P., Reidel, Dordrecht, Holland.

White, G.J., Rainey, R., Hayashi, S.S., & Kaifu, N., 1987. *Astron. Astrophys.*, **173**, 337.

White, G.J., 1988. In: *Millimetre and Submillimetre Astronomy*, Kona, Hawaii. ed A.S. Webster.

Wynn-Williams, C.G., Genzel, R., Becklin, E.E. & Downes, D., 1984. *Astrophys. J.*, **281**, 271.

Zeldovich, Y.B., & Raizer, Y.P., 1966. *Physics of shock waves and high temperature hydrodynamic phenomena*, eds. Hayes, W.D., & Probstein, R.F., Academic press, New York and London.

Finally...

This thesis not only represents the end of three and a little bit happy years at Edinburgh but also the transition from the amateur to professional ranks. The necessary increase in appreciation to get from the staring through telescopes stage to the increasing short-sightedness due to staring at VDU's all night long would have never occurred if not for the knowledge, skill and enthusiasm of my supervisor Peter Brand. It would certainly have been very difficult without the loan of a bedroom during my first month in Edinburgh, thanks Peter and Eileen. Even though hard to see the information being relayed to the VDU's was vastly improved by Tom Geballe, his ability at getting the most out of UKIRT's instruments amazes me still. Peter and Tom along with Mike Burton need to be thanked for their scientific input and for being great fun to observe and work with. Mike Smith, the younger, is thanked for all those little chats.

I cannot forget all the other lads and lasses, both present and those that have since passed on. I thank you all for making the observatory a lively, friendly and more humane place to work and live. If I do not single you out here, well sorry, but there are some who deserve special thanks. It seems I have spent the last three years with a total difference of opinion with Phil Blanco. Thanks for being just ever so slightly insane. Dave Nicholoson has kept me company over the the few months while this was written and he as well as Karl Glazebrook have saved my sanity on more than one occasion by convincing me to have the odd drink or two. Of the friends I have made in Edinburgh, Mike is thanked not only for the many pints but also for being a member from the valley and Mad Johnny is, put simply, Mad. The transition from layman to amateur was quickened by all the members of Cleethorpes and District Astronomical Society. Their keeness has helped to keep things in perspective, in particular Barry & George, Andy & Karen and Paul (foothills are dangerously distracting) are thanked for the fun times had while looking for that damned comet. Many old friends need a special mention. Yet another Mike is thanked for not only being a close friend but is also blamed for my life as a vegan (or β pictoran as a another Mike put it!). Steve's rapid return to the right upon obtaining a car and mortgage was astounding, Tim's peaked cap even more so. Geoff for his Holmes impression and Steve for being himself. If any person left out feels offended it is a tough life and well sorry. The Sing When We're Fishing team are thanked for all the wittiscisms. I acknowledge the SERC for keeping me alive, barely.

The largest and most heartfelt thanks have to go to all the members of my family and to my parents in particular. Their continual support, encouragement and understanding (if not of the science, but one day...) especially when I was young has helped more than anything else. It is corny but literally none of this would have been possible without them. I have therefore dedicated this thesis to them.

Spatial variations of the 3 μm emission features within Orion's Bar

A. Moorhouse, T.R. Geballe, L.J. Allamandola, A.G.G.M. Tielens & P.W.J.L. Brand

Abstract

We have obtained 3 μm spectra of the Orion Bar region, at three positions corresponding to different distances from the exciting source. The recently discovered unidentified features at 3.46, 3.51, and 3.57 μm are clearly visible. The spectra show that the 3.4 and 3.51 μm emission features increase in intensity relative to the strong 3.3 μm feature as the distance from the exciting source increases. The implications for polycyclic aromatic hydrocarbons and recent ideas concerning their ultraviolet excitation and spatial evolution are discussed.

7.1 Observations

The Orion Bar is an ionization front, seen edge on and located approximately 2 arc minutes south east of the trapezium stars. The neutral molecular material beyond the ionization front is a strong emitter of the bright unidentified features in the 3–12 μm waveband. The emission is also known to be extended in a direction perpendicular to the ionization front.

Spectra from 3.1–3.7 μm have been obtained at three positions in the neutral bar, Aitken's position 4 at R.A. = $5^h\ 32^m\ 52.4^s$ and declination = $-5°\ 27'\ 3.5''$ (1950 coordinates; Aitken *et al.* 1979), and 10″ and 20″ south of position 4. All observations were made at UKIRT using CGS2 with a beam size of 5″. At all positions the well known strong 3.3 μm feature can be seen (Figure 7.1), in addition there are weaker bands at 3.4, 3.46, 3.51 and (marginally above the noise) 3.57 μm. The last three bands were only recently discovered by de Muizon *et al.* (1986). The plateau of emission from 3.25–3.60 μm seen in other objects (Geballe *et al.* 1985) is also visible. All of the features decrease in intensity to the south of position 4. It is clear, however, that the 3.40 and 3.51 μm bands do not decrease as rapidly as the others. Similar behaviour of the 3.4 μm feature is seen in the Red Rectangle (Geballe *et al.* 1988).

7.2 Interpretation

The frequencies of absorption features in the laboratory spectra of aromatic molecules are close to the frequencies of the brighter astronomical emission features. Current thinking is that the astronomical bands arise from ultraviolet excitation of the most stable members of polycyclic aromatic hydrocarbons (PAHs), which could exist in the interstellar medium as free molecules or as

Dust in the Universe, eds. Bailey, M.E. & Williams, D.A., 67–71.

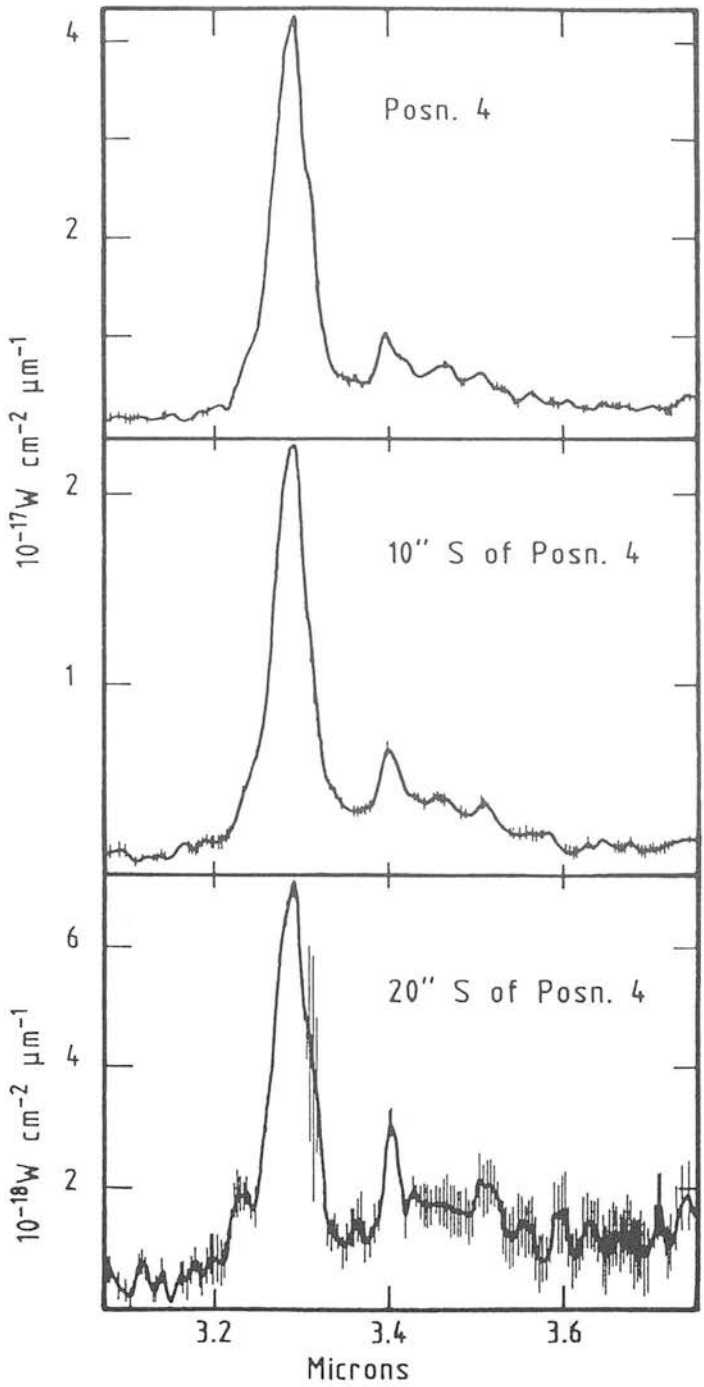

Figure 7.1: The three spectra taken at the locations indicated in the Orion Bar. The spectra have been Hanning smoothed to a resolution of 0.009 μm.

small amorphous particles (Duley & Williams 1981, Léger & Puget 1984, Allamandola *et al.* 1985). The main bands between 3 and 12 μm are assigned to various C−C and C−H stretch and bend-stretch modes in PAHs which are thought to contain between 20–50 carbon atoms (d'Hendecourt & Léger 1987).

There have been two suggestions for the interpretation of the weak features in the 3 μm spectra. One is that some of these features are vibrational overtones of the C−H stretch (Barker *et al.* 1987). The second, suggested by Duley & Williams (1981) for the — at that time unresolved — 3.4 μm band, is that all of the weak features are fundamental vibrations of molecular subgroups attached to the PAHs (de Muizon *et al.* 1986).

A: The features as vibrational overtones

The fundamental vibrational C−H stretch is always close to 3.3 μm for PAHs. The overtone transitions are shifted to longer wavelengths because of anharmonicity in the potential. The emission features at 3.40 and 3.51 μm are close to the expected wavelengths of the 2–1 and 3–2 vibrational transitions of CH in PAHs (Barker *et al.* 1987), thus suggesting their identity as overtone transitions.

The $v = 2$ vibrational modes are more easily excited in smaller rather than larger PAHs. This is because smaller PAHs contain fewer atoms, and therefore fewer vibrational modes throughout which the photon energy can be distributed. The probability of enough energy being deposited in the C−H stretch to excite the high levels will thus be larger for the smaller PAHs. The smaller PAHs will, however, be more susceptible to destruction by ultraviolet radiation.

When the amount of energy which is deposited in the molecule exceeds a critical value CH bond rupture will occur (Tielens *et al.* 1987). Once a CH bond is broken, there are fewer modes throughout which the energy of a second absorbed photon can be distributed, and hence another CH bond will rupture. If this can occur before attachment of a hydrogen atom onto the free bond, the PAH will quickly become dehydrogenated.

The spatial variations of the features could then be qualitatively explained by the following scenario. At position 4, near to the exciting star, there is a high flux of radiation and only the larger PAHs survive. These large PAHs are unlikely to emit from $v \gtrsim 2$. Further away from position 4 the radiation flux is far less and the smaller PAHs will be able to survive. There will thus be relatively more emission from the excited levels.

B: The features as vibrational modes of molecular subgroups

Laboratory experiments (d'Hendecourt & Léger 1987) show that aliphatic subgroups such as $-CH_3$ and $-C_2H_5$ produce transitions between 3.3 μm and 3.6 μm. It has been suggested that such subgroups attached to PAHs could be responsible for the weak features (de Muizon *et al.* 1986, de Muizon *et al.* 1987). The relative strengths of the features might then be due to different

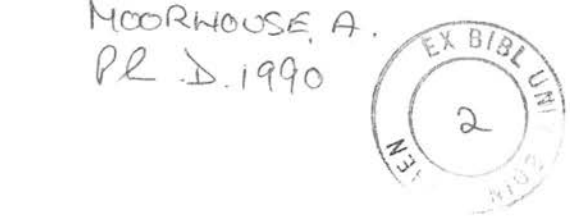

THE ASTROPHYSICAL JOURNAL, 334:L103–L106, 1988 November 15

RATIOS OF MOLECULAR HYDROGEN LINE INTENSITIES IN SHOCKED GAS: EVIDENCE FOR COOLING ZONES

P. W. J. L. BRAND,[1] A. MOORHOUSE,[1] M. G. BURTON,[2] T. R. GEBALLE,[3,4] M. BIRD,[1] AND R. WADE[5]

Received 1988 February 3; accepted 1988 August 19

ABSTRACT

Column densities of molecular hydrogen have been calculated from 19 infrared vibration-rotation and pure rotational line intensities measured at peak 1 of the Orion molecular outflow. The run of column density with energy level is similar to a simple cooling zone model of the line-emitting region, but is not well fitted by predictions of *C*-shock models current in the literature.

Subject headings: infrared: spectra — interstellar: molecules — molecular processes — shock waves

I. INTRODUCTION

The discovery of line emission from shocked molecular hydrogen in the Orion molecular cloud OMC-1 (Gautier *et al.* 1976) stimulated a series of theoretical studies (Kwan 1977; London, McCray, and Chu 1977; Hollenbach and Shull 1977) of the structure of molecular shocks. Observations of an extremely supersonic range of velocities in the H_2 1–0 $S(1)$ line profile (Nadeau and Geballe 1979) prompted several workers (Draine 1980; Chernoff, Hollenbach, and McKee 1982; Draine, Roberge, and Dalgarno 1983) to develop magnetically moderated *C*-shock models.

In this *Letter* we present data from the brightest part of the OMC-1 outflow, peak 1 ($5^h32^m46^s$, $-5°24'02''$ [1950] Beckwith *et al.* 1978). The data consist of a set of molecular hydrogen line intensities observed between 2 μm and 4 μm, which cover a wide range of upper level energies (6500–25,500 K).

II. OBSERVATIONS

All of the observations of peak 1 were made at the United Kingdom 3.8 m Infrared Telescope on Mauna Kea. Most of them utilized the facility cooled grating spectrometer. The beam diameter of this instrument was set to 5″; the resolving power was typically 500. Standard chopping and nodding (60″ EW) practices were employed. The stars BS 1552 and BS 1713 were used for flux calibration. All of the 3 μm lines were measured in 1985 November; most of the 2 μm lines were observed in 1987 January and February. In addition, during the latter period a number of the strong lines in the 2 and 3 μm bands were measured in a single scan so that their relative intensities could be determined. The reduced 2 μm spectrum from 1987 January is shown in Figure 1. The 3 μm spectrum has been published elsewhere (Geballe 1986).

Several 2 μm H_2 lines, including the 4–3 $S(3)$ and 3–2 $S(2)$ (which had not previously been observed), were measured at peak 1 in 1988 January. These data were obtained using the facility CVF spectrometer in series with an ambient temperature Fabry-Perot interferometer. The beam diameter was 12″, and the velocity resolution was $\sim$120 km s^{-1}. Chopping and nodding practices were as above. The 1–0 $S(1)$ line was measured with this instrument, so that the former two line intensities could be scaled to previously measured H_2 lines and thus be included in the analysis. The 4–3 $S(3)$ line is the highest excitation H_2 line yet observed in the 2 μm band; its spectrum is shown inset in Figure 1 together with that of the 3–2 $S(2)$ line.

III. ANALYSIS AND RESULTS

The intensities of lines measured by the cooled grating spectrometer were determined by least-squares fitting Gaussian profiles to the observed lines, together with polynomials to the continua. Because of pointing and beam size differences between the different observations sets, the spectra were scaled to one another using the previously described spectrum that contained lines common to the various 2 and 3 μm spectra. The resulting line intensities are presented in Table 1. We note that the relative intensities of the 2 μm lines measured by us are consistent with those observed by Oliva and Moorwood (1988).

Of the approximately 30 H_2 lines detected, only those 19 lines whose intensities were believed to be free from significant uncertainties (e.g., due to attenuation by telluric absorption lines) were considered for further analysis. Observed column densities, N_0 (assuming no extinction), were determined from the observed intensities using transition probabilities from Turner, Kirby-Docken, and Dalgarno (1977). The extinction may be estimated by comparing intensities of lines which arise from a common upper energy level. In the present data set the 1–0 $S(1)$, 1–0 $Q(3)$, and 1–0 $O(5)$ lines may be used. Assuming $A_\lambda \propto \lambda^{-1.5}$ we determine that $A_K = 0.8 \pm 0.3$. The dereddened column densities in the last column of Table 1 assume this form of the extinction law. If it is assumed that $A_\lambda \propto \lambda^{-1.0}$, the derived extinction is $A_K = 1.0 \pm 0.3$. However, the derived ratios of dereddened column densities are not changed significantly from those in Table 1.

Figure 2 is a plot of the dereddened column density in each level divided by that predicted for a slab of gas at 2000 K. The data are presented in this way in order to show the deviation from such a constant temperature environment, which has often been considered to be characteristic of the H_2 line-emitting region. A Boltzmann distribution at any other temperature is a straight line in this diagram. The best-fit single excitation temperature for the data is $\sim$2200 K, which is consistent with most previous observations of H_2 lines in OMC-1 (e.g., Knacke and Young 1981). However, it is clear that no straight line will be a satisfactory fit to all of the data points.

[1] Department of Astronomy, University of Edinburgh.
[2] NASA/Ames Research Center.
[3] Joint Astronomy Centre, Hilo, Hawaii.
[4] Foundation for Astronomical Research in The Netherlands—ASTRON.
[5] Royal Observatory, Blackford Hill, Edinburgh.

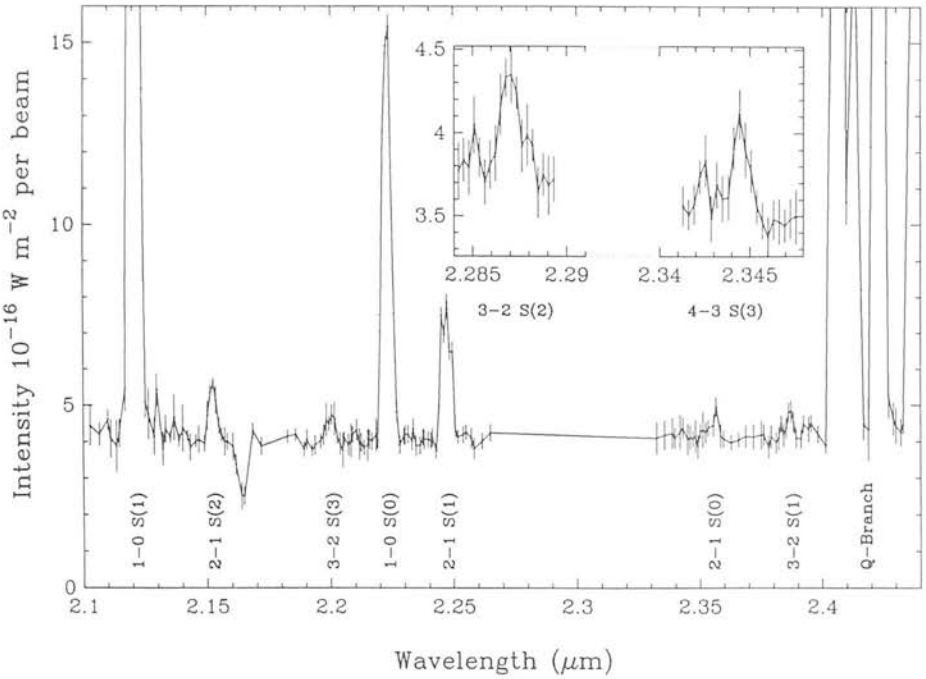

FIG. 1.—Raw 2 μm spectrum from 1987 January, obtained at a resolution of 0.004 μm. Lines used in the analysis are labeled. The feature at 2.166 μm is due to B n the offset beam. The inset is the spectrum of the 3–2 $S(2)$ and 4–3 $S(3)$ lines, at a resolution of 0.0009 μm, and with the same flux scale as the main diagram.

TABLE 1

PARAMETERS AND INTENSITIES OF OBSERVED H_2 LINES

Line	Wavelength[a] (μm)	Upper Level Energy[a] (K)	Flux Density[b] (10^{-16} W m^{-2})	Dereddened Column Density[c]/g_j (10^{18} m^{-2})
1–0 $S(7)$[d]	1.7480	12818	4.2 ± 0.4	...
1–0 $S(1)$	2.1218	6956	50.1 ± 0.5	326.3 ± 2.9
2–1 $S(2)$	2.1542	13150	1.6 ± 0.1	14.8 ± 1.2
3–2 $S(3)$	2.2014	19086	0.8 ± 0.1	1.9 ± 0.2
1–0 $S(0)$	2.2235	6471	12.2 ± 0.2	467.5 ± 11.1
2–1 $S(1)$	2.2477	12550	4.3 ± 0.1	18.8 ± 0.8
3–2 $S(2)$	2.2870	18386	0.8 ± 0.2	2.5 ± 0.6
4–3 $S(3)$	2.3445	23955	0.5 ± 0.1	0.6 ± 0.1
2–1 $S(0)$	2.3556	12095	0.9 ± 0.1	22.5 ± 4.5
3–2 $S(1)$	2.3846	17818	0.8 ± 0.1	3.1 ± 0.8
1–0 $Q(1)$[d]	2.4066	6149	40.0 ± 5.0	...
1–0 $Q(2)$[d]	2.4134	6471	16.5 ± 2.0	...
1–0 $Q(3)$	2.4237	6956	45.1 ± 5.0	367.0 ± 41.0
1–0 $Q(4)$[d]	2.4375	7585	16.0 ± 2.0	...
1–0 $O(4)$[d]	3.0039	6471	13.4 ± 2.0	...
1–0 $O(5)$	3.2350	6956	25.7 ± 2.1	299.0 ± 25.0
2–1 $O(5)$[e]	3.4378	12550	2.1 ± 0.3	16.9 ± 2.4
0–0 $S(17)$	3.4857	25541	1.5 ± 0.5	0.21 ± 0.07
1–0 $O(6)$	3.5007	7584	4.3 ± 0.6	167.0 ± 22.0
0–0 $S(16)$	3.5475	23461	0.8 ± 0.4	0.38 ± 0.18
0–0 $S(15)$	3.6261	21413	3.5 ± 0.6	0.74 ± 0.13
2–1 $O(6)$[d]	3.7236	13150	2.2 ± 0.3	...
0–0 $S(14)$[d]	3.7244	19405		...
1–0 $O(7)$	3.8075	8365	9.2 ± 0.8	145.0 ± 12.0
0–0 $S(13)$	3.8461	17445	8.4 ± 0.9	3.11 ± 0.03
0–0 $S(12)$	3.9960	15542	3.8 ± 0.4	5.8 ± 0.6
2–1 $O(7)$[d]	4.0540	13891	1.4 ± 0.4	...

[a] Obtained from Dabrowski 1984.

[b] In a 5″ aperture at peak 1, except for the 3–2 $S(2)$ and 4–3 $S(3)$ lines, which were in a 12″ aperture. These latter two fluxes need to be divided by 2.9 to scale with those in a 5″ aperture [based on a measurement of the 1–0 $S(1)$ line through the 12″ aperture]. The 2 μm line fluxes combine two sets of measurements. The 3 μm line fluxes have been multiplied by a factor of 1.07 from the observed values based on a composite 2 and 3 μm spectrum.

[c] Assumes $A_\lambda \propto \lambda^{-1.5}$ with $A_K = 0.8$. All values apply to a 5″ aperture.

[d] Line detected, but either contaminated by telluric absorption lines, blended with other lines, or observed with incomplete spectral coverage. Intensities not reliable enough to be included in the analysis.

[e] Blended with 0–0 $S(18)$, but we estimate the contamination is $< 5\%$.

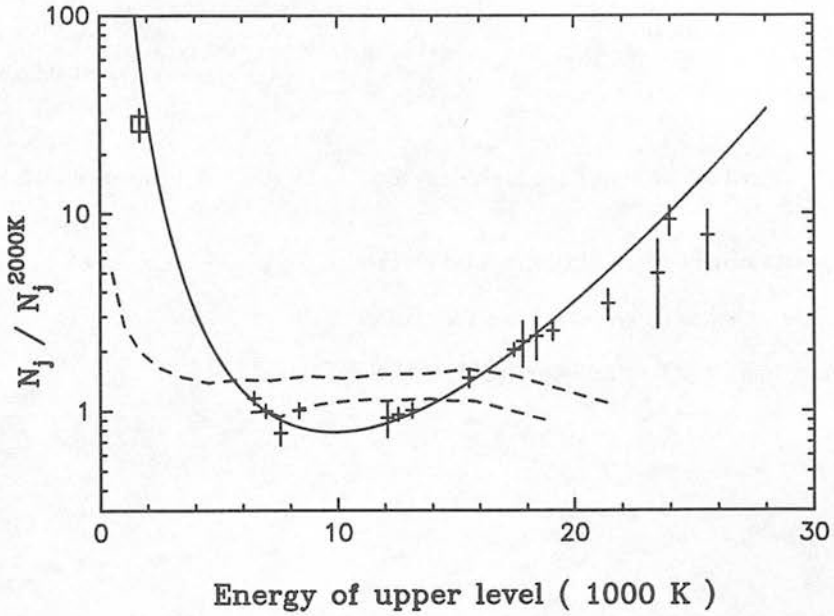

FIG. 2.—Plot of the ratios of observed, dereddened H_2 column densities to those from a Boltzmann distribution at 2000 K [normalized so that the 1–0 $S(1)$ ratio is unity] vs. upper energy level. Error bars are $\pm 1\ \sigma$. The continuous line is from the cooling flow calculations described in the text, drawn through the 1–0 $S(1)$ point. The dashed lines are the predictions of the C-shock models for OMC-1 by Draine and Roberge (1982) and by Chernoff, Hollenbach, and McKee (1982). The upper line is for pure rotational lines. The box represents the value of the 0–0 $S(2)$ line observed by Beck *et al.* (1979).

The weak, high-excitation lines are considerably more intense than would be expected from a straight line fit based on the strong, low-excitation lines. Since weak and strong lines come from both the 2 and the 3 μm spectra and correspond to both ortho- and para-H_2, neither errors in scaling, errors in dereddening, nor any particular ortho-para ratio can be the cause of the curvature in the locus of data points in Figure 2.

A significant contribution to the high-v lines from fluorescence is highly unlikely at peak 1, since the intensity of the 3–2 $S(2)$ line decreases with that of the 1–0 $S(1)$ line just off-source, but within the ionized nebula. It is clear on theoretical grounds that intensities of the weak, high-J pure rotational lines at peak 1 cannot be significantly enhanced by fluorescent emission.

IV. DISCUSSION

The solid curve in Figure 2 is the prediction from a "toy" calculation (which nevertheless contains all the major features of the full calculation) of column density in the cooling zone behind a hydrodynamic shock. The cooling rate is taken to be $\Lambda = \Lambda_0 T^s$ W (H_2 molecule)$^{-1}$, with s set to 4.7 to match roughly the calculations (Hollenbach and McKee 1979; Burton 1986) of cooling by thermalized H_2. If the shock is strong enough, the H_2 column density per state at level j with energy T_j degrees Kelvin is approximately

$$N_j/g_j \propto \int e^{-T_j/T}(Q\Lambda)^{-1}\,dT \propto T_j^{-s} - (T_j + T_v)^{-s}, \quad (1)$$

where the partition function Q is approximated by $AT(1 - e^{-T_v/T})$ with $T_v = 6000$ K.

A proper calculation of column density in a J-shock cooling zone, and a corresponding investigation of C-shocks, is being prepared for publication.

The cooling flow calculation described above provides a surprisingly good fit to the observed data. The apparent range of temperatures is naturally explained by the shape of the cooling function, independently of local conditions such as the shock velocity. This is consistent with other evidence (Brand *et al.* 1988) which shows that the ratio of a pair of H_2 lines with upper energy levels at 8365 K and 17,458 K respectively, is constant throughout the outflow.

In a calculation with the detailed shape of the cooling function properly treated, a better fit will result. Current C-shock models provide a poor fit to the wide range of H_2 data now available, and it appears that a superposition of several C-shocks may be required. The dashed curves are from the C-shock calculations by Draine and Roberge (1982) and Chernoff, Hollenbach, and McKee (1982).

We wish to thank the staff of the United Kingdom Infrared Telescope for friendly and able assistance during the several observing runs from which this *Letter* resulted. A. M. and M. B. are supported by SERC studentships. This work was done, in part, while M. G. B. held a National Research Council NASA Research Associateship at Ames Research Center.

REFERENCES

Beck, S. C., Lacy, J. H., and Geballe, T. R. 1979, *Ap. J. (Letters)*, **234**, L213.
Beckwith, S., Persson, S. E., Neugebauer, G., and Becklin, E. E. 1978, *Ap. J.*, **223**, 464.
Brand, P. W. J. L., Toner, M. P., Webster, A. S., Geballe, T. R., and Williams, P. M. 1988, *M.N.R.A.S.*, submitted.
Burton, M. G. 1986, Ph.D. thesis, University of Edinburgh.
Chernoff, D. F., Hollenbach, D. J., and McKee, C. F. 1982, *Ap. J. (Letters)*, **259**, L97.
Dabrowski, I. 1984, *Canadian J. Phys.*, **62**, 1639.
Draine, B. T. 1980, *Ap. J.*, **241**, 1021.
Draine, B. T., and Roberge, W. G. 1982, *Ap. J. (Letters)*, **259**, L91.
Draine, B. T., Roberge, W. G., and Dalgarno, A. 1983, *Ap. J.*, **264**, 485.
Gautier, T. N., III, Fink, U., Treffers, R. R., and Larson, H. P. 1976, *Ap. J. (Letters)*, **207**, L29.
Geballe, T. R. 1986, in *Summer School on Interstellar Processes*, ed. D. J. Hollenbach and H. A. Thronson (NASA TM 88342), p. 129.

Hollenbach, D. J., and McKee, C. F. 1979, *Ap. J. Suppl.*, **41**, 553.
Hollenbach, D. J., and Shull, J. M. 1977, *Ap. J.*, **216**, 419.
Knacke, R. F., and Young, E. T. 1981, *Ap. J.* (*Letters*), **249**, L65.
Kwan, J. 1977, *Ap. J.*, **216**, 713.
London, R., McCray, R., and Chu, S-I. 1977, *Ap. J.*, **217**, 442.
Nadeau, D., and Geballe, T. R. 1979, *Ap. J.* (*Letters*), **230**, L169.
Oliva, E., and Moorwood, A. F. M. 1988, *Astr. Ap.*, **197**, 261.
Roberge, W. G., and Dalgarno, A. 1982, *Ap. J.*, **255**, 176.
Turner, J., Kirby-Docken, K., and Dalgarno, A. 1977, *Ap. J. Suppl.*, **35**, 281.

M. BIRD, P. W. J. L. BRAND, and A. MOORHOUSE: University of Edinburgh, Department of Astronomy, Royal Observatory, Blackford Hill, Edinburgh EH9 3HJ, Scotland

M. G. BURTON: NASA/Ames Research Center, MS 245-6, Moffett Field, CA 94035

T. R. GEBALLE: Joint Astronomy Centre, 665 Komohana Street, Hilo, HI 96720

R. WADE: Royal Observatory, Blackford Hill, Edinburgh EH9 3HJ, Scotland

THE ASTROPHYSICAL JOURNAL, 341:278–287, 1989 June 1

SPATIAL VARIATIONS OF THE 3 MICRON EMISSION FEATURES WITHIN UV-EXCITED NEBULAE: PHOTOCHEMICAL EVOLUTION OF INTERSTELLAR POLYCYCLIC AROMATIC HYDROCARBONS

T. R. GEBALLE,[1,2] A. G. G. M. TIELENS,[3,4] L. J. ALLAMANDOLA,[3] A. MOORHOUSE,[5] AND P. W. J. L. BRAND[5]

Received 1988 June 17; accepted 1988 October 28

ABSTRACT

We have obtained 3 μm spectra at several positions in the Orion Bar region and in the "Red Rectangle," the nebula surrounding HD 44179. The recently discovered weak emission features at 3.40, 3.46, 3.51, and 3.57 μm (2940, 2890, 2850, and 2800 cm^{-1}) are prominent in the Orion Bar region. The 3.40 μm and 3.51 μm features increase in intensity relative to the dominant 3.29 μm (3040 cm^{-1}) feature when going from the ionized to the neutral zone across the Orion Bar. The spectrum obtained in the Red Rectangle, 5″ north of HD 44179, is somewhat similar to those in the Orion Bar. However, only a weak and rather broad 3.40 μm feature is present at the position of HD 44179. These spectra demonstrate that some of the 3 μm emission components vary independently of each other and in a systematic way within UV-excited nebulae. This spatial variation is discussed in terms of the UV excitation and photochemical evolution of polycyclic aromatic hydrocarbons and related molecular structures. The spatial behavior of the weak emission features can be understood qualitatively in terms of hot bands of the CH stretch and overtones and combination bands of other fundamental vibrations in simple PAHs. An explanation in terms of emission by molecular sidegroups attached to the PAHs is less straightforward, particularly in the case of the Red Rectangle and other evolved, mass-losing objects. We estimate PAH sizes of 20–50 carbon atoms based on the susceptibility of PAHs to destruction by the far ultraviolet fields present in the Orion Bar and the Red Rectangle; the size range is similar to independent estimates made previously.

Subject headings: infrared: spectra — interstellar: molecules — nebulae: individual (Red Rectangle) — nebulae: Orion Nebula

I. INTRODUCTION

Recent observations of the 3 μm unidentified emission features found in many UV-excited nebulae have revealed that their spectra are considerably more complex than had earlier been appreciated. Although the dominant feature is the well-known 3.29 μm (3040 cm^{-1}) band, other features at 3.40, 3.46, 3.51, and 3.57 μm (2940, 2890, 2850, and 2800 cm^{-1}) are present in some objects and, in addition, the above features appear to be perched on a rounded "plateau" of emission, above the flat continuum, which extends approximately from 3.2 to 3.6 μm (3100 to 2800 cm^{-1}) (Geballe *et al.* 1985; de Muizon *et al.* 1986; Nagata *et al.* 1988). These features have been attributed to the vibrations of polycyclic aromatic hydrocarbons (PAHs) and to related species (e.g., Duley and Williams 1981; Leger and Puget 1984; Allamandola, Tielens, and Barker 1985; Sakata *et al.* 1984; de Muizon *et al.* 1986; Borghesi, Busoletti, and Colangeli 1987). However, precise molecular identifications of the emitting species are unknown.

Clues to the origin of the unidentified 3 μm emission features might be found, not only by accurate determination of their wavelengths and profiles or by studies of their intensity variations from source to source, as have been done previously (e.g., Geballe *et al.* 1985), but also by studying their spatial variations within extended sources. The most basic of the latter approaches is to study the dependence of feature strengths with distance from the star which pumps the emission. We have taken this last approach by obtaining spectra from 3.1 to 3.7 μm (3225 to 2700 cm^{-1}) at three locations in the Orion Bar which are located at different distances from the Trapezium stars, and by observing the Red Rectangle at two locations, one on HD 44179 itself and the other 5″ north of that star. At most of these locations fairly accurate UV fluxes can be estimated. Knowledge of the spectrum and flux of the ultraviolet radiation field is crucial to proper understanding of the physical conditions experienced by the emitting material and can be used to place constraints on the structure of the emitters. This information, in turn, sheds light on the spatial, chemical, and physical evolution of the band carriers and their environment.

II. OBSERVATIONS

All spectra were obtained at the United Kingdom 3.8 m infrared telescope on Mauna Kea, using the facility liquid and solid nitrogen–cooled grating spectrometer with a 5″ aperture. A spectrum of the Red Rectangle, which consists of 12 individual scans, was obtained in 1984 December, 5″ north of the central star HD 44179. A spectrum obtained with the aperture centered on the star already has been published (Geballe *et al.* 1985); however, a second such spectrum, obtained in 1987 January with the aperture centered on the star, is presented here. Total integration times were 18 and 1.1 minutes, respectively. During both of these measurements a chopper throw of ~40″ (EW) was used. Most of the Orion Bar measurements were obtained in 1986 December. The locations observed were position 4 (Aitken *et al.* 1979) and 10″ and 20″ south of this position. The number of independent spectra and the total integration times at these positions were 4, 6, and 7 and 15, 22, and 26 minutes, respectively. An additional 16 spectra at the 20″ south position were obtained in 1987 August and brought the total amount of observing time at this position to about

[1] Joint Astronomy Centre, Hilo, Hawaii.
[2] Foundation for Astronomical Research in the Netherlands (ASTRON).
[3] NASA/Ames Research Center.
[4] Space Sciences Laboratory, University of California (Berkeley).
[5] Royal Observatory Edinburgh.

TABLE 1

PEAK INTENSITIES OF EMISSION FEATURES

SOURCE	PEAK SPECTRAL INTENSITY OF FEATURE (10^{-17} W cm^{-2} μm^{-1})[a]				
	λ (μm) = 3.29	3.40	3.46	3.51	3.57
	ν (cm^{-1}) = 3040	2940	2890	2850	2800
Orion Position 4	3.9	0.50	0.20	0.17	0.10
Orion Position 4 (10″ S)	2.0	0.35	0.06	0.11	0.05
Orion Position 4 (20″ S)	0.50	0.13	<0.02	0.06	<0.02
Red Rectangle (HD 44179) ...	160.	10.	<5.	<5.	...
Red Rectangle (5″ N)	4.5	0.6	<0.2	0.2	<0.15

[a] Above continuum plus plateau for Orion Bar; above adjacent flux density levels for Red Rectangle.

2 hr. During all Orion Bar observations the chopper throw was 120″ (EW), so that the reference beam, although well within the ionized gas of the Orion Nebula, was off of the extended infrared continuum emission (see Sellgren 1981).

The spectra obtained 5″ north of HD 44179 in 1984 December were sampled every one-half resolution element. All other spectra were sampled every one-third resolution element. The spectral resolution was $\sim$0.0075 μm ($\sim$6.5 cm^{-1}); however, the spectra as shown here are Hanning-smoothed and have a resolution of $\sim$0.009 μm ($\sim$8 cm^{-1}).

The co-added spectra were divided by spectra of early-type stars observed during the same nights and were then multiplied by Planck functions corresponding to assumed fluxes and temperatures of these stars. For the Orion Bar measurements the calibration star was BS 1713 (L = 0.13, T = 10,000 K); for the Red Rectangle the stars were BS 2294 (L = 2.66, T = 18,000 K) and BS 1899 (L = 3.53, T = 25,000 K). The final spectra of the Orion Bar and of the Red Rectangle are displayed in Figures 1 and 2. The poor signal-to-noise ratios near 3.31 μm in these spectra are caused by strong absorption by telluric CH_4. Peak intensities of most of the emission features are given in Table 1.

III. DESCRIPTION OF SPECTRA

a) Orion Bar

The three spectra of the Orion Bar (Fig. 1) show the unidentified emission features superposed on weak continua. The spectrum at position 4 shows the well-known emission peaks at 3.29 and 3.40 μm and, in addition, peaks at 3.46, 3.51, and (marginally above the noise level) 3.57 μm. The latter three features were only recently discovered in IRAS 21282+5050 and in GL 437 by de Muizon *et al.* (1986) and have now also been identified in NGC 7027 (Nagata *et al.* 1988) as well as in the ρ Oph source, WL 16 (T. R. Geballe, unpublished). The "plateau" of emission extending from 3.2 to 3.6 μm is also evident in all three Orion Bar Spectra; such emission has also been observed previously in several sources (Geballe *et al.* 1985; de Muizon, d'Hendecourt, and Geballe 1987). The emission features in the Orion Bar decrease in intensity to the south of position 4. However, it is clear that the 3.40 and 3.51 μm features do not decrease as rapidly as the others. In particular the ratio of peak intensities of the 3.40 and 3.29 μm features is 0.13 at position 4, 0.18 10″ to the south, and 0.26 20″ to the south. The peak intensities of the 3.51 μm feature are 0.04, 0.06, and 0.12 relative to those of the 3.29 μm feature at these positions. Note that the ratios of the integrated intensity of each of the weaker features relative to the 3.29 μm feature is roughly a

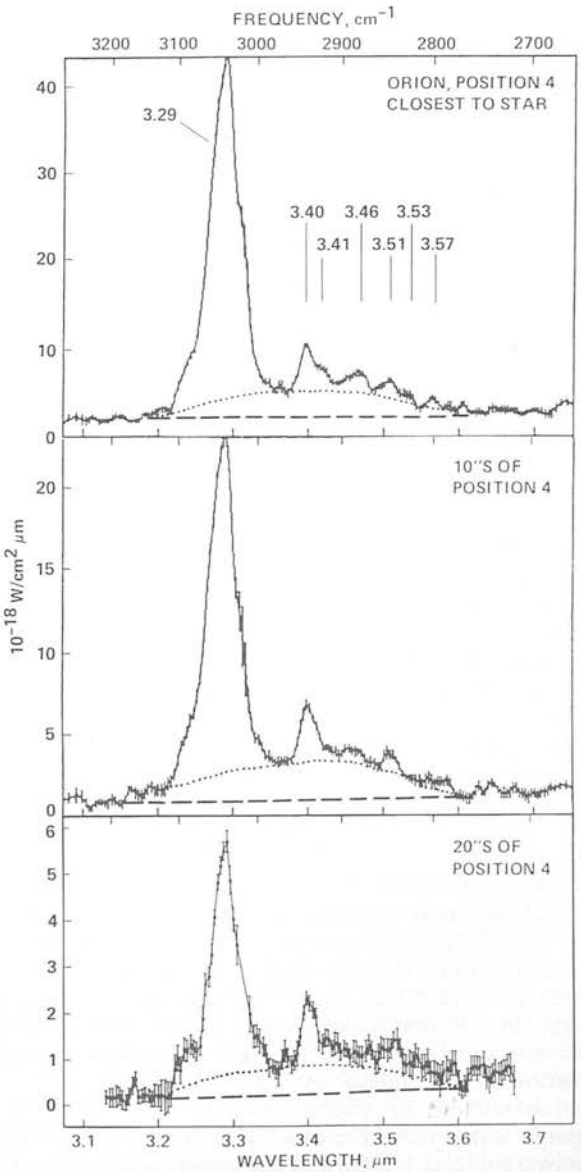

FIG. 1.—Spectra at 3 μm obtained in a 5″ beam at three locations within the Orion Bar. The spectral resolution is 0.009 μm. Dotted lines indicate the "plateau," dashed lines, the underlying continuum. Wavelengths of emission features are indicated in the top panel. Error bars are ± 1 σ.

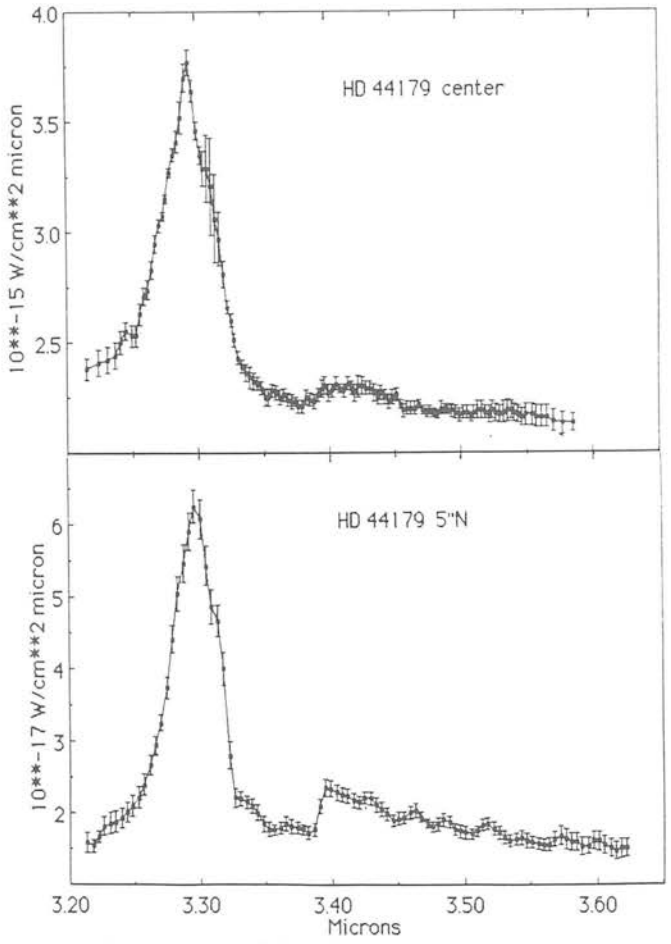

FIG. 2.—Spectra at 3 μm of the Red Rectangle obtained using a 5″ beam at the position of the exciting star and 5″ north of it.

factor of 2 less than the ratio of the peak intensities, because the width of the 3.29 μm emission is about twice that of each weaker feature.

In contrast to the behavior of the 3.40 and 3.51 μm features, the 3.46 μm component appears to be reduced in strength relative to the 3.29 μm feature 10″ south of position 4. At the 20″ south location there is no evidence for this feature at all. It also appears that the long-wavelength shoulders, present on the 3.40 and 3.51 μm features at position 4, decrease to the south. These shoulders may be due to independent and unresolved emission features at 3.415 and 3.53 μm.

b) Red Rectangle

Somewhat similar behavior to that in the Orion Bar is seen in the Red Rectangle spectra (Fig. 2). The spectrum observed at the position of HD 44179 shows a strong 3.29 μm feature and a weak, rather broad 3.40 μm feature superposed on a strong continuum. There is little evidence of the 3.2–3.6 μm plateau, although the 3.40 μm feature appears to be somewhat broader than in most other sources exhibiting it. At the off-star position the continuum, as judged by the flux densities at 3.2 and 3.6 μm, is reduced in spectral intensity by a factor of 150 (compared with a reduction of a factor of $\sim$450 measured for unresolved sources), but the 3.29 μm feature has decreased by a factor of only 36. The ratio of peak intensity (above the continuum) of the 3.40 μm feature to that of the 3.29 μm features has markedly increased, from 0.06 at HD 44179 to 0.13 at the 5″ north position. The short-wavelength cut-on of the 3.40 μm feature appears to occur slightly shortward of the cut-on in Orion, and the peak of the feature shows a similar shift, although these differences are only marginally significant.

In addition to the 3.29 μm and 3.40 μm features, some weak spectral structures appear in the 5″ north spectrum. The weaker ones of these (3.43, 3.48, 3.57 μm) are probably the result of smoothing noise fluctuations in the spectrum. The most prominent of the weak features is at 3.51 μm; we believe that this feature is real. Note that this is one of the features seen to become relatively more prominent going across the Orion Bar, and that it is not seen at HD 44179. The reality of the next most prominent feature, at 3.46 μm, is questionable. Thus regarding the 3.29 μm, 3.40 μm, and 3.51 μm features, the trend is similar to that in the Orion Bar; the ratios of the latter two to the former increase with increasing distance from the stellar (UV) source. We also note that the 3 μm spectrum of HD 44179 obtained by Tokunaga *et al.* (1988) in a 2″.7 aperture is consistent with the above pattern; it shows no 3.40 or 3.51 μm features at all.

The present spectrum obtained at the location of HD 44179 (Fig. 2, *top panel*) shows some slight differences from a similar spectrum published by Geballe *et al.* (1985). Two faint emission features at 3.46 and 3.52 μm were marginally present (although not commented upon) in the earlier spectrum. Because of their proximity to two of the new features found by de Muizon *et al.* (1986), it was suggested by the latter authors that they might be the same ones. However, in the present spectrum of HD 44179 there is no evidence for these emission features. Moreover, it has been determined that spurious features at these wavelengths can be generated by dividing the spectrum of a bright continuum source by that of a late-type star which contains strong OH absorption lines (Tokunaga *et al.* 1988). The present spectrum of HD 44179 was divided by that of a hot star, and should contain no such spurious emission features.

c) Width of the 3.29 Micron Feature

Tokunaga *et al.* (1988) found that within their 2″.7 aperture the FWHM of the 3.29 μm feature in HD 44179 is only 0.023 μm ($\sim$20 cm^{-1}), roughly half that observed in other sources (Geballe 1984; Geballe *et al.* 1985; de Muizon *et al.* 1986; Nagata *et al.* 1988). Our spectra of the Orion Bar and of HD 44179 obtained in a 5″ beam, yield deconvolved FWHMS of $\sim$0.040 μm ($\sim$37 cm^{-1}) and $\sim$0.035 μm ($\sim$32 cm^{-1}), respectively. They were made at a lower spectral resolution than used by Tokunaga *et al.*, but one which easily resolved the feature. A recent (1988 October) spectrum of HD 44179, obtained by us in a 2″.5 aperture, confirms the narrow width found by Tokunaga *et al.*

There are some difficulties in determining the widths of 3.29 μm features, largely due to the deep and only partially resolved telluric CH_4 absorption on the long-wavelength side of the feature and the difficulty in determining the continuum level. These cause uncertainties of perhaps 0.005 μm (5 cm^{-1}) in the FWHMs. In determining the FWHMs given above, we have used a straight line to interpolate across the 3.31–3.32 μm interval. However, the Tokunaga *et al.* (1988) spectrum shows that the major difference between the profiles of the 3.29 μm feature in HD 44179 and in other objects occurs on the short-wavelength side of the 3.29 μm feature, where the atmospheric transmission is fairly good. The results of Tokunaga *et al.*, combined with ours, imply that the width of the 3.29 μm

feature can vary significantly, not only from source to source, but also with position in a source.

IV. DISCUSSION

The 3.29 μm feature has long been ascribed to emission from the C—H stretch in aromatic systems. Because of its high intensity relative to the lower frequency emission features, even far from the powering source, the carriers have to be small, containing 20–50 carbon atoms. Such molecular-sized aromatic entities are generically called polycyclic aromatic hydrocarbons (see Allamandola, Tielens, and Barker 1987 for a review).

Detailed spectra of the emission features in the 3 μm region should provide strong constraints on the carriers once laboratory spectra of realistic analogs become available. Within the framework of the PAH hypothesis, two general classes of interpretations for the weaker features (at 3.40, 3.46, 3.51, and 3.57 μm) already have been suggested. One is that some of these features are vibrational "hot bands" (e.g., $v = 2$–1 and 3–2) of the C—H stretch, blending with combination bands involving the low frequency C—C stretching and bending modes (Barker, Allamandola, and Tielens 1987). The other is that they are fundamental vibrations of molecular subgroups attached to the basic PAH structure (Duley and Williams 1981; de Muizon *et al.* 1986). Below we discuss the present spectra, which show positional variations in the relative strengths of these emission features, in the context of the above interpretations. At present each explanation can accommodate at least some of these observations, mainly because of the lack of laboratory data regarding these transitions in free PAHs. Of course, both explanations may actually contribute. Each explanation will be discussed in turn, within the context of what is currently known.

a) Vibrational Overtones and Hot Bands

In PAHs the fundamental C—H stretching vibration always occurs close to 3.29 μm. Anharmonicitiy of the vibrational potential as a function of atomic separation causes the transitions between higher adjacent vibrational levels (i.e., $v = 2$–1, $v = 3$–2, ...; often called "hot bands") to be shifted to successively longer wavelengths (lower frequencies). Two of the weak emission features observed in these and other objects, those at 3.40 and 3.51 μm, are quite close to, although not exactly at, the wavelengths of the 2–1 and 3–2 vibrational transitions of the C—H stretch in the small aromatic hydrocarbons, benzene, napthalene, and anthracene (Barker, Allamandola, and Tielens 1987). The anharmonicities of ionized and larger PAHs are not yet determined but are likely to be similar. It is possible that some of them might provide an exact match.

Absorption of an ultraviolet (UV) photon by a molecule is followed by a rapid redistribution of the photon energy among the various vibrational modes of the molecule. In the absence of any other deactivation route, this is followed by spontaneous deexcitation via infrared fluorescence. In the case of PAHs the latter process takes about 0.1 s. The PAHs which are believed to dominate the near-infrared and mid-infrared emission spectrum are thought to contain 20–50 carbon atoms (Leger and Puget 1984; Allamandola, Tielens, and Barker 1985). The larger molecules in this range contain many times more vibrational modes than can be simultaneously excited by a single UV ($h\nu < 13.6$ eV) photon. Thus population of high-energy modes such as C—H stretches in $v = 2$ or higher states will be unusual occurrences. However, because smaller PAHs have fewer modes, more frequent excitation above the $v = 1$ levels is expected for them. By the same token the smaller PAHs will also be more susceptible to photodissociation processes by the UV radiation field (Tielens *et al.* 1987).

For a highly vibrationally excited PAH, H loss is much more likely than fragmentation of its carbon skeleton. This is because the aromatic C—H bond strength ($\sim$4.5 eV) is significantly lower than the aromatic C—C bond strength (5.5 eV; cf. Table 2) and because at least two C—C bonds have to be broken simultaneously in order to lose a C atom. This requires 11 eV and a simultaneous bond excitation, a very improbable pair of events. Indeed, photodestruction is thought to play only a minor role in the breaking up of the carbon skeletons of interstellar PAHs (Crawford, Tielens, and Allamandola 1985). Emission of IR photons (IR fluorescence) and C—H bond rupture are competing relaxation mechanisms for highly vibrationally excited PAHs, but C—H bond rupture will dominate only when the amount of energy which is deposited in the molecule exceeds a critical threshold, E_c, whose value depends strongly on the size of the PAH and the internal excitation energy (Tielens *et al.* 1987). Small decreases in the size of the molecule or small increases in the internal excitation energy (e.g., the energy of the absorbed UV photon) will increase the probability of H loss by large factors. If reattachment of hydrogen is unlikely before the following UV photon with $E > E_c$ is absorbed, a small PAH eventually will be stripped of all of its H atoms.

Thus in regions with strong UV fields (e.g., at the surface of a molecular cloud or near the exciting star), interstellar PAHs with sizes below a critical value will be quickly dehydrogenated. Larger PAHs will not be dehydrogenated at all, but because these have many vibrational modes, little emission from the $v = 2$ or higher levels will occur, even in the intense UV field near the star. In a shielded environment, such as a molecular cloud (e.g., 20″ S of position 4 in the Orion Bar), or sufficiently far from the exciting star, rehydrogenation dominates over UV destruction, and all PAHs are completely hydrogenated. The smaller ones will be highly excited upon absorption of a UV photon and will emit strongly in the hot bands (i.e., near 3.40 and 3.51 μm). The resultant spectra of the region will be strongly dependent on the details of the PAH size distribution, but clearly, the observed spatial variations in the relative strengths of the 3.29, 3.40, and 3.51 μm bands shown in Figures 1 and 2 could be a natural consequence of this model.

To determine if this explanation is tenable, one must estimate how susceptible small PAHs are to dehydrogenation by UV radiation in the Orion Bar and the Red Rectangle. Within the framework of this model, the intensity ratios of the 3.29 to 3.40 μm features 10″ south of position 4 in the Orion Bar and 5″ north of HD 44179 in the Red Rectangle imply that the smallest hydrogenated PAHs contain about 15–20 carbon atoms, depending on the spectrum of absorbed UV photons (Barker, Allamandola, and Tielens 1987), In contrast, at position 4 and (especially) at HD 44179 the PAHs responsible for the 3.40 μm emission contain about 50% more C atoms. It is likely that this is because of the complete dehydrogenation of the smaller ones at the latter positions. Using quantum RRK theory (Barker 1983) one can calculate the C—H bond rupture rate as a function of PAH size and vibrational energy content. Tielens *et al.* (1987) show that the UV threshold for efficient dehydrogenation of PAHs containing about 18–20 carbon

TABLE 2

PHYSICAL PROPERTIES OF SIDEGROUPS ON POLYCYCLIC AROMATIC HYDROCARBONS

SIDEGROUP[a]	BENZENE DERIVATIVE	BOND[b]	ENERGY[b] (eV)	H STRETCHING MODE[c] (cm^{-1})	H STRETCHING MODE[c] (μm)	NOTES
Hydrogen	Benzene	C_6H_5-H	4.47	3030	3.29	
	Benzene	$C-C_5H_6$	11.0	...	...	1
Methyl	Toluene	$C_6H_5CH_2-H$	3.69	2925 s	3.42	2
	Toluene	$C_6H_5CH_2-H$		2870 m	3.48	
	Toluene	$C_6H_5-CH_3$	4.0	...	...	
Ethyl	Ethylbenzene	$C_6H_5CH_2-CH_3$	3.1	2926 s	3.42	
	Ethylbenzene	$C_6H_5CH_2-CH_3$	3.1	2853 m	3.51	
Methylene	Benzyl	$C_6H_5-CH_2$	4.9	2986	3.35	3, 4
	Benzyl	$C_6H_5-CH_2$	4.9	3062	3.27	
	Benzyl	C_6H_5CH-H	4.47	...	...	
Hydroxyl	Phenol	C_6H_5O-H	3.69	3610	2.77	5
	Phenol	C_6H_5-OH	4.5	...	...	
		C_6H_5-O	3.2	...	...	
Amine	Aniline	C_6H_5NH-H	3.47	3481	2.87	
	Aniline	C_6H_5NH-H	3.47	3395	2.95	
	Aniline	$C_6H_5-NH_2$	4.0	...	...	
Aldehydic hydrogen ..	Benzaldehyde	C_6H_5CO-H	3.21	2820	3.55	6
	Benzaldehyde	C_6H_5CO-H	3.21	2730	3.66	

[a] Structural formulae shown in Fig. 3.

[b] Energy of bond denoted by — (Benson 1965)

[c] Peak frequencies and wavelengths of H stretching modes (Bellamy 1966) Variation of about 10 cm^{-1} (0.01 μm) likely within a class of compounds. The indicators s and m denote strong and moderate intensities.

NOTES.—(1) Elimination of a carbon atom from the carbon backbone of a PAH requires two bonds to be broken simultaneously (thus 11.0 eV; Crawford *et al.* 1985). (2) Frequencies are for methyl groups directly attached to a benzene ring. In pure, saturated aliphatic hydrocarbons, the CH stretching frequencies are 2960 and 2870 cm^{-1} (3.38 and 3.48 μm). (3) Phenyl is a very stable radical (see text). (4) Theoretically calculated frequencies (Lutoshkin, Kotorlenko, and Krugylak 1972). Actual values may be slightly different. (5) Frequency and wavelength are for isolated hydroxyl group. If strong intramolecular hydrogen bonding occurs, peak shifts to $\sim$3200 cm^{-1} (3.13 μm). (6) Presence of two bands is due to a Fermi resonance of the aldehydic CH stretching mode with overtones of the bending vibrations.

atoms is about 75,000 cm^{-1} (1300 Å). Therefore to estimate the dehydrogenation rates in these objects one must know the UV flux in the 912–1300 Å range.

i) *The Orion Bar*

In the Orion Bar region most of the emission in the features originates in the neutral zone adjoining the H II region (Sellgren 1981; Bregman *et al.* 1988). The UV flux in the above band incident from θ^1 Ori C (T = 40,000 K) is estimated to be 3×10^{12} cm^{-2} s^{-1}, from the observed far-infrared intensity (cf. Werner *et al.* 1976; Tielens and Hollenbach 1985*b*). Multiplying this by an assumed PAH UV cross section (5×10^{-16} cm^2) yields an H loss rate of 1.5×10^{-3} s^{-1}. Assuming that rehydrogenation occurs with unit efficiency upon each H atom–PAH collision, the rehydrogenation rate is given by the expression, $R = 10^{-9} n$ s^{-1} (Tielens *et al.* 1987). At the Orion Bar, where $n = 10^5$, the rehydrogenation rate is then 10^{-4} s^{-1}. Clearly for such small PAHs, dehydrogenation dominates at position 4. For slightly larger PAHs ($\sim$25 C atoms), however, the critical UV photon energy for dehydrogenation falls above the Lyman limit, and they will be completely hydrogenated.

The emitting material 10″ and 20″ south of the bar is embedded in the neutral zone where the UV field is heavily attenuated. Assuming that the observed intensity of the 3.29 μm feature directly measures the flux of pumping UV photons, (i.e., that most of the 3.29 μm feature is due to large, completely hydrogenated PAHs), the UV field 20″ south of position 4 is eight times less than at position 4 (i.e., $\tau_{UV} \simeq 2$). The C—H rupture rate is then calculated to be about 2×10^{-4} s^{-1}, comparable to the rehydrogenation rate. If instead the 3.29 μm emission is dominated by smaller, partially dehydrogenated PAHs, then the UV field, and thus the C—H rupture rate, will be lower than estimated above. In either case it appears that dehydrogenation of PAHs close to the surface of a molecular cloud can quantitatively explain the observed spatial variations of the 3 μm spectra in the Orion Bar.

ii) *The Red Rectangle*

A similar analysis of the emission in the Red Rectangle leads to a slightly different model than above. Speckle observations at 2.2 μm have recently been made of this object, and show that its 1/e dimensions are 0.″8 × 0.″6 (Beckers *et al.* 1988). Our observations of the line-to-continuum ratio indicate that the 3.29 μm emission is slightly more extended. Therefore we evaluate the physical conditions at a distance of 1″ from HD 44179. For this star, we take the distance (330 pc) and luminosity (1×10^3 $L_\odot$) from Cohen *et al.* (1975), use T = 10,000 K to estimate that about 0.009 of the luminosity is radiated between 912 and 1300 Å (Kurucz, Peytremann, and Avrett 1974), and obtain a UV photon flux in this band of 6×10^{12} cm^{-2} s^{-1} at a radius of 1″. This flux is twice that at position 4 in Orion and implies that the H loss rate from PAHs containing 20 carbon atoms is $\sim 3 \times 10^{-3}$ s^{-1}. The hydrogen density

is not well known for this object. Hα measurements indicate a density of $\sim 100\ \mathrm{cm}^{-3}$ at a distance of 15″ in the lobes (Warren-Smith, Scarrott, and Murdin 1981). Assuming that the nebula is due to a steady outflow from HD 44179, the density at 1″ is $2 \times 10^4\ \mathrm{cm}^{-3}$, which translates into a rehydrogenation rate of $2 \times 10^{-5}\ \mathrm{s}^{-1}$. Thus, in the region of brightest 3.29 μm emission, small PAHs probably are rapidly dehydrogenated; indeed, conditions appear to be considerably harsher than those in the Orion Bar.

It must be cautioned, however, that the geometry of the Red Rectangle suggests the presence of a bipolar flow; hence, the emission close to HD 44179 might actually originate within a circumstellar disk, whose density cannot easily be guessed. Whether the weakness of the 3.40 μm band close to HD 44179 can be attributed to photochemically driven dehydrogenation depends critically on the assumed density of the emitting circumstellar material.

A further problem is encountered in evaluating the conditions 5″ north of HD 44179. Due to geometric dilution, the UV field will have dropped by a factor of 25 compared to its value at $r = 1''$. In an outflow the density also will have decreased by this factor, so that the ratio of dehydrogenation and rehydrogenation rates should remain approximately constant within the nebula, until attenuation by dust becomes dominant. As the 3.29 μm feature has decreased by only a factor of 36 at the 5″ north position, significant attenuation of UV radiation by dust appears unlikely (i.e., $\tau_{\mathrm{UV}} \sim 0.4$). Thus, unless the density is much higher 5″ north of HD 44179 than expected, the relative spatial variations of the 3 μm emission features in the Red Rectangle cannot be explained by the above simple model.

However, an important, and perhaps crucial, distinction between the conditions close to HD 44179 and those of the Orion Bar region is the intensity of the entire illuminating UV field (evaluated over all UV wavelengths longward of 912 Å). At a distance of 1″ from HD 44179 the absorption rate of all such UV photons by PAHs is about $0.1\ \mathrm{s}^{-1}$, which is about 30 times larger than in the Orion Bar. Consequently, events governed by the absorption of two UV photons within a radiative relaxation time scale (i.e., $\Delta t_{\mathrm{abs}} < t_{\mathrm{IR}} = 0.1$ s) occur at least 10^3 times more frequently in the Red Rectangle than at position 4 in Orion. The increased likelihood of a high internal excitation energy, even larger than the Lyman limit, coupled with the (possible) low rehydrogenation rate, should result in the dehydrogenation of much larger PAHs close to HD 44179 than in the Orion Bar. Since the rate of two-photon events is proportional to r^{-4}, rehydrogenation will quickly dominate beyond a certain distance. Therefore two-photon events may be able to explain the weakness or absence of the 3.40 and 3.51 μm emission features close to HD 44179.

Thus within the framework of the "hot band" interpretation of the 3.40 and 3.51 μm features, the spatial dependence of these features both in Orion and in HD 44179 can be interpreted in terms of photochemically driven dehydrogenation of PAHs. The steep dependence of the dehydrogenation rate on the molecular size (Tielens *et al.* 1987) implies that the smallest PAHs, which are responsible for most of the emission in the 3.40 and 3.51 μm features, contain less than 25 C atoms. In the Red Rectangle, within 1″ of HD 44179, somewhat larger PAHs may also be dehydrogenated. The intensity ratio of the 3.29 μm and 3.40 μm features independently implies that the smallest hydrogenated PAHs present contain 15 to 20 carbon atoms (see, e.g., Barker, Allamandola, and Tielens 1987). The similarity of these size estimates is no coincidence, as both the emission in the hot bands as well as dehydrogenation depend on appreciable population of the higher vibrational levels of the CH stretching mode.

Finally, within this anharmonicity picture, not all of the weaker features in the 3 μm region are due to hot bands of the CH stretching vibrations. Some could be attributed to overtones (i.e., $v = 2$–0) and combination bands of the CC stretching vibrations, whose fundamentals occur in the 5–9 μm region. These would not be affected by dehydrogenation of the small PAHs. The weak 3.46 and 3.53 μm features in Orion may be examples of this emission since their spatial variations suggest a different origin than the 3.40 and 3.51 μm features. This idea is supported by laboratory spectra of several PAHs, some of which (i.e., coronene and pyrene) show weak, narrow absorption features at the former wavelengths as well as a broad, weak feature from 3.2 to 3.6 μm (Cyvin and Klaboe, reproduced in Allamandola, Tielens, and Barker 1987). The absence of these features in the spectrum of HD 44179 implies then that the PAH family responsible for the emission in this source is somewhat different from that in Orion. Such a compositional difference is also implied by the strikingly different 5–13 μm spectrum observed from this source (Cohen, Tielens, and Allamandola 1985; Cohen *et al.* 1986). Although the Orion Bar and the Red Rectangle are associated with objects in vastly different evolutionary stages, it is tempting to speculate that such compositional differences are created by the different intensities of the UV fields where most of the emitting PAHs are located.

b) Molecular Sidegroups

Figure 3 shows structural formulae of some typical sidegroups that can attach to PAHs. Table 2 lists physical properties of these sidegroups. Included in the table are the XH— stretching frequencies of each sidegroup when attached to benzene (i.e., each benzene derivative). In the sidegroup picture the best candidates for the bands in the 3.4–3.6 μm region are CH stretching vibrations of saturated aliphatic subgroups,

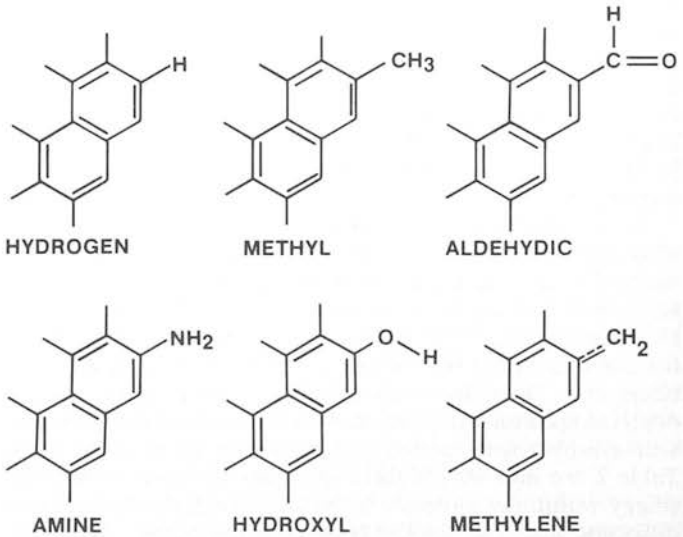

FIG. 3.—Structural formulae of some possible sidegroups on PAHs. The hexagonal networks schematically indicate the carbon backbone of the PAHs. Sidegroups, each of which would replace one H atom, are indicated only on one of the possible edge positions of a PAH. The "methylene" group actually refers to a relatively stable radical (see text).

such as $-CH_3$ and $-C_2H_5$ (Duley and Williams 1981; de Muizon *et al.* 1986; de Muizon, d'Hendecourt, and Geballe 1987). Although close, such saturated aliphatic hydrocarbon sidegroups do not provide an exact match to the observed spectral structure in the 3 μm region. However, it has been suggested that for ionized, dehydrogenated, or electronically excited PAHs these bands would be shifted and might provide a better match (de Muizon *et al.* 1986). Finally, one might perhaps expect the presence of sidegroups other than CH_2 and CH_3, notably CH and NH_2. However, due to their low binding energies, such sidegroups are very susceptible to photochemical destruction, and their expected intensities are small.

The present observations, particularly those of the Orion Bar, provide some constraints on sidegroup identifications. The observed 3.40 and 3.51 μm bands might be attributed to (shifted) methyl or methylene CH stretching vibrations. In contrast, since the observed 3.40 and 3.46 μm bands are decoupled, the latter cannot be the (shifted) methyl or methylene symmetric stretching vibration. Indeed, the difference in spatial behaviors of the 3.40 and 3.51 μm features relative to the other weak features (3.415 μm, 3.46 μm, 3.53 μm) is not readily explained within the sidegroup model (see below). However, even within the sidegroup model, $\Delta v = 1$ emission from higher vibrational levels of the CH stretching mode, and overtones and combination bands of the low-frequency CC stretching vibrations are expected at some level.

In the case that several of the weak bands are emitted by different molecular sidegroups, their intensities relative to other bands are a measure of the ratio of aromatic to aliphatic groups attached to the PAHs. The integrated band strengths for gas-phase PAHs with and without sidegroups are not known, but may be similar, as in the case of benzene derivatives (Gribov and Smirnov 1962; Wexler 1967). If so, the observed ratio (5–10) of the band intensity at 3.29 μm to the sum of those at longer wavelengths is simply the ratio of the number of aromatic to aliphatic H atoms in the emitting species. Assuming that each saturated aliphatic group contains three H atoms, the ratio of aromatic H atoms to aliphatic sidegroups is 15–30. This suggests that saturated aliphatic sidegroups are at best only a minor component of the IR-emitting PAHs. Attributing the emission to PAHs containing 20–50 carbon atoms with about 10–20 edge atoms results in an average of one sidegroup (other than H) per PAH, although one might construct models in which sidegroups dominate the peripheral groups on small PAHs and are absent on larger ones (see below).

In the sidegroup model, variations in the relative strengths of the features may be attributed to differences in the degrees to which different sidegroups survive exposure to the UV radiation field and the different rates of sidegroup reattachment after dissociation. It is therefore important to consider the binding energies of the various bonds involved with aliphatic sidegroups. These are summarized in Table 2. In view of the observed spectral structure, we restrict ourselves mainly to the aromatic hydrogen, methyl, and methylene groups. Examining Table 2, we infer that if there were just sufficient vibrational energy within the molecule to break a bond, the first ones to dissociate would be the C—H bond in the methyl side group and the C—C bond which connects methyl groups to a larger saturated aliphatic hydrocarbon sidegroup (i.e., $-CH_2-CH_3$). In both cases a very stable radical is produced because the unpaired electron on the remaining CH_2 sidegroup can participate in the aromatic π molecular orbital. In the case of methyl-benzene, the benzyl radical is formed. Due to the increased binding energy, further hydrogen loss from this stripped-down methyl group is about as likely as the loss of peripheral aromatic hydrocarbons. Thus, photochemistry will tend to convert saturated aliphatic hydrocarbon sidegroups into CH_2 radical sidegroups. Subsequently, the PAH may lose further hydrogens from this sidegroup, peripheral aromatic H atoms, or both, depending on the exact binding energies involved. Finally, loss of the carbon in the sidegroup may become important. As in the case of the anharmonic model, fragmentation of the carbon backbone of the PAH is expected to be of little importance.

i) *A Model for the Orion Bar Emission*

The above considerations suggest the following simple model for the photochemical evolution of PAHs in clouds near sources of intense far-UV radiation, such as in Orion. At a distance within the molecular cloud corresponding to $A_V \sim$ 5–10 mag, a small PAH (<25 carbon atoms) is likely to absorb a UV photon and lose an aromatic H during the lifetime of the region ($\sim 10^5$ yr for Orion). Because most of the hydrogen is locked up in H_2, abundances of atomic C and O are comparable to that of atomic H, while atomic N is somewhat less abundant (Tielens and Hollenbach 1985*a*). A PAH which has lost an H atom there is likely to grow an aliphatic sidegroup containing O, C, H, and, to a lesser extent, N. The expected sidegroups at this cloud depth may consist of an aliphatic carbon backbone with hydroxyl (e.g., OH), aldehydic (e.g., HC=O), amine (NH_2), and methyl and methylene (e.g., $-CH_3$, $-C_2H_5$) functional groups attached (cf. Fig. 3). Closer to the cloud surface ($A_V < 5$ mag) the UV field will photodissociate H_2 and atomic H will be more abundant than C and O, so the strengths of the sidegroup features relative to the 3.29 μm feature will decrease. In terms of the spatial behavior of the emission features, only the 3.40 and 3.51 μm features are even qualitatively consistent with the above model. However, since for small PAHs the photochemical rupture and rehydrogenation time scales are much shorter than the dynamical evolution of the Orion region, the composition of the sidegroups on PAHs should reflect the composition of the gas phase, and thus within the Orion Bar region observed ($A_V < 1$) only aromatic H groups are expected. One is then forced to assume that the smallest PAHs present in Orion have a time scale for photochemical evolution which is comparable to the lifetime of the region and, thus, will not have "equilibrated" with the gas phase. Possibly, the observed sidegroups might result from the photochemical evolution of PAHs accreted onto ice grain mantles (Allamandola 1988).

In principle, in the sidegroup model, the 3.4–3.6 μm features could originate in slightly larger PAHs than in the anharmonic model, as the average energy per oscillator is not required to be as high for emission in the CH_2 and CH_3 stretching vibrations as that needed to pump $v = 2$ and 3 levels of the aromatic CH stretch. Somewhat larger PAHs are also implicated if the observed variations are interpreted, as above, as implying a time scale of $\sim 10^5$ yr for photochemical evolution. Note that a short lifetime for the emitting PAHs immediately implies emission in CH stretch "hot bands," since a radiation field which destroys PAHs populates excited vibrational levels in the process. Thus, if $v = 1$–0 vibrations in sidegroups are the only cause of the weak 3 μm features, a long photochemical time scale for these PAHs is actually a necessity.

To summarize this discussion, in the Orion Bar the observed spatial intensity pattern of the 3.40 and 3.51 μm features relative to the 3.29 μm (fundamental CH stretch) feature is qualitatively similar to that expected from sidegroups, but the patterns seen for the other combinations of weak features do not match expected behavior. In addition, if the sidegroup model is valid, it appears that the PAHs must acquire sidegroups by some means other than UV photodehydrogenation followed by reactions with gas-phase species.

ii) *The Red Rectangle*

The situation in the Red Rectangle is quite different from that in Orion, because the 3 μm emitting material has been freshly synthesized from atomic gas formerly within HD 44179. In the harsh environment very close to the star, PAHs can only be formed without aliphatic sidegroups. As the PAHs move to greater distances from the star, conditions moderate to the point where sidegroups could survive. However, unless the carbon elemental abundance is extremely high (C/H $\gtrsim$ 1), complete hydrogenation is expected to dominate over sidegroup formation. Thus, we see no simple model that can account for the observed spatial variations in the 3 μm spectrum of the Red Rectangle within the context of the sidegroup model. In fact, this argument may apply to the structure in the 3 μm spectra in all outflow sources, such as planetary nebulae (NGC 7027) and other evolved objects (e.g., IRAS 21282+5050) which produce PAHs locally.

d) The ^{13}C—H Stretch

When the ^{12}C—H fundamental stretch occurs at 3.29 μm the ^{13}C—H fundamental stretch occurs at 3.42 μm. Thus ^{13}C may be responsible for the weak, long wavelength shoulder sometimes observed on the 3.40 μm feature. In Orion the emitting material is interstellar, where ^{12}C/^{13}C is $\sim$40 (e.g., see Hawkins and Jura 1987), in reasonable agreement with the strength of the 3.415 μm shoulder, after subtraction of the underlying broad component (plateau). In evolved objects mixing of CNO-processed material from the interior can lead to observed values of ^{12}C/^{13}C as low as $\sim$4. The spectrum of HD 44179 by Tokunaga *et al.* (1988), which shows no detectable 3.40 μm or 3.415 μm feature, demonstrates that ^{12}C/^{13}C is at least 50 in that object. CO observations of NGC 7027, another object which has a clear-cut 3.40 μm band, yield ^{12}C/^{13}C > 36 (Thronson 1983). Here, the ^{13}C may be responsible for the observed shoulder on the 3.40 μm emission feature.

e) Line Widths

In general the width of the 3.29 μm feature (FWHM $\sim$ 0.04 μm) is about twice that of the weaker features (FWHM $\sim$ 0.025 μm). The latter are somewhat difficult to determine accurately due to their blending with other weak features as well as their placement relative to the strong, underlying plateau, or "quasi continuum." We noted earlier that the 3.29 μm feature obtained with a 2".7 aperture centered on HD 44179 (Tokunaga *et al.* 1988) has a narrower width ($\sim$0.023 μm) than it does in our spectrum obtained with a 5" aperture, or in any other object observed to date. We also note that the 3.40 μm feature observed on HD 44179 (Fig. 2) is either a blend of more than one feature, or is unusually broad. Thus it appears that the widths of some of these features can vary substantially. In this section we will discuss possible interpretations of these observations, although we realize that further observational tests of these effects are warranted.

The width of an IR fluorescent feature is determined by the combined effects of the time-scale for intramolecular vibrational energy transfer (the Heisenberg uncertainty relation, $\Delta E\,\Delta t > \hbar$), intensity enhancement and blending with weaker modes that are close in frequency (i.e., Fermi resonance), and small shifts in frequency of the emitting mode between different molecules within the family of interstellar PAHs (Allamandola, Tielens, and Barker 1985). The first is generally cited for the widths of the narrower observed emission features (e.g., at 3.29 μm and 6.2 μm), while the last may be responsible for the broad 7.7 μm feature and the plateau of emission underneath the 11.3 μm feature (Allamandola, Tielens, and Barker 1985; Cohen, Tielens, and Allamandola 1985).

In the case that intramolecular energy transfer dominates, the width will reflect the density of states at the internal excitation energy and the coupling of these states with the emitting mode. Since the density of such states is a strong function of the excitation energy, one might expect that the widths of "hot bands" are much greater than those of the fundamentals. Likewise, given their similar excitation energies, one might expect that the CH stretching modes of CH_3 and CH_2 have widths similar to that of aromatic H. However, recent elegant studies of the line widths of overtones of the CH stretching modes in benzene (Reddy, Heller, and Berry 1982), as well as of other molecules, have shown that intramolecular energy transfer from a particular mode to the general thermal bath usually takes place through a very limited number of so-called doorway states. Apparently, partly due to near-energy resonance and partly due to the geometric structure of the molecule, the couplings to these states (other fundamental modes which are close in frequency, as well as overtones and combination bands of lower frequency fundamentals) are very strong, leading to a very fast energy transfer ($\Delta t \sim 10^{-13}$ s). The "doorway" states of the particular modes under consideration themselves couple rapidly with a slightly different set of "doorway" states, so that coupling of a particular vibrational mode with all of the other available modes in the thermal bath occurs on a much slower, diffusion time scale. Nevertheless, all modes communicate on a time scale much less than the typical time for IR emission (0.1 s), so that the assumption of statistical distribution of the available energy over all modes, used in calculating IR emission spectra (e.g., Allamandola, Tielens, and Barker 1985) is fully justified. The line width, however, is determined by those "doorway" modes that dominate the energy transfer from the energy level in question, and the observed widths of the 3.29 μm and 6.2 μm features is in general agreement with that expected from such time scales (Allamandola, Tielens, and Barker 1985).

Since the actual line width of a fluorescing mode depends to a large extent on the coupling to a few states, no large increase in line width with vibrational excitation energy is expected. In fact, experimental studies on benzene show that the width of CH stretching modes increases slightly for the first few modes, but decreases again for even higher modes. In view of the absence of laboratory data on astrophysically relevant PAHs, the decrease in line width for "hot bands" or sidegroups is not presently in conflict with the PAH hypothesis.

Although the line width of the 3.29 μm emission feature generally has been interpreted only in terms of energy transfer time scales, the observations of a large variation in the linewidth by Tokunaga *et al.* (1988) suggest that other contributions should be considered. In particular, close to HD 44179 perhaps even the largest PAHs contain only a few H atoms. Since the

3.29 μm line width is probably dominated by interactions with the stretching modes of other peripheral H atoms on the PAH, such an isolation in HD 44179 might lead to a narrower emission feature. Similarly, we note that in benzene a Fermi resonance between the CH stretching vibration and an overtone or combination band of CC stretching modes gives rise to a strong band at 3.25 μm (3080 cm^{-1}), close to that of the fundamental aromatic CH stretch (Herzberg 1945). The absorption spectrum of coronene and, to a lesser extent, pyrene, also show a strong overtone or combination band in this wavelength region (Cyvin and Klaboe, reproduced in Allamandola, Tielens, and Barker 1987). Blending of these two emission features and broadening by intramolecular energy transfer will give rise to an increased width and perhaps a slight shift in frequency of the CH stretching mode. The narrow 3.29 μm feature observed in a small beam around HD 44179 may then reflect a difference in composition of the PAH family responsible for the emission in this source. That is, the PAHs which dominate the emission within 1″ of HD 44179 may lack this overtone or combination band.

Such a compositional difference in the PAH family close to HD 44179 has already been suggested on the basis of its 5–8 μm spectrum, which shows a "7.7 μm emission feature" which peaks at much longer wavelengths ($\sim$8.0 μm) than in Orion (Cohen *et al.* 1986; Bregman *et al.* 1988; Allamandola, Tielens, and Barker 1987). This might mean that an overtone or combination band of the "7.7 μm" CC stretch is involved in broadening the 3.29 μm emission feature. In that case, one would expect that other sources that show a large wavelength shift in the peak of the 7.7 μm feature (e.g., CPD $-56°8032$ and He 2–113; Cohen *et al.* 1986) would also show a narrower 3.29 μm feature. The observed variations of this feature in the Red Rectangle would suggest that this Fermi resonance is associated with the smallest PAHs. Very close to HD 44179, such species may have lost all of their aromatic H atoms, and, in the absence of the fundamental CH stretch, the intrinsic strengths of the overlapping overtone or combination band would decrease considerably. The 3.29 μm band would then be dominated by the CH stretch in somewhat large PAHs, which do not possess this Fermi resonance. Further laboratory and astronomical studies are needed to test these speculations.

V. CONCLUSION

The spectra presented here provide unambiguous evidence for the presence of several components to the 3 μm emission spectrum of UV-excited nebulae which vary independently of one another within each nebulae. The observed spatial behavior of these features, in conjunction with laboratory studies, suggests that the weak 3.46 and 3.53 μm features may be due to overtones and combination bands of low-frequency CC stretching vibrations. The observed spatial variations of the intensities of the 3.40 and 3.51 μm features relative to that of the 3.29 μm feature can be attributed to the photochemical evolution of the interstellar PAH family within UV-excited nebulae. In the Orion Bar, these two features can be either "hot bands" ($v = 2$–1, 3–2) of the CH stretch in simple PAHs (containing only aromatic H atoms), or emission in the CH stretching modes of saturated aliphatic subgroups. However, in the Red Rectangle, whose emitting material is mass recently lost from the central star, the same type of spatial variations appear difficult to explain in the context of the sidegroup model. Therefore, if the 3.40 and 3.51 μm features in the Orion Bar region are emitted by the same molecular species as they are in the Red Rectangle, one must seriously question whether sidegroups are involved. Given the paucity of relevant laboratory data and the ingenuity of theoreticians, however, both interpretations of these features still must be considered viable. The observed photochemical evolution of interstellar PAHs implies that the emission carriers are small (between 20 and 50 C atoms, depending on the model adopted). It is significant that estimates of PAH sizes obtained from this work are similar to those previously obtained from other considerations.

Progress in understanding the identifications and emission mechanisms of the various features awaits the availability of laboratory spectra. However, it is also important to quantitatively test further the dependency of the weak emission features on the UV radiation field. Additional observational tests might be carried out on planetary nebulae and other objects that show the 3 μm features. We note, for example that the 3 μm spectra of the planetary nebulae NGC 7027 and BD $+30°3639$ are considerably different (Geballe *et al.* 1985; Nagata *et al.* 1988). In BD $+30°3639$, where the 3.29 μm emission occurs rather close to the exciting star, the emission features in the 3.4–3.6 μm region are weak or absent, similar to HD 44179. In NGC 7027, where the emission occurs at an angular distance from the star perhaps 5 times greater (and hence where the UV radiation field is likely considerably less intense), the 3.4–3.6 μm features are relatively prominent. Spectra at different locations within the above objects might prove illuminating.

We wish to thank the staff of UKIRT for its support of this research. Some of the data described herein were obtained during UKIRT Service observing time. We are indebted to Professor Cyvin of Trondheim University, Norway for pointing out some important spectroscopic characteristics of condensed aromatics and to A. Tokunaga for a number of helpful comments. This work was partially supported by NASA grant 188-41-57 at NASA/Ames.

REFERENCES

Aitken, D. K., Roche, P. F., Spenser, P. M., and Jones, B. 1979, *Astr. Ap.*, **76**, 60.
Allamandola, L. J. 1988, in *Carbon in the Galaxy*, ed. J. Tarter (NASA CP), in press.
Allamandola, L. J., Tielens, A. G. G. M., and Barker, J. R. 1985, *Ap. J. (Letters)*, **290**, L25.
———. 1987, in *Polycyclic Aromatic Hydrocarbons and Astrophysics*, ed. A. Leger *et al.* (Dordrecht: Reidel), p. 255.
Barker, J. R., 1983, *J. Chem. Phys.*, **77**, 301.
Barker, J. R., Allamandola, L. J., and Tielens, A. G. G. M. 1987, *Ap. J. (Letters)*, **315**, L61.
Beckers, J. M., Christou, R. G., Probst, R. G., Ridgway, S. T., and von der Luhe, O. 1988, preprint.
Bellamy, L. J. 1966, *The Infrared Spectra of Complex Molecules* (New York: Wiley).
Benson, S. W. 1965, *J. Chem. Ed.*, **42**, 502.
Borghesi, A., Busoletti, E., and Colangeli, L. 1987, *Ap. J.*, **314**, 422.
Bregman, J., Allamandola, L. J., Tielens, A. G. G. M., Geballe, T. R., and Witteborn, F. C. 1988, *Ap. J.*, submitted.
Cohen, M., *et al.* 1975, *Ap. J.*, **196**, 179.
Cohen, M., Allamandola, L. J., Tielens, A. G. G. M., Bregman, J. D., Simpson, J., Witteborn, F. C., Wooden, D., and Rank, D. 1986, *Ap. J.*, **302**, 737.
Cohen, M., Tielens, A. G. G. M., and Allamandola, L. J. 1985, *Ap. J. (Letters)*, **199**, L93.
Crawford, M. K., Tielens, A. G. G. M., and Allamandola, L. J. 1985, *Ap. J. (Letters)*, **293**, L45.
de Muizon, M., d'Hendecourt, L. B., and Geballe, T. R. 1987, in *Polycyclic Aromatic Hydrocarbons and Astrophysics*, ed. A. Leger *et al.* (Dordrecht: Reidel), p. 287.

de Muizon, M., Geballe, T. R., d'Hendecourt, L. B., and Baas, F. 1986, *Ap. J. (Letters)*, **306**, L105.
Duley, W. W., and Williams, D. A. 1981, *M.N.R.A.S.*, **196**, 269.
Geballe, T. R. 1984, in *Workshop on Laboratory and Observational Infrared Spectra of Interstellar Dust*, ed. R. D. Wolstencroft and J. M. Greenberg (Edinburgh: Royal Observatory), p. 93.
Geballe, T. R., Lacy, J. H., Persson, S. E., McGregor, P. J., and Soifer, B. T. 1985, *Ap. J.*, **292**, 500.
Gribov, L. A., and Smirnov, V. N. 1962, *Soviet Phys.—Uspekhi*, **4**, 919.
Hawkins, I., and Jura, M. 1987, *Ap. J.*, **317**, 374.
Herzberg, G. 1945, *Molecular Spectra and Molecular Structure. II. Infrared and Raman Spectra of Polyatomic Molecules* (Princeton: van Nostrand Co.).
Kurucz, R. L., Peytremann, E., and Avrett, E. H. 1975, *Blanketed Model Atmospheres For Early Type Stars* (Washington: Smithsonian Astrophysical Observatory).
Leger, A., and Puget, J. L. 1984, *Astr. Ap.*, **137**, L5.
Lutoshkin, V. I., Kotorlenko, L. A., and Krugylak, Y. A. 1972, *Teor. Eksp. Khim.*, **8**, 542.
Nagata, T., Tokunaga, A., Sellgren, K., Smith, R. G., Onaka, T., Nakada, Y., and Sakata, A. 1988, *Ap. J.*, **326**, 157.
Reddy, K. V., Heller, D. F., and Berry, M. J. 1982, *J. Chem. Phys.*, **76**, 2814.
Sakata, A., Wada, S., Tanabe, T., and Onaka, T. 1984, *Ap. J. (Letters)*, **287**, L51.
Sellgren, K. 1981, *Ap. J.*, **245**, 138.
Thronson, H. A. 1983, *Ap. J.*, **264**, 599.
Tielens, A. G. G. M., Allamandola, L. J., Barker, J. R., and Cohen, M. 1987, in *Polycyclic Aromatic Hydrocarbons and Astrophysics*, ed. A. Leger *et al.* (Dordrecht: Reidel), p. 273.
Tielens, A. G. G. M., and Hollenbach, D. J. 1985*a*, *Ap. J.*, **291**, 722.
———. 1985*b*, *Ap. J.*, **291**, 747.
Tokunaga, A. T., Nagata, T., Sellgren, K., Smith, R. G., Onaka, T., Nakada, Y., Sakata, A., and Wada, S. 1988, *Ap. J.*, **328**, 709.
Warren-Smith, R. F., Scarrott, S. M., and Murdin, P. 1981, *Nature*, **292**, 317.
Werner, M. W., Gatley, I., Harper, D. A., Becklin, E. E., Loewenstein, R. F., Telesco, C. M., and Thronson, H. A. 1976, *Ap. J.*, **204**, 420.
Wexler, A. S. 1967, *Appl. Spectrosc. Rev.*, **1**, 9.

L. J. Allamandola and A. G. G. M. Tielens: NASA/Ames Research Center, MS 245–6, Moffett Field, CA 94035

P. W. J. L. Brand and A. Moorhouse: Royal Observatory, Blackford Hill, Edinburgh EH9 3HJ, Scotland

T. R. Geballe: Joint Astronomy Centre, 665 Komohana Street, Hilo, HI 96720

High Spectral Resolution Observations of Fluorescent Molecular Hydrogen in Molecular Clouds

Michael G. Burton [1,2] T.R. Geballe [3,4] P.W.J.L. Brand [5]
A. Moorhouse [5]

[1] NASA Ames Research Center
[2] University of California at Irvine
[3] Joint Astronomy Centre, Hilo, Hawaii
[4] Foundation for Astronomical Research in The Netherlands - ASTRON
[5] Department of Astronomy, University of Edinburgh

Submitted to the *Astrophysical Journal*
Accepted 1 · 1990

August 29, 1989

Abstract

The 1–0 S(1) line of molecular hydrogen has been observed at high spectral resolution (16 $km s^{-1}$ FWHM) in several sources where the emission was suspected of being fluorescent. In NGC 2023, the Orion Bar and Parsamyan 18 the S(1) line is unresolved, and the line centre close to the rest velocity of the ambient molecular cloud. Such behaviour is expected for UV-excited line emission. The H_2 linewidths in molecular clouds thus can serve as a diagnostic for shocked and UV-excitation mechanisms; if the lines are broader than several $km s^{-1}$ or velocity shifts are observed across a source it is likely that shocks are responsible for the excitation of the gas.

Subject headings: infrared: spectra – interstellar: molecules – molecular processes – nebulae: Orion nebula.

I Introduction

The fluorescence of molecular hydrogen (H_2) gas in the interstellar medium is now a firm observational phenomenon (*e.g.*, Gatley *et al.* 1987). In this process infrared line emission from H_2 follows the absorption of a UV photon by the molecule, raising it to an excited electronic state, and subsequent decay to an excited vibrational level of the ground electronic state (*e.g.*, Black & Dalgarno 1976). The fluorescence is the radiative decay, via infrared vibration-rotation transitions, down the vibrational ladder. It has been a matter of common practice to distinguish between fluorescent and shock-excited H_2 emission by comparing intensities of lines from several vibrational levels. In low density gas ($\preceq 10^4\,\mathrm{cm}^{-3}$), fluorescence is characterised by strong emission lines from excited vibrational levels, with, in particular, a 1–0 S(1)/2–1 S(1) line ratio of ~ 2 (*e.g.*, Black & Dalgarno 1976, Hollenbach & Shull 1977, Black & van Dishoeck 1987). The observed spectra in the reflection nebulae NGC 2023 (Gatley *et al.* 1987) and Hubble 12 (Dinerstein *et al.* 1988) are characteristic of fluorescent emission. In contrast, shock-excited spectra, in which the H_2 levels are collisionally excited, are dominated by emission lines from the v=0 and 1 levels, with, in particular a 1–0 S(1)/2–1 S(1) line ratio of ~ 10 (*e.g.*, Kwan 1977, London, McCray & Chu 1977, Shull & Hollenbach 1978, Draine & Roberge 1982, Chernoff, Hollenbach & McKee 1982). Shock-excited emission has been observed in many sources, most notably the star forming region OMC–1 (*e.g.*, Gautier *et al.* 1976, Beckwith *et al.* 1978, Scoville *et al.* 1982, Brand *et al.* 1988).

Recent theoretical work has shown that discriminating between the two exciting mechanisms on the basis of line intensities (in particular by using the ratio of the 1–0 S(1) and 2–1 S(1) lines) is not straightforward in all cases. In a photodissociation region (PDR) (*e.g.*, a molecular cloud illuminated by UV radiation, see Tielens & Hollenbach 1985a) which is sufficiently dense ($\succeq 10^5\,\mathrm{cm}^{-3}$), collisional de-excitation of radiatively populated levels can move the level populations towards a thermal distribution and give the spectrum the appearance of shocked emission (Sternberg & Dalgarno 1989, Burton, Hollenbach &

Tielens 1989a). In addition, it is possible that emission from certain kinds of shocks may appear 'fluorescent'. If the shock speed is sufficiently fast ($\gtrsim 40$ km s^{-1}) to dissociate all of the H_2, which then reforms on the surfaces of dust grains in cooler downstream regions, and is subsequently ejected, a 'reformation' spectrum will result. The details of this process are somewhat uncertain, but Hollenbach & McKee (1989) suggest that highly excited vibrational lines may result, similar to those produced in the UV-excited radiative cascade.

Several recent observations of H_2 emission line spectra show characteristics of both emission processes. In the Orion Bar, an ionisation front (IF) associated with the Trapezium stars, Hayashi *et al.* (1985) found that the ratio of the 1–0 and 2–1 S(1) lines varies from unity to about 10, the latter value occurring just behind the IF. The authors speculate that radiative excitation is occurring everywhere, but that just behind the IF a shocked layer exists, the shock wave being driven by the expansion of the HII region. However it is hard to drive such a shock wave faster than ~ 3 km s^{-1} (Hill & Hollenbach 1978), which is too slow to significantly excite the vibrational levels of H_2. A plot of energy level against column density shows the lower level lines having apparent excitation temperatures of ~ 2000 K, typical of 'shocks', while ratios of higher level lines are typical of 'fluorescence' (Hippelein & Münch 1989). Tanaka *et al.* (1989) find that both radiative and thermal contributions are required to explain the excitation temperatures measured in some planetary nebulae, HII regions and reflection nebulae. In other planetary nebulae (*e.g.*, the Dumbbell, the Ring and NGC 6720; Zuckerman & Gatley 1988), the H_2 appears to be shock-excited on the evidence of line ratios. However, there appear to be no plausible forces available to drive a shock in order to match the intensity of the H_2 line emission (unless the collision rate coefficients have been severely underestimated and/or H–H_2 collisions dominate over H_2–H_2); yet there is an abundance of UV photons available for pumping the molecules.

In molecular clouds there is another way to distinguish between shock-excited and fluorescent line emission, through the velocity dispersion of the excited gas. Shocks are associated with bulk motions and high velocities. Velocity widths are observed to be large

in shocks, occasionally greater than $100\,\mathrm{km\,s^{-1}}$ (*e.g.*, as in the bipolar outflows OMC–1 (Nadeau & Geballe 1979, Scoville *et al.* 1982) and DR 21 (Garden *et al.* 1986), and the supernova remnant IC 443 (Burton 1987)). Even in shocked sources where the lines are currently unresolved, such as the bipolar outflow NGC 2071, evidence for motions may be seen by comparing the emission velocities at different locations (Burton *et al.* 1989b). In contrast, fluorescent emission should occur at the ambient cloud velocity and the line width should be just the thermal or turbulent velocity dispersion of the cloud. This is $< 3\,\mathrm{km\,s^{-1}}$ and thus unresolvable with current observing techniques.

We have therefore conducted a program to measure the velocity profiles of H_2 lines in several fluorescent, or suspected fluorescent sources. We have observed the profiles at high spectral resolution, although the low surface brightness of the line emission necessitated the use of a large aperture, which in turn somewhat degraded the resolution. In this paper we show that the H_2 lines in most or all of the sources observed are quite narrow, a result consistent with their line emission being due to fluorescence.

II Observations

The profiles of the H_2 1–0 S(1) ($2.1212544\,\mu\mathrm{m}$) line in the sources listed in Table 1 were measured at the United Kingdom Infrared Telescope (UKIRT) on Mauna Kea, Hawaii on January 20 and 21 1988, utilizing a scanning Fabry–Perot interferometer (FP) in series with a circular variable filter (CVF) with resolving power 120, tuned to transmit at $2.12\,\mu\mathrm{m}$. The aperture diameter was 8 arcsec FWHM, which degraded the resolution of the FP from $12\,\mathrm{km\,s^{-1}}$ (its value in parallel light) to approximately $16\,\mathrm{km\,s^{-1}}$. Spatial chopping and nodding were performed, with a throw of 120 arcsec E–W. Other details of the observations are listed in Table 1. The FP was scanned over ranges of 60–85 $\mathrm{km\,s^{-1}}$, in steps of $5\,\mathrm{km\,s^{-1}}$. Adjacent orders of the FP are separated by 450 $\mathrm{km\,s^{-1}}$, thus 5 orders of the FP are included within the FWHM of the CVF. We are aware of four lines which may possibly contaminate

the 1–0 S(1) profiles. The 3–2 S(4) line, two orders away at 2.1274 μm, lies $-28\,\mathrm{km\,s^{-1}}$ from the line centre of the 1–0 S(1) line, and the 8–6 O(4) line at 2.1210 μm lies at $-36\,\mathrm{km\,s^{-1}}$. The 7–5 O(6) line, at 2.1084 μm, four orders away, and thus significantly attenuated, lies at $-39\,\mathrm{km\,s^{-1}}$(all wavelengths in standard air, from Black & van Dishoeck, 1987, and Bragg, Brault & Smith, 1982). We estimate that in a shocked source the contamination by each line will be less than 1% of the 1–0 S(1) line (Brand *et al.* 1988), but that in a (low-density) fluorescent source the contamination will be (not including attenuation) $\sim$ 6%, 7% and 3% respectively (Black & van Dishoeck 1987). The HeI 3^3P–4^3 multiplet, with weighted mean wavelength 2.112022 μm (Litzén, 1970), will occur at $+31\,\mathrm{km\,s^{-1}}$ if it is emitted in the same source as the 1–0 S(1) line and at the same local velocity. (N.B. The uncertainty in the last figure of these wavelengths results in a ± 3 $\mathrm{km\,s^{-1}}$ error in the velocity shifts above.)

The S(1) profiles are shown in Figure 1, together with the profile of an Argon lamp line (19 $\mathrm{km\,s^{-1}}$ FWHM; the Ar profile is pressure broadened from the 16 $\mathrm{km\,s^{-1}}$ FWHM of the instrument) at 2.1338708 μm (in vacuo, Norlén 1973). The peak emission velocities have been shifted to $0\,\mathrm{km\,s^{-1}}$ and the fluxes normalised to unity. Details are given in Table 2. Velocities of line centres were measured relative to OMC–1 Peak 2, and are estimated to be correct to $\pm 3\,\mathrm{km\,s^{-1}}$. Drifting of the FP plates was monitored by periodically measuring the frequency of maximum line emission at Peak 2; the drift over the course of a night was steady and totalled $5\,\mathrm{km\,s^{-1}}$, and thus was negligible for any single observation. Line fluxes are given relative to Peak 2.

III Results

In Figure 1 it can be seen that the 1–0 S(1) line at OMC–1 Peak 2 is resolved, with an observed FWHM $37\,\mathrm{km\,s^{-1}}$ (consistent with Nadeau & Geballe 1979). For the Orion Bar, NGC 2023 and Parsamyan 18, the S(1) line is essentially unresolved with FWHMs ranging

from 16 to 20 $\mathrm{km\,s^{-1}}$. The S(1) line in OMC–2 is somewhat broader. There are features at about the 10 percent level of the peak flux at $\sim -30\,\mathrm{km\,s^{-1}}$ in several of the profiles, which may be due to higher excitation lines coming through other orders of the FP (see §2). For Parsamyan 18 8W there is a feature at $\sim +35\,\mathrm{km\,s^{-1}}$, which may be due to the HeI 4S–3P line; this feature is not seen in any other sources. For the Orion Bar, OMC–2, NGC 2023 and Parsamyan 18 the S(1) line emission velocity is, within the errors, at the velocity of the ambient molecular cloud determined by CO line observations (see Table 2).

IV Discussion

The observed narrow line profiles are centred at the rest velocity of the respective ambient molecular clouds, which is as expected for UV–excited line emission. However such profiles could be produced by a single shock moving perpendicular to the line of sight. Thus these data are in themselves insufficient to demonstrate that the emission is fluorescent. Therefore, in the rest of this section we discuss additional evidence for fluorescence in the four sources that are observed.

NGC 2023 The reflection nebula NGC 2023, excited by a B1.5 star HD 37903, is the source where the first clear identification of fluorescent H_2 line emission was made (Gatley *et al.* 1987, Black & van Dishoeck 1987). Many other observed phenomena are best interpreted as occurring on the surface of the molecular cloud as a result of UV irradiation (*e.g.*, Pankonin & Walmsley 1976, Crawford *et al.* 1985, Witt & Schild 1988, Burton *et al.* 1989c) and have a close spatial coincidence with the H_2 line emission. Thus the evidence for H_2 fluorecence is particularly convincing in NGC 2023.

Parsamyan 18 The reflection nebula P 18 has a 1–0/2–1 S(1) line ratio of 1.7, as expected for fluorescent line emission (Sellgren 1986). The UV–excited infrared emission bands at 3.3 μm (Gatley *et al.* 1987), 6.2, 7.7 μm and 11.3 μm (Cohen *et al.* 1986), have been observed. The H_2 1–0 S(1) line and the 3.3 μm emission feature are morphologically similar

(Burton *et al.* 1989c). Thus, the observed narrow H_2 line profile is entirely consistent with the previous understanding of the excitation of the H_2.

The Orion Bar From the variation of the 1–0/2–1 S(1) line ratio across the ionization front in the Orion Bar, Hayashi *et al.* (1985) concluded that both UV-excitation from the Trapezium stars, and shock–excitation driven by the expansion of the HII region were responsible for the H_2 line emission. As pointed out earlier, however, it is difficult to drive such a shock wave sufficiently fast to excite the vibrational H_2 lines. In addition, the H_2 line emission peaks 15" away from the ionization front, whereas it would be expected to occur immediately adjacent to the front if the H_2 were shock–excited. A detailed model of the region by Tielens & Hollenbach (1985b) fits the observed [OI] 63 μm and 146 μm, [CI] 609 μm, [CII] 158 μm and low-lying CO rotational lines by a PDR model with density 2×10^5 cm^{-3} and a UV–field appropriate to that measured for the Trapezium stars. The high-excitation H_2 lines observed by Hippelein & Münch (1989) require a density of $\sim 10^6$ cm^{-3} in the same UV–field for this model (Burton *et al.* 1989a), but a possible underestimation of H_2 collisional de-excitation rates may lower this density to a value closer to that determined from the fine-structure lines. The 3.3 μm emission feature also originates in a neutral region behind the ionization front (Sellgren 1981, Aitken *et al.* 1979). However, images of the 3.3 μm feature and the S(1) line are not identical, with the S(1) line peaking a further 10" away from the ionization front than the 3.3 μm feature (Burton *et al.* 1989c). The strongest S(1) emission occurs in the region assigned as shock-excited by Hayashi *et al.* (1985). Emission from the 3.3 μm feature does arises here too, although its intensity is reduced relative to that closer to the ionization front.

On the basis of these data and the current H_2 spectra, we cannot rule out the possibility that some of the H_2 line emission from the Orion Bar is shock-excited, although it seems clear from the narrow linewidths that the bulk of the emission is fluorescent. It appears likely that much of the H_2 line emitting gas is sufficiently dense ($> 10^5 - 10^6$ cm^{-3}) that collisions thermalise the vibrational levels of the H_2 molecules before they can radiate. The emission spectrum therefore appears similar to that expected from hot, shocked gas, and

the lines are narrow and emitted at the rest velocity of the cloud, as observed.

OMC-2 H_2 line emission in OMC–2 is centred on IRS4, (Fischer, Righini-Cohen & Simon 1980, Thronson & Thompson 1982) and extends $\sim$ 90" NNE as a narrow 'jet' (Burton, Garden & Russell, in preparation). The present observations were centred on a bright clump situated about half way along the 'jet'. No infrared sources have been observed in the region of this 'jet'. On the basis of a 1–0/2–1 S(1) line ratio of 7 for the emission on IRS4, Thronson & Thompson (1982) argue for shock-excitation of the gas. The noise level on their 2–1 S(1) line is high however, so the interpretation is subject to some doubt. ^{12}CO line emission is seen with wings extending to $\pm 6\,\mathrm{km\,s^{-1}}$ away from line centre around IRS4 (Fischer *et al.* 1985). The emission is slightly bipolar, with axis extending NNE from IRS4 and centred at about (10E,20N) from the source; *i.e.*, in a direction similar to the 'jet' seen in the S(1) line. IRS4–N is the most luminous member of the star cluster making up OMC–2 and appears to be surrounded by a disk oriented E–W (Pendleton *et al.* 1986, Rayner *et al.* 1989). This disk may collimate an outflow from IRS4–N. Thus, on this evidence, it seems plausible to assume that the S(1) line emission from OMC–2 is shocked. However, the line profile observed is narrow (although somewhat broader than one would expect from a quiescent cloud), and the emission velocity is close to the rest velocity of the cloud. These are indicative of fluorescence, but could also be consistent with a low velocity shock, or a faster one travelling in the plane of the sky. The observed CO velocities are also too small to significantly populate the vibrational H_2 levels if there are shocks moving with the same velocities. However, examples are known (*e.g.*, DR 21, Garden *et al.* 1986) where observed H_2 velocities far exceed those observed in CO. Further observations of the H_2 line emission, in particular spectra and profiles taken at several positions along the 'jet', are required in order to determine the source of excitation.

V Conclusions

We have measured the profile of the H_2 1–0 S(1) line at high resolution in several sources where the emission is suspected of being fluorescent. In each case we find that the line is narrow and the emission velocity is close to that of the ambient cloud. This is as expected in sources excited by UV–radiation, but is not commonly observed in shock–excited sources. Thus in some cases high resolution spectroscopy can provide an additional diagnostic for distinguishing between shocks and fluorescence. Taken together with other evidence, it is clear that the H_2 line emission in NGC 2023, Parsamyan 18 and the Orion Bar result from fluorescence. In OMC–2 we cannot distinguish yet between shocks and fluorescence.

Acknowledgements

We wish to thank the staff of the United Kingdom Infrared Telescope for friendly and able assistance. AM is supported by an SERC studentship. This work was done, in part, while MGB held a National Research Council N.A.S.A. Research Associateship at Ames Research Center.

Table 1 : Observing Log

Object	(0,0) Position	Integration time per point (sec)	Number of spectral points
The Orion Bar	$5^h32^m55^s.4$ $-5°26'50".7$	40	13
θ_2 Ori A			
OMC–2	$5^h32^m59^s.8$ $-5°11'30".1$	35	18
IRS4–S			
NGC 2023	$5^h39^m07^s.3$ $-2°16'58"$	50	15
HD 37903			
Parsamyan 18	$6^h57^m16^s.6$ $-7°42'16"$	60	17
Star A			
OMC–1	$5^h32^m48^s.2$ $-5°24'30"$	4	43
Peak 2			

Table 2 : Source Parameters

Source	Offset (arcsec)	Observed FWHM of Line ($km\,s^{-1}$)	Velocity of 1–0 S(1) Line ($km\,s^{-1}$)	Velocity of Ambient Cloud ($km\,s^{-1}$)	Relative Flux
The Orion Bar	38.5W 9.3S ($10\,\mu m$ peak[2])	20	+14.5	+11[1]	0.0095
	30W 18S (Position 4[1])	17	+14		0.029
	45W 25S (H_2 peak)	17	+11.5		0.046
OMC-2	18E 50N (H_2 peak)	23	+13	+10.5[3]	0.030
NGC 2023	78S 9W (H_2 peak)	17	+11	+11[4]	0.031
Parsamyan 18	8W	19	+15.5	+13.4[5]	0.011
	7W 12N	16	+15.5		0.015
OMC-1 Peak 2	0E 0N	37	+13	+9	1.0

An approximate line flux for OMC-1 Peak 2 is 4×10^{-19} W cm^{-2} through an 8" aperture (Beck & Beckwith 1983). All velocities are with respect to the local standard of rest. H_2 velocities are estimated to be accurate to $\pm 3\,km\,s^{-1}$. They were measured relative to the line centre at Peak 2, for which the values given are from Nadeau & Geballe (1979). Other references, for quiescent cloud velocities and positions are as follows : (1) Hayashi *et al.* 1985; (2) Becklin *et al.* 1976; (3) Fischer *et al.* 1985; (4) Gatley *et al.* 1987; (5) Wooden & Cohen (private communication).

References

Aitken, D.K., Roche, P.F., Spenser, P.M. & Jones, B., 1979. *Astr. Ap.*, **76**, 90.

Beck, S.C. & Beckwith, S., 1983. *Ap. J.*, **271**, 175.

Becklin, E.E., Beckwith, S., Gatley, I., Mathews, K., Neugebauer, G., Sarazin, C. & Werner, M.W., 1976. *Ap. J.*, **207**, 770.

Beckwith, S., Persson, S.E., Neugebauer, G. & Becklin, E.E., 1978. *Ap. J.*, **223**, 464.

Black, J.H. & Dalgarno, A., 1976. *Ap. J.*, **203**, 132.

Black, J.H. & van Dishoeck, E.F., 1987. *Ap. J.*, **322**, 412.

Bragg, S.L., Brault, J.W. & Smith, W.H., 1982. *Ap. J.*, **263**, 999.

Brand, P.W.J.L., Moorhouse, A., Burton, M.G., Geballe, T.R., Bird, M. & Wade, R., 1988. *Ap. J. (Letters)*, **334**, L103.

Burton, M.G., 1987. *Q.J.R.A.S.*, **28**, 269.

Burton, M.G., Garden, R.P. & Russell, A.P.G.R. (in preparation).

Burton, M.G., Geballe, T.R. & Brand, P.W.J.L., 1989b. *M.N.R.A.S.*, in press.

Burton, M.G., Hollenbach, D.J. & Tielens, A.G.G.M., 1989a. in *Infrared Spectroscopy in Astronomy*, 22nd ESLAB Symposium (ESA SP–290), Salamanca, Spain, Dec 7–9 1988. ed B. Kaldeich (in press).

Burton, M.G., Moorhouse, A., Brand, P.W.J.L., Roche, P.F. & Geballe, T.R., 1989c. in *Interstellar Dust, I.A.U. Symp. 135*, eds. L.J. Allamandolla & A.G.G.M. Tielens (in press).

Chernoff, D.F., Hollenbach, D.J. & McKee, C.F., 1982. *Ap. J. (Letters)*, **259**, L97.

Cohen, M., Allamandola, L., Tielens, A.G.G.M., Bregman, J., Simpson, J.P., Witteborn, F.C., Wooden, D. & Rank, D., 1986. *Ap. J.*, **302**, 737.

Crawford, M.K., Genzel, R., Townes, C.H. & Watson, D.M., 1985. *Ap. J.*, **291**, 755.

Dinerstein, H.L., Lester, D.F., Carr, J.S. & Harvey, P.M. 1988. *Ap. J. (Letters)*, **327**, L27.

Draine, B.T. & Roberge, W.G., 1982. *Ap. J. (Letters)*, **259**, L91.

Fischer, J., Righini-Cohen, G. & Simon, M., 1980. *Ap. J. (Letters)*, **238**, L155.

Fischer, J., Sanders, D.B., Simon, M. & Solomon, P.M., 1985. *Ap. J.*, **293**, 508.

Garden, R., Geballe, T.R., Gatley, I. & Nadeau, D., 1986. *M.N.R.A.S.*, **220**, 203.

Gatley, I., Hasegawa, T., Suzuki, H., Garden, R., Brand, P., Lightfoot, J., Glencross, W., Okuda, H. & Nagata, N., 1987. *Ap. J. (Letters)*, **318**, L73.

Gautier, T.N. III, Fink, U., Treffers, R.R. & Larson, H.P., 1976. *Ap. J. (Letters)*, **207**, L29.

Hayashi, M., Hasegawa, T., Gatley, I., Garden, R. & Kaifu, N., 1985. *M.N.R.A.S.*, **215**, 31P.

Hill, J.K. & Hollenbach, D.J., 1978. *Ap. J.*, **225**, 390.

Hipplelein, H.H. & Münch, G., 1989. *Astr. Ap.*, (in press).

Hollenbach, D.J. & McKee, C.F., 1989. *Ap. J.*, (in press).

Hollenbach, D.J. & Shull, J.M., 1977. *Ap. J.*, **216**, 419.

Kwan, J., 1977, *Ap. J.*, **216**, 713.

Litzén, U. 1970. *Physica Scripta*, **2**, 103.

London, R., McCray, R. & Chu, S.-I, 1977, *Ap. J.*, **217**, 442.

Nadeau, D. & Geballe, T.R., 1979, *Ap. J. (Letters)*, **230**, L169.

Norlén, G., 1973. *Physica Scripta*, **8**, 249.

Pankonin, V. & Walmsley, C.M., 1976. *Astr. Ap.*, **48**, 341.

Pendleton, Y., Werner, M.W., Capps, R. & Lester, D., 1986. *Ap. J.*, **311**, 360.

Rayner, J., McCaughrean, M., Aspin, C. & McLean, I., 1989. *M.N.R.A.S.*, (submitted).

Scoville, N.Z., Hall, D.N.B., Kleinmann, S.G. & Ridgway, S.T., 1982. *Ap. J.*, **253**, 136.

Sellgren, K., 1981. *Ap. J.*, **245**, 138.

Sellgren, K., 1986. *Ap. J.*, **305**, 399.

Shull, J.M. & Hollenbach, D.J., 1978. *Ap. J.*, **220**, 525.

Sternberg, A. & Dalgarno, A., 1989. *Ap. J.*, **338**, 197.

Tanaka, M., Hasegawa, T., Hayashi, S.S., Brand, P.W.J.L. & Gatley, I., 1989. *Ap. J.*, **326**, 207.

Tielens, A.G.G.M. & Hollenbach, D.J., 1985a. *Ap. J.*, **291**, 722.

Tielens, A.G.G.M. & Hollenbach, D.J., 1985b. *Ap. J.*, **291**, 747.

Thronson, H.A. & Thompson, R.I., 1982. *Ap. J.*, **254**, 543.

Witt, A.N. & Schild, R.E., 1988. *Ap. J.*, **325**, 837.

Zuckerman, B. & Gatley, I., 1988. *Ap. J.*, **324**, 501.

Figure Captions

Figure 1 The observed profiles of the H_2 1–0 S(1) line, at 2.1218 μm, in the sources NGC 2023, OMC–2, Parsamyan 18, the Orion Bar, and, for reference, in the shock-excited source OMC–1. An Argon lamp line is shown for each profile. All profiles have been normalised to unit flux and have had their central velocity set to 0 $km\,s^{-1}$. Relative fluxes, FWHM's and V_{LSR} emission velocities are given in Table 2.

Authors' Addresses

P.W.J.L. BRAND, and A. MOORHOUSE: University of Edinburgh, Department of Astronomy, Royal Observatory, Blackford Hill, Edinburgh EH9 3HJ, Scotland, U.K.

MICHAEL G. BURTON: N.A.S.A. Ames Research Center, MS 245-6, Moffett Field, CA 94035.

T.R. GEBALLE: Joint Astronomy Centre, 665 Komohana Street, Hilo, HI 96720.

Figure 1.

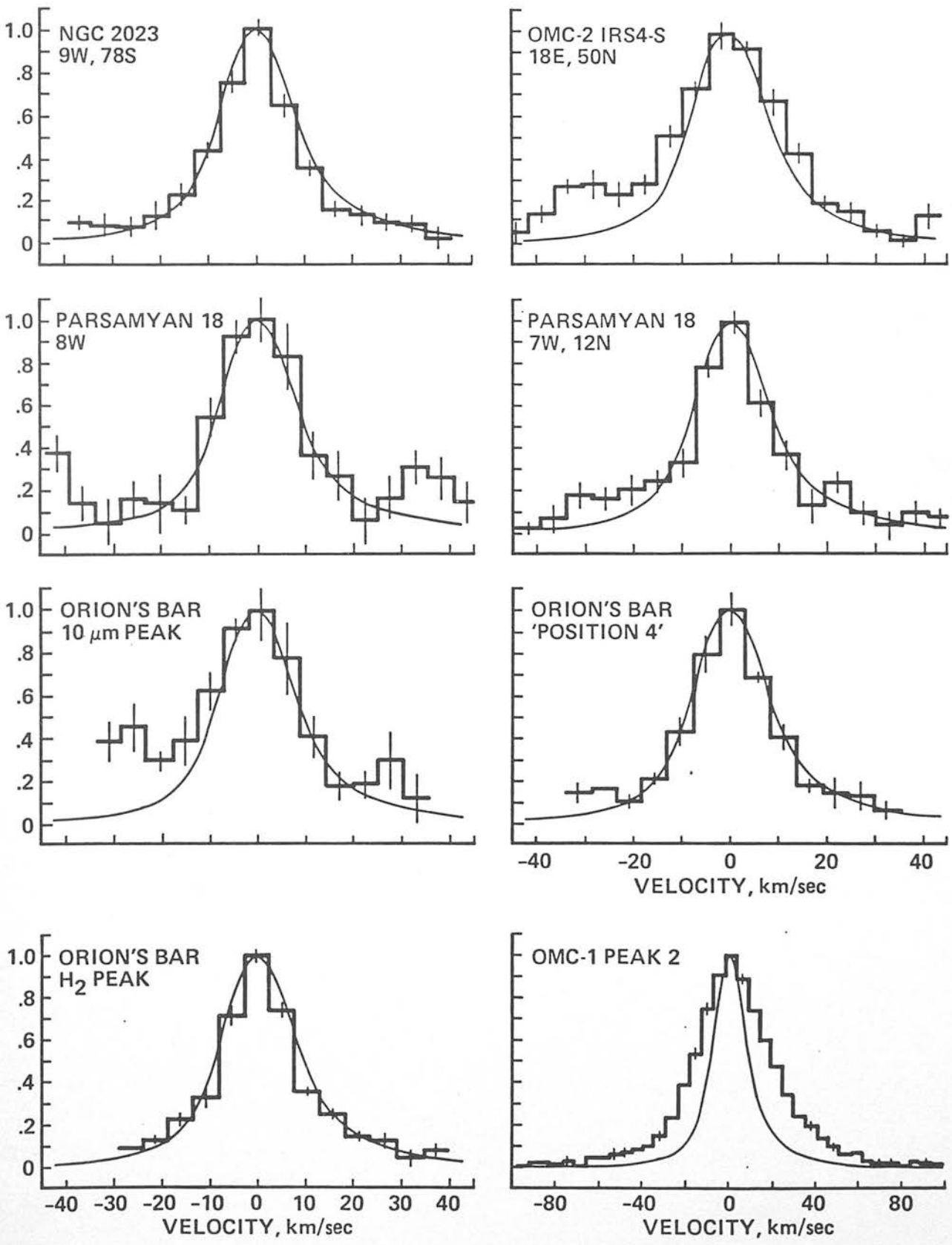

BURTON

$$\frac{\text{cm}^{-2}}{N_H (10^{-21})} = 2$$

$\tau = 1 \qquad N_H = \frac{10^{21}}{2} = 5 \times 10^{20} \text{ cm}^{-2} \qquad 5 \times 10^{14} \text{ cm}$

$$\frac{\lambda \tau}{N_H} = 1 \times 10^{-26}$$

$$N_H = 10^{26} \lambda = 2 \times 10^{+22} \qquad 2 \mu m.$$

40

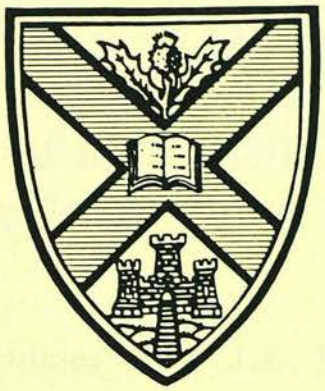

Edinburgh Astronomy Preprint

Number 11/89

July 1989

Velocity profiles of high excitation molecular hydrogen lines

A. Moorhouse
P.W.J.L. Brand
T.R. Geballe
M.G. Burton

University of Edinburgh Department of Astronomy
Royal Observatory, Blackford Hill, Edinburgh EH9 3HJ, Scotland
Telephone: 031-667 3321 Telex 72383

Accepted for publication
in Monthly Notices of the Royal Astronomical Society

Velocity profiles of high excitation molecular hydrogen lines

A. Moorhouse,[1] P.W.J.L. Brand,[1]
T.R. Geballe[2] and M.G. Burton[3,4]

1. Department of Astronomy, Royal Observatory Edinburgh, Blackford Hill, Edinburgh EH9 3HJ.

2. Joint Astronomy Centre, 665 Komohana Street, Hilo, HI 96720, USA.

3. N.A.S.A. Ames Research Center, MS 245-6, Moffett Field, CA 94035., USA.

4. University of California at Irvine, Irvine, CA 92717, USA.

Summary

Profiles of three lines of molecular hydrogen near 2.2 μm , originating from widely spaced energy levels, have been measured at a resolution of 32 km s^{-1} at Peak 1 in the Orion molecular outflow. The three lines (1-0 S(1), 2-1 S(1) and 3-2 S(3)) are found to have identical profiles. This result rules out any significant contribution to the population of the higher energy levels of molecular hydrogen at Peak 1 by fluorescence, is inconsistent with multiple C shock models which produce higher excitation temperatures at larger shock velocities, and is generally consistent with emission from multiple J-type shocks.

1 Introduction

Observations in Orion of the v=1-0 S(1) molecular hydrogen line (e.g. Nadeau & Geballe, 1979) demonstrated that some of the shocked gas is undergoing motions in excess of 70 km s^{-1} relative to the quiescent molecular cloud. Similar highly supersonic motions of shocked H_2 are observed in other star forming regions (*e.g.* Doyon & Nadeau 1988; Garden *et al.* 1986), and are presumed to be associated with the interaction of a high velocity wind from a young stellar object and a molecular cloud being impacted by the wind. However the line emission at these high velocities defies easy explanation (*e.g.* Brand *et al.* 1989a).

The atomic and molecular line emission in Orion has been modelled by several authors as arising in a magnetically moderated C-type shock (Draine & Roberge 1982; Chernoff, Hollenbach & McKee 1982). However, the intensities of weak, high excitation, molecular hydrogen lines are considerably stronger than the predictions from the C-shock models, and appear consistent with a hydrodynamic or J-type shock (Brand *et al.* 1988). This conclusion presupposes that there is insignificant emission in these weak high excitation lines from fluorescence, which would be observed as a narrow unresolved component to the line core. Conversely in C-shocks the excitation temperature increases as the shock velocity increases (Draine, Roberge & Dalgarno 1983). Comparison of the 1-0 S(1) with lines of similar excitation energy, but from longer wavelengths (Geballe *et al.* 1986; Scoville *et al.* 1982), show that slightly higher excitation lines display stronger high velocity wings. This was interpreted by the above

authors as an effect of extinction through the outflow and different locations of the high and low velocity gas. However, it is not clear if these differences are due, in part, to real differences in the velocity distributions of the different energy levels involved. By observing lines which are from widely different upper energy levels, but are very close in wavelength, effects of differential extinction are minimal, and any intrinsic differences in the velocity distributions can be ascertained.

2 Observations

The observations displayed in fig. 1 were all made at the United Kingdom Infrared Telescope on the night of the 21 January 1988. The indium antimonide photometer/low resolution spectrometer (UKT9) was used in conjunction with an ambient temperature Fabry Perot interferometer (FP), whose passband has a full width at half maximum of 25 km s^{-1} in parallel light. The circular variable filter (CVF) in UKT9 acted as an order isolator, although it transmits several adjacent orders. The FP was stepped at intervals of 10 km s^{-1} , providing a fully sampled spectrum. The aperture size was 12 arcsec, degrading the resolution of the FP to 32 km s^{-1} . Standard nodding and chopping (60 arcsec E-W) were performed. All observations were of Peak 1 (R.A. = $5^h\ 32^m\ 46.2^s$, Dec = -5° 24′ 02″ ; Beckwith *et al.* 1978). Molecular hydrogen 1-0 S(1), 2-1 S(1) and 3-2 S(3) lines were observed. The blue wing of the 3-2 S(3) line is blended with the 4-3 S(5) line, which is observed for the first time. Further details are given in Table 1.

Absolute velocity calibration of the H_2 lines was achieved by comparing their wavelengths calculated from the energy levels of Dabrowski (1984) with nearby lines from an argon lamp. The FP was regularly monitored for velocity drift, by observing the argon lamp before and after each observation. The uncertainty in the velocity calibration is 5 km s^{-1} , the main source being drift of the FP during the observations, which thus very slightly degrades the instrumental profile for the long integrations. The measured peak velocity for each of the profiles is quoted in Table 2 as well as the relative intensities and upper energy levels of the lines. The peak of the 1-0 S(1) profile is at +4km s^{-1} close to the velocity of the ambient molecular cloud (+9km s^{-1} ;Goldsmith, Plambeck & Chiao 1975). The velocity of the peaks of the other profiles

are, within the measurement errors, identical to that of the 1-0 S(1). The absolute flux scale was not determined because of uncertainties in the numbers and relative strengths of orders transmitted by the CVF.

3 Results

The spectrum of the 1-0 S(1) line is shown in fig. 1(a). The error bars are plus/minus one standard deviation. The signal to noise is very high, so for clarity a bar ten times the length of the average error bar is plotted in the top right. The solid curve is a cubic spline fitted through the data points. The dashed line is the measured lamp profile which, since the lamp line is unresolved, may be taken to be the instrumental profile. The spline fit will be used to compare other lines to the 1-0 S(1) line. It is clear from fig. 1 that the errors in the 1-0 S(1) data are very small. Errors in comparing the profiles of fainter lines with the spline fit will thus be due largely to the measurement errors in these lines.

The 2-1 S(1) line profile is presented in fig. 1(b). The solid line is the least squares fit to these data using the cubic spline from the 1-0 S(1) line plus a flat continuum. In this fit $\chi^2 = 39$ with 42 data points. It is thus apparent that there are no measurable differences between the observed 1-0 S(1) and 2-1 S(1) profiles.

The 3-2 S(3) line profile is displayed in fig. 1(c). It is blended with the 4-3 S(5) line (2.009 μm) at -61 km s^{-1} relative to the 3-2 S(3) line. The rise in intensity beyond $+100$ km s^{-1} is the blue wing of the 1-0 S(0) line, approximately two FP orders away from the 3-2 S(3) line and partially transmitted by the CVF. On the LSR velocity scale in the diagram it would peak at 215 km s^{-1} . The solid line is again a least squares fit to the data, except that in this case a flat continuum plus three cubic splines with the correct velocity offsets were fitted to the data. The amplitude of the 4-3 S(5) line was set to 0.10 times the 3-2 S(3) line. This is the ratio calculated from a J shock model fitted to many molecular hydrogen lines in the 2-3 μm region (Brand *et al.* 1988). The value of χ^2 is 22. There are 39 data points, and three free parameters. The dashed lines show the individual contributions from the lines. Again it is evident that there are no differences between the 3-2 S(3) profile and the 1-0 S(1) profile. If the ratio of blended lines is left as a free parameter, the best fit value is 0.3, with a χ^2 of 20.

It is noted that the values of χ^2 for this data is smaller than would be expected, this is likely due to the high continuum to line ratio (about 10), so the formal errors are dominated by continuum variations.

The 4-3 S(5) line is the highest excitation line yet detected in shocked gas. It is weak, and so it is not obvious that the data constrain its profile. This question was examined by fitting an instrumental profile instead of the 1-0 S(1) spline to this line. The result is shown in Fig. 2. It is clear that this a worse fit, in this case the χ^2 increases to 26, and so we infer that the 4-3 S(5) line possesses a broad profile, which is consistent with the 1-0 S(1) profile.

In order to quantify the fraction of flux that a narrow (*e.g.* fluorescent) line could contribute to the broad lines, a combination of the instrumental profile and the 1-0 S(1) spline was fitted to the data , the relative amplitudes being left as free parameters. The 3-sigma upper limit to the fraction of each observed profile which could be produced by a narrow line was : for the 2-1 S(1) line 0.03, for the 3-2 S(3) line 0.20, and for the 4-3 S(5) line 0.6.

4 Discussion

4.1 Limits on fluorescence and reformation

The Orion molecular outflow lies behind the optical HII region M42. The interface layer between the two gives rise to fluorescent H_2 emission (Hayashi *et al.* 1985). Such fluorescent emission is a likely contaminant of the line emission observed toward the molecular outflow region. However, the fluorescent emission is considerably narrower than the present resolution (Burton *et al.* 1989b), so that line emisson at moderate and high velocities must originate in shocked gas. The 60 arcsec chop, was chosen in order to sample line emission away from the outflow, but still within the HII region, largely subtracting any foreground fluorescence. The upper limits to narrow features in the profiles represent limits to fluorescent contamination of the line emission seen toward the outflow region. From the similarity of all the lines we conclude that any fluorescent contribution from the photodissociation region is insignificant.

Theoretically the fluorescent contribution to the v= 3 and 4 lines is expected to be much less than the above limits. The average intensity of the 1-0 S(1) line emission

observed from the photodissociation region is approximately 500 times smaller than that from Peak 1 (Tielens & Hollenbach 1985). At Peak 1 the 3-2 S(3) line is one fiftieth of the 1-0 S(1) (Brand *et al.* 1988). Even if fluorescence were able to produce as much flux in the 3-2 S(3) line as the 1-0 S(1), the contribution from the photodissociation region to the 3-2 S(3) would be only ten percent of that from the shocked outflow. The fluorescent component is likely to be much less, since the fluorescent models of Black & van Dishoeck (1987) predict that at most the 3-2 S(3) is twenty percent of the 1-0 S(1). A similar argument holds for the 4-3 S(5) line.

The above discussion refers only to the foreground fluorescence from the photodissociation region. Fluorescence in the fast moving gas can be ruled out by the observed line ratios (Brand *et al.* 1988) and the present result of similar profiles, implying that the H_2 line ratios are independent of velocity. The ratios are totally unlike any fluorescence models (i.e. Black & van Dishoeck 1987), and show a smooth increase in excitation temperature as the energy of the upper level of the transition increases. Recentley it has been pointed out that in regions of high density, collisions will thermalize the lower vibrational levels of UV-excited molecules (i.e. see review by Sternberg 1989, and references therin), however this cannot produce the range of excitation temperatures observed and, more importantly, there would still be strong emission from vibrational levels far higher than are actually observed.

Molecular hydrogen is completely collisionally dissociated in J-type shocks with velocities greater than 25 km s^{-1} (Kwan 1977), and in magnetohydrodynamic C-type shocks at velocities greater than 45 km s^{-1} (Draine & Roberge 1982). Thus, the large width of these H_2 lines is not easy to explain. Molecular hydrogen is known to reform on the surfaces of cool dust grains (Hollenbach & Salpeter 1971; Duley & Williams 1984), at gas temperatures so low that H_2 line emission is no longer collisionally excited. It is likely that the H_2 will reform in an excited state (*e.g.* Duley & Williams 1986, Hollenbach & McKee 1989). However such excited molecules will be collisionally deexcited in the dense ($\geq 10^{13}$ m^{-3}) gas behind the shock front. Therefore we do not believe that molecule reformation can account for the high velocity, high excitation line emission.

4.2 Shock models

It is clear from the foregoing discussion that an individual simple shock wave (either J- or C-type) cannot lead to the large range of emission velocities observed in excited H_2 lines. A high velocity bow shock, either from a wind passing a high density clump or a bullet propagating into a lower density medium, suffers from similar problems, and cannot in itself lead to broad profiles (Brand *et al.* 1989a). An oblique C-type shock can broaden the profile beyond what would be produced by a J-type shock, but the range is still too small to account for the observations. Finally, the possibility that the high velocity line emission is due to scattering off fast moving grains has been ruled out by measurements of profiles of the 1-0 O(7) line at 3.8 μm (Geballe *et al.* 1986) and by spectropolarimetry of the 1-0 S(1) line (Burton *et al.* 1988).

It therefore seems most plausible that the observed H_2 line profile along a given line of sight is produced by an ensemble of low velocity shocks, some of which are occurring in molecular gas that is co-moving with the molecular outflow, as suggested by Chevalier (1980) and by Nadeau, Geballe & Neugebauer (1982). Observational evidence for this interpretation has been found by Scoville *et al.* (1982), Geballe *et al.* (1986) and, perhaps most strongly, by Geballe & Garden (1989), although geometric models of the emission region are not obvious (*e.g.* Brand *et al.* 1989a).

If indeed the line emission is due to a superposition of shocks, the similarity of the profiles of lines with widely differing upper energy levels constrains the shock type. This is because in a J-shock, the line emitting H_2 has already been accelerated and is cooling rapidly, so the temperature distribution is independent of the shock velocity. In a C-shock, much of the line emitting gas is in LTE. at a temperature which is a strong (monotonically increasing) function of the shock speed. For example, J-shocks give significant emission only for shock velocities between 10 km s^{-1} (below this the temperature behind the shock front is not high enough to excite much H_2 before the gas cools) and 25 km s^{-1} (the dissociation limit). For shock velocities between these limits the excitation temperature of any particular line pairs is constant. The emission from J-shocks is more dependent on the pressure (through the amounts of dissociational to radiative cooling($\propto n^2$ and n respectivley)), even over two orders of magnitude the excitation temperature derived from the 2-1 S(1)/1-0 S(1) ratio varies only from 1800 to 2200 K. The appearance of C-shocks is dependent on many parameters (i.e shock

velocity, magnetic field strength, ionisation fraction and density) in a 36 km s^{-1} shock (applied to Orion by Draine, Roberge & Dalgarno 1983) the excitation temperature of the 2-1/1-0 lines is 2700 K and drops to 800 K for 20 km s^{-1} . The line profiles of a superposition of J-shocks will be similar for all upper state energies, unless there are large variations in the shock pressure . However, for a superposition of C-shocks, higher excitation lines are very sensitive to the parameters of the shock. The present results then, when interpreted in terms of multiple shock events along the line of sight, clearly favour J-type over C-type shocks. Several recent and independent observational tests (Brand *et al.* 1988, 1989b; Burton *et al.* 1989a), in Orion and elsewhere, also favour J-shocks.

5 Conclusions

We have presented velocity profiles at Peak 1 of three molecular hydrogen lines arising from widely differing energy levels. All three are virtually identical in shape and peak at the same velocity. This implies that:

(i) fluorescent contributions from the photodissociation region cannot be large;

(ii) the bulk of the high velocity emission is not due to H_2 that has reformed following a fast (dissociative) shock;

(iii) If the line profiles are due to a superposition of shocks along the line of sight, the shocks are more likely to be J-type than C-type.

Acknowledgements

We thank the staff of UKIRT for their friendly and helpful assistance in obtaining the observations. AM was supported by an SERC studentship, and MGB held a National Research Council NASA Research Associateship at Ames Research Center during this work.

References

Beck, S.C., Bloemhof, E.E., Serabyn, E., Townes, C.H., Tokunaga, A.T, Lacy, J.H. & Smith H.A., 1982. *Astrophys. J.*, **253**, L83.

Beckwith, S., Persson, S.E., Neugebauer, G. & Becklin, E.E., 1978. *Astrophys. J.*, **223**, 464.

Black, J.H. & van Dishoeck, E.F., 1987. *Astrophys. J.*, **332**, 412.

Brand, P.W.J.L., Moorhouse, A., Burton M.G., Geballe, T.R., Bird, M., Wade, R., 1988. *Astrophys. J.*, **334**, L103.

Brand, P.W.J.L., Toner, M.P., Geballe, T.R. & Webster, A.S., 1989a. *Mon. Not. R. astr. Soc.*, **237**, 1009.

Brand, P.W.J.L., Toner, M.P., Geballe, T.R., Webster, A.S., Williams, P.M., & Burton, M.G., 1989b. *Mon. Not. R. astr. Soc.*, **236**, 929.

Burton, M.G., Brand, P.W.J.L., Geballe, T.R. & Webster, A.S., 1989a. *Mon. Not. R. astr. Soc.*, **236**, 409.

Burton, M.G., Geballe, T.R., Brand, P.W.J.L., & Moorhouse, A., 1989b. in preparation.

Burton, M.G., Hough, J.H., Axon, D.J., Hasegawa, T., Tamura, M., McCaughrean, M.J. & McLean, I.S., 1988. *Mon. Not. R. astr. Soc.*, **235**, 161.

Chernoff D.F., Hollenbach D.J. & Mckee C.F., 1982. *Astrophys. J.*, **259**, L97.

Chevalier, R.A., 1980 *Astrophys. J.*, **259**, L97.

Dabrowski, I., 1984. *Canadian J. Phys.*, **62**, 1639.

Doyon, R. & Nadeau, D., 1988. *Astrophys. J.*, **334**, 883.

Draine, B.T., 1980. *Astrophys. J.*, **241**, 1021.

Draine, B.T. & Roberge W.G., 1982. *Astrophys. J.*, **259**, L91.

Draine, B.T. & Roberge W.G. & Dalgarno, 1983. *Astrophys. J.*, **264**, 485.

Duley W.W. & Williams, D.A., 1984. *Interstellar Chemistry,* Academic press, London.

Duley W.W. & Williams, D.A., 1986. *Mon. Not. R. astr. Soc.*, **223**, 177.

Garden, R., Geballe, T.R., Gatley, I. & Nadeau, D., 1986. *Mon. Not. R. astr. Soc.*, **220**, 203.

Geballe, T.R., & Garden, R.P., 1989, in preparation.

Geballe, T.R., Persson, S.E., Simon, T., Lonsdale, C.J., & McGregor, P.J., 1986. *Astrophys. J.*, **302**, 693.

Goldsmith, P.F., Plambeck, R.L. & Chiao, R.Y., 1975. *Astrophys. J.*, **196** L39.

Hayashi, M., Hasegawa, T., Gatley, I., Garden, R.P. & Kaifu, N., 1985. *Mon. Not. R. astr. Soc.*, **215**, 31p.

Hollenbach, D.J. & McKee, C.F., 1989. *Astrophys. J.*, in press.

Hollenbach, D.J. & Salpeter, E.E., 1971. *Astrophys. J.*, **163**, 155.

Kwan, J., 1977. *Astrophys. J.*, **216**, 713.

Nadeau, D., Geballe, T.R., 1979. *Astrophys. J.*, **230**, l169.

Nadeau, D., Geballe, T.R. & Neugebauer, 1982. *Astrophys. J.*, **253**, 154.

Scoville, N.Z., Hall, D.N.B., Kleinmann, S.G. & Ridgway, S.T., 1982. *Astrophys. J.*, **253**, 136.

Sternberg, A., 1989. in the proceedings of 22^{nd} Eslab symposium on infrared spectroscopy in astronomy, Salamanca, 7-9^{th} December 1988.

Tielens A.G.G.M. & Hollenbach D., 1985. *Astrophys. J.*, **291**, 747.

Table 1 : Observing Log

Line	Wavelength[1] (microns)	Integration time[2] per point (sec)	Number of points
1-0 S(1)	2.1218	8	43
2-1 S(1)	2.2477	48	42
3-2 S(3)	2.2014	96	39
4-3 S(5)	2.2009	96	39

1. Calculated from energy levels of Dabrowski (1984).

2. Total integration time includes time spent on and off source.

Table 2 : Line parameters

Line	Energy Level[1] (Kelvins)	relative intensity	Velocity of peak[2] intensity (km s^{-1})
1-0 S(1)	6956	100	4
2-1 S(1)	12550	9	0
3-2 S(3)	19086	2	3
4-3 S(5)	25623	0.2	6[3]

1. Calculated from energy levels of Dabrowski (1984).

2. With respect to local standard of rest.

3. Not well constrained by data, error is 10 km s^{-1} .

Figure Captions

Figure 1 Profiles of molecular hydrogen lines at Peak 1 in OMC—1; (a) The 1-0 S(1) line (dots, with error bars); a cubic spline (solid curve) fitted through the data points and an Argon lamp line (dashed curve) profile. (b) The 2-1 S(1) line where the spline shown in (a) is fitted to the data (solid curve); and (c) The 3-2 S(3) line, fitted by a spline model with components due to (dotted curves) the 3-2 S(3) (v=0 km s^{-1}), 4-3 S(5) (v= -61 km s^{-1}), and the 1-0 S(0) (v=215 km s^{-1}) lines. In all of the above the dotted line represents the underlying continuum.

Figure 2 Same data as in Fig. 1(c), except that the 4-3 S(5) has been fitted with the instrumental profile.

Figure 1.

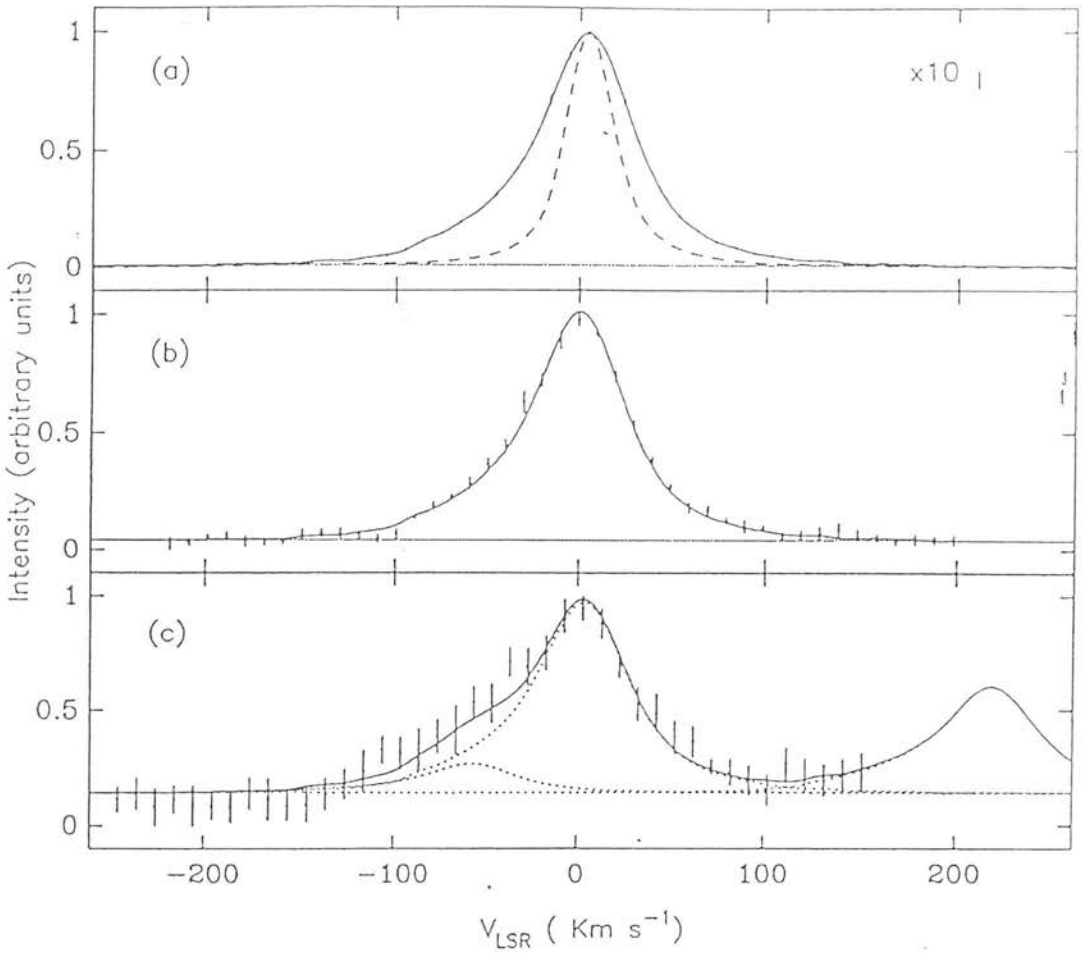

Figure 2